

Department Biologie II
Anthropologie und Humangenetik
Ludwig-Maximilians-Universität München

**Nuclear gene positioning in the context of
evolutionary conservation and genomic
innovation in vertebrates**

Florian Grasser

Dissertation der Fakultät
für Biologie der Ludwig-Maximilians-Universität München
Eingereicht am 15.07.2008

Nuclear gene positioning in the context of evolutionary conservation and genomic innovation in vertebrates

Dissertation der Fakultät

für Biologie der Ludwig-Maximilians-Universität München

vorgelegt von

Dipl. Biol. Florian Grasser

aus München

Gutachter:

PD Dr. Stefan Müller

Prof. Dr. Thomas Cremer

Tag der mündlichen Prüfung: 12.11.2008

1. Summary	8
2. Introduction	10
2.1 Nuclear genome architecture	10
2.1.1 Chromosome territories	10
2.1.2 Subchromosomal domains, genes and gene cluster	11
2.1.3 Chromatin folding and interaction between genomic loci	12
2.1.4 Current models of a functional nuclear architecture	14
2.2 Histone modifications	15
2.2.1 Histone code	15
2.2.2 Histone 3 lysine 4 methylation	16
2.2.3 Histone 3 lysine 9 methylation	17
2.2.4 Histone 3 lysine 27 methylation	17
2.3 Chromosomal genome organization in mouse and chicken	17
2.3.1 Mouse genome	17
2.3.2 Chicken genome	18
2.4 Evolutionary DNA sequence conservation in vertebrates	18
2.4.1 Coding sequences	18
2.4.2 Ultraconserved noncoding sequence (UCS) cluster	19
2.4.3 The Dach1 gene locus and flanking UCS clusters	20
2.4.4 The Bcl11a gene locus and its genomic neighborhood	22
2.5 Evolutionary genomic innovation in vertebrates:	23
The Casein gene locus	
2.6 Embryonic development of mouse and chicken	25
2.6.1 Primitive streak stage	25
2.6.2 Organogenesis	25
2.7 Skin appendages	26
2.7.1 Evolution of skin appendages	26
2.7.2 Postnatal mammary gland	27
2.7.3 Mammalian hair and avian feather follicles	28
2.8 Aims of the work	29
3. Material and methods	31
3.1 Workflow	31

3.2 Cell material	31
3.2.1 Embryonic mouse and chicken fibroblasts	31
3.2.2 Mouse and chicken embryos	32
3.2.3 Tissue of adult mouse and chicken	32
3.3 Cell material fixation and cryosectioning	33
3.3.1 Metaphase preparation from embryonic fibroblasts	33
3.3.2 Fixation of embryonic fibroblasts for 3D-FISH	34
3.3.3 Fixation of embryos and adult tissue	35
3.3.4 Cryoprotection and cryosectioning for chromogenic RNAish and 3D-FISH	35
3.3.5 Freezing and cryosectioning for RNA FISH and qPCR	36
3.4 Preparation of RNA, DNA and embryonic powder	37
3.4.1 DNA isolation and preparation of cot-1 DNA from chicken liver	37
3.4.2 Isolation of BAC clone DNA from bacterial cultures	38
3.4.3 Extraction of embryonic powder	39
3.4.4 Isolation of total RNA and cDNA from tissue	40
3.4.5 Isolation of mRNA and cDNA from laser microdissected tissue	41
3.5 Gene expression analysis	43
3.5.1 Probe design and labelling for RNAish	43
3.5.2 Whole mount RNAish on embryos	47
3.5.3 Chromogenic RNAish on tissue sections	48
3.5.4 RNA FISH on tissue sections	50
3.5.5 Relative qPCR using the TaqMan technique	51
3.5.5.1 Probe design and labeling for qPCR	52
3.5.5.2 qPCR from laser microdissection derived cDNA	53
3.6 DNA Fluorescence in situ hybridisation (FISH)	55
3.6.1 Phi29 amplification and Nick translation labeling of BAC clone DNA	56
3.6.2 DOP-PCR amplification and labeling of chromosome painting probes	58
3.6.3 Preparation of FISH probe sets	59
3.6.4 Metaphase FISH	60
3.6.5 3D-FISH on embryonic fibroblasts	61
3.6.6 3D-ImmunoFISH on embryonic fibroblasts	61
3.6.7 3D-FISH on tissue cryosections	63
3.6.8 3D-FISH on RNAish tissue cryosections	64
3.7 Microscopy	65
3.7.1 Binocular microscopy	65
3.7.2 Phase contrast microscopy	65
3.7.3 Laser microdissection microscopy	65
3.7.4 Epifluorescence microscopy	65
3.7.5 Confocal laser scanning microscopy	66

3.8 Image Processing	67
3.8.1 Adobe photoshop 7.0	67
3.8.2 Huygens Essential 3.5	67
3.8.3 Image J 1.38	67
3.8.4 AMIRA 3.1.1	68
3.9 Quantitative evaluation of 3D confocal image stacks	68
3.9.1 3D relative radial distribution (3D-RRD)	68
3.9.2 Enhanced distance measurement (EDMT)	68
3.9.3 Nuclear Volume and Roundness (EDMT)	68
3.9.4 Higher order DNA conformation (DistAng)	69
3.10 Statistical analysis	70
3.11 Web based resources	70
3.12 Materials	71
3.12.1 Chemicals	71
3.12.2 Nutrient medium and additives	72
3.12.3 Enzymes, nucleic acids, oligonucleotides and BAC clones	72
3.12.4 Antibodies and Avidin conjugates	75
3.12.5 Buffers and solutions	75
3.12.6 Commercial Kits and Solutions	80
3.12.7 Technical devices	81
3.12.8 Software	82
4. Results	83
<hr/>	
4.1 Nuclear topology of evolutionary conserved genomic regions	84
4.1.1 Hot spots of ultraconserved noncoding sequence (UCS) clusters	84
4.1.1.1 Experimental design	84
4.1.1.2 Nuclear radial arrangement of UCS clusters	85
4.1.1.3 Histone modifications in UCS cluster regions	87
4.1.1.4 Results summary of UCS hot spots	88
4.1.2 Dach1 and flanking conserved noncoding sequence clusters	88
4.1.2.1 Experimental design	88
4.1.2.2 Dach1 mRNA expression pattern and quantification	90
4.1.2.3 Nuclear radial arrangement of the Dach1 locus	91
4.1.2.4 Distance to the chromosome territory surface of the Dach1 locus	94
4.1.2.5 Mean higher order chromatin conformation of the Dach1 region	95
4.1.2.6 Results summary of Dach1	97

4.1.3 Bcl11a and its flanking genomic regions	98
4.1.3.1 Experimental design	98
4.1.3.2 Bcl11a mRNA expression pattern	99
4.1.3.3 Nuclear radial arrangement of the Bcl11a region	101
4.1.3.4 Distance to the chromosome territory surface of the Bcl11a region	103
4.1.3.5 Mean higher order chromatin conformation of the Bcl11a region	105
4.1.3.6 Results summary of Bcl11a	107
4.2 Nuclear topology of a mammalian genomic innovative region	108
4.2.1 Experimental design	108
4.2.2 Casein genes mRNA expression pattern	110
4.2.3 Nuclear radial arrangement of Casein region	110
4.2.4 Distance to the chromosome territory surface of Casein region	113
4.2.5 Mean higher order chromatin conformation of the Casein region	114
4.2.6 Results summary of Csn genes	117
5. Discussion	118
5.1 Technical aspects of this work	119
5.1.1 RNA expression analysis	119
5.1.2 3D image acquisition, processing and analysis	121
5.2 Nuclear chromosome territory and gene positioning	122
5.2.1 Chromosome territory positioning	122
5.2.2 Nuclear radial gene positioning	124
5.2.2.1 Correlation with gene density	124
5.2.2.2 Correlation with gene expression	125
5.2.2.3 Evolutionary genomic conservation and innovation	127
5.2.3 Geometrical constraints	129
5.3 Gene positioning with respect to the chromosome territory	132
5.4 Higher order 3D chromatin structure	133
5.4.1 Global higher order chromatin conformation	133
5.4.2 Local higher order chromatin conformation	133
5.5 Conclusions	136
6. Supplementary material	139
7. Literature	140

Publications	154
---------------------	------------

Curriculum Vitae	156
-------------------------	------------

Acknowledgement	158
------------------------	------------

1. Summary

The nuclear topology of ultraconserved non-coding sequence (UCS) clusters, the Dach1, the Bcl11a and the Casein (Csn) gene region was investigated by 3D-FISH on tissue sections from certain developmental stages of mouse and chicken. Native tissue sections are advantageous compared to ex vivo cultured cells in these analysis, the latter were included in control experiments. Moreover the comparative approach allowed for functional conclusions concerning evolutionarily conserved motives of higher order nuclear architecture.

UCS clusters in vertebrates represent potential enhancer or chromatin boundary elements. Together with their flanking UCS, the transcription factors Dach1 and Bcl11a can be considered the tip of evolutionary genomic sequence conservation in vertebrates. In addition, the antidromic Bcl11a region is flanked to one side by a gene-dense region. In contrast the casein genes are a genomic innovation introduced in the mammalian lineage, flanked by sequences with conserved homology in other vertebrates.

In this study, ImmunoFISH on embryonic fibroblasts of mouse and chicken combined delineation of certain histone methylations and visualization of five separate UCS clusters. Further, by combining DNA FISH and chromogenic RNAish in selected tissues the results on the nuclear topology were placed in the context of the expression status of targeted genes. The observed expression differences were validated by RNA FISH and qPCR from laser-microdissected tissue.

The five UCS clusters, although selected from gene deserts showed histone modifications characteristic for euchromatin. In addition, the UCS clusters lack for colocalization in a specific nuclear compartment, suggesting discrete functions of each individual UCS cluster.

Furthermore the three-dimensional quantitative positional analysis of the targeted Dach1, Bcl11a, Csn and and flanking regions in interphase nuclei revealed the nuclear radial arrangement (I) and the distance to the harboring chromosome territory (CT) surface (II). The local chromatin conformation in these regions was captured by interphase distance and angle measurements (III).

(I) Strikingly the nuclear positions of Dach1, Bcl11 and Csn were evolutionarily largely conserved between homologous mouse and chicken tissue but not necessarily between cell types in one species. The Dach1 locus and flanking UCS clusters were stably localized in the nuclear periphery, whereas the antidromic Bcl11a region showed considerable positional flexibility. In neither case the radial positioning could be directly linked to the expression activity, however for Bcl11a it was possibly influenced by the tissue-specific expression of the flanking genes. In stark contrast, upon gene expression during lactation the Csn locus was clearly - and

reversibly - relocalized to the nuclear center. In the transcriptionally silent state in the mouse, and irrespective of the absence of Csn in chicken, in both species the entire region was stably positioned in the periphery.

(II) The locus positioning with respect to the CT surface was species-specific, and was not directly influenced by gene expression. All genomic loci resided stably associated close to or within the core CT.

(III) Overall, the species specific local higher order 3D chromatin conformation was not comprehensively changed by the gene activity of Dach1 or Bcl11a, but considerably by the strong activity of Csn genes. Of importance, gene density was the most reliable indicator for a decondensed chromatin state. In the Csn region extensive chromatin backfolding was observed restricted to lactation, possibly caused by geometrical constrained deformation of the chromatin fiber, but not in the Dach1 or Bcl11a region flanked by clustered UCS.

In conclusion the nuclear radial arrangement was found best conserved during evolution among homologous tissues, and is hence potentially functionally most important compared to the localization within the CT and the local chromatin conformation. Contrary to the moderately expressed trans-dev genes Dach1 and Bcl11a, the strong expression of Csn genes resulted in higher-order chromatin remodeling that was strikingly reversible after lactation. Thus the nuclear genome architecture is inseparably correlated with gene density, and in some instances gene expression in greater genomic regions, and is potentially further influenced by geometrical constraints within a CT. Most importantly these alternating effects can vary among tissues and developmental stages.

2. Introduction

2.1 Nuclear genome architecture

2.1.1 Chromosome territories

Chromosome territories (CTs), as distinct entities in the interphase nucleus of higher eukaryotes were already observed by Theodor Boveri in 1909 (Boveri 1909). The concept of CTs was experimentally proofed beginning with the with the microbeam experiments of (Cremer et al. 1982). Recently the multi color FISH experiments of (Bolzer et al. 2005) allowed to visualize all human 46 chromosome territories in a single cell nucleus.

The radial arrangement of CTs in the nucleus is nonrandom (Cremer et al. 2006; Meaburn and Misteli 2007, for recent review). In general CTs showed a gene density driven positioning in spherical nuclei but a chromosome size driven positioning in ellipsoid nuclei (Bolzer et al. 2005). These findings were also confirmed in nuclei of mouse (Mayer et al. 2005), chicken (Habermann et al. 2001) and a wide range of primates (Neusser et al. 2007). In particular the radial position of human chromosomes 18 and 19 CTs difference was driven by gene density. Although being of nearly equal size the gene-rich chromosome 19 was shown to be located in the nuclear interior and the gene-poor chromosome 18 at the nuclear border in spherical lymphoblastoid cells (Croft et al. 1999). Furthermore this orientation is well conserved in primate evolution (Tanabe et al. 2002) and in cancer (Cremer et al. 2003). Remarkably in fattened ellipsoid fibroblast nuclei of species with pronounced chromosome size differences a size correlated radial position was found (Bolzer et al. 2005; Neusser et al. 2007; Sun et al. 2000). Moreover radial localization preference of CTs could result in preferential neighborhoods of CTs with similar gene content or size, respectively. However no fixed neighborhoods of entire CTs were revealed (Bolzer et al. 2005; Mayer et al. 2005; Parada et al. 2004). Notwithstanding the detected preferential spatial proximity of genomic loci resulting from this radial arrangement likely enhanced the probability of reciprocal chromosome rearrangement (Bickmore and Teague 2002; Roix et al. 2003, Neusser et al. unpublished data).

These probabilistic orientation preferences still do allow for CT position differences between cell types, differentiation and developmental stages and even among the two homologous CTs in the same nucleus. Cell type specific positioning was revealed for various CTs in humans (Croft et al. 1999) mouse (Mayer et al. 2005) and chicken (Stadler et al. 2004), e.g. during developmental differentiation of human adipocytes (Kuroda et al. 2004) and mouse T-cells (Kim et al. 2004). Cell type differences are most likely driven by pattern modifications of chromatin along the

chromosome (Meaburn and Misteli 2007). These patterns can be governed by alterations of gene activity, replication timing or epigenetic modifications and may be in addition superimposed by differences of the nuclear size and shape (for review Cremer et al. 2006; Lanctot et al. 2007).

2.1.2 Subchromosomal domains, genes and gene cluster

Although the results of CT positioning in the nucleus indicate comprehensible functional chromatin architecture the CT position differences between cell types and differentiation stages still cannot be satisfyingly explained. Therefore recent research on chromatin architecture focused on subchromosomal structures and in particular on cluster of genes and single genes during defined developmental and cell type states (Kumaran and Spector 2008; Lanctot et al. 2007).

Distinct chromosome arm and band domains build up CTs (Dietzel et al. 1998; Lemke et al. 2002) and exhibit an internal polarity with gene-poor (Kupper et al. 2007; Murmann et al. 2005; Nogami et al. 2000) and late replicating chromatin (Grasser et al. 2008; Visser et al. 1998) facing the nuclear border whilst gene-dense or early-replicating chromatin localized in the nuclear interior. Further the radial probabilistic polarity of CTs is influenced by the cell type (Kupper et al. 2007) and by geometrical constraints within a chromosome territory (Grasser et al. 2008). By conclusion, gene density over mbp size regions is at present considered the best prediction parameter for nuclear chromatin localization. While the predictive quality of replication timing (Grasser et al. 2008) and gene activity (Kupper et al. 2007; Murmann et al. 2005) may be inferior.

Nevertheless, upon gene activity changes numerous case studies documented relocalization of genes and gene clusters referencing different nuclear landmarks. For example, IgH in committed B lymphocytes (Kosak et al. 2002), c-maf in T cells (Hewitt et al. 2004), Mash1 in neuronal cells (Williams et al. 2006) and Cftr in adenocarcinoma cells (Zink et al. 2004) relocalized to the nuclear center upon gene expression activation. Next, the beta-Globin locus was first transcriptionally activated and then moved to the nuclear interior, suggesting that gene expression is the cause and not the effect of relocalization (Ragoczy et al. 2006).

On the other side transcriptional activation did not necessarily lead to locus translocation. For instance, the interferon-gamma locus was constantly located in the nuclear periphery irrespectively of its transcriptional status (Hewitt et al. 2004). Furthermore active gene expression of a transgenic product was maintained in the nuclear periphery (Kumaran and Spector 2008; Mahy et al. 2002a). Moreover, not only the afore mentioned Mash1 locus was drawn to the nuclear center but also the neighboring genes up to 2mbp distance, regardless of their activity status.

Actively expressed genes were also found inside of CTs (Verschure et al. 1999). Contradictory genes, from the mouse Hox d cluster upon gene activation were shown

to loop away from the CT in one tissue or to remain stably associated with the CT in the other tissue (Morey et al. 2007). Further, some genes were found to loop out from their harboring CT upon transcriptional activation (reviewed in Fraser and Bickmore 2007). Osborne et al. 2004 found genes looping out from the interphase chromosome in mouse erythroid progenitor cells to reach transcription factories. In addition, genes from different genomic loci can occasionally share the same transcriptional factory and thereby come into close proximity at so-called expression hubs (Osborne et al. 2007).

Taken together gene density and gene expression determine the position of single genes regarding nuclear landmarks. However the scenario is far less clear than for CT positioning in the nucleus. Various case studies for both, a conservative or an adaptive nuclear architecture upon expressional activation exist and the decision criteria are still not well understood.

2.1.3 Chromatin folding and interaction between genomic loci

How the densely packed metaphase chromosomes are transformed into interphase CTs is still elusive (see Nemeth and Langst 2004 for review). CTs, initially believed to be rather impermeable structures (Kurz et al. 1996), likely have a sponge like structure with channels extending throughout (Albiez et al. 2006). This model gained further acceptance since gene expression was detected also in the interior of CTs (Mahy et al. 2002a; Mahy et al. 2002b; Verschure et al. 1999). However, still very little is known about the chromatin folding states of CTs that separate the genome into functional domains. While, the primary DNA structure, made up by the DNA phosphodiester backbone and the nucleosome are well understood (resolution at 1.9 angstrom, Schalch et al. 2005), already the structure of the so-called 30nm fiber, made up of nucleosome interactions, is under debate (solenoid model vs. zig-zag-model), and even less is known about the higher-order chromatin folding (Tremethick 2007 for review). The higher-order chromatin structure in the interphase nucleus, observed in early electron microscopic studies by Okada and Comings 1979 was rosette shaped and Belmont and Bruce 1994 measured chromatin fibers of different thickness, from 10-30nm up to 100-130nm in the interphase nucleus without defining the precise structure. Further, the random-walk-giant-loop-model from Sachs et al. 1995 and Yokota et al. 1995 proposed that the higher-order chromatin is organized into loops of about 5 mbp and that these loops are connected via flexible chromatin linkers of about 200 kbp, the so-called chromatin backbone. The giant-loop-random-walk-model was postulated from interphase distance measurements between genomic loci about 4mbp apart. Contradictory, other measurements between genomic loci, suggested a multiloop-subcompartment-model (Knoch 2002; Münkler and Langowski 1998), emanating from the 30nm fiber that is folded into rosette-like small loops that are connected by chromatin linkers of variable size. Further, in favor

of rosette formation it was shown that the maintenance of CTs requires chromatin backfolding (Cremer et al. 2000; Munkel et al. 1999). In conclusion, the state of knowledge is that the various degrees of chromatin in the interphase nucleus show hierarchical states of twisting, looping, back folding and condensation, without the disclosure of the exact structures.

Nonetheless it was demonstrated that genome-wide, gene-dense regions are in general more decondensed than gene-poor regions and further that the impact of gene expression on the degree of condensation was considered as minor (Gilbert et al. 2004). Moreover a gene rich, orthologous DNA segment of mouse and human displayed extended chromatin structure conserved in both species (Mahy et al. 2002a). In general the distribution of RIDGEs (regions of high gene expression) and anti-RIDGEs correlated very well with gene density (Caron et al. 2001; Goetze et al. 2007) making a genome wide separation of gene density and expression difficult. The size of RIDGEs fitted with the conserved 20mbp blocks of synteny between mouse and human, which argues for an evolutionary conserved nuclear organization to group the genome into co-expressed, similarly condensed chromatin segments (Kosak and Groudine 2004b). Further condensed chromatin distribution was found to be similar in differentiated cells of the same lineage, but the pattern varied among nuclei of different cell types (Leitch 2000). Therefore the chromatin state may reflect not only the gene density but also the differential state of the cell and may be involved in the establishment and propagation of the tissue specific pattern of gene expression (Francastel et al. 2000).

The transcription status is likely mediated by insulator elements that can link chromatin to the lamina and to nuclear pores (Nemeth and Langst 2004) or help to regulate gene expression by forming specific chromatin interactions (Gaszner and Felsenfeld 2006 for review). Beside also specific enhancer promotor interactions require locus specific chromatin folding (Gaszner and Felsenfeld 2006). Such transient long-range interactions of chromatin can be captured by the chromatin-conformation-capture technique (de Laat and Grosveld 2007; Dekker 2008; Gondor et al. 2008). Prominent examples for long-range chromatin loops towards specific nuclear sites are the over 1000 olfactory receptor genes that interact with one enhancer element resulting in the coordinated expression of only one olfactory receptor gene per neuron (Lomvardas et al. 2006), the colocalization of active genes to so-called transcription factories (Osborne et al. 2004) and the co-localisation of locus regulatory elements and alternatively expressed genes from the T-helper cell pathway to form a functional expression unit (Spilianakis et al. 2005). Most recent, the mono- or diallelic colocalisation upon estradiol stimulation of TF1 and GREB1 in 90% of analyzed nuclei within only 5min was revealed (Nunez et al. 2008). It was also noticed that chromatin could move over long distances, likely directed by the actin-myosin machinery (Chuang et al. 2006; Dundr et al. 2007). In contrast,

movement of the bulk chromatin loci in living cells is restricted to the maximum of only 0.5 μ m (0.1% of the nuclear volume) (Chubb and Bickmore 2003) for review) and movements were mainly limited to the G1 phase (Walter et al. 2003).

In a nutshell, the exact organization of higher order chromatin structures is not clear and it is general assumed that gene-rich chromatin (and RIDGEs) lead to a decondensed chromatin structure. Although most chromatin is packed and positioned rather stably in the interphase nucleus of higher eukaryotes, dynamically changing long-range and site-specific higher structures encompassing large-scale decondensation can be formed in response to gene activity. The decision factors for an adaptive chromatin folding and interactions are also largely unknown.

2.1.4 Current models of a functional nuclear architecture

The nucleus is composed of highly compartmentalized chromatin domains (Misteli 2005, 2.1.1-2.1.3). The structure of CTs and chromosome substructures down to the single gene level is largely stable and predominantly determined by local gene density. However, structures are prone to be modified in adaptation to cellular processes, mainly upon gene activation (Cremer et al. 2006, 2.1.1-2.1.3).

The important aspects of a functional nuclear architecture assuming the IC-CT model are summarized in figure 2.1 (from Cremer et al. 2001). CTs are complex folded and have a sponge like structure that is pervaded by channels and lacunas. Occasionally transcriptionally active chromatin loops protrude from CTs (figure 2.1 a). Furthermore distinct subchromosomal domains with actively transcribed genomic loci are positioned away from heterochromatin and inactive loci (black) are in contact to heterochromatin (figure 2.1 b). In CTs hierarchical chromatin folding is present, with the decondensed perichromatin region (yellow) next to the IC and the most condensed chromatin to the CT interior (figure 2.1 c). Moreover, CTs show a polar organization with early replicating chromatin (green) and mid replication chromatin (red) at the nuclear lamina (light yellow) (figure 2.1 d). Active genomic loci (white) locate to the surface of chromatin domains, while inactive inactive loci (black) locate to the inside. Hence, active loci gain direct contact to the nuclear protein machinery (orange) (figure 2.1 e). This nuclear protein machinery is organized into distinct patterns (orange) within the IC compartment (green). The chromatin is hierarchically folded with active genomic gene rich loci (white) in decondensed chromatin state and inactive, gene poor loci with a compact chromatin structure (figure 2.1 f).

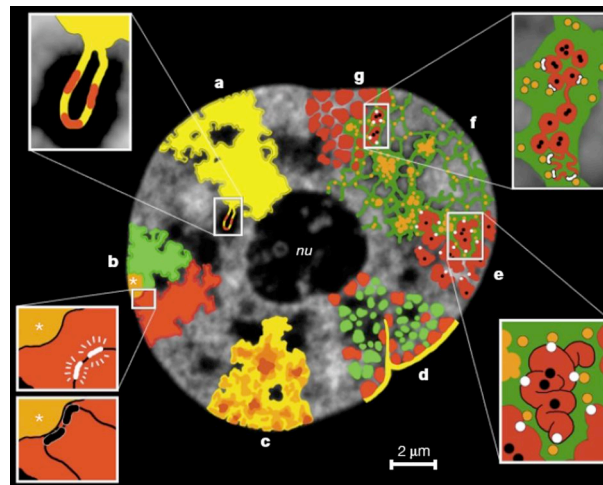


Figure 2.1: Current model of the functional nuclear architecture from Cremer et al. 2001) (see main text for details).

Nevertheless, it is still controversially discussed how the chromatin free space in the nucleus, the IC is organized in detail (figure 2.1 f) (see (Albiez et al. 2006). Although proteins, involved in transcription, replication, the cell cycle and chromatin maintenance are organized in sophisticated patterns to compartmentalize the nuclear processes into spatial domains (e.g. SC35 speckels, cajal-bodies, nucleoli, PML bodies or Rad 51 foci) (Lamond and Spector 2003) (figure 2.1) the assembly of these domains and how the evacuation of RNA to the nuclear pores is assured is still matter of debate. Whereas (Albiez et al. 2006) favored the interchromation compartment (IC) model, a network of channels and lacunas throughout the entire nucleus and into CTs and comprising the domains for nuclear processes and all protein and RNA transport, (Branco and Pombo 2006) proposed an extensive intermingling of chromatin domains resulting in a overall CT overlap of about 20%. Further this intermingling was believed to be necessary to explain the frequency of interchromosomal rearrangements.

2.2 Histone modifications

2.2.1 Histone code

Chromatin comprises the histone octamers and DNA that is wrapped around in 1.65 coils (146bps). Histones are evolutionarily deeply conserved basic proteins with a high affinity to the acidic DNA (DeLange et al. 1969). The N-terminal tails of histones can be covalently modified at distinct amino acid positions (figure 2.2, Schones and Zhao 2008; Verdone et al. 2005). These modifications then orchestrate accessory protein binding, influence the chromatin condensation (e.g. histone acetylation decondenses the chromatin) and affect in a combinatorial way the gene expression (Schones and Zhao 2008). In this worked we focused on histone 3 trimethylation on

lysine 4, 9, and 27 residues in several targeted genomic regions that are predominantly characteristic for the main chromatin states – euchromatin, facultative heterochromatin and constitutive heterochromatin, respectively. Antibodies to these histone modifications are most useful to annotate sequences because H3 methylation patterns are rather stably maintained (Jenuwein 2006) and evolutionarily strongly conserved at human and mouse orthologous loci, irrespectively of the sequence conservation (Bernstein et al. 2006b). Noteworthy the epigenetic state is a complex interplay of over 50 known histone modifications, DNA methylation (at CpGs), nucleosome positioning and other factors. Therefore the described methylation pattern predominantly but not exclusively characterizes a specific chromatin state (Figure 2.2 B, Peters et al. 2003).

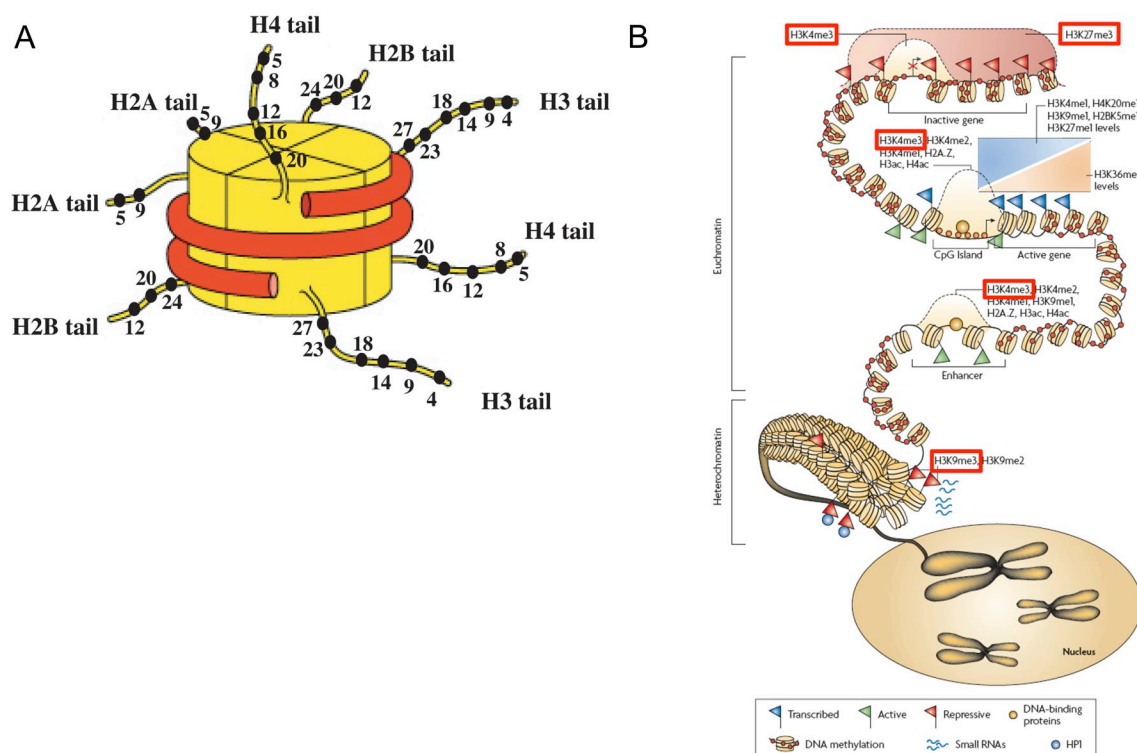


Figure 2.2: (A) Histone octamer (yellow) wrapped by 1.65 coils of DNA (red). N-terminal tails of histones stick out and are free to covalent chemical modifications. This work focuses on the trimethylation of histone 3 lysine residues at amino acid positions 4, 9 and 27. (Verdone et al. 2005) (B) Chromosomes are divided into decondensed euchromatic and condensed heterochromatic regions. H3K4me3 is highly enriched in transcription start sites of active genes. H3K27me3 is mainly present in broad domains that encompass inactive genes, the facultative heterochromatin. H3K9me is characteristic for constitutive heterochromatic regions and serves as platform for HP1 binding (H3Kme3 modifications boxed in red) (Schones and Zhao 2008).

2.2.2 Histone 3 lysine 4 methylation

H3K4me3 is a marker for euchromatin (Henikoff et al. 2004) that is transcriptionally active and harbors mostly ubiquitously expressed house keeping genes. Further H3K4me3 corresponds with DNase sensitive sites, high transcriptional levels, histone

acetylation, is highly enriched in promoter regions and extends significantly into transcribed regions (Barski et al. 2007; Liu et al. 2005; Pokholok et al. 2005). These findings were confirmed in drosophila, mouse and humans (Bernstein et al. 2005; Kim et al. 2005; Roh et al. 2006; Schubeler et al. 2004). Contradictory high levels of H3K4me3 were also detected in silent promoter regions maybe to keep chromatin in a poised state for gene activation (Martens et al. 2005; Roh et al. 2006; Squazzo et al. 2006).

2.2.3 Histone 3 lysine 9 methylation

H3K9me3 marks constitutive heterochromatin (Peters et al. 2003), which includes almost no genes and is mainly found in pericentromeric regions. Moreover H3K9me3 serves as loading platform for heterochromatic proteins, correlates with H4K20me3, is enriched near the boundaries of large heterochromatin blocks (Barski et al. 2007) and contributes to the formation and transcriptional repression (Martens et al. 2005). Contradictorily the H3K9me3 pattern was also found in 3'ends of active and inactive zinc finger genes, but the function there is still speculative (Barski et al. 2007).

2.2.4 Histone 3 lysine 27 methylation

Histone 3 lysine 27 trimethylation marks facultative heterochromatin (Peters et al. 2003) that is in contrary of constitutive heterochromatin, in a reversible condensed chromatin state and keeps tissue specific genes inactive. For instance H3K27me3 inversely correlates with gene activation and the distribution pattern in nuclei is broader than for H3K4me3 (Boyer et al. 2006; Roh et al. 2006; Squazzo et al. 2006). Although in general there is nearly no overlap between H3K27me3 and H3K4me3 patterns (Zinner et al. 2006) both modifications can coexist at promoter and regulatory elements to decide about gene expression levels (Roh et al. 2006). Their interplay likely takes a crucial role during ES cells differentiation (Bernstein et al. 2006a).

2.3 Chromosomal genome organization in mouse and chicken

2.3.1 Mouse genome

The mouse genome consists of 3421mbp DNA, 37.5% derived from transposable elements, 5% derived from interspersed repeats (Mouse sequencing consortium 2002) and to date, 22,010 protein-coding genes (about 1% of the genome) were identified (NCBI m37, april 2007). Nearly the entire genome is covered by BAC clones, which can be obtained from public resource centers (bacbac.chori.org). The mouse karyotype displays 19 acrocentric chromosome pairs plus the sex chromosomes x and y. Mouse chromosomes vary in size between 197mbp and

61mbp. Compared to humans the mouse karyotype is highly rearranged showing 96 homologous segments (Graphodatsky et al. 2008). The last common ancestor of mouse and human lived 91 ± 2 million years ago (Hedges 2002). We investigated the nuclear position of mouse chromosomes 5 (156mbp, 8.8genes/mbp), 11 (122mbp, 14.0genes/mbp) and 14 (125mbp, 6.5genes/mbp) by chromosome painting.

2.3.2 Chicken genome

With 1051mbp the chicken genome has, roughly 40% the genome size of mammals. In contrast to 40-50% in mammalian species, only 15% of the chicken genome is represented by repetitive sequences (Burt et al. 1999). Only 4,782 protein-coding genes were identified so far (WASHU2, may 2006). However, the chicken consortium suggested 20,000-23,000 genes (Consortium 2004). Chicken was the first sequenced non-mammalian genome and BAC clones covering most parts can be obtained from a resource center (bacbac.chori.org). The avian and mammalian evolutionary lineages separated about 310 million years ago (Hedges 2002). The average conserved homologous segment length between chicken and human is about 30-40cM (Consortium 2004) but the exact number of rearrangements separating chicken and human chromosomes is yet unknown. Although the total number is believed to be lower or equal to mouse and human (Consortium 2004). This estimation is supported by a high similarity of the chicken karyotype to the proposed ancestral vertebrate karyotype (Kohn et al. 2006) (Nakatani et al. 2007) and an accelerated rate of chromosomal rearrangement in the mammalian lineage (Burt et al. 1999). The chicken karyotype displays 9 pairs of macrochromosomes and 30 pairs of microchromosomes (Griffin et al. 2007). Macrochromosomes tend to be gene-poor and AT rich compared to the gene dense and GC rich microchromosomes (Schmid et al. 2005). The chromosomes range in size from 201mbp to less than 1mbp. We defined the nuclear localization of the metacentric chicken macrochromosomes 1 (201mbp, 3.4genes/mbp), 3 (114mbp, 3.2genes/mbp) and 4 (94mbp, 3.8genes/mbp).

2.4 Evolutionary DNA sequence conservation in vertebrates

2.4.1 Coding sequences

Only 1-2% of vertebrate genomes are protein coding and the majority thereof are evolutionarily conserved (Nei and Kumar 2000). In detail 18,968 from 21,541 human genes (NCBI 36, may 2005) have orthologs in 11 sequenced vertebrates, including mouse and chicken (Matsuya et al. 2008). Furthermore protein coding exons show 90% alignment in human-mouse-rat and still around 72% alignment between human and chicken (Consortium 2004). Recently it was revealed that not only the sequence

of genes but also their expression level and tissue specificity is remarkable conserved in mammals (Liao and Zhang 2006).

2.4.2 Ultraconserved noncoding sequence (UCS) cluster

Comparative vertebrate genome sequence analysis revealed that around 3-8% of the vertebrate genome is under purifying selective constraints. It is widely accepted that evolutionary conservation provides indirect evidence for functional importance (reviewed in Siepel et al. 2005). Besides protein coding or RNA coding sequences, hundreds of ultraconserved non-coding sequences (UCS), presenting the tip of sequence conservation in vertebrates were detected. UCS were identified by whole genome alignments using different sets of vertebrate or even metazoan species, various search algorithms, sequence identity thresholds and length limits (Bejerano et al. 2005; Dermitzakis et al. 2002; Sandelin et al. 2004; Siepel et al. 2005; Woolfe et al. 2005). The genome browser Ancora (Engstrom et al. 2008) offers UCS location and UCS density blots over different genomes.

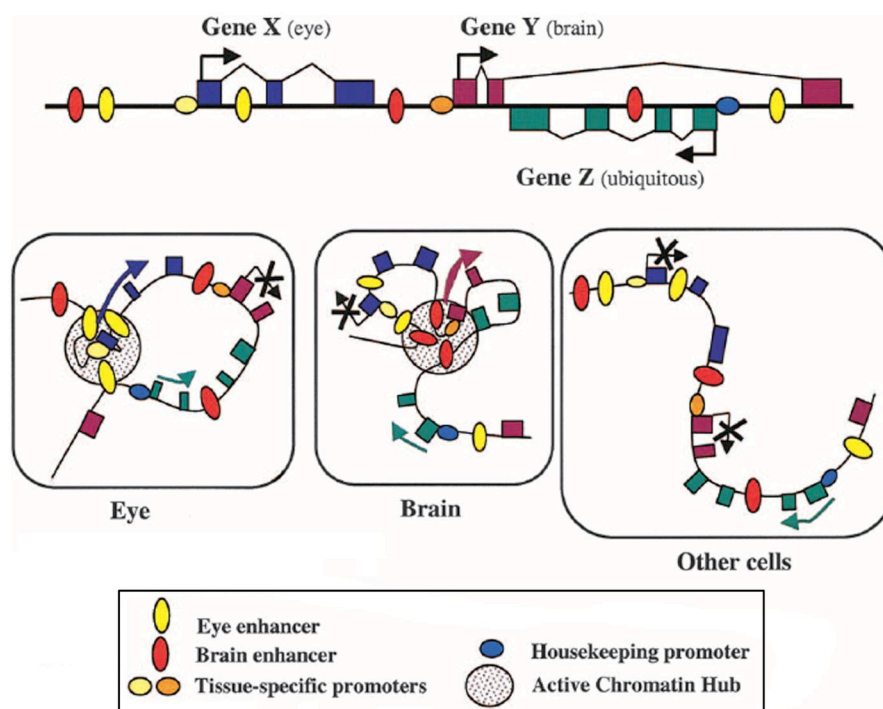


Figure 2.3: Hypothetical cis regulatory module with tissue-specific expression of genes. UCS function as cis elements. They tune gene expression, alternative splicing and chromatin compaction. This requires transient chromatin interactions and foldings and therefore the chromatin structure of the locus is determined by a combination of cis activities that control the chromatin structure. Specific chromatin interactions are transiently established or prevented (taken from Kleinjan and van Heyningen 2005).

The vast majority of UCS was identified in proximity to trans-dev genes (mostly transcription factors) that play key roles during vertebrate embryogenesis. UCS can reside intronic, 5' and 3' to genes and thereby form clusters of UCS spanning genomic regions of few mbps. Although the function of most UCS is still

uncharacterized the applied sequence annotation algorithms predicted that most UCS are cis regulatory elements (McEwen et al. 2006; Pennacchio et al. 2007). Hence, UCS may act as enhancers or silencer elements to coordinate the spatio-temporal transcription factor expression and/or alternative splicing. This functionally implies discrete binding of transcription factors and transient long-range chromatin interactions between UCS and the promoter regions of trans-dev genes. Further UCS can serve as boundary elements to separate differentially compacted chromatin regions (Gaszner and Felsenfeld 2006). Therefore clustered UCS form cis regulatory modules (Arnone and Davidson 1997) and might determine the chromatin structure of trans-dev gene loci (figure 2.3). Interestingly the cis regulatory modules align with vertebrate conserved synteny blocks, suggesting selection against chromosomal rearrangements in these regions (Kikuta et al. 2007). Indeed chromosomal rearrangements and mutations causing human disease were detected in genomic regions harboring UCS clusters (reviewed in Kleinjan and van Heyningen 2005), highlighting the functional importance of UCS. Moreover the ability of selected UCS to drive spatio-temporal reporter gene expression was shown in vivo in mouse embryos (Nobrega et al. 2003; Pennacchio et al. 2006), frog embryos (de la Calle-Mustienes et al. 2005) and fish embryos (de la Calle-Mustienes et al. 2005; Kimura-Yoshida et al. 2004; Woolfe et al. 2005). Notably, the detected reporter gene expression spatio-temporally overlapped in part with the in vivo expression patterns of the close-by trans-dev gene in all cases. On the other hand knock-out mice lacking single UCS were fertile and healthy with no altered phenotype (Ahituv et al. 2007). This indicates that UCS cluster function combinatorially as cis regulatory modules (figure 2.3) and that single UCS might be dispensable.

2.4.3 The Dach1 gene locus and flanking UCS cluster

The DACH1 gene is located on human chromosome 13 (70,910,099-71,339,331bp), with orthologs on mouse chromosome 14 (98,186,066-98,568,762bp) and chicken chromosome 1 (160,767,258-161,137,822bp). Human DACH1 is encoded by 12 exons and displays alternative splicing variants (Ayres et al. 2001). Dach1 lies centrally in a gene desert ranging from 2.94 mbp in mouse, 2.60 mbp in human to 1.52 mbp in chicken (NCBI). The nearest gene annotations are KLHL1 and LOC440145 in human or the corresponding orthologs in other vertebrates. Both in the 5' and 3' flanking gene deserts prominent clusters of UCS were identified (Sandelin et al. 2004; Woolfe et al. 2005, figure 2.4).

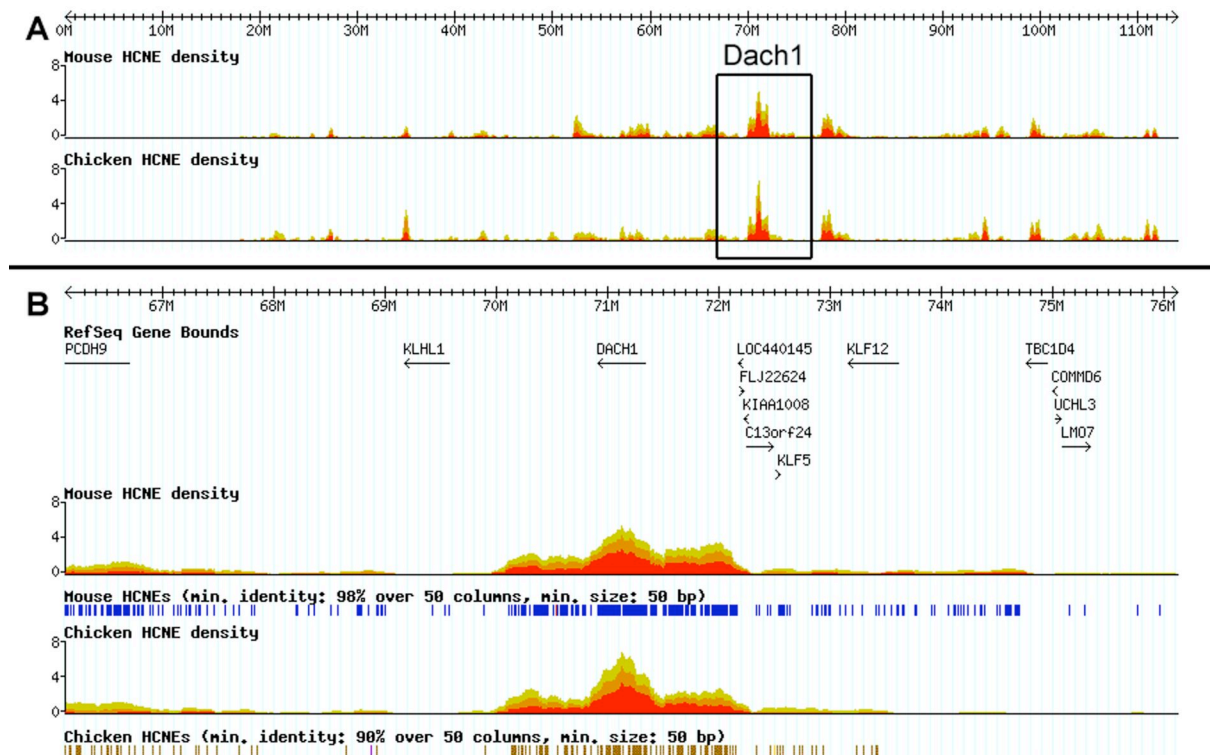


Figure 2.4: UCS density maps from the ANCOR genome browser (Engstrom et al. 2008) in mouse and chicken referred to the human genome. (A) UCS density map along human chromosome 13. Note the prominent clustering of UCS around Dach1. (B) Magnified view of the Dach1 region. The greater Dach1 region locates to human-mouse-chicken synteny block. UCS reside exclusively in the gene desert around Dach1.

Furthermore, UCS that were selected from the Dach1 region, are capable to drive tissue-specific gene expression in vivo of a reporter gene in transgenic mouse embryos (5 out of 7 tested UCS) (Nobrega et al. 2003). Thus Dach1 is presently the best-characterized cis regulatory UCS module.

The in vivo expression pattern of Dach1 in mouse, chicken and fly is well characterized (Caubit et al. 1999; Davis et al. 1999; Kida et al. 2004; Mardon et al. 1994, data herein). The gene expression level and the tissue specificity (limb, genital, nervous system, eye) are evolutionarily conserved (Davis et al. 2008), arguing for a conserved function of Dach1 in evolution. Dach1 encodes a putative transcriptional cofactor that was initially identified in drosophila (Davis et al. 2008). Drosophila dachshund mutants display abnormal development of retina, limbs, genital and brain (neural cell differentiation) (Mardon et al. 1994; Martini et al. 2000; Miguel-Aliaga et al. 2004; Shen and Mardon 1997). In vertebrates two paralogs Dach1 and Dach2 have been identified (Davis et al. 2008 and refs therein). Surprisingly, neither Dach1 (Backman et al. 2003; Davis et al. 2001) nor Dach2 (Davis et al. 2006) knock out mice showed abnormalities in retina, limbs, genital or brain development. Dach1 knock out mice die postnatal within 24h for unknown reasons, whereas Dach2 knock out mice are healthy and fertile (Davis et al. 2008). In summary these observations

point to redundant developmental pathways in vertebrates and clearly shows that only Dach1 is essential for life.

2.4.4 The Bcl11a gene locus and its genomic neighborhood

The Bcl11a (CTIP-1, Evi-9) gene locus resides on human chromosome 2 (60,531,806-60,634,137bp), mouse chromosome 11 (23,978,117-24,074,123bp) and chicken chromosome 3 (1,823,953-1,883,382bp). Human BCL11A is encoded by 5 exons that are transcribed in four alternative isoforms (Liu et al. 2006). Bcl11a marks the border between gene-dense chromatin to the one side and a gene desert to the other side. In the flanking gene-dense region the oncogene rel and the house keeping genes Paplog (poly-A polymerase gamma) and Xpo1 (exportin1) are located. In the gene desert comprising 2.21 mbp in human, 1.44 mbp in mouse and 0.9 mbp in chicken no genes were annotated between BCL11A and FANCL and the respective vertebrate orthologs (human, NCBI 36). Instead, evolutionary footprint studies uncovered densely clustered UCS in the gene desert (Sandelin et al. 2004; Woolfe et al. 2005, figure 2.5).

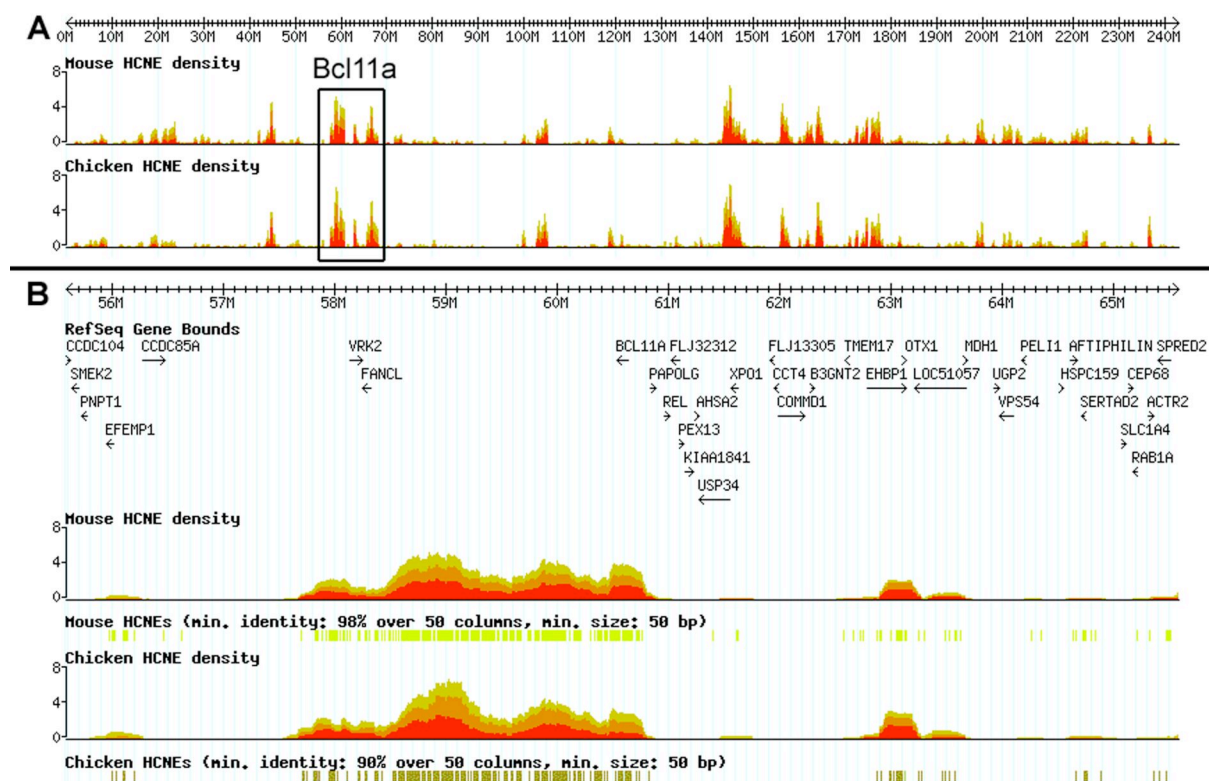


Figure 2.5: UCS (= HCNE, highly conserved non-coding element) density maps from the ANCOR genome browser (Engstrom et al. 2008) in mouse and chicken referred to the human genome. (A) On human chromosome 2 UCS clusters are prominent around Bcl11a. (B) Zoom into the Bcl11a region. The greater Bcl11a region locates to human-mouse-chicken synteny block. UCS reside in the non-genic region to one side of the Bcl11a gene whereas the other side is gene-rich and depleted from UCS.

Bcl11a orthologs have been identified across all vertebrate species (www.ensembl.org) and the presence of paralogous genes Bcl11a and Bcl11b suggest that the Bcl11 precursor was already present before the vertebrate whole genome duplication. Further, Bcl11a is in the category of the most conserved protein-coding genes between human and mouse (94% at sequence and 95% at protein level, (Bejerano et al. 2005). Even the transcription pattern of mouse Bcl11a is identical to that found in humans (Su et al. 2002). High transcription levels were detected in lymphoid tissue, plasmacytoid dendritic cells and in both fetal and adult brain (Satterwhite et al. 2001; Su et al. 2002). The expression of Bcl11a in mouse embryos was identified as quite ubiquitous in the limb bud, the branchial arches and throughout the CNS from E10 to E18.5 (Leid et al. 2004). Before E12.5 the expression pattern appeared quite diffuse but from E12.5 onward it appeared mostly restricted. Bcl11a expression data from the chicken is so far not available.

BCL11A, a Krüppel-like zinc finger protein interacts with BCL6 (Nakamura et al. 2000), COUP-TF (Avram et al. 2002) and with itself (Liu et al. 2006). BCL11A can directly bind to a GC-rich promoter sequence (5'-GGCCGG-3') and thereby repress the transcription of other genes, independently of the interaction with BCL6 or COUP-TF (Avram et al. 2002). Most likely the repression by BCL11A encourages SIRT1 and is leading to Histone 3 and 4 deacetylation in the promoter regions of the repressed genes (Senawong et al. 2005). Finally, knock out mice of Bcl11a die on postnatal day one underlining its importance in postnatal development (Liu et al. 2006).

2.5 Evolutionary genomic innovation in vertebrates:

The casein gene locus

Whole genome duplication, segmental duplication and gene duplication followed by mutation and gain of new functions is one of the key mechanisms driving genomic innovation. One or two rounds of whole genome duplication are believed to have shaped the vertebrate genome (Dehal and Boore 2005; Gu et al. 2002; Van de Peer 2004). 25% of vertebrate genes present in paralogous pairs are hallmarks of these events. Further, segmental duplications (>90% sequence identity, >1kb) represent about 5% of the human genome (Eichler et al. 2001). Gene duplications most likely result in loss of function in one of two copies. Alternatively, mutations in both gene copies may create complementary functions or both copies may retain their original function. Only rarely one of the copies retains the original function while the other copy acquires a novel evolutionarily advantageous function.

A prime example of genomic innovation by duplication and gain of novel function is the exclusively mammalian casein gene cluster. Casein, the major milk protein evolves fast and it is believed that the casein gene cluster emerged from the

secretory calcium binding phosphoprotein family (SSCP). SSCP proteins are involved in calcium storage (dentin, bone, enamel, milk, salivary gland) and share common sequence features (reviewed in Kawasaki and Weiss 2006). (Kawasaki et al. 2007) proposed the evolutionary origin of SSCPs as set of duplication events. First, SPARC (= osteonectin) and SPARCL1 in vertebrates evolved from the founder SPARC during whole genome duplication. Tandem gene duplication then led to two SPARCL1 copies, which adapted complementary functions of surface tissue (enamel, milk, saliva) and body tissue (bone, dentin). Whereas SPARC and SPRACL1 are still associated in puffer fish, intrachromosomal rearrangements separated the two loci in mammals, for example by 17mbp in mouse and human. Further, parallel gene duplications and eliminations of old genes resulted in phenotypic changes. For example an eggshell matrix protein in the avian lineage and milk and saliva in the mammalian lineage are encoded by SSCPs (figure 2.6).

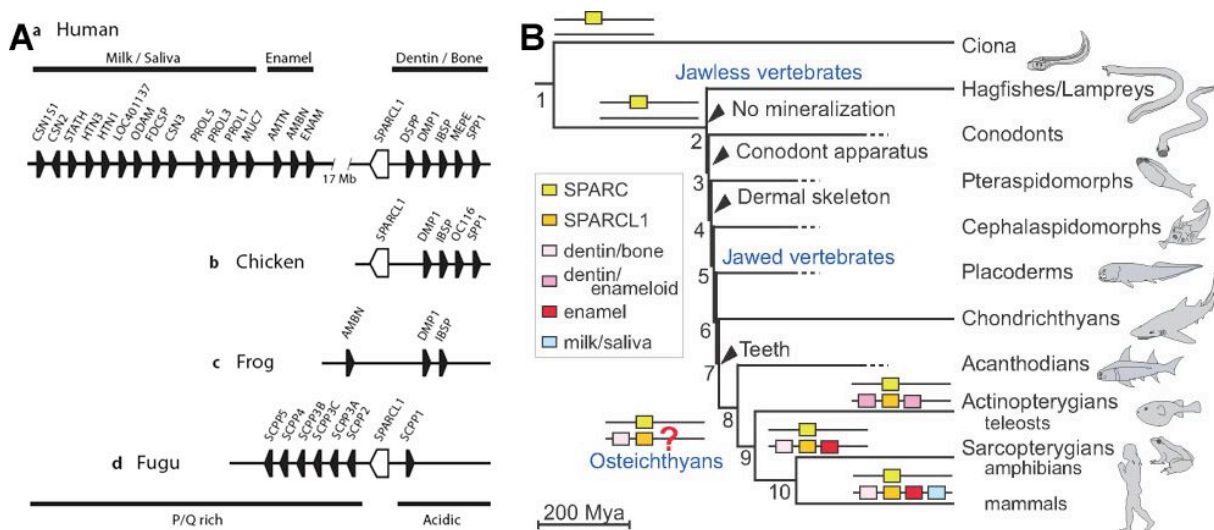


Figure 2.6: (A) Present SSCP gene cluster in vertebrates. Arrowheads indicate the genomic orientation (Kawasaki et al. 2007) (B) Several genomic innovation steps in the vertebrate lineage contributed to the formation of the mammalian casein cluster (light blue) (Kawasaki and Weiss 2006).

The mammalian Casein gene cluster comprises genes for enamel, saliva and milk. Mammalian milk proteins are acidic and proline-rich phosphoproteins encoded by 3-4 genes (calcium-sensitive casein) and one physically linked gene (kappa-casein) with functional association spanning a gene cluster of 250-350kb (Rijnkels et al. 2003, figure 2.7). Whereas in human four genes, CSN1S1, CSN2, CSN1S2A and CSN3 exist, in mouse five genes, Csn1s1, Csn2, Csn1s2a, Csn1s2b and Csn3 are present. The Csn gene cluster is gene-rich but displays a low GC content (34.5% in mouse). Moreover, caseins differ extensively at the coding sequence level (67% identity between mouse and human), with no conservation difference between exons and introns but the organisation and orientation in the gene cluster is highly conserved among mammals (Rijnkels 2002). The high degree of evolutionarily sequence

differences reflects an adaptation to the nutrition needs of the newborns in each species. Furthermore caseins genes are expressed in a developmental-stage and tissue specific manner (Rijnkels et al. 2003, data herein).

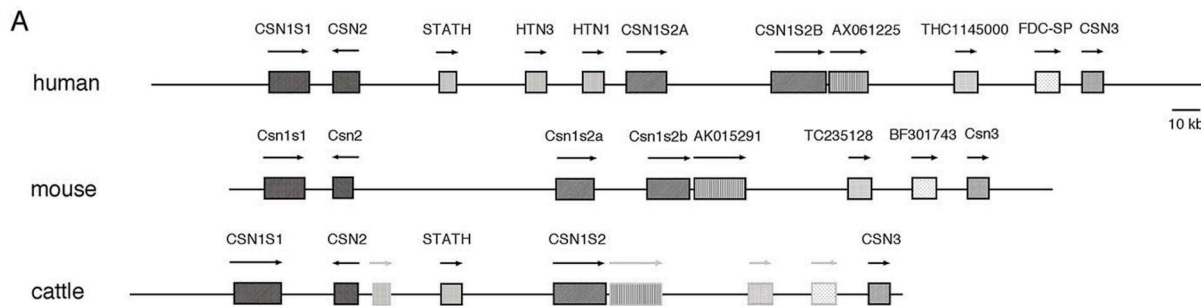


Figure 2.7: Comparative map of the mammalian Casein gene cluster in human, mouse, rat and cattle. Although the sequence shows only little and exon-intron indistinguishable sequence conservation the relative position and orientation of caseins is highly conserved (Kawasaki and Weiss 2006).

2.6 Embryonic development of mouse and chicken

2.6.1 Primitive streak stage

The early development of mouse and chicken differs strongly. Mice are viviparous, and the homeothermic conditions inside the female mouse guarantee a constant development and the birth of 8-20 newborns after 21d. In contrast chicken embryogenesis occurs in ovo. After egg laying the chicken embryo arrests its development until breeding and the chick hatches after 21d. However chicken embryos show stage variation after the same time of incubation of about 1 day (Hamburger and Hamilton 1992) because the exact developmental stage is influenced by temperature, freshness of the eggs and different breeds.

Mouse E7.0 and chicken E21h are at the primitive streak stage that is formed during early vertebrate development as one of the first signs of gastrulation, still ahead to head formation and the first somite. Cells from the germ lines ectoderm, mesoderm and entoderm are separated at this stage. In more detail the chicken primitive streak already reached its maximal length (about 1.88mm, after 18-19h) after 21h but the embryo is before formation of the head fold (Hamburger and Hamilton 1992). Mouse E7.0 is at the early mid-primitive streak stage. Here the intraembryonic mesoderm firstly appears and extra-embryonic ectoderm and subjacent mesoderm cells proliferate to form the posterior amniotic fold (Kaufmann 1992).

2.6.2 Organogenesis

Organogenesis is very similar between mouse and chicken (figure 2.10). Skin, pigment cells and neurons emerge from the ectoderm, muscle cells, red blood cells, kidney tubule cells and mesenchymal cells develop from the mesoderm and lung aveolar cells, thyroid cells and pancreatic cells differentiate from the endoderm.

Mouse E13.0 (Theiler stage 21) and chicken E5.5 (HH stage 28) are analogous developmental stages (figure 2.8). The digits differentiate from the limb bud and the neurons grow from the brain ventricles outward. Mouse E13.0 is characterized by 52-55 pairs of somites. The hump in mouse head of E11.5 to 12.5 has disappeared. Instead the pinna and first details of the vibrissae are visible. Webbing is clearly seen in digital interzones and slightly more pronounced in the forelimb. The major parts of the brain, in particular the lateral ventricles, neopallial cortex expands and the pituitary gland differentiates develop further (Kaufmann 1992). Chicken E5.5 is characterized by the first incidence of the beak and the visceral arch morphology. Five digits and 4 toes are distinct with the second digit and the third toe longer than the others resulting in a pointed structure of the toe-plate. As in mouse E13.0 the brain extensively differentiates and expands (Hamburger and Hamilton 1992).

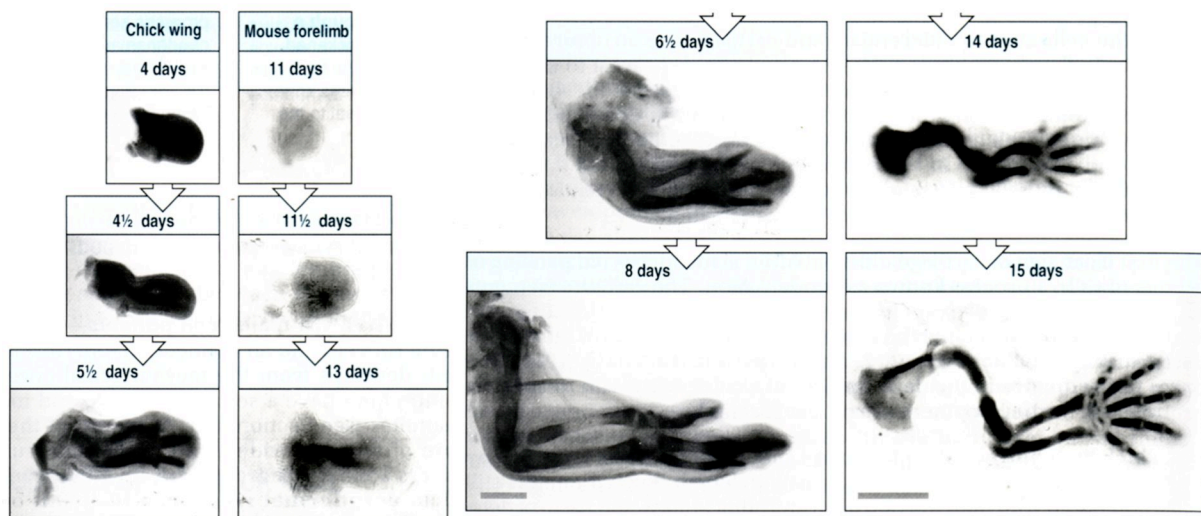


Figure 2.8: Analogous developmental stages of the chicken wing and the mouse forelimb (modified from Lewis Wolpert – Principles of Development). (Scale bar 1mm)

2.7 Skin appendages

2.7.1 Evolution of skin appendages

In this work we further concentrated on the comparison of epithelial cells from mammalian hair, mammary gland and avian feather. Mammary gland, hair and feather develop from skin via an ectodermal placode followed by formation of a bud, resulting in specific organogenesis (Pispa and Thesleff 2003; Mikkola 2007, figure 2.9). Hair and feathers furthermore share the same follicular structure (Yue et al. 2005). In all-three skin appendages epithelial stem cells give rise to a proliferative trait (Pispa and Thesleff 2003). Further ablation of epithelial Shh signalling, resulting in unexpected transformation of hair follicles to a strikingly mammary gland fate underlines the link between hair follicle and mammary gland development (Gritti-Linde et al. 2007).

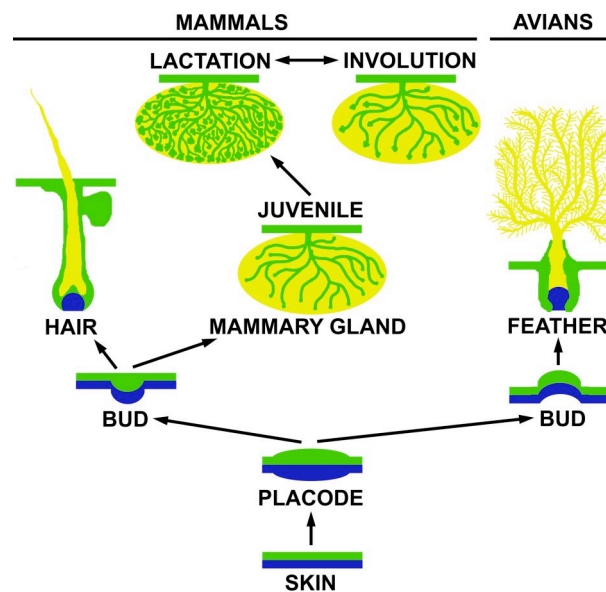


Figure 2.9: Development of hair, mammary gland and feather from skin. Epithelial cells are shown in green and mesodermal cells in blue. The developmental onset via a thickened placode a bud precursor is shared. Mammary gland predominantly develops postnatally from the juvenile to the lactating state and cyclical with each pregnancy from lactating state back to the involuted state. Epithelial cells line the lactal ducts and alveoli in mammary gland and lie in the outer root seath of hair and feather.

2.7.2 Postnatal mammary gland

The mammary gland is an organ innovation of the mammalian lineage and this organ is eponymous to this vertebrate class. Mammary gland derives from an ancestral apocrine-like gland that was associated with hair follicle (Oftedal 2002b). In monotremes the mammary gland is still associated with a hair patch instead of forming a nipple and during early development of marsupials vestigial mammary hair is found (Oftedal 2002a). Contrasting other organs the mammary gland predominantly develops postnatal (Brisken and Rajaram 2006; Hennighausen and Robinson 2005 for review): With each pregnancy an expanded lobulo-alveolar compartment rises on the simple tree-like ductal compartment (Alveogenesis) of the mammary gland. Further, a series of differentiation and proliferation processes during Lactogenesis convert mammary epithelial cells of the ductal compartment from a nonsecretory state to a secretory state. Then, after weaning of the pups the entire alveolar compartment undergoes apoptosis and is remodelled to return to a virgin-like state (Involution) (Hennighausen 1997, figure 2.10).

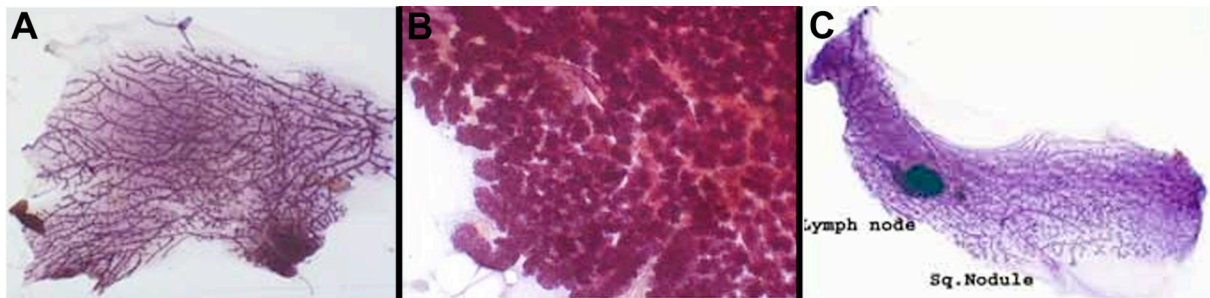


Figure 2.10: Hematoxylin and eosin staining of postnatal mammary gland developmental stages. (A) Simple tree-like structure of milk ducts embedded in the fat pad in a juvenile mouse before first pregnancy. (B) Lactating mammary gland. Nearly the entire fat is replaced by an expanded lobulo-alveolar system. (C) Involved mammary gland after pregnancy (ccm.ucdavis.edu).

Lactation correlates with an over 100% increase of RNA expression (Mustafa), mainly caused of the expression of Casein genes. Casein stores Calcium and by that assures a fast growth of calcified tissue like teeth and bone in the newborns (Kawasaki and Weiss 2006).

2.7.3 Mammalian hair and avian feather follicles

Hair, as the mammary gland, is only present in the mammalian lineage, however hair evolutionarily appeared earlier (Ofteidal 2002b) because hair but not mammary gland is found fully developed in marsupials. Hair displays a complex organ architecture comprising distinct compartments (figure 2.11): The dermal papilla plays an important role for the developmental and differentiation signaling, the basal hair matrix gives rise to all epithelial cells except in the outer root sheath, and the inner root sheath (IRS) separates the outer root sheath (ORS) from the hair shaft (Schlake 2007). Moreover, the hair possesses a cyclical renewal capacity based on stem cells. Although feather in birds evolved independently from hair, the organs share the same follicular structure. Both organs are composed of a basal dermal papilla, the ORS emerged from epithelial cells and the IRS separating the ORS from the pulp (figure 2.11). In contrast to the bilateral symmetry of a flight feather the down shows a simple radial symmetry. Feather can also be regenerated in circles from stem cells (Yue et al. 2005).

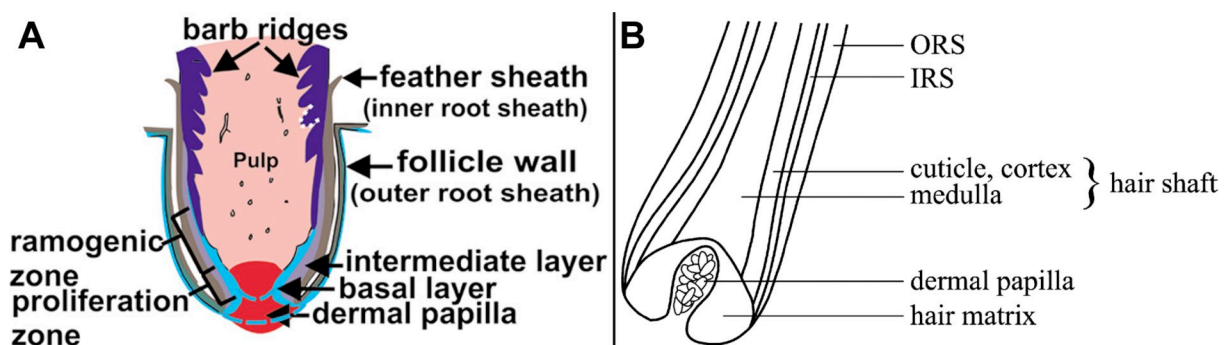


Figure 2.11: Longitudinal schematic sections of a feather (from (Yue et al. 2005) (A) and a hair (from (Schlake 2007) (B)). Both organs share the follicular structure with the basic dermal papilla, the inner (IRS) and the outer root sheath (ORS). Epithelial cells in both organs are located in the outer root sheath.

2.8 Aims of the work

The parameters defining a functional higher-order nuclear genome architecture are still only partially understood. It is generally accepted that local gene density shapes the radial nuclear arrangement of the genome and predisposes for an open chromatin conformation. However, developmental stage, chromosomal genome organization, and cell type specific gene activity may or may not lead to modifications of this pattern. For example, gene activity was shown to alternatively result in relocalization to the nuclear center, looping away from the core CT, site-specific chromatin folding, decondensation of chromatin or to have no detectable effects altogether.

In this work we will focus on the analysis of the nuclear topology of UCS (ultraconserved non-coding sequences) clusters, the *Dach1*, the *Bcl11a* and the *Csn* gene region in transcriptionally silent and expressing tissue from mouse and chicken. 3D-FISH experiments to tissue cryosections of both species will be performed, in order to address developmental, evolutionary genome rearrangement, cell type and gene activity related aspects of nuclear architecture.

Thereby, the among vertebrates exceptionally highly conserved UCS clusters, *Dach1* and *Bcl11a* genes will be compared to the exclusively mammalian *Csn* genes, representing an important region of genomic innovation. Some UCS were recently functionally characterized as enhancer or boundary elements, however, so far their nuclear topology is uncharacterized. The *Dach1* gene is located centrally in a large gene desert harboring UCS clusters on both sides, while the *Bcl11a* gene marks the border between a gene desert containing UCS clusters and a gene-rich region. In addition to these evolutionarily conserved local genomic features, the uniform karyotype of mouse contrasts the heterogenous karyotype of chicken. Thus, the comparison between mouse and chicken, concerning gene density and chromosome size, will allow for drawing conclusions on the impact of genomic rearrangements. In contrast, the *Csn* gene cluster is only present in mammals and is flanked by genomic regions represented by *Sult1b1* and *Igj*, which are evolutionarily conserved throughout vertebrates. Analysis of the *Csn* locus should reveal the effect of evolutionary sequence insertion and the consequences of dramatic gene expression changes during lactation.

First, ImmunoFISH to embryonic fibroblasts for the delineation of distinct histone methylation patterns should reveal the chromatin state in UCS cluster regions. In

addition, 3D-FISH to tissue of mouse and chicken embryos should test for preferential radial positioning and for nuclear colocalization of separate UCS clusters. Second, Dach1, Bcl11a and Csn expression analyses by RNAish will be combined with DNA FISH of the respective gene and UCS probes to correlate the expression status of the targeted genes with their topology referring to the nucleus and the respective chromosome territory surface. Further the local 3D chromatin conformation, including the flanking genomic regions, should be captured by interphase angle and distance measurements to gain information about chromatin compaction and folding in these regions. The gene positioning of Dach1 and Bcl11a will be determined in transcriptionally active and silent embryonic tissue of mouse and chicken, whereas the localization of Csn will be studied in mouse hair follicles, chicken feather follicles and mouse mammary gland from a juvenile, a lactating and a retired breeder mouse.

We expect that the results will elucidate the influence of UCS in the Dach1 and Bcl11a region, the gene expression changes of Dach1, Bcl11a and Csn, the arrangement and density of genes in the Dach1, Bcl11a and Csn region, cell type specification in native tissue and finally of evolutionary sequence conservation and genomic innovation between mouse and chicken to shape a functional higher order nuclear architecture.

3. Material and Methods

3.1 Workflow

The workflow should present the consecutive cell biological, molecular biological and data acquisition steps of all basic techniques described herein, from the starting material to the evaluated results. The protocols for RNAish on tissue sections and 3D FISH on tissue sections can be consecutively combined with only minor modifications that are noted in 3.6.8.

FISH on metaphases	3D FISH on cultured cells	3D Immuno FISH on cultured cells	3D FISH on tissue sections
3.2.1	3.2.1	3.2.1	3.2.2 / 3.2.3
3.3.1	3.3.2	3.3.2	3.3.3
3.4.1	3.4.1	3.4.1	3.3.4
3.4.2	3.4.2	3.4.2	3.4.1
3.6.1	3.6.1	3.6.1	3.4.2
3.6.2	3.6.2	3.6.2	3.6.1
3.6.3	3.6.3	3.6.3	3.6.2
3.6.4	3.6.5	3.6.6	3.6.3
3.7.2	3.7.2	3.7.3	3.6.7
3.7.4	3.7.3	3.7.5	3.7.3
3.8.1	3.7.5	3.8.2	3.7.5
	3.8.3	3.8.3	3.8.3
	3.9.1	3.9.1	3.8.4
	3.9.2	3.9.2	3.9.1
	3.9.3	3.9.3	3.9.2
	3.9.4	3.9.4	3.9.3
	3.10	3.10	3.9.4
			3.10
RNAish whole mount embryos	RNAish tissue sections	RNA FISH on tissue section	qPCR from tissue material
3.2.2	3.2.2 / 3.2.3	3.2.2	3.2.2
3.3.3	3.3.3	3.3.3	3.3.5
3.3.4	3.3.4	3.3.4	3.4.5
3.4.3	3.4.4	3.4.4	3.5.5
3.4.4	3.5.1	3.5.1	3.5.5.1
3.5.1	3.5.3	3.5.4	3.5.5.2
3.5.2	3.7.1 / 3.7.2	3.7.5	3.7.3
3.7.1	3.8.1	3.8.3	
3.8.1			

3.2 Cell material

3.2.1 Embryonic fibroblasts from mouse and chicken

Material

- DMEM medium including 15% FCS, 4 mM L-glutamine, penicillin/streptomycin
- 1x PBS
- Trypsin 0,05% (v/v), 0,02% EDTA (v/v) in 1x PBS
- T75cm² tissue culturing flasks
- Serological pipettes

Embryonic mouse fibroblasts (gift from Prof. Dr. Horst Hameister, Universitätsklinikum Ulm, Germany) and embryonic chicken fibroblasts (kindly provided by PD Dr. Christian Grund, Institute for Avian Disease, Ludwig-Maximilians-University, Oberschleißheim, Germany) were grown in T75cm² tissue culturing flasks and incubated at 37°C, 5%CO₂ and 80% relative humidity. Culture comprised of 15% fetal calf serum, 5ml Penicillin/Streptomycin, 4mM L-glutamin. 5% chicken serum was added when culturing of chicken embryonic fibroblasts. Upon confluence cells were proteolytically detached with trypsin and sub-cultivated in a 3:1 ratio.

3.2.2 Embryos of mouse and chicken

Material

- Timed pregnant CD- 1 mice (Charles River laboratories, Sulzfeld)
- Fertilized chicken eggs (Hühnerbrüterei Hölzl, Moosburg)
- 1x PBS
- Scissors, fine forceps, spatula
- Filter paper (125mm)
- RNAlater (Applied Biosystems, AM 7020)

Embryos from E7.0 and an E13.0 timed pregnant CD-1 mice were dissected with scissors and forceps as described at <http://www.swarthmore.edu> and mouse E7.0 was further isolated from the uterus under a binocular using fine forceps.

Fertilized chicken eggs were incubated for 21h or 5.5 days at 39°C, 5%CO₂ with 80% relative humidity. Chicken eggshell was opened with scissors after the desired time of incubation and released into a petri dish. Chicken E5.5 was gathered using a spatula and chicken E21h with a filter paper ($\varnothing \approx 1.5\text{cm}$), both from the top of the yolk sac. After cutting around the filter paper with scissors the chicken E21h sticks to the filter paper and was further processed together with the underlying filter paper.

Mice and chick embryos were rinsed in ice-cold PBS for subsequent fixation (see 3.3.2) and snap freezing (see 3.3.5) or stored in RNAlater for total RNA isolation (see 3.4.4).

3.2.3. Tissue of adult mouse and chicken

Material

- CBL 57 or CD1 mice (MPI for biochemistry, Planegg-Martinsried)
- Poulard (Institute for avian disease, Oberschleißheim)
- 1x PBS
- Scissors, fine forceps, spatula, razor blade
- Filter paper (125mm)

- RNAlater (Applied Biosystems, AM 7020)

Mouse Mammary gland and skin tissue was dissected out of wild type CBL 57 or CD1 mice. Mice were kindly provided by Dr. Markus Moser (MPI of biochemistry, Planegg-Martinsried, Germany). The 5 mammary gland pairs of mouse are located subcutaneous in the thoracic and groin region (figure 3.1). Mammary gland pair no.4 was obtained from a fertile juvenile mouse (12-14wk old), a lactating mouse and a retired breeder mouse after complete involution (at least 4wk after weaning of pups). Skin was obtained from the juvenile mouse and hair was removed with a razor blade. Poulard skin of the chest with downy feather was kindly provided by Prof. Dr. Rüdiger Korbel (Institute for Avian Disease, Ludwig Maximilians University, Oberschleissheim). Downy feather were shaved of. All tissue was rinsed in ice cold PBS until fixation (see 3.3.2) or stored in RNAlater for total RNA isolation (see 3.4.4).

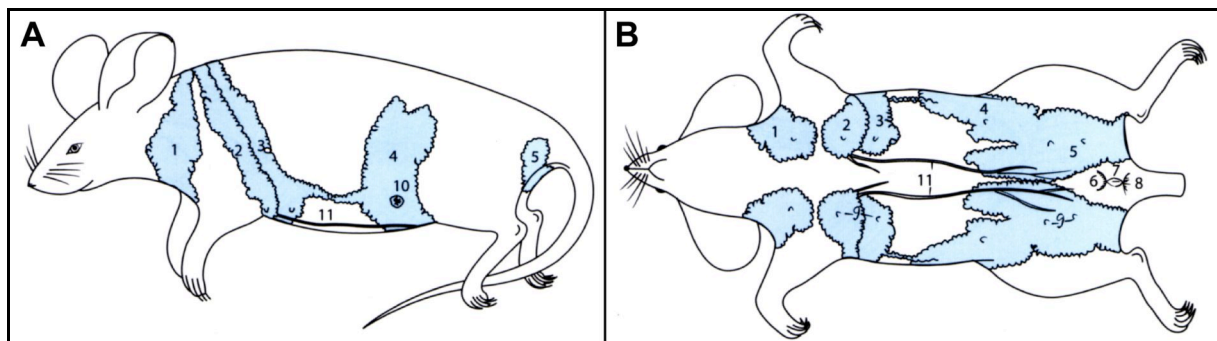


Figure 3.1: Position of the 5 mammary gland pairs in mouse: (A) lateral view, (B) dorsal (The laboratory mouse, H.Hedrich. Elsevier academic press, p.119)

3.3 Cell material fixation and cryosectioning

3.3.1 Metaphase preparation from embryonic fibroblasts

Material

- Colcemid-solution (10 mg colcemid/ml H₂O bidest) in 1x PBS
- Trypsin 0.05% (v/v), 0.02% EDTA (v/v) in 1x PBS
- Hypotonic solution: 0.075 M KCl
- Fixative: methanol/ glacial acetic acid 3:1 (v/v)
- Ethanol (70%, 90%, 100%)
- 4mg/ml pepsin in 0.01N HCl
- Heraeus Biofuge pico
- Certomat® R/H incubator
- Lauda E100 waterbath with lid

In order to prepare metaphases for cell cycle arrest at metaphase the spindle poison colcemid (10 μ l/ml) was added for 30min to a dividing, sub-confluent cell culture of mouse or chicken primary fibroblasts. First, cells were detached with trypsin and spun down at 157g for 10min. After that, the supernatant was discarded, the pellet was resuspended in hypotonic buffer and incubated 15-20min at 37°C. Swelling of nuclei was stopped by adding 1ml of fixative. The cell suspension was then spun (157g, 10min) down, resuspended in fixative, fixed for at least 25min at -20°C and cyclically washed 2-3x by spinning down and resuspension in fixative. The cell suspensions were stored at -20°C. Thereafter metaphase spreads from the cell suspension were prepared in a 55°C floating metal box according to (Deng et al. 2003) under standardized conditions. Next proteins were digested with pepsin solution (4mg/ml pepsin in 0.01N HCl for 1.5-2.5min at 37°C) and the metaphase spreads were incubated for 1h at 60°C to improve the FISH probe and the antibody accessibility. Last quality and quantity of metaphase spreads were checked under a phase contrast microscope.

3.3.2 Fixation of embryonic fibroblasts for 3D-FISH

Material

- 1x PBS (pH 7.4)
- 2x SSC
- 4% Paraformaldehyde in PBS 1x pH 7.4
- 0.5% Triton X-100
- 20% Glycerol in 1x PBS
- Liquid nitrogen
- 0.1N HCl
- 2mg/ml pepsin in 0.01N HCl
- 50% formamide/2x SSC (pH = 7.0)

To prepare fixed and 3-dimensionally preserved fibroblast nuclei for in situ hybridization experiments primary fibroblasts of mouse and chicken were grown on 26x76mm cover slips to 60-80% confluency in DMEM with 15% FCS. Thereafter, cells were fixed in 4% paraformaldehyde /1xPBS for 10min to maintain best possible the 3D-conformation of the nucleus. For 3D-Immuno-FISH fixed cells were stored in 1xPBS (see 3.6.6). Otherwise, permeabilization for normal 3D-FISH cell-fixations in five steps allow efficient FISH and antibody penetration: (1) treatment in 0.5% Triton X-100 in PBS for 20min plus 3x5min washes in 1x PBS; (2) 20% glycerol in PBS for; at least 1h (3) 4 freezing/thawing cycles in liquid nitrogen plus 3x5min washes in 1x PBS; (4) incubation in 0.1N HCl for 8min including 3x5 in 3x5min in 1x PBS (5) pepsinization (2mg/ml pepsin in 0.01N HCl at 37°C for 5-8min) followed by 2x5min 2x

SSC equilibration (Solovei et al. 2002). Finally, slides were stored in 50% formamide/2x SSC (pH = 7.0) at 4°C until 3D-FISH (see 3.6.5).

3.3.3 Fixation of embryos and adult tissue

Material

- 1x PBS (pH 7.4, DEPC treated)
- Paraformaldehyde 4% in PBS 1x pH 7.4
- DEPC
- Test-Tube-Rotator 34528

Tissue was fixed in 4%PFA 1xPBS (DEPC) at 4°C over night in a rotation wheel to maintain the tissue integrity and nuclear 3-dimensional morphology. All solutions in contact with tissue for later RNA isolation were stirred over night with 0.1% active DEPC and subsequently autoclaved, to (di-ethyl-propyl carbonate) block RNase activity by DEPC-binding to secondary and tertiary amines, hydroxy and thiol groups present in the enzymes catalytic domain and is pyrolyzed to ethanol and CO₂ during autoklaving. Next, fixed tissue was either processed for cryosections (3.3.4) or whole mount RNAish (3.5.2).

3.3.4 Cryoprotection and cryosectioning for chromogenic RNAish and 3D-FISH

Material

- 1x PBS (pH 7.4, DEPC treated)
- Paraformaldehyde 4% in PBS 1x pH 7.4
- 0.1M phosphate buffer pH 7.4
- 5% sucrose in 0.1M phosphate buffer
- 12.5% sucrose in 0.1M phosphate buffer
- 20% sucrose in 0.1M phosphate buffer
- Dry ice
- 95% ethanol
- Razor blades
- Test-Tube-Rotator
- Tissue freezing medium (JUNG, Oder Number 0201 08926)
- Poly-A-Way Disposable Embedding molds (T-12)
- CM3000 Cryostat
- Super Frost®Plus slides

After fixation (see 3.3.3) tissue was cryoprotected in an increasing sucrose gradient in 0.1M phosphate buffer to prevent the tissue from drying and freezing injury by ice crystal formation. Then, tissue was washed 2x10min in 0.1M phosphate buffer,

equilibrated for 1h each in 5%, 12.5% at RT and finally over night in 20% sucrose in 0.1M phosphate buffer at 4°C on a rotation wheel. The day after the tissue was cut with a razor blade to fit the embedding mold dimensions. The embedding mold was filled with tissue freezing medium and tissue was orientated with a pipette tip. Chicken E21h, hindlimbs of mouse E13.0 and chicken E5.5, skin of mouse and chicken and mouse mammary gland were orientated horizontally. Mouse E7.0, head of mouse E13.0 and head of chicken E5.5 were orientated vertically. Finally, tissue blocks were frozen in a dry ice 95% ethanol bath (-78°C) and stored at -80°C until cryosectioning. 20µm cryosections were cut in a cryostat-microtome at -17°C, taken up with a room tempered Super Frost®Plus object slide and replaced to -80°C.

3.3.5 Freezing and cryosectioning for RNA FISH and qPCR

Material

- 1x PBS (pH 7.4, DPEC treated)
- Paraformaldehyde 4% in PBS 1x pH 7.4
- Liquid nitrogen
- Tissue freezing medium (JUNG, Oder Number 0201 08926)
- Poly-A-Way Disposable Embedding molds (T-12),
- CM3000 Cryostat
- Super Frost®Plus slides
- 1mm PEN-membrane slides
- 70%, 90%, 100% ethanol
- Hematoxylin
- H₂O (DEPC treated)

After dissection of mouse E13.0 the embryos were (see 3.2.2) placed in an embedding mold without fixation and immediately frozen to prevent RNA damage. Therefore embryos were quickly embedded in tissue freezing medium and snap frozen in liquid nitrogen (-196°C) to avoid RNA degradation and to prevent tissue damage from ice crystal formation, because snap freezing in liquid nitrogen below -140°C produces vitreous ice with an amorphous structure. Tissue blocks were stored at -80°C until tissue sectioning in a cryostat-microtome at -17°C. After the uptake of cryosections, afore cut at 14µm with a room tempered sterile Super Frost®Plus object slide the cryosections were directly placed on dry-ice and subsequently fixed 15min in 4% PFA in 1xPBS (DPEC) in advance to RNA FISH (see 3.5.4). In contrast, 8µm cryosections for qPCR were mounted on sterilized (baked 3h at 180°C) 1mm PEN-membrane slides, then rapidly fixed 2.5min in ice cold 70% ethanol, briefly rinsed 3x in H₂O (DPEC), stained 1min in hematoxylin, washed 1min in H₂O (DPEC),

briefly dehydrated in a 70%, 90% and 100% ethanol series and finally placed on dry ice until the shortly consecutive laser microdissection (see 3.4.5).

3.4 Preparation of RNA, DNA and embryonic powder

3.4.1 DNA isolation and preparation of cot-1 DNA from chicken liver

Material

- Chicken liver
- 2% SDS lysis buffer (see 3.12.5)
- Proteinase K
- 5M NaCl
- Ethanol
- RNase A
- TE buffer
- Phenol-Chloroform-Isoamylalcohol (25:24:1)
- ddH₂O
- 0.3M NaCl
- 2x nuclease-S1-buffer (see 3.12.5)
- Certomat® R/H shaking incubator
- Glass pasteur pipettes 230mm
- Centrifuge Jouan C 3i
- Haereus Biofuge pico
- DNA/RNA calculator GeneQuantII
- Easy-Cast Electrophoresis-System
- Polytron homogenizer
- Ultrasonic sonicator SW220F

Cot-1 DNA was isolated from chicken liver to later block repetitive DNA in combinatorial FISH probe sets (see 3.6.3). As first step chicken genomic DNA was isolated from 4x4g fresh chicken liver (Höhenrainer, Viktualienmarkt, Munich, Germany). Therefore, each 4g liver was homogenized in 2.5ml lysis buffer using a polytron homogenizer (Ultra Turrax), thereafter filled up to 25ml with 2% SDS lysis buffer and incubated 1h at 37°C. Proteinase K was added to the lysate in a final concentration of 0.1mg/ml and protein was digested for 24h at 50°C in a shaker incubator. Then, the protein was precipitated by adding 10ml 5M NaCl. After vortexing for 15sec the precipitate was spun down at 2775g for 15min. The 4x supernatant was collected and the contained DNA was precipitated by adding 2Vol of 100% ethanol. The precipitated DNA was fished using a glass loop, washed 2x in 70% ethanol and briefly air-dried. Next, the DNA was resuspended in 10ml TE-buffer

at 37°C for 12h on a shaking incubator. With a final concentration of 20µl/ml of RNase in TE-buffer the RNA digested was digested for 2h at 37°C on the next day. Then purification of DNA from digested RNA was performed with an equal volume of Phenol-Chloroform-Isoamylalcohol (25:24:1). After centrifugation at 2354g for 5min the upper phase was transferred to 2Vol ethanol and the DNA was left to precipitate in ethanol for 1h at -20°C. After that precipitated DNA was spinned down at 8500rpm (rotor JS13) for 20min. The supernatant was discarded and ethanol residues were removed with a pipette. Finally, the genomic DNA pellet was resuspended in 1.68ml ddH₂O. DNA quality and yield were checked on a 1% agarose gel and photometrically measured (expected yield approx. 5mg genomic DNA/g liver).

Subsequently, 75mg of genomic DNA were mixed with 10ml TE-buffer and fractioned to 300-600bp by ultrasonic sonification (7x2min on ice). The fragment size was controlled by gel electrophoresis.

The most highly repetitive genomic DNA portion is referred to as Cot-1 DNA. Cot-1 DNA can be isolated from fragmented genomic DNA by denaturation and following renaturation at defined salt concentration (0.3M NaCl), temperature (65°C) and time (44sec). The time can be calculated from the DNA concentration in TE-buffer (7.5g/l) and the average molecular weight of a nucleotide (330g/mol) with the equation $Co^{-1} = t$:

$$Co \text{ (DNA concentration)} = m/M = 7.5g/l / 330g/mol = 2.27 \times 10^{-2} \text{ mol/l}$$

$$t \text{ (sec)} = 1 / Co = 1 / 2.27 \times 10^{-2} = 44 \text{ sec}$$

Hence, the fragmented DNA was denatured at 96°C for 6min, transferred to 65°C and 640µl 5M NaCl were added. After 44sec the renaturation was terminated by adding with 10.6ml ice-cold 2x nuclease-S1-buffer. Single stranded DNA was then digested with 10.000U (25µl) nuclease-S1 at 37°C for 30min. Double stranded Cot1-DNA was extracted with 1Vol Phenol-Chloroform-Isoamylalcohol (25:24:1) and precipitated with 2Vol ethanol as described above. After centrifugation (8500rpm, rotor JS13, 20min) the DNA Pellet was resuspended in ddH₂O to a final concentration of 3.4 µg/µl, and stored at -20°C until further use (see 3.6).

3.4.2 Isolation of BAC clone DNA from bacterial cultures

Material

- LB medium (see 3.12.5)
- Chloramphenicol Stock (50mg/ml)
- 50% glycerol
- P1, P2, P3 buffer (see 3.12.5)
- Isopropanol
- 70% ethanol
- Certomat® R/H incubator

- Haereus Biofuge pico
- Easy-Cast™ Electrophoresis-System

Agar staps from BAC clones (*E. coli* transfected a BAC vector) were purchased from <http://bacpac.chori.org> (listed under 3.12.3). BAC vectors carried genomic inserts from mouse or chicken and the isolated DNA was used in DNA FISH probe sets to specifically target genomic sites (see 3.6). Therefore, 7ml LB medium cultures with chloramphenicol (conc. 15µg/ml) were inoculated and cultured at 37°C for 16h under vigorous shaking. The next day 300µl of bacterial culture was added to 300µl 50% glycerol (autoclaved) and stored at -80°C as backup for further cultures. BAC clone DNA was isolated from the remaining bacterial culture according to <http://bacpac.chori.org>, <http://www.rzpd.de> with minor modifications from Dr. Steffen Dietzel (Ludwig-Maximilians-University, Munich). Bacteria were spun down for 15min at 3075g and resuspended in 0.5ml P1 buffer. Subsequently, 0.5ml P2 buffer and 0.5ml P3 buffer were added with gently shaking after each step. Tubes were placed on ice for 5min and then directly centrifuged for 10min at 15115g. The resulting pellet contains all proteins and bacterial genomic DNA whereas BAC clone DNA from the supernatant was transferred to a new tube. Thereafter, the DNA was precipitated with 0.8ml isopropanol at -20°C for 20min and spun down for 15min at 15115g. The supernatant was removed and the pellet was washed with 0.5ml 70% ethanol. Next, the pellet was air dried and resuspended in 50µl H₂O. Isolation of BAC clone DNA was checked on a 1% agarose gel. The BAC clone DNA concentration was increased by evaporation to about 25µl using a vacuum centrifuge and finally stored at -20°C until phi29 amplification (see 3.6.1).

3.4.3 Extraction of embryonic powder

Material

- 1x PBS (pH= 7.4)
- Acetone
- Haereus Biofuge pico
- Spatula
- Filter paper (125nm)
- Polytron homogenizer Ultra Thurax

Embryonic powder, to block unspecific antibody epitopes during RNAish detection (see 3.5.2) was prepared following the protocol published at <http://www.paperyglyphs.com>. Mouse E13.0 embryos were homogenized in a minimum volume of ice cold PBS. Afterwards, 4Vol of acetone were added to the embryos, mixed and incubated for 30min on ice for precipitation of proteins.

Homogenized embryos were spun down for 10min at 10000g, washed once with acetone and spun down again. The pellet was then spread on a filter paper and air dried over night. The next day embryonic powder was collected using a spatula and stored at 4°C until whole mount RNAish (see 3.5.2).

3.4.4 Isolation of total RNA and cDNA from tissue

Material

- peqGold RNAPure™ (peqLab, Article number 12-6834-01)
- Chloroform
- Isopropanol
- 75% ethanol
- H₂O (DEPC treated)
- SuperScript™ II or III RT kit (Invitrogen, Cat.No. 12574-018)
- RNase H
- RNeasy Mini Kit (QiaGen, Cat.No. 74104)
- Polytron homogenizer
- DNA/RNA calculator GeneQuantII
- Easy-Cast™ Electrophoresis-System
- Thermo Block TDB-120

Total RNA and further cDNA was isolated from tissue to serve as input for the generation of RNA in situ probes (see 3.5.1). Total RNA from mouse lactating mammary gland, mouse E.13.0 and chicken E5.5 tissue was isolated using peqGold RNAPure™ following the manufacturer's tissue isolation protocol. First, tissue was homogenized on ice in 2ml peqGold RNAPure™ per 100mg tissue. The homogenate was then incubated for 5min at RT to ensure dissociation of nucleotide complexes. 0.2ml chloroform per ml of PeqGold RNAPure™ were added to the sample, thereafter incubated for 3min at RT and directly centrifuged for 10min at 12000g. The upper aqueous phase contained the RNA whereas protein and DNA remained in the intermediate and lower phenol phase. The upper phase was then transferred to a tube containing 0.5ml isopropanol per 1ml of aqueous phase. RNA was precipitated over night at -20°C. The following day the RNA was centrifuged at 4°C for 10min at 12000g. The pellet was washed twice with 75% ethanol and centrifuged again after each washing step (4°C, 10min, 12000g). Thereafter, the pellet was briefly dried before resuspension in RNase free H₂O. Next, the RNA concentration (OD 260nm and dilution factor) and purity (ratio OD 260nm/OD 280nm) was photometrically checked in 1xTE. For intact total RNA the OD ratio 260nm/280nm should be at least 1.7. For mammary gland the initial RNA quality was below 1.7 and therefore the RNA quality was enhanced using the RNeasy Mini Kit (Qiagen, see 3.5.1 for use)

purification procedure. Then RNA quality and quantity was determined with 1.5µg HeLa total RNA as a standard. For high quality RNA the band for 28S RNA should be twice as strong as the 18S RNA band on a 1.2% formamide gel and both bands should be distinct. Finally, the yield was estimated in comparison to the control. Total RNA was stored at -20°C and is stable for at least 6months. Storage of RNA concentrations below 1µg/µl results in faster RNA degradation and should be avoided.

In a second step the isolated total RNA was reverse transcribed to cDNA with Invitrogen SuperScript™ II or III RT kit (Invitrogen) (figure 3.2). For this 5µg of total RNA were mixed with 1µl of Oligo(dT)₁₈ primer, 10mM dNTP mix and adjusted to 12µl with RNase free water. The oligo T primer binds to the polyA tail of mRNA. The reaction was incubated for 5min at 65°C to resolve secondary RNA structures and cooled down on ice. Thereafter, 5µl 5x FirstStrand buffer and 2µl 0.1M DTT were added and the reaction was incubated for 2min at 42°C. Reverse Transcription was then started by adding 1µl SuperScript™ RT enzyme and carried out for 50min at 42°C. Subsequent incubation at 70°C for 15min thermally stopped the reaction. The RNA template was digested with 1µl RNase H (NEB) at 37°C for 20min leaving only single stranded cDNA intact. The cDNA was stored at -20°C until 2nd strand synthesis (see 3.5.1).

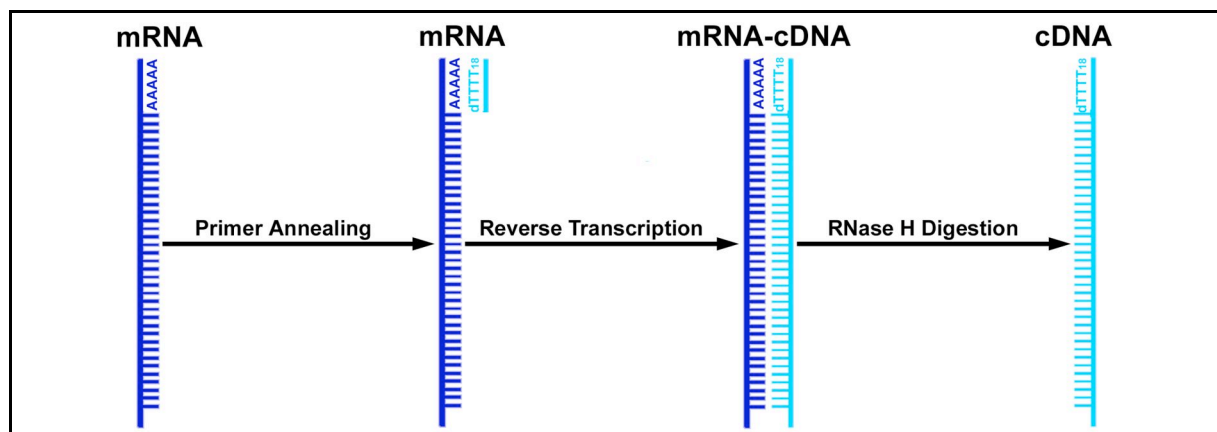


Figure 3.2: Steps of reverse transcription from mRNA to cDNA using an oligo(dT)₁₈ primer

3.4.5 Isolation of mRNA and cDNA from laser microdissected tissue

Material

- QuickPick™ RNA SML mRNA kit (Bio-Nobile, 42022)
- AffinityScript™ QPCR cDNA Synthesis Kit (Stratagene, #600559)
- PALM AdhesiveCap (200µl)
- PickPen® 1-M magnetic tool
- PickPen Tips (bulk 96)
- PALM MicroBeam
- Thermo Block TDB-120

mRNA and cDNA was extracted from fixed issue sections to quantify RNA expression levels in tissue (see 3.5.5). Therefore, hematoxylin stained 8 μ m vertical cryosections from mouse E13.0 on dry-ice (see 3.3.5) were immediately inserted in the laser microdissection system (Zeiss MicroImaging, Bernried). The tissue was mounted on a UV-light absorbing 1mm PEN-membrane coated slide. The dissection area on the slide was marked by the PALM software, then cut from the surrounding by the focused pulsed laser (accuracy 1 μ m) and finally laser pressure catapulted to an adhesive cap right above the tissue (figure 3.3). The ns long laser pulses did not heat up the tissue. Further, the system was operating without direct contact to the specimen and without using any liquids. The PALM AdhesiveCap (200 μ l) contained a silicon pad to which the tissue material sticks. After tissue collection the AdhesiveCap was closed and placed on ice until the subsequent mRNA isolation.

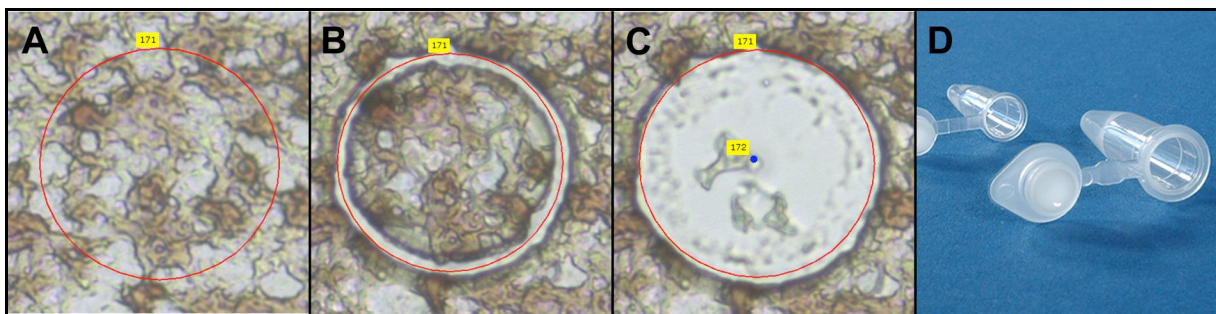


Figure 3.3: Laser microdissection from hematoxylin stained mouse E13.0 tissue (A) Selection (B) laser microdissection (C) laser pressure catapulting (D) AdhesiveCap with silicone lid (D taken from <http://www.zeiss.de>)

mRNA was isolated from dissected tissue with the QuickPickTM RNA SML mRNA kit (BioNobile, Finland) by oligo(dT)₃₀ paramagnetic particles and a magnetic QuickPickTip covered by a sterilized silicone cap (baked for 3h, 180°C) following the protocol for less than 1000 cells (figure 3.4). For hybridization of the polyA mRNA to the particles, 100 μ l lysisbuffer and 15 μ l of paramagnetic particles were added directly to the AdhesiveCap and incubated for 8min at RT upside down. Next, the particles were transferred with the magnetic tip to 2x in 100 μ l BufferA and 1x in 100 μ l Buffer B to remove unspecifically bound material as pre-mRNA, rRNA, tRNA or snRNA. The silicon tip was used to agitate the particles for 15sec before transfer to the next buffer step. Finally, the magnetic particles were released into 6.5 μ l RNase free H₂O. The mRNA was simultaneously thermally released from the particles 5min at 70°C. Magnetic particles were removed with the magnetic tip to avoid any risk of the particles to impair in downstream reactions.

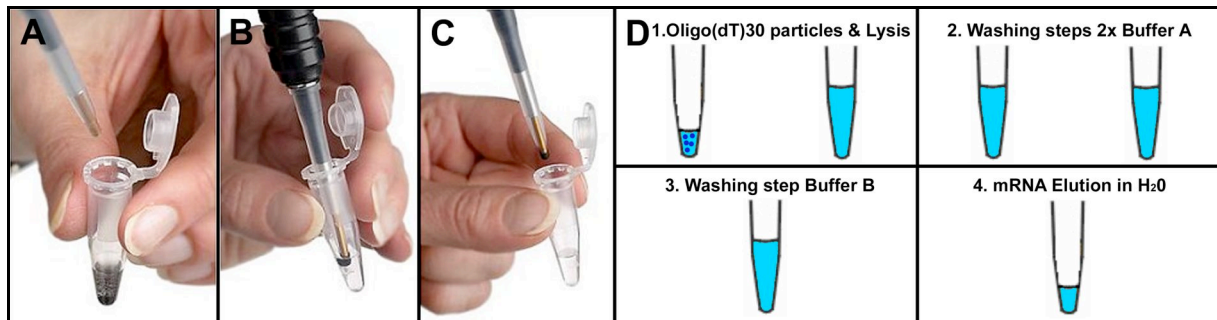


Figure 3.4: (A-B) Magnetic Oligo(dT)₃₀ particles uptake with the PickPen® 1-M. (D) Experimental steps for mRNA isolation with the QuickPick™ RNA SML mRNA kit (pictures modified from <http://www.bio-nobile.com>).

The entire isolated mRNA was then reverse transcribed (table 3.2) to cDNA in a single reaction batch using the AffinityScript™ QPCR cDNA Synthesis Kit (Stratagene). Reaction was made up of 6.5 µl mRNA, 10µl of cDNA Synthesis Master Mix, 3µl Oligo(dT) primer and 1µl RT/RNase Block Enzyme Mixture. The reaction was equilibrated 5min at RT and reverse transcription was carried out for 1h at 42°C. The reaction was stopped for 5min at 95°C and placed on ice until qPCR analysis was performed (see 3.5.5).

3.5 Gene expression analysis

3.5.1 Probe design and labeling for RNAish

Material

- QIAquick gel extraction kit (QiaGen, Cat.No. 28704)
- Isopropanol
- NEB cutting enzymes
- DIG or Biotin RNA labeling mix (Roche, Cat.No. 11 277 073 910, 11 685 597 910)
- RNeasy Mini kit (QiaGen, Cat.No. 74104)
- 2-Mercaptoethanol
- Easy-Cast Electrophoresis System
- Techni TC-312 Thermal Cycler
- Heraeus Biofuge pico

RNA in situ hybridization is a technique to visualize gene expression sites in the cellular context. A primer pair is required which amplifies specifically a cDNA fraction of the target gene and next the reverse transcription with simultaneous labeling to generate a detectable RNA antisense probe to the expressed target mRNA. Here, RNAish probes against mouse and chicken Dach1, mouse and chicken Bcl11a, mouse Csn1s2a and Csn3 were designed.

As a first step the respective cDNA sequences were downloaded from public databases (www.ensembl.org, www.ncbi.nlm.nih.gov). Primer pairs were designed to

amplify a cDNA fraction were chosen with respect to the following issues: (1) Alternative splicing was checked and probes limited to amplify fractions present in all splice variants. (2) For evolutionarily comparative analysis between mouse and chicken cDNAs were aligned (http://www.ch.embnet.org/software/LALIGN_form.html) and primers were selected to amplify the most conserved regions. (3) Primers were chosen which span at least two exons or ideally span one splicing exon-exon border to distinguish from genomic DNA contamination. (4) Primers were blasted (www.ensembl.org/Multi/blastview) against the reference genome to minimize cross annealing. (5) Finally attention was paid to general rules for primer design according to Innis and Gelfand (Innis and Gelfand 1990). To allow for reverse transcription of the 2nd strand amplification product from cDNA, the forward and reverse primer were end modified with a T7 or T3-promotor sequence, respectively, plus 4 basepairs to protect the promotor region from the polymerase 5'-3' exonuclease activity during PCR set up and amplification. 3.12.3 summarizes the sequences of all selected primer pairs.

To set up the PCR reaction conditions the melting points of the primer were calculated ($T_m = 2^{\circ}\text{C} \times (A + T) + 4^{\circ}\text{C} \times (C + G)$). 5 PCR cycles of high stringency were followed by 25 cycles of low stringency with shorter denaturation and a shorter annealing time, closer to the primer melting point temperature. Cycles with low stringency allow amplification from the cDNA template and later high stringency favor amplification only from the products of cycles with low stringency. Thereby, amplification of unspecific longer or from similar annealing sites was suppressed. Selected PCR and conditions reaction for each target gene are summarized in table 3.1 and 3.2.

		Bcl11a		Dach1		Mouse Csn	
Cycles	Time	Mouse	Chicken	Mouse	Chicken	Csn1s2a	Csn3
1x	4min	94°C	94°C	94°C	94°C	94°C	94°C
6x	1min	94°C	94°C	94°C	94°C	94°C	94°C
low	1min	59°C	59°C	57°C	54°C	60°C	60°C
stringency	1min 30sec	72°C	72°C	72°C	72°C	72°C	72°C
25x	30sec	94°C	94°C	94°C	94°C	94°C	94°C
high	30sec	61°C	61°C	60°C	62°C	63°C	63°C
stringency	1min 30sec	72°C	72°C	72°C	72°C	72°C	72°C
1x	5min	72°C	72°C	72°C	72°C	72°C	72°C

Table 3.1: PCR conditions for gene specific 2nd strand amplification from isolated cDNA

2nd strand PCR	Reaction
cDNA	2.0µl
TAPS3	2.5 µl
Fw Primer (25pmol/µl)	0.5 µl
Rev Primer (25pmol/µl)	0.5 µl
dNTP Mix (2.5mM each)	2.0 µl
Taq pol	0.5 µl
ddH ₂ O	17 µl
TOTAL	25.0 µl

Table 3.2: PCR reaction for gene specific 2nd strand amplification from isolated cDNA

If necessary, the 2nd strand amplification product was gel purified in order to remove any unspecific PCR coproducts using the QIAquick gel extraction kit. In this case the entire PCR reaction was separated by agarose gel electrophoresis, stained with ethidium bromide and the specific amplification product was cut out under UV light with a sterile scalpel. The gel piece was then weight, dissolved in 3Vol of puffer GQ at 50°C for 10min and mixed afterwards with 1Vol of isopropanol.

Otherwise, in case of no unspecific PCR coproducts the 2nd strand reaction was diluted in 5Vol of buffer PB1.

Both, the dissolved gel piece and the directly diluted 2nd strand reaction were purified from the PCR reagents and/or from the dissolved agarose with the QIAquick PCR Purification Kit following the protocol “using a microcentrifuge”. Buffer PB1 diluted PCR product or buffer GQ dissolved gel piece with isopropanol was bound to the QIAquick column for 45sec at 10000g and the flow through was discarded. Columns were then washed once with 0.5ml buffer GQ for dissolved agarose input and always with 0.75ml buffer PE, thereafter centrifuged for 45sec at 10000g and placed in a new tube. The DNA was then eluted from the column by adding 30µl H₂O, incubation at RT for 1min and centrifugation for 1min at 10000g. The eluate contained about 28µl of purified 2nd strand PCR product and was store at -20°C.

Afterwards the PCR product was control digested with a afore selected single cutter enzyme (<http://tools.neb.com/NEBcutter2/index.php>) and expected fragment lengths were verified on a 1% agarose gel with the 1kb and 100bp ladder standard (figure 3.5).

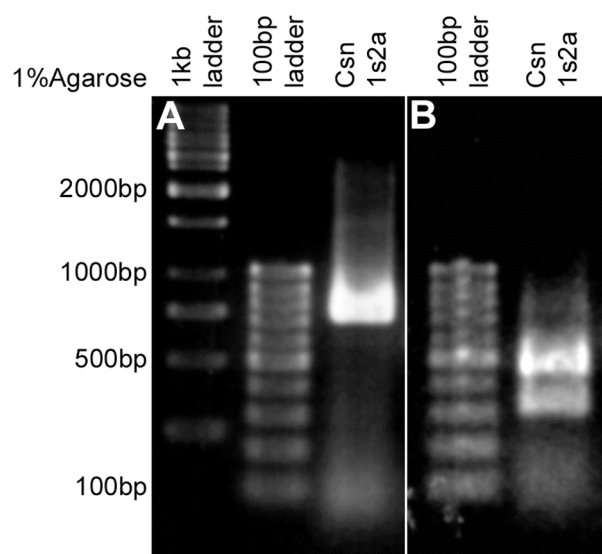


Figure 3.5: 1% Agarose gel electrophoresis (100V, 40min), stained with Ethidium Bromide: (A) 2nd strand amplification product for mouse Csn1s2a from lactating mammary gland cDNA (product size: 710bp), (B) Control digestion with single cutter KpnI (NEB) (cutting site: 432/428bp).

To generate a labeled RNA antisense probe against the mRNA of the target gene the 2nd strand product was used as template. The reverse transcription reaction was driven by the T7 promotor region added to the PCR primer. Simultaneously with the reverse transcription, the RNA probe was labeled by incorporation of Digoxigenin-UTP or Biotin-UTP (DIG or Bio RNA labeling mix, Roche). The reverse transcription reaction was set up as shown in table 3.3 and incubated for 3h at 37°C.

T7/T3 RNA Anti-/Sense	Reaction
2nd strand PCR product	2.0µl
Transcription Buffer 10x	2.5 µl
DIG/Bio RNA labeling Mix	0.5 µl
RNAguard	0.5 µl
0.1M DTT	2.0 µl
T7/T3 RNA pol	0.5 µl
H2O (DEPC treated)	5.5 µl
TOTAL	20.0 µl

Table 3.3: T7/T3 RNA antisense or sense strand reverse transcription reaction using the DIG or Bio RNA labeling Mix, Roche.

Subsequently, DIG or Bio labeled RNA antisense probe was purified from input DNA and reagents using the QiaGen RNeasy Mini kit. Reverse transcription product was adjusted to 100µl with RNase free water and mixed with 350µl buffer RLT (freshly set up with 2-Mercaptoetanol). Next, 250µl ethanol were added and mixed thoroughly. The entire volume was applied to an RNeasy mini column where the RNA was bound to the column by centrifugation for 15sec at 8000g. The column was washed twice with 0.5ml buffer RPE followed by centrifugation steps for 15sec and 2min, respectively at 8000g. The RNA was then eluted from the columns by adding twice

30µl RNase free water each time followed by centrifugation for 1min at 8000g. DIG or Bio labeled RNA antisense probe was finally sized-checked on a normal agarose gel and stored at -20°C, to be used for RNA chromogenic (see 3.5.2, 3.5.3) or fluorescent (3.5.4) expression detection in tissue.

3.5.2 Whole mount RNAish on embryos

Material

- 25%, 50%, 75%, 100% methanol
- H₂O₂
- Proteinase K
- PBT
- 4% PFA in PBT
- Hybridization mix
- Washing solution I, solution II, solution III
- DIG RNA antisense probe (see 3.5.1)
- Anti-Digoxigenin-AP (Fab Fragments)
- Embryonic powder (see 3.4.3)
- MABT
- NTMT
- NBT/BCIP
- Glycerol / 4% PFA (1:1)
- Lauda E100 waterbath
- Thermo Block TDB-120

Whole mount RNAish was performed on mouse E13.0 and chicken E5.5 embryos according to (Wilkinson 1992), with some modifications. In principle, sites of expression were targeted by hybridization of a sequence specific Digoxigenin labeled RNA antisense probes to the target mRNA. Digoxigenin was further detected by an alkaline-phosphatase-coupled antibody. Alkaline phosphatase hydrolyzes BCIP (5-Bromo-4-Chloro-3'-Indolyphosphate p-Toluidine Salt). This hydrolyzed intermediate dimerized with the help of NBT (Nitro-Blue Tetrazolium Chloride) to a blue indigo dye (figure 3.6). Thus, the insoluble Indigo precipitates indicate sites of expression whereas expressionally silent sites stay unstained.

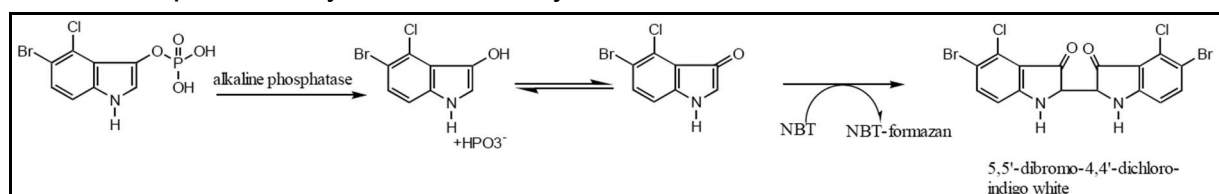


Figure 3.6: Chemical reaction NBT (Nitro-Blue Tetrazolium Chloride) and BCIP (5-Bromo-4-Chloro-3'-Indolylphosphate p-Toluidine Salt) to indigo (5,5'-Dibromo-4,4'-Dichloro-indigo white)

All solutions used were treated with DEPC (see 3.3.3) and all following steps were carried out in a 2.0ml Eppendorf tubes. After fixation (see 3.3.3) embryos were sequentially dehydrated in 25%, 50%, 75% and 100% methanol for each 5min and then stored in 100% methanol at -20°C until hybridization to block endogenous alkaline phosphatase by methanol and avoid unspecific indigo precipitates.

At day one of the procedure the embryo was taken from -20° and bleached for 1h in 6% H₂O₂ in 80% methanol. RNAish is a relative detection method of gene expression and tissue bleaching equaled the tissue pigmentation. The embryo was then rehydrated in 50% and 25% methanol and washed in PBT 3x 5min. Further digestion with Proteinase K (20µg/ml), 1h for mouse E13.0 and 40min for chicken embryo E5.5 permeabilized the embryo to allow probe penetration. Embryos were then washed in PBT 3x5min and stabilized by postfixation for 3h in 4% PFA. Three washing steps in PBT for 5min each were followed by prehybridization in hybridization mix for 1h at 70°C. Next, 27.5µl of DIG RNA antisense probe (see 3.5.1) were diluted in 0.5ml hybridization mix. Probe hybridization was carried out over night at 70°C.

The second day, unbound and unspecifically bound probe was removed by performing and added to stringency washes in solution 1 (3x30min, 70°C), solution 2 (3x 30min, 66°C) and solution 3 (30min, 66°C and 2x 30min 68°C). Afterwards embryos were then equilibrated 2x5min in MABT and further incubated in MABT 2x30min at 70°C and to increase the signal to noise ratio. Unspecific antibody epitopes were blocked for 1h in blocking solution. Simultaneously anti-DIG antibody coupled to alkaline phosphatase was blocked: A needle tip of embryonic powder (see 3.4.3) was dissolved in 2ml of blocking solution for 1h at 70°C, chilled on ice and the anti-DIG antibody diluted 1:2000. The Antibody solution was rotated for 2h at 4°C and centrifuged down for 10min at 10000g. Subsequently, the supernatant was applied to the embryo and incubated over night at 4°C.

The third day, unbound and false bound antibody was removed by washing in MABT 9x 30min at RT. The embryo was washed 3min and equilibrated for 15min in NTMT. NTMT buffer (pH = 9.4) has the basic pH required the conversion of BCIP to the Indigo dye. Staining was performed with 1,4 µl BCIP (Stock: 75mg/mL) and 1,1 µl NBT (Stock: 100mg/mL) per ml of NTMT in the dark. Depending on the probe the staining was stopped after 50min to over night with PBT followed by postfixation in 4% PFA over night. Finally, the embryo was imaged under the binocular and could be stored in 50% 4%PFA/ 50% glycerol at 4°C.

3.5.3 Chromogenic RNAish on tissue sections

Materials

- DEPC
- 1x PBS (DEPC treated)

- 5x SSC (DEPC treated)
- 4% PFA in 1x PBS (DEPC treated)
- Proteinase K
- Hybridization Mix
- RNA-DIG-Antisense-Probe (see 3.5.1)
- 2x SSC
- 0.1x SSC
- Buffer 1, Buffer 2, Buffer 3
- NBT/ BCIP
- TE Buffer
- 95% Ethanol
- 50% Formamide in 2x SSC (pH 7.0)
- Anti-Digoxigenin-AP (Fab Fragments)
- NBT/BCIP
- Fixogum rubber cement
- Coverslips 20x20 mm

The technical principle of RNAish of tissue sections was the same as described above for whole mount embryos. However the reduced complexity of a 20 μ m tissue cryosection (see 3.3.4) in comparison to a whole mount embryo allowed simplify the protocol following (Braissant and Whali 1998). The protocol was applied to sections of mouse mammary gland, mouse E13.0 and chicken E5.5 embryos.

On day one, cryosections were taken from -20°C and air-dried for 2h. Air-drying is necessary to guarantee that the tissue stays on the object slide at all times of the protocol. Next, tissue was fixed in 4%PFA for 20min. Endogenous and contamination RNase activity on the slide was blocked by incubation in 0.1% active DEPC, 2x for 15min (in the fume hood). All used solution were afore made RNase free by DEPC treatment (see 3.3.3). Sections were then equilibrated for 5min in 5xSSC. Immediately afterwards the sections were prehybridized in hybridization mix for 2h at 58°C. Hybridization probe was combined by adding 0.5 μ l DIG RNA antisense probe (3.5.1) to 20 μ l hybridization mix. To avoid direct contact the hybridization area was covered with a 20x20mm coverslip glued to spacers (figure 3.7) and next sealing with fixogum prevented drying-up. Probe hybridization was allowed at 58°C over night.

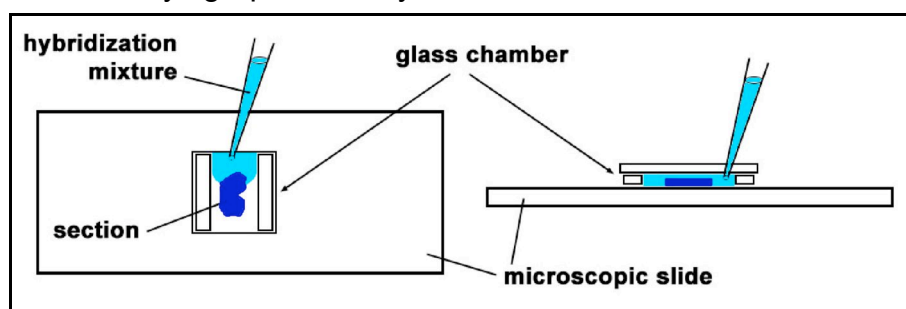


Figure 3.7: Glass chamber for in situ hybridization on tissue sections to avoid direct tissue cover slip contact. (modified from Irina Solovei, Ludwig-Maximilians-University, Munich)

On day two, stringency washes were carried out for 30min in 2xSSC, 1h in 2xSSC at 65°C and 1h in 0.1xSSC at 65°C. Afterwards the sections were equilibrated in buffer 1 for 10min. Alkaline phosphatase coupled anti-DIG antibody was diluted 1:4000 in buffer 2. The antibody was then incubated for 2h at RT on the sections. Next, the sections were washed 2x in 15min in buffer 1. To set the basic conditions for staining the sections were equilibrated for 5min in buffer 3 (pH=9.5). The staining reaction was started with 4.5µl BCIP and 3.5µl NBT per ml of buffer 3. Dye precipitation was quenched after 1 h to over night with 1xTE. Unspecific background was then removed with 95% ethanol. Finally, sections were imaged in deionized H₂O under a binocular and stored in 50%FA in 2xSSC if further used for DNA FISH (see 3.6.6).

3.5.4 RNA FISH on tissue sections

Materials

- DEPC
- 1x PBS (DEPC treated)
- 5x SSC (DEPC treated)
- 4% PFA in 1x PBS (DEPC treated)
- Proteinase K
- Hybridization Mix
- RNA-DIG-Antisense-Probe (see 3.5.1)
- 2x SSC
- 0.1x SSC
- 4x SSC 0.1% Saponin, 0.1% Triton X-100, 2% BSA
- 4x SSC 0.1% Triton X-100
- Antibodies: Mouse-anti-Streptavidin-cy5, Goat-anti-Mouse-cy5
- 2µg/µl DAPI in 4xSSCT
- Vectashield
- Coverslips 20x20mm, 26x74mm
- Fixogum rubber cement
- Oligonucleotides
- Brilliant II QPCR Master Mix (Stratagene, Cat.no. 929551)
- Fast Optical 96-well Reaction Plate (0.1ml)
- Optical Adhesive Cover
- Abi 7500 Fast qPCR system

Although chromogenic RNAish allowed visualization of expressional active area in tissue by eye the sites of expression in the nucleus stayed unrevealed. In contrast

RNA FISH visualized the sites of expression in the nucleus that could be monitored with the confocal microscope to gain information about the spatial control of expression. The RNA FISH procedure on cryosections was modified from the protocol for RNAish on tissue sections (see 3.5.3). In contrast to RNAish, here snap frozen unfixed embryos were used for cryosectioning (see 3.3.5) and sections were immediately processed for RNA FISH. The Bio RNA antisense probe was detected using anti-Biotin antibodies coupled to a fluorescent dye and not by an enzymatic reaction.

The first day of the procedure is identical to RNAish protocol on tissue sections (see 3.5.3). Importantly, sections were taken from dry ice and were immediately fixed in 4%PFA.

The stringency washing steps of the second day were time reduced as follows: 30min in 2xSSC at RT, 30min in 2xSSC at 65°C and 30min in 0.1xSSC at 65°C. Unspecific antibody epitopes were blocked for 20min in 0.1%Saponin, 0.1% Triton X-100, 2% BSA in 4xSSC. Subsequently, probe detection by antibodies was performed by sequential incubation with mouse-anti-Streptavidin-cy5 (1:100), Goat-anti-Mouse-cy5 (1:100) and mouse-anti-Streptavidin-Cy5 (1:100), because Cy5 does not interfere with the autofluorescence of the tissue. Each antibody was incubated for 2.5h at 37°C followed by 3x 10min washing steps in 0.1% Triton X-100 in 4xSSC at 37°C. Sections were counterstained with DAPI (4',6-diamidino-2-phenylindole, 2µg/µl in 4xSSC) for 20min, mounted with Vectashield and kept in the dark on 4°C until confocal microscopy (see 3.7.5).

3.5.5 Relative qPCR using the TaqMan technique

TaqMan hydrolysis probes were used to quantify the PCR amplification over cycles under constant PCR conditions (for PCR conditions table 3.4). In general a TaqMan probe hybridized to the target cDNA in between the forward and the reverse primer and was modified 5' by an reporter dye and 3' by an quencher which suppresses the reporter fluorescence by FRET (Fluorescence resonance energy transfer). During elongation the DNA polymerase degraded the TaqMan probe with its 5'-3' exonuclease activity. Thus the 5'reporter dye was released from the 3'quencher and the increasing fluorescence was detected by the qPCR system over cycles (figure 3.8).

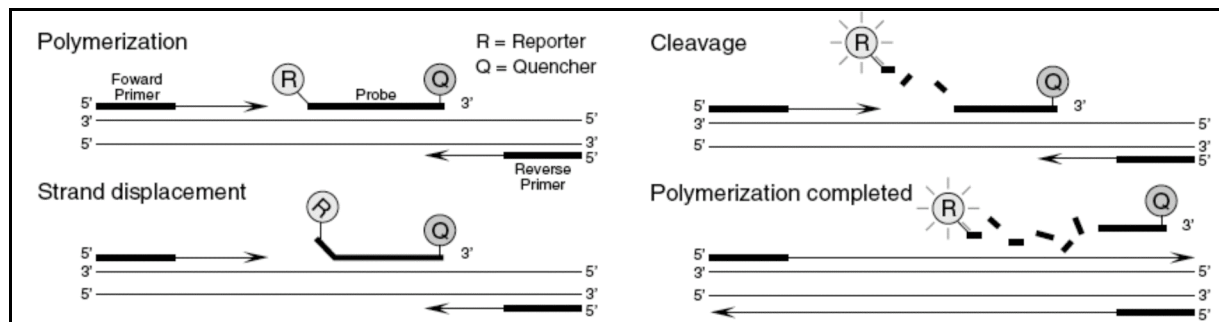


Figure 3.8: Principle of TaqMan quantification in qPCR reactions. During polymerization the leading strand displaces the TaqMan probe 5'. The 5'-3' exonuclease activity of the DNA polymerase cleaves the reporter dye from the quencher. The increasing fluorescence over time is quantified by the qPCR system. (modified from <http://www.stratagene.com>)

3.5.5.1 Probe design and labeling for qPCR

As for RNAish techniques the first step was to design a primer pair to amplify a specific region from cDNA sequence of the target gene (downloaded from www.ensembl.org or <http://www.ncbi.nlm.nih.gov>). In addition, essential was a TaqMan hydrolysis probe to quantify amplification after each cycle in the subsequent qPCR run (see 3.5.5 for details). The TaqMan oligonucleotide was 5' modified by FAM (Fluorophor) and 3' by Dabcyl (non-fluorescent quencher) and bound between the primer pair. The ABI 7500 Fast qPCR system (Applied Biosystems) was supplied by the Primer Express 3.0 software. This software automatically designed the primer pair and TaqMan probe from any input cDNA sequence according to the rules in figure 3.9. Most importantly, the melting point of the primers should be 58-60°C, the melting point of the TaqMan probe 68-70°C and the amplified sequence should be short, between 50 and 150bp, to fit the standardized qPCR conditions (see 3.5.5.2). In addition, a BLAST search (<http://www.ensembl.org/Multi/blastview>) against the reference genome was performed to exclude unspecific amplification products. Primer and Probe sets against mouse *Actb*, *Bcl11a*, *Dach1* and *Gapdh* were designed and are summarized in 3.12.3.

Primer T _m		Probe T _m	
Min Primer T _m	58	Min Probe T _m	68
Max Primer T _m	60	Max Probe T _m	70
Max Difference in T _m of Two Primers	2	Probe GC Content	
Primer GC Content		Min Probe %GC Content	30
Min Primer %GC Content	30	Max Probe %GC Content	80
Max Primer %GC Content	80	Probe Length	
Max Primer 3' GC's	2	Min Probe Length	13
Primer 3' End Length	5	Max Probe Length	30
Primer 3' GC Clamp Residues	0	Probe Composition	
Primer Length		Max Probe G Repeats	3
Min Primer Length	9	Max Num Ambig Residues in Probe	0
Max Primer Length	40	No G at 5' End in Probe	true

Figure 3.9: Primer Express 3.0 guidelines for primer design and TaqMan probe design (modified from Primer Express 3.0 software)

3.5.5.2 qPCR from laser microdissection derived cDNA

Materials

- Oligonucleotides
- Brilliant II QPCR Master Mix (Stratagene, Cat.no. 929551)
- Fast Optical 96-well Reaction Plate (0.1ml)
- Optical Adhesive Cover
- Abi 7500 Fast qPCR system

The used Abi 7500 Fast qPCR system worked in the 96-well plate format sealed with an adhesive cover. Using the Brilliant II QPCR Master Mix (Stratagene) 25 μ l qPCR reactions per well were set up as shown in table 3.4. PCR conditions resulted from a series of test runs for optimization with different concentration of the primer, the TaqMan probe and the reference dye, and could vary for the amplification of other target genes than used herein (Bcl11a, Dach1, Csn1s2a, Csn3). To adjust the variance between different wells a passive reference dye was used (Texas Red). Fluorescence was normalized between the reporter dye and the reference dye. The system was equipped with 5 fluorescence filters and read out the increasing fluorescence of the reporter dye and of the passive reference dye after each cycle (annealing step) and thereafter normalized automatically with the passive reference dye.

A			B	
Cycles	Time	Temperature	qPCR	Reaction
1x	10min	95°C	cDNA from tissue	X μ l
50x	15sec	94°C	2x Mastermix	12.5 μ l
	30sec	60°C	TaqMan probe (10pmol/ μ l)	0.625 μ l
			Fw primer (20pmol/ μ l)	0.5 μ l
			Rev primer (20pmol/ μ l)	0.5 μ l
			Reference dye (10pmol/ μ l)	0.375 μ l
			PCRgrade H2O	X μ l
			TOTAL	25.0 μ l

Table 3.4: qPCR set-up: (A) qPCR cycle conditions for TaqMan cDNA amplification (B) qPCR reaction (X μ l cDNA = 2.0-9.5 μ l, X μ l PCRgradeH2O = 0.5-8.5 μ l).

After the qPCR run the data was relatively quantified with the delta-delta-Ct-method (Livak and Schmittgen 2001) in combination with the geometric-averaging-of-internal-control-genes-method for accurate normalization (Vandesompele et al. 2002). The Ct (= threshold cycle) value marked the cycle in which the reporter fluorescence increased significantly over the background fluorescence. Thus the Ct point marked the beginning of the exponential amplification phase (= log phase). The internal control genes were housekeeping genes (Actb and Gapdh) with a very constant expression level in all tissue and were used for normalization in respect to the target

gene (see (Vandesompele et al. 2002). The qPCR run was started and afterwards evaluated in five steps (figure 3.10 for an example): (1) Ct values for the two internal control genes and the target gene were defined from the amplification curve (Delta Rn vs cycle, Rn = Fluorescence) by setting a threshold in the 7500 Fast System Software. (2) The geometrical mean Ct was calculated from CTs of the two internal control genes. (3) The geometrical mean Ct was then subtracted from the Ct value of the target gene. (4) Steps one to three were done for expressional active and inactive cDNA amplification and the resulting Ct values were subtracted from each other. (5) Finally, the normalized relative expression level difference resulted from the exponentiation of the Ct difference expressed vs. nonexpressed to the basis 2. The basis 2 indicates the doubling of the PCR product with each cycle of PCR amplification.

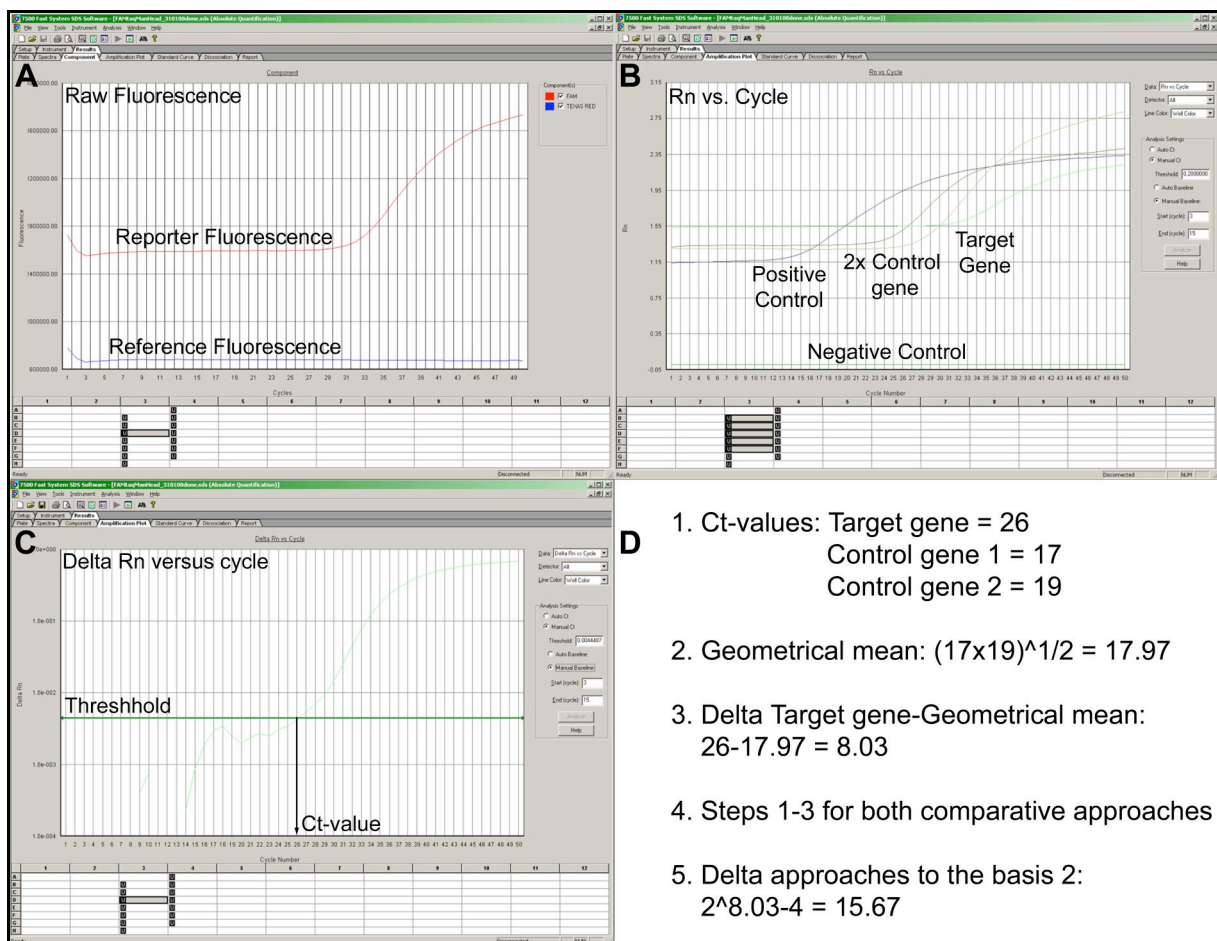


Figure 3.10: (A) Raw fluorescence data over 50 cycles qPCR of the reporter dye and the reference dye (B) Normalized fluorescence difference increase over 50 cycles of qPCR. Positive control with 2.0 μ l cDNA from total RNA mouse E13.0, negative non-template control, 2x control gene and target gene from cDNA from mRNA laser microdissection. (C) Determination of the Ct-values by setting threshold for each qPCR reaction. (D) Calculation steps to obtain the normalized relative gene expression difference between two sample sets. The example results in an expression difference of 15.67 fold. (A-C Screenshots from 7500 Fast software)

3.6 DNA Fluorescence in situ hybridisation (FISH)

The technique of DNA Fluorescence in situ hybridization (FISH) allows for the specific detection and localization of DNA fragments by fluorescently labeled probes on metaphase spreads, in vitro interphase cells or in native tissue by essential compromise five steps: (1) Preparation and labeling of DNA probes, (2) preparation of the in situ specimen (3) denaturation and hybridization of the sample and the probe, (4) stringency washes and (5) detection of hybridization signals.

Probes can be labeled non-radioactively either directly using fluorophore-dUTPs (Tamra, TexasRed) or indirectly by hapten-dUTPs (Biotin, DIG, DNP). Denaturation is implicit to allow probe hybridization to sample sequences with high complementarity. The fast reassociation of the in excess added unlabeled cot-1 DNA (see 3.4.1) suppresses probe hybridization to repetitive sample sequences (= chromosome in situ suppression hybridization). Together with the use of cot-1 DNA the signal to noise ratio of a DNA-FISH experiment is influenced by temperature and salt concentration of post hybridization washing steps. Hapten labeled probe to sample hybridization is finally detected by specific antibodies couple to a fluorophore and DNA counterstained with DAPI (table 3.5 for fluorophores and antibodies). Fluorescence can be visualized by light microscopy in combination with specific filter sets or with a filter-free acoustooptical beam splitter (see 3.7). The experimental parameters influencing a DNA FISH are summarized in table 3.6.

Label	#	Detection Layer	Dilution	Absorption	Emission
Tamra				542nm	568nm
Texas Red				583nm	603nm
Bio-a	1	Streptavidin-Cy5	1/100	649nm	670nm
	2	Goat-anti-Streptavidin-Bio	1/150		
	3	Streptavidin-Cy5	1/100	649nm	670nm
Bio-b	1	Av-Alexa488	1/200	495nm	519nm
Dig	1	Mouse-anti-Dig-Cy5	1/100	649nm	670nm
	2	Goat-anti-Mouse-Cy5	1/100	649nm	670nm
DNP-a	1	Rabbit-anti-DNP	1/150		
	2	Goat-antiRabbit-Alexa488	1/150	495nm	519nm
DNP-b	1	Rabbit-anti-DNP	1/150		
	2	Goat-antiRabbit-Alexa514	1/200	513nm	533nm
DAPI		DNA counterstain	2µg/µl	358nm	461nm

Table 3.5: Used fluorophores, haptens and antibodies for detection of FISH probes. Detection scheme a for Biotin and Digoxigenin was used in 5-color FISH experiments, label scheme b in 6-color FISH experiments. DNA was counterstained with DAPI.

Formamid	In the hybridization mix lowers the DNA melting temperature and thereby prevents the cells material from heat injury
Salt concentration	Determines the ion strength of hybridization and denaturation solutions, stabilization of the DNA double strand
Dextran sulfate in the Hybridization Mix	Internal polymer, that triples the hybridization speed. Dextran sulfate builds a matrix in the hybridization solution resulting in local probe concentration without influencing the stringency
cot-1 DNA	Saturation with cot-1 blocks hybridization to repetitive DNA segments
Bovine serum albumin	Protein solution that blocks antibody binding to unspecific epitopes
Tween 20 detergent	Decreases the surface tension and by that facilitates the antibody penetration
Salmon sperm DNA	Saturation with salmon sperm DNA blocks hybridization to unspecific DNA binding sites

Table 3.6: Experimental parameters influencing the stringency of DNA FISH experiments.

3.6.1 Phi29 amplification and Nick translation labeling of BAC clone DNA

Materials

- BAC clone DNA (see 3.4.2)
- Illustra GenomiPhi V2 DNA amplification kit (GE Healthcare, Code 25-660-30)
- 10x NT-buffer
- dNTP-mix (0.5mM each dATP, dCTP, dGTP, 0.1mM dTTP)
- dUTP-label (1mM) (Tamra, Biotin, DNP, Texas Red)
- 2-Mercaptoethanol (0,1M)
- DNase I
- DNA Polymerase I
- ddH₂O
- Techne TC-312 Thermal Cycler
- Waterbath 15°C

Isolated BAC clone DNA (see 3.4.2) was amplified using the illustra GenomiPhi V2 DNA amplification kit and afterwards fragmented and labeled directly with fluorophore-dUTPs or indirectly by hapten in a Nick translation reaction.

Whole genome amplification using Phi29 polymerase was introduced by (Dean et al. 2001) and resulted in 5-7µg DNA from a minimum of 10ng DNA starting template. Its principle was an isothermal (30°C) rolling circle amplification, based on the prolonged extension of an oligonucleotide primer annealed to a circular template DNA. Thus a continuous sequence of tandem copies of the circle was synthesized (figure 3.11). Exponential amplification was driven from each strand independently by random hexamer primers and a cascade of strand displacement reactions. Phi29 polymerase possessed an extreme processivity and was highly accurate, because of its 3'-

5' exonuclease proof reading activity, resulting in an average amplification length of around 10kb.

GenomiPhi DNA amplification was set up by mixing 1µl of isolated BAC clone DNA with 9µl of template buffer. DNA was denaturated 3min at 95°C and directly chilled on ice. Subsequently, 9µl of reaction buffer and 1µl of enzyme mix were added. Amplification was carried out for 2h at 30°C. Thereafter, the reaction was thermally stopped for 10min at 65°C. All steps were performed sequentially in a thermal cycler. Phi29 amplified DNA was stored at -20°C.

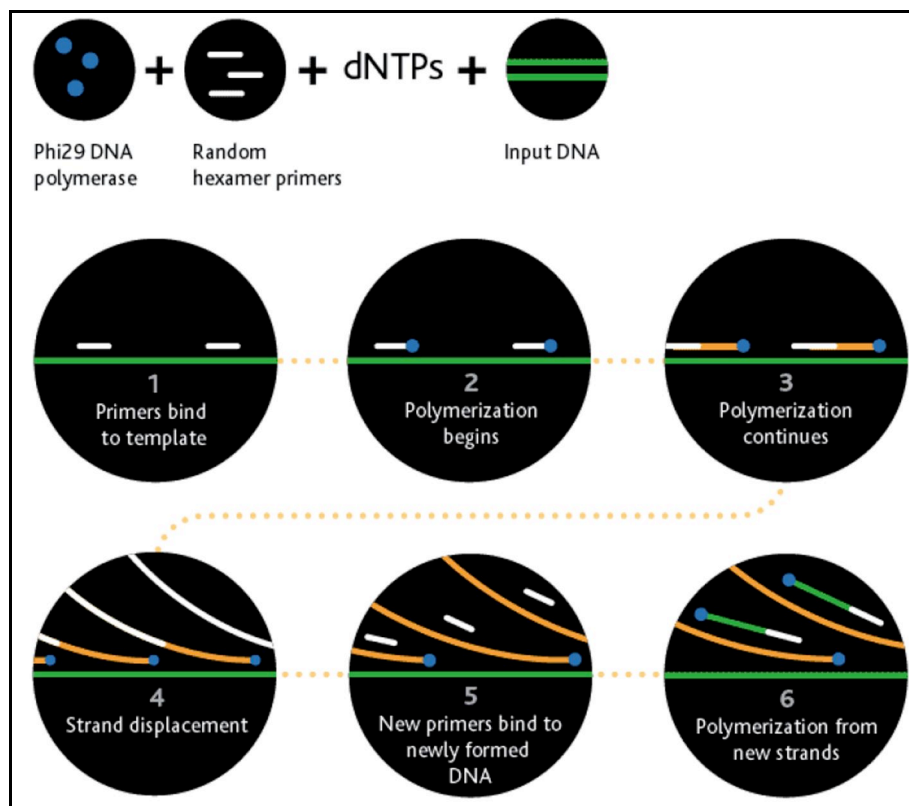


Figure 3.11: Overview of the GenomiPhi V2 DNA amplification (from GE Healthcare)

Subsequent nick translation was used to incorporate labeled-dUTP in Phi29 amplified BAC clone DNA and to fragment DNA to 200-1000bp, in order to allow probe detection and penetration in DNA FISH experiments (see 3.6.3). Nick translation was driven by the interplay of the two enzymes, DNA polymerase I and DNase I. DNase I caused single stranded “Nick” breaks in the DNA template that were targeted by the DNA polymerase I. For repair, starting from the Nick the polymerase catalyzed elongation 5' to 3' and thereby incorporated labeled dUTP and replaced (translates) the nick. DNA was fragmented if DNase I was introducing a 2nd Nick on the opposite strand. Further, per µg DNA a 50µl Nick translation was set up as depicted in table 3.7, was incubated for 1h 45min at 15°C and stopped afterwards on ice (4°C). Tamra-dUTP or TexasRed-dUTP were used to directly label the probe and DNP-dUTP (2-,4-Dinitrophenol), Bio-dUTP or DIG-dUTP for indirect labeling. 1.8µl of

Phi29 amplified DNA equaled about 1µg DNA input and was used per 50µl Nick translation reaction. As DNase I is degraded over time it is important to adjust the working concentration and reaction time accordingly. The desired DNA length (200-1000bp) was checked with 5µl Nick translation reaction on a 1.8% agarose gel and the remaining reaction further digested if necessary. The labeled and fragmented BAC clone DNA was thereafter used in DNA FISH experiments (see 3.6.3).

Nick Translation	Reaction
GenomiPhi product	1.8 µl
NT-buffer 10x	5.0 µl
dNTPmix	5.0 µl
2-mercaptoethanol	5.0 µl
dUTP-label	1.0 µl
Dnase I (1:100-1:200)	1.0 µl
DNA polymerase I	0.8 µl
ddH2O	30.4 µl
TOTAL	50.0 µl

Table 3.7: Nick translation reaction set-up

3.6.2 DOP-PCR amplification and labeling of chromosome painting probes

Materials

- 6-MW amplified chromosome paints
- 6-MW primer (20µM)
- dNTP-Mix (2.5 mM each)
- label dNTP mix (dATP, dCTP, dGTP 2.5 mM each, dTTP 1.8mM)
- Tamra dUTP
- ddH₂O
- 20x W1 (Sigma P-7516)
- Taq-Polymerase
- 10x TAPS 3 (see 3.12.8)
- Techne TC-312 Thermal Cycler
- Easy-Cast™ Electrophoresis System

Chromosome specific painting probes, to target whole chromosomes in interphase nuclei, for mouse chromosomes 5,11,14 (kindly provided by N. Carter Sanger Institute, Hinxton, UK) and chicken chromosomes 1,3,4 (described in (Habermann et al. 2001)) were generated from flow-sorted chromosomes and were readily DOP-PCR amplified with the 6MW-Primer (Telenius et al. 92). The 6MW-Primer sequence (see 3.13.3) has 6 degenerated nucleotide binding sites ($2^6 = 4096$ potential binding targets) in its middle and statistically binds each 1kb to human DNA. Hence, the label PCR run amplified small fragments in the size of 500-1000bp that are effective for DNA FISH (see 3.6.3-3.6.6) and represented the sequence complexity of the entire

chromosome. The same primer was used for reamplification and labeling PCR. Reamplification and labeling PCR (for conditions table 3.8) were run under high stringency conditions to allow amplification only from the PCR product of the primary DOP-PCR product and not from genomic DNA. The painting probe quality was stable for at least five successive rounds of reamplification. All chromosome paints were directly fluorescent labeled by incorporation of Tamra-dUTP. The PCR reactions were set up as summarized in table 3.8 and carried out in a thermal cycler. Label PCR product was concentrated about 100ng/ μ l.

A			B		
Cycles	Time	Temperature	DOP-PCR	Reamp.	Label
1x	3min	94°C	Chromosome paint	1.1 μ l	1.1 μ l
	1min	94°C	6MW-primer	2.5 μ l	2.5 μ l
30x	1min	62°C	TAPS 3 buffer	2.5 μ l	2.5 μ l
	1min30sec	72°C	dNTP	1.5 μ l	
1x	7min	72°C	label dNTP		1.5 μ l
			Tamra-dUTP		1.5 μ l
			20xW1	1.25 μ l	1.25 μ l
			Taq polymerase	0.5 μ l	0.5 μ l
			ddH2O	15.65 μ l	14.15 μ l
			TOTAL	25.0 μ l	25.0 μ l

Table 3.8: (A) PCR conditions for DOP-PCR amplification (B) DOP-PCR reaction with chromosome paint 6MW product for reamplification and label amplification.

3.6.3 Preparation of FISH probe sets

Materials

- Labeled BAC clones
- Labeled chromosome paints
- Mouse cot-1 DNA (500 μ g/ml)
- Chicken cot-1 DNA (see 3.4.1)
- Salmon sperm DNA (1mg/ml)
- Ethanol
- 3M Sodium acetate
- Hybridization buffer (see 3.12.8)

Labeled BAC clone DNA (see 3.6.1) and labeled chromosome painting probes (see 3.6.2) were joined to FISH probe sets. Therefore, desired quantities of label reaction, cot-1 DNA, salmon sperm DNA, 0.1V of 3M sodium acetate and 2.5V of ethanol were mixed. Salmon sperm DNA as carrier DNA and the salt concentration aid efficient DNA precipitation by ethanol. DNA was precipitated at -20°C for 30min, spinned down for 15min at 15115g. Next, the DNA pellet was dried for 1.5-2.5min at 65°C and resuspended in hybridization buffer over night at 39°C by vigorous shaking. Used quantities per probe were dependent on the specimen and are shown in table 3.9.

	chromosome paint	BAC	cot-1 DNA	salmon sperm DNA
Metaphase FISH	1.5 µg	1 µg	7.5µg	5µg
3D-FISH cultur cells	7.5 µg	2 µg	25µg	10µg
3D-FISH tissue sections	10 µg	3 µg	25µg	10µg

Table 3.9: Quantities of labeled chromosome paint DNA, labeled BAC clone DNA, Cot-1 DNA and salmon sperm DNA in FISH experiments to metaphases, 3D-fixed embryonic fibroblasts and tissue cryosections.

3.6.4 Metaphase FISH

Materials

- 70% formamide (v/v) in 1x SSC (pH = 7.0)
- 0.1xSSC
- 2xSSC
- 4xSSCT
- 1x PBS
- 1x PBS, 0.5% Triton-X-100
- Vectashield
- 3% BSA in 4xSSCT; 1%BSA in 4x SSCT
- Fixogum rubber cement
- Antibodies
- DAPI (2µg/ml)
- Cover-slips 15x15mm, 24x60 mm
- Lauda E100 waterbath

FISH on metaphases was used to verify the locus specificity of all BAC clone DNAs together with the harboring chromosome paint probe. Correct hybridization was judged by the position on the correct chromosome in the expected region. This procedure is crucial because, BAC clone DNA can compromise insert sequences with high sequence identity to other genomic loci, as sequence duplications or high dispersed repeats, that can not be suppressed by cot-1 DNA. In addition, the fully automated clone picking procedure from micro titer plates has an error rate of about 10% to pick the wrong BAC clone. Metaphases spreads were prepared according to 3.3.1 and FISH probe sets used as depicted in 3.6.3.

FISH probe set were denaturated for 7min at 72°C and preannealing of cot-1 DNA was allowed for 30min at 37°C. In parallel the metaphase slide was denaturated at 72°C in 70%FA in 2xSSC (pH = 7.0) for 1.5min and dehydrated stepwise in 70%, 90% and 100% ethanol, each for 3min. The probe was then applied on the dried metaphase sample, covered with a 15mmx15mm cover slip, sealed with rubber cement (Fixogum) and left to hybridize over night at 37°C.

The next day the cover slip was removed, followed by stringency washing steps in order to remove unbound and unspecifically hybridized probe for 3x 5min in 0.1xSSC at 62°C. Next, unspecific antibody epitopes were blocked in 3%BSA in 4xSSCT for

20min at 37°C. Antibodies for hapten labeled probe detection were diluted in 1%BSA in 4xSSC-T and the slide was incubated for 45-60min at 37°C. Haptens were fluorescently detected using 1-3 serial incubated antibodies (table 3.5). Excess and unspecifically bound antibody was removed after each incubation step by washing in 4xSSCT for 3x 5min at 42°C. DNA was then counterstained in 2µg/µl DAPI in 4xSSCT for 5min. Finally, the slide was rinses in 4xSSCT to remove excess DAPI solution. Prior to epifluorescent microscopy (see 3.7.3), slides were mounted in antifade solution and covered with a 24x66mm cover slip. Slides were stored at 4°C in the dark.

3.6.5 3D-FISH on embryonic fibroblasts

Materials

- See 3.6.4

FISH to 3D preserved embryonic fibroblasts (see 3.3.2) was carried out as an in vitro control for FISH to in vivo fixed tissue cryosections.

Initially, probe and 3D-fixed cells were denaturated: the probe was incubated for 7min at 72°C and left for prehybridization of cot-1 DNA for 30min at 37°C. 3D-fixed cells were denaturated for 2.5min in 70%FA in 2xSSC (pH = 7.0) and transferred to 50%FA in 2xSSC at 4°C until hybridization. To preserve the 3D morphology of fixed cells, any drying up during handling was avoided. The probe was then applied to the 3D-fixed cells and the slide was sealed with a 15x15mm cover slip and rubber cement. Hybridization was carried out at 37°C for 2 days.

Consecutively, post hybridization stringency washes and antibody detection were done as in metaphase FISH experiment (see 3.6.4), but, counterstaining in 2µg/µl DAPI in 4xSSCT was prolonged to 10min. Hybridized cover slips were finally mounted with antifade and covered with an object slide. Slides were kept at 4°C in the dark.

3.6.6 3D-ImmunoFISH on embryonic fibroblasts

Materials

- See 3.6.4
- 4% BSA in PBST
- 2% BSA in PBST
- additional antibodies
 - rabbit-anti-H3K4me3
 - rabbit-anti-H3K9me3
 - rabbit-anti-H3K27me3
 - goat-anti-rabbit-Biotin

- Techne Dry-Block DB20

3D-Immuno FISH was used to combine the fluorescent detection of distinct histone modifications and of DNA probes. Certain histone modifications are prevalent to active euchromatin, facultative heterochromatin or constitutive heterochromatin and predominantly mark the respective DNA segments (see 2.3).

Immunohistology to detect proteins and cell nucleus permeabilization for efficient 3D-FISH are two conflicting aims. In general, proteins and especially the extracellular matrix and the cytoskeleton hinder the FISH probe to penetrate the nucleus and are therefore destroyed unspecifically during cell permeabilization of 3D-fixed cells by HCl, liquid nitrogen and pepsine. To overcome this limitation, a protocol was developed by (Zinner et al. 2006) to sequentially detect protein and DNA, followed by joint antibody detection. Two steps in the protocol are essential. Firstly, the detection of histone proteins with an antibody coupled to biotin and secondly a post fixation step in 1% PFA for stabilization of cellular morphology. Thus, the epitope-antibody interactions persist through cell permeabilization and denaturation and can be fluorescently detected together with the FISH probe. The Biotin-Avidin affinity is very strong (<http://www.weizmann.ac.il>) and the Biotin epitopes seem to be more inert to the FISH procedure than conventional antibodies.

In a first step, fixed fibroblast cells (see 3.3.2) were taken from 1xPBS and permeabilized in 0.5% Triton X-100 for 15min. Unspecific epitopes were then blocked in 4% BSA/PBST for 10min at 37°C. The histone specific antibodies (rabbit-anti-H3K4me3, rabbit-anti-H3K9me3 or rabbit-anti-H3K27me3) were diluted 1:200 in 2% BSA/PBST and slides incubated for 1h at 37°C. Slides were next washed for 2x5min in 1xPBST. Goat-anti-rabbit-Biotin in 2%BSA/PBST (1:100) was added for 1h at 37°C to detect the primary anti histone antibody. After 2x 5min washing steps in 1xPBST the cells were post-fixed in 1% PFA in 1xPBS. Cells were further permeabilized prior to 3D-FISH in 0.1N HCl for 10min, additionally permeabilized in 0.5% Triton X-100 in 1xPBS for 5min followed by 45 min cryoprotection in 20% glycerol 1xPBS and 4x repeated freezing and thawing in liquid nitrogen. Cells were washed 2x5min in 2xSSC and stored in 50%FA in 2xSSC (pH= 7.0) at 4°C for 24-48h.

Subsequent cells were digested in pepsine (2mg/ml pepsin in 0.01N HCl at 37°C for 5-8min) as described in 3.3.2 with the addition of a 1% PFA in 1xPBS cell fixation step for 3min directly after pepsin inactivation in 1xPBS. Cells were returned to 50%FA in 2xSSC (pH= 7.0) at 4°C for some hours.

The same as usual DNA FISH probe set containing 50%FA (see 3.6.2) was then added on the cell and hybridization area sealed with rubber cement. In contrast to conventional 3D-FISH procedure probe and sample were denaturated together on a hot-block at 72°C for 2min 45sec in hybridization buffer, because denaturation of the

sample in 70%FA resulted in decreased signal strength of histone modification detection. The slide was left to hybridize for 2 days at 37°C.

Post hybridization stringency washes, antibody detection, counterstaining with DAPI, mounting of slides and slide storage was performed as for conventional 3D-FISH experiments (see above).

3.6.7 3D-FISH on tissue cryosections

Materials

- 10mM sodium citrate (pH = 6.0)
- 70% formamide (v/v) in 1x SSC (pH = 7.0)
- 0.1xSSC
- 2xSSC
- 4xSSC, 0.1% Triton X-100
- 1x PBS
- 1x PBS, 0.5% Triton-X-100
- Vectashield
- 2%BSA, 0.1% Saponin, 0.1%Triton X-100 in 4xSSC
- Fixogum rubber cement
- Antibodies (table 3.5)
- DAPI (2 μ g/ml)
- Cover-slips 12x12mm, 24x60 mm
- Microwave (600W)
- Techne Dry-Block DB20
- Lauda E100 waterbath

The 3D-FISH protocol to tissue cryosections was established and published during the course of this work, in collaboration with Dr. I. Solovei and Dr. C. Lanctôt (Solovei 2007). The much higher 3D complexity of native tissue, in comparison to fixed in vitro cells, required a dedicated FISH protocol with special adaptations and changes of most steps. 3D-FISH experiments with probe sets (see 3.6.3) were performed on tissue cryosections (see 3.3.4) of different mouse mammary gland postnatal developmental stage, mouse E7.0 and chicken E21h.

Tissue cryosections were taken from -80°C and placed at 37°C over night to increase the adhesiveness to the object slide and increase 3D-FISH probe penetration ability. The next day, the tissue was incubated for 10min in 10mM sodium citrate (pH = 6.0) and was then placed in a microwave. The tissue was microwaved at 600W until boiling. The microwave was immediately switched off at this point for 1min, and then again heated up until boiling until a total time of 5min was reached.

Tissue was cooled down for 10min at RT, washed twice 5min in 2xSSC and placed to 50%FA in 2xSSC (pH = 7.0) at 4°C at least over night or up to several months.

Next, the DNA FISH probe was pipetted onto the tissue and the hybridization area was sealed with rubber cement and a 12x12mm hybridization chamber (see 3.5.4). To allow for probe penetration into the tissue, the slide was prehybridized for 3-4h at 42°C. For denaturation, a dry block at 82°C for 5min was used. Hybridization of probes was allowed for 3 days at 37°C.

Subsequently, the hybridization chamber was removed and stringency washes were performed as follows: 2 steps of 10min in 2xSSC and 1 step of 10min in 0.1xSSC. Unspecific epitopes were blocked in 2%BSA/0.1% Saponin/0.1%Triton X-100/4xSSC for 20min at 37°C. Saponin and Triton X-100 are detergents further enhancing the antibody penetration into the tissue. Antibodies for sequential hapten detection (see 3.6) were also diluted in 2%BSA/0.1% Saponin/0.1%Triton X-100/4xSSC and slides were incubated for 2.5h at 37°C. The long antibody incubation time was indispensable for effective antibody penetration. After each antibody incubation step the slides were washed 3x 5min in 0.1% Triton X-100/4xSSC at 37°C. The specimen was counterstained either in 2µg/µl DAPI for 20min or in 10µm TOPRO-3 in PBST for 20min, briefly washed in 4xSSC/0.1% Triton X-100 and finally embedded in antifade. Slides were stored at 4°C for confocal microscopy (see 3.7.5)

3.6.8 3D-FISH on RNAish tissue cryosections

Materials

- See 3.6.7

To analyse the nuclear topology with respect to the expression status of the gene locus, targeted by an FISH probe, in complex tissue we sequentially combined chromogenic RNAish (see 3.5.3) with 3D-FISH on the same tissue cryosection. The indigo precipitate at expression sites of target gene was fully stable throughout the entire FISH procedure and could be monitored in the confocal microscope by phase contrast (see 3.7.5). Thus data could be highly confidentially collected from tissue showing a transcriptional active or inactive state of the target gene locus.

Tissue sections were taken from 50%FA in 2xSSC (pH = 7.0) at 4°C and were equilibrated in 10mM sodium citrate (pH = 6.0). As the insoluble indigo precipitate complicated the FISH probe penetration into the nuclei it was necessary to prolong microwave heating in 0.1M sodium citrate from 5min to a total time of 20min. Tissue was cyclically heated up to 600W until boiling and cooled down for 1min. After a cooling down step for 10min at RT, the slides were washed 2x 5min in 2xSSC and placed back to 50%FA in 2xSSC (pH = 7.0) at 4°C over night. Optionally, in case of probe-penetration problems, tissue can be further microwaved the next day or can be

permeabilized additionally with acetone to enhance the tissue accessibility. For protein precipitation treatment with acetone the tissue was incubated in 1xPBS for 10min, placed for 5min in acetone at -20°C, washed in 1xPBS for 1h and returned subsequent to 50%FA in 2xSSC (pH = 7.0).

Hybridization, stringency washes, antibody detection and counterstaining with DAPI were carried out as for 3D-FISH on tissue cryosections without RNAish (see 3.6.7).

3.7 Microscopy

3.7.1 Binocular microscopy

A Zeiss Axiovert 40c or a Zeiss, Stemi 2000-C binocular, both equipped with a Canon PowershotG5 digital camera was used to image chormogenic RNAish experiments on whole mount embryos (see 3.5.2) and tissue cryosections (see 3.5.3).

3.7.2 Phase contrast microscopy

Phase contrast microscopy, performed with a Zeiss, Axiovert 25, coupled a to Canon PowershotG5 digital camera was used to take pictures from tissue-cryosections (see 3.5.3). Further, embryonic fibroblast cell cultures, 3D fixed specimen during pepsine digestion and appropriate hybridization areas were inspected under this microscope.

3.7.3 Laser microdissection microscopy

The used PALM MicroBeam laser microdissection (LCM) system was selectively used to collect cell material from tissue cryosections in a PALM Adhesive Cap (0.2ml) (see 3.4.5) and was equipped with a N₂ UV-laser=337nm emitting pulses of 3ns full width half maximum FWHM duration. The laser beam was coupled into an Axiovert 200 inverted microscope equipped with a CCD camera, a motorized, computer-controlled stage (ROBOT) and a Zeiss LD Plan Neofluar 40/0.5 objective.

3.7.4 Epifluorescence microscopy

FISH experiments to metaphase chromosomes (see 3.6.4) were visualized using a Zeiss, Axiovert2 epiflourescence microscope with a motorized microscope stage and a HBO 100W lamp as light source. 630x magnified images were taken with an 63x objective (Planapochromat) and a system coupled cooled CCD camera (Photometrics KAF 400). The system was equipped with the SP100 – Filterset for Multi-color FISH (Chroma) using DAPI (Ex 350nm, Em 470nm), FITC (Ex 470 nm, Em 522nm), Cy3 (Ex 530nm, Em 565nm), Texas Red (Ex 603nm, Em 631nm) and Cy5 (Ex 630nm, Em 667nm) sequentially. The software Smart Capture 2.0 (Digital

Scientific, Cambridge, England) was used to capture digital images, and to control objectives and fluorescent filters were controlled via the software (see 3.8.1).

3.7.5 Confocal laser scanning microscopy

Light optical serial sections of 3D-fixed specimen were captured using three different Leica laser scanning confocal systems: LCS SP1, LCS SP2 AOBS, LCS SP5 AOBS (table 3.10). By focusing the laser light in one point the specimen was illuminated in only that point. Scattered light above and below the confocal plane was masked by the confocal pinhole. Thus the photomultiplier detected only fluorescence emission light from one point in one plane (a voxel). The specimens were scanned voxel wise in all planes resolution in an image stacks offering the analysis of the nuclear architecture in 3D. Compared to conventional light microscopy confocal microscopy results in a much better resolution. However, the resolution is limited in xy by the defraction limit and in z by the light wavelength and the numerical aperture (Abbe limit $(d) = \lambda/2 \times NA$).

Parameter	LCS SP1	LCS SP2 AOBS	LCS SP5 AOBS
Laserlines	488nm, 544nm,633nm	405nm,458nm,476nm, 488nm, 496nm, 514nm, 561nm, 594nm, 633nm	405nm,458nm,476nm, 488nm, 496nm, 514nm, 561nm, 594nm, 633nm
Photomultiplier	3x PMT	4x PMT	5x PMT
Objective	100x Plan-Apochromat oil immersion 1.4	63x Plan-Apochromat oil immersion 1.4	63x Plan-Apochromat oil immersion 1.4
Scanmode	Between frames	Between frames	Between frames
Frame average	4	4	4
z- step	150nm	150nm	150nm
xy pixel size	49-56nm	52-93nm	47-93nm
Image size	512x512px	512x512px	512x512px

Table 3.10: Technical data for image acquisition with the used LCS SP systems

The LCS SP1 offered three fixed laser lines (488nm, 544nm, 633nm) to excite three different fluorophors: Alexa 488, Tamra and Cy5 or TOPRO-3. It was used to scan chicken E21h embryos and control experiments on embryonic fibroblasts.

The LCS SP5 AOBS system replaced the LCS SP2 AOBS system. Both systems were equipped with acoustooptical beam splitters (AOBS). The AOBS, a combination of a prism and mirrors, adjusts the fixed laserlines (405nm, 458nm, 476nm, 488nm, 496nm, 514nm, 561nm, 594nm and 633nm) to the probe fluorescence (DAPI, Tamra, Alexa 488, Alexa 514, Texas Red and Cy5). Further, the Leica SP detectors allowed to tune the emission bands for all fluorescent channels and hence the separation of excitation and emission of up to 6 fluorescent channles. The LCS SP2 AOBS was used to image all experiments on mouse E7.0, of Dach1 and Bcl11a. The LCS SP5 AOBS was utilized for all experiments related to casein.

3.8 Image Processing

3.8.1 Image Adobe photoshop 7.0

Metaphase FISH images (see 3.7.4) and image galleries of 3D images (see 3.7.5) were further processed with Adobe Photoshop 7.0. Images were corrected for brightness, contrast, color, resolution and size and finally merged to multicolor images.

3.8.2 Huygens Essential 3.5

The Huygens Essential 3.5 software was used to deconvolve the blur in 3D confocal image stacks to further increase the resolution of confocal microscopy by applying an iterative algorithm, the so-called point spread function (PSF). Deconvolution was applied to all image stacks of 3D-Immuno-FISH (see 3.6.6) that were later used for colocalization measurements (see 3.9.2). First 3D-confocal image stacks (resolution 50x50x120nm in 512x512px images) of Tetraspeck Beads of defined size (\varnothing 175nm) were captured in all fluorescent channels. Next, the PSF, separate for each fluorescent channel, was calculated in Huygens Essential. The PSF was an algorithm that was reconstructing the bead of defined size (\varnothing 175nm) from the blurred 3D confocal image. Based on these algorithms the Huygens software corrected all confocal images automatically for scattered light and by that mathematically increased the resolution in light optical sections.

3.8.3 Image J 1.38

All light optical serial sections obtained by confocal microscopy (see 3.6) were processed with Image J. The freeware software Image J was additionally supplied with homemade plugins written by Dr. Joachim Walther and Dr. Boris Joffe (Ludwig-Maximilians-University, Munich).

First, the sections were corrected in z for chromatic aberration. This was necessary because optical lenses have a different defraction index for different wavelengths of light. The focal point of long wavelength light is above the one of short wavelength light. Therefore light optical serial sections of Tetraspeck Beads (\varnothing 500nm) were obtained in all fluorescent channels. The fluorescent channels were then made congruent in Image J and the resulting shift values were used to correct the experimental series. For that single optical sections of image stacks were cut at the end or the beginning of each fluorescent channel.

Then the shift corrected image stacks were further processed for brightness and contrast, unspecific fluorescent background was cut and pictures smoothed by Gaussian blur before the 3D-evaluation. The DAPI counterstain was either segmented from tissue sections with Amira 3.1.1 (see 3.8.4) or otherwise processed

as the fluorescent channels with Image J. The segmented tissue counterstain was used to subtract the fluorescent signals belonging to a particular nucleus in the image stack from the surrounding tissue in advance to processing. Further scale bars were set in images. Finally, before sending the processed files to the quantitative evaluation programs (see 3.9) a user-defined threshold was set to select the voxles incorporated in the evaluations.

3.8.4 AMIRA 3.1.1

As Image J failed to separate single nuclei from the tissue surrounding the counterstain of single nuclei were segmented in 3 dimensions from confocal image stacks by hand in AMIRA 3.1.1 (figure 3.12). Therefore the DAPI tissue image sections were loaded to Amira by adding the proper xyz Voxel dimensions. Via the function sequences *Labelling* → *Label field* and next *View* → *Layout* → *4 Viewer* the tissue section was exhibited separately in x,y and z dimension. Next, the *Exterior* was set to black and the *Inside* to white. Using the *Brush Tool* three optical sections were assigned and filled (*Selection* → *Fill*) in x,y and z. Based on that information AMIRA then calculated with *Selection* and *Warp* a 3-dimensional image of the nucleus. This nucleus was outlined with the function sequence *3D* → *Selection* → + and exported via *File* → *Save Data as* → *2D Tiff*. The 2D Tiff files were loaded into Image J (via *Import* → *image sequence*) and used for image processing (see 3.8.3).

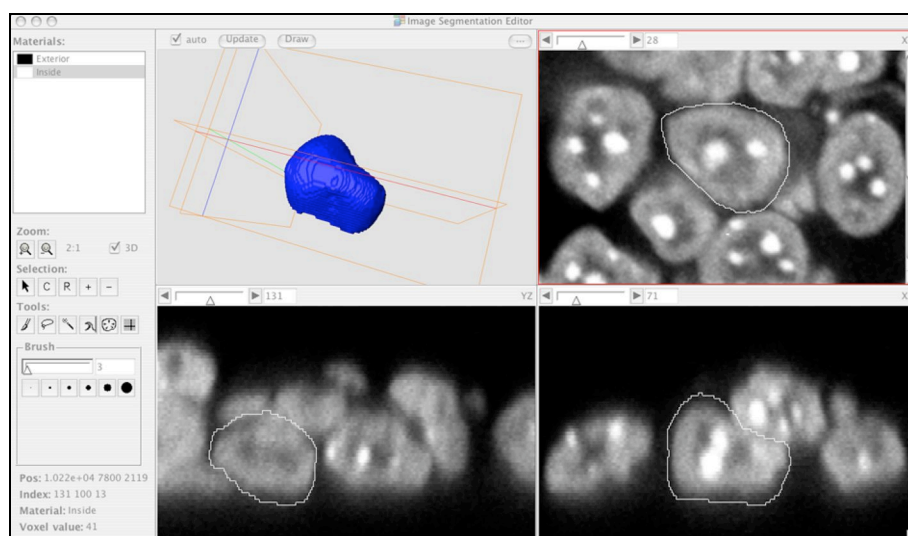


Figure 3.12: Reconstruction of DAPI counterstain from mouse E13.0 neurons in a 20 μ m tissue cryo-section.

3.9 Quantitative evaluation of 3D confocal image stacks

3.9.1 3D relative radial distribution (3D-RRD)

The 3D-RRD software calculated the radial distribution in percentage of DNA FISH probes (see 3.6) referring to the nucleus (developed from Johann von Hase,

Kirchhoff institute for physics, Heidelberg, see (Cremer et al. 2001). Hence, this program normalized for different sizes of nuclei resulting from cell cycle or cell type specific differences.

As 3D-RRD operated with thresholds values between 0 (all pixels) and 1 (no pixel) whereas ImageJ operated with 256 grayscales of 8-bit images the before collected values were adopted. In a first step the program calculated the intensity gravity center of the nucleus. Based on the gravity center the border of the nucleus was determined in a vector-based manner. That way the nuclear space was subdivided into 25 equidistant shells, following the shape of the nucleus. Each signal voxel of each fluorescent channel was then assigned to a shell resulting in the probe distribution per shell averaged over all nuclei. This results were plotted as an Excel graph and the mean relative radius (ARR) of each fluorescent channel in each nucleus was used for pairwise statistical testing between experiments (3.10).

3.9.2 Enhanced distance measurement tool (EDMT)

The enhanced distance measurement tool (EDMT) (programmed by Tobias Thormeyer, Ludwig-Maximilians-University, Munich, see Albiez et al. 2006) was used to measure the shortest distance in nm to the surface of a reference structure and is independent of the shape and the size of this reference. As reference structures chromosome territories and immunostaining of histone codes were chosen. The program converted the 8-bit gray scale images from image J (see 3.8.4) to binary images (black and white), applying the user set threshold determined in Image J and a minimum object size to exclude unspecific objects from the evaluation. The distance to the reference structure was calculated in a voxel-based manner. The step size of measurements was identical with scanned z-step distance in the confocal image stacks. The resulting distance distribution of each fluorescent channel weighted over all evaluated nuclei was graphically illustrated in Excel. The mean distances of each fluorescent channel in each nucleus were used for pair-wise statistics (see 3.10).

3.9.3 Nuclear Volume and Roundness (EDMT)

By evaluating the nucleus against itself, as the reference and as evaluation channel in EDTM the number of surface voxels and the total number of volume voxles was obtained. Then the nuclear volume was calculated from the total number of voxels by applying the scanned xyz voxel dimensions. The nuclear roundness was estimated by dividing the number of total voxles by the number of surface voxels. Smaller roundness values indicated that the nucleus differed more from the perfect sphere. Volumes and roundness of experiments were statistically tested in pairs (see 3.10).

3.9.4 Distances and angles (DistAng)

The program distances and angles (DistAng) was developed by Tobias Thormeyer (Ludwig-Maximilians-University, (Grasser et al. 2008). The program measured euclidian distances and angles between signal gravity centers in confocal image stacks based on the xyz voxel dimensions. Evaluated signals were user-defined by an intensity-dependent object threshold and a minimum object size resulting in binary images (black and white). Next, the program defined the combined geometrical center of all objects in each fluorescent channel. Therefore, it was necessary to save the two homologous DNA FISH signals segments as separate images in ImageJ (see 3.8.4) before running the evaluation. A programmed matrix listed all possible angles and distances between up to four fluorescent channels. An algorithm calculated mean distances and angles and the standard deviation of the mean. Experimental data was tested pair-wise using with the U-test (see 3.10).

3.10 Statistical analysis

All statistical tests were performed using the U-test (Mann-Whitney rank sum test). The U-test (equivalent to the Wilcoxon test) is a non-parametric test for assessing whether two samples of observations come from the same distribution or not. The test allows comparison of the non-normal but similar distributed datasets herein and is recommended by Ronneberger et al. 2008 and <http://www.vislab.ch>. p values below 0.05 (statistical probability < 95%) were accepted as significant different distributions.

3.11 Web based resources

Link	Task
http://www.ncbi.nlm.nih.gov/sites/entrez	UniGene Expression profiler
http://www.ensembl.org/index.html	Genome Browser, Genome BLAST search
http://genome.ucsc.edu/	Genome Browser, BAC End Pairs, Most Conserved
http://www.informatics.jax.org/	Mouse Genome Informatics
http://embryology.med.unsw.edu.au/	Embryogenesis
http://www.hspp.ucla.edu/wonglab/Conc-calculator.htm	RNA/DNA concentration calculator from OD measurements
http://www.ch.embnet.org/software/LALIGN_form.html	Alignment of short sequence motives
http://tools.neb.com/NEBcutter2/index.php	Restiction enzyme cutting site search
http://www.vislab.ch/Lehre/EST/est.html	Decision tree for statistical testing
http://www.swarthmore.edu/NatSci/sgilber1/D_B_lab/Mouse/mouse_dissection.html	Dissection of mouse embryos from pregnant mice

3.12 Materials

3.12.1 Chemicals

Chemicals	Company
Acetone	Merck, Darmstadt, Germany
Agarose SeaKem ME	FMC Rockland, Rockland, USA
BCIP	Gibco-BRL, Karlsruhe, Germany
Bromophenol Blue	Sigma-Aldrich, Deisenhofen, Germany
BSA (for SSC solution)	ICN Biomedicals, Frankfurt, Germany
BSA (for PBS solution)	Sigma-Aldrich, Deisenhofen, Germany
Colcemid (10µg/ml)	Biochrom AG, Berlin, Germany
Chloramphenicol	Sigma-Aldrich, Deisenhofen, Germany
DAPI	Sigma-Aldrich, Deisenhofen, Germany
Denhardts	Invitrogen, Scotland
Dextran sulfate	Amersham Pharmacia, Wien, Austria
Diethyl-pyro-carbonate	Sigma-Aldrich, Deisenhofen, Germany
Dextran sulfate	Sigma-Aldrich, Deisenhofen, Germany
Diethyl-ether	Merck-Schuchardt, Hohenbrunn, Germany
DMSO	Sigma-Aldrich, Deisenhofen, Germany
Dry-ice (CO ₂ (l))	Air Liquide, Düsseldorf, Germany
DTT	Sigma-Aldrich, Deisenhofen, Germany
EDTA	Merck, Darmstadt, Germany
Ethanol	Merck, Darmstadt, Germany
Ethidium-bromide	Sigma-Aldrich, Deisenhofen, Germany
Formamide	Merck, Darmstadt, Germany
Formamide deionised	Sigma-Aldrich, Deisenhofen, Germany
Fixogum	Marabu, Tamm, Germany
Glacial acid	Merck, Darmstadt, Germany
Glycerine	Merck, Darmstadt, Germany
HCl 1N	Merck, Darmstadt, Germany
Hematoxylin	Merck, Darmstadt, Germany
Magnesiumchloride Hexahydrate	Merck, Darmstadt, Germany
Mercaptoethanol	Merck, Darmstadt, Germany
Methanol	Merck, Darmstadt, Germany
MgCl ₂ x 6 H ₂ O	Merck, Darmstadt, Germany
MOPS	MP Biomedicals, Solon, USA
Na ₂ HPO ₄ x H ₂ O	Merck, Darmstadt, Germany
NaH ₂ PO ₄ x 2H ₂ O	Merck, Darmstadt, Germany
NBT	Gibco-BRL, Karlsruhe, Germany
Nitrogen (l)	Air Liquide, Düsseldorf, Germany
Paraformaldehyde	Merck, Darmstadt, Germany
Potassium Chloride	Merck, Darmstadt, Germany
Saponin	Serva, Heidelberg, Germany

SDS	Sigma-Aldrich, Deisenhofen, Germany
Sodium acetate	Merck, Darmstadt, Germany
Sodium chloride	Merck, Darmstadt, Germany
Sodium dihydrogenphosphat	Merck, Darmstadt, Germany
Sodium hydrogenphosphate	Merck, Darmstadt, Germany
Succhrose	Merck, Darmstadt, Germany
TAPS	Sigma-Aldrich, Deisenhofen, Germany
TOPRO-3	Molecular Probes, Carlsberg, USA
Tris	Sigma-Aldrich, Deisenhofen, Germany
Tris-Hcl (pH 8.0)	Sigma-Aldrich, Deisenhofen, Germany
Triton X-100	Merck, Darmstadt, Germany
Tween-20	Merck, Darmstadt, Germany
W1 Detergent	Sigma-Aldrich, Deisenhofen, Germany

3.12.2 Nutrient medium and additives

Nutrient medium	Company
FBS Superior	Biochrom AG, Berlin, Germany
Penicillin/Streptomycin	Biochrom AG, Berlin, Germany
DMEM with stable Glutamin	Biochrom AG, Berlin, Germany

3.12.3 Enzymes, nucleic acids, oligonucleotides and BAC clones

Enzymes	Company
DNA Polymerase I	Roche, Mannheim, Germany
Nuclease S1	Roche, Mannheim, Germany
Pepsin	Sigma-Aldrich, Deisenhofen, Germany
Proteinase K	Roche, Mannheim, Germany
Restrictionenzymes	New England Biolabs, Ipswich, UK
Rnase A	QiaGen, Hilden, Germany
Rnase H	New England Biolabs, UK
Superscript reverse transcriptase	Invitrogen, Scotland, UK
T3 RNA polymerase	Roche, Mannheim, Germany
T7 RNA polymerase	Roche, Mannheim, Germany
Taq – polymerase	Amersham, Braunschweig, Germany
Trypsin/EDTA	Biochrom AG, Berlin, Germany

Nucleic acids	Company
Aminoallyl dUTP	Sigma-Aldrich, Deisenhofen, Germany
Baker's yeast RNA	Sigma-Aldrich, Deisenhofen, Germany
Biotin	Molecular Probes, Carlsbad, USA

Chicken Cot-1 DNA	Home made
Deoxynucleoside Triphosphat Set (dNTPs)	Roche, Mannheim, Germany
Digoxigenin	Molecular Probes, Carlsbad, USA
Dinitrophenol	Molecular Probes, Carlsbad, USA
Gene Ruler® 100bp DNA ladder	Fermentas, St. Leon-Rot, Germany
Gene Ruler® 1kb DNA ladder	Fermentas, St. Leon-Rot, Germany
Lamda/Hind III ladder	Roche, Mannheim, Germany
Mouse Cot-1 DNA	Gibco-BRL, Karlsruhe, Germany
Salmon sperm DNA	Gibco-BRL, Karlsruhe, Germany
Tamra	Molecular Probes, Carlsbad, USA
TexasRed	Molecular Probes, Carlsbad, USA

Oligonucleotides	Sequence 5'-3' (ordered at MWG-Biotech, Ebersberg)
6MW-primer	CCGACTCGAGNNNNNNATGTGG
T7 Bcl11a Fw mouse	TACGAATTAACCCCTCACTAAAGGGGAGATGCACACGGAGCTCTAATCC
T3 Bcl11a Rev mouse	TACGTAATACGACTCACTATAGGGGAGATCGCATGACTTGGACTTGACC
T7 Bcl11a Fw chicken	TACGAATTAACCCCTCACTAAAGGGGAGACAGGACTAGGTGCAGAGTGC
T3 Bcl11a Rev chicken	TACGTAATACGACTCACTATAGGGGAGAAGATCGAACTCCTTCTCCAGC
T7 Csn1s2a Fw mouse	TACGAATTAACCCCTCACTAAAGGGGAGAGTGAGGAATCATCTGCCAGC
T3 Csn1s2a Rev mouse	TACGTAATACGACTCACTATAGGGGAGATGCAGTTAATACGGCTCCACAG
T7 Csn3 Fw mouse	TACGAATTAACCCCTCACTAAAGGGGAGATCGTAGTTGTGAATATTCTGGC
T3 Csn3 Rev mouse	TACGTAATACGACTCACTATAGGGGAGATGCTGCAGTTGAGGACACTGG
T7 Dach1 Fw mouse	TACGAATTAACCCCTCACTAAAGGGGAGAGTAGCAGCAGCAGCTGCCG
T3 Dach1 Rev mouse	TACGTAATACGACTCACTATAGGGGAGAGGAGGTAGTGGTTGTCCATGC
T7 Dach1 Fw chicken	TACGAATTAACCCCTCACTAAAGGGGAGACAAGATGGTGGATCTGAGG
T3 Dach1 Rev chicken	TACGTAATACGACTCACTATAGGGGAGAAGAGCTCCATCTTCAGC
qPCR Actb Fw	ACGGCCAGGTCATCACTATTG
qPCR Actb Rev	CAAGAAGGAAGGCTGGAAAAGA
qPCR Actb TaqMan	FAM-CAACGAGCGGTTCCGATGCCCC-Dabcyl
qPCR Bcl11a Fw	TCAAGCTGGAGAAGGAGTTTGAC
qPCR Bcl11a Rev	GCGAGCCACTGCGAATACA
qPCR Bcl11a TaqMan	FAM-CGGCCGCGATGCCTAACACG-Dabcyl
qPCR Dach1 Fw	TTAGCCATCCTCTCAACCATCTG
qPCR Dach1 Rev	GCATCATCATAAAAGGAAGTTCCA
qPCR Dach1 TaqMan	FAM-AGCACAGCCACCTTCCGCCAAA-Dabcyl
qPCR Gapdh Fw	GACGGCCGCATCTTCTTGT
qPCR Gapdh Rev	CACACCGACCTTACCATTTT
qPCR Gapdh TaqMan	FAM-CAGTGCCAGCCTCGTCCCGTAGA-Dabcyl

Underlined sequence: T7 or T3 promotor sequence

Lab ID	BAC clone ID	Region	Species	Genomic locus
11	RP24-338O2	5'Dach1	MMU	chr14:97,283,971-97,467,211

12	RP23-195C20	5'Dach1	MMU	chr14:97,470,666-97,663,785
13	RP23-414J2	5'Dach1	MMU	chr14:97,687,399-97,889,113
14	RP24-118H12	5'Dach1	MMU	chr14:97,891,271-98,060,902
15	RP23-17E17	Dach1 gene	MMU	chr14:98,160,911-98,402,842
16	RP24-86G10	Dach1 gene	MMU	chr14:98,402,009-98,567,946
17	RP23-167A7	3'Dach1	MMU	chr14:98,700,437-98,899,660
18	RP24-296L19	3'Dach1	MMU	chr14:98,827,383-99,014,875
19	RP24-318D24	3'Dach1	MMU	chr14:99,033,144-99,219,003
20	RP24-83O8	3'Dach1	MMU	chr14:99,187,682-99,398,697
21	CH261-99M7	5'Dach1	GGA	chr1:160,389,150-160,565,419
22	CH261-126B13	5'Dach1	GGA	chr1:160,590,328-160,746,225
23	CH261-178B1	Dach1 gene	GGA	chr1:160,758,691-160,939,180
24	CH261-116N16	Dach1 gene	GGA	chr1:160,949,443-161,111,939
25	CH261-5O20	3'Dach1	GGA	chr1:161,167,811-161,345,706
27	RP24-158C9	Bcl11a gene	MMU	chr11:23,929,452-24,082,617
28	RP23-378N18	3'Bcl11a	MMU	chr11:24,294,373-24,475,845
29	RP23-187D4	3'Bcl11a	MMU	chr11:24,582,413-24,791,910
30	RP23-271I6	3'Bcl11a	MMU	chr11:24,951,704-25,176,260
31	RP23-270B24	3'Bcl11a	MMU	chr11:25,298,737-25,482,459
32	RP23-257B4	3'Bcl11a	MMU	chr11:25,574,727-25,787,115
33	RP23-232O13	3'Bcl11a	MMU	chr11:25,891,070-26,097,060
34	RP23-414P6	5'Bcl11a	MMU	chr11:23,138,721-23,358,674
35	CH261-85B24	Bcl11a gene	GGA	chr3:1,732,461-1,901,439
36	CH261-67F7	5'Bcl11a	GGA	chr3:1,403,944-1,645,629
37	CH261-172J9	5'Bcl11a	GGA	chr3:1,189,917-1,364,613
38	CH261-75C5	5'Bcl11a	GGA	chr3:933,424-1,160,861
39	CH261-117L22	3'Bcl11a	GGA	chr3:2,182,959-2,356,663
127	RP24-167M18	3'Meis1	MMU	chr11:18,551,129-18,698,261
128	CH261-104M14	3'Meis1	GGA	chr3:10,593,852-10,820,885
129	RP23-224N6	3'Zfx1b	MMU	chr2:44,990,628-45,141,686
130	CH261-89C14	3'Zfx1b	GGA	chr7:35,087,237-35,310,000
131	RP23-438F24	3'Zfp536	MMU	chr7:37,754,594-37,922,530
132	CH261-117L3	3'Zfp536	GGA	chr11:9,543,172-9,758,619
133	RP23-138E8	3'Foxp2	MMU	chr6:14,874,863-15,067,127
134	CH261-44N4	3'Foxp2	GGA	chr1:27,927,549-28,141,738
138	RP23-380F12	5'Csn	MMU	chr5: 87,792,870-87,986,557
139	RP23-314H12	Csn cluster	MMU	chr5:88,140,018-88,316,955
140	RP24-472J1	3'Csn	MMU	chr5: 88,967,666-89,209,414
141	CH261-187A23	5'pseudo Csn	GGA	chr4:51,503,522-51,695,896
142	CH261-110C4	Pseudo Csn	GGA	chr4:52,373,840-52,568,888
143	CH261-121A24	3'pseudo Csn	GGA	chr4:53,150,259-53,315,793

Genomic locus identified in UCSC genome browser (mouse assembly july 2007, chicken assembly may 2006). 5' and 3' indicated relative position up- or downstream from to the reference gene.

3.12.4 Antibodies and Avidin conjugates

Antibody	Company
Anti-Digoxigenin-AP (Fab-Fragments)	Roche, Mannheim, Germany
Mouse-anti-Streptavidin Cy5	Biotrend, Köln, Germany
Goat-anti-Streptavidin-Biotin	Dianova, Hamburg, Germany
Goat-anti-Mouse Cy5	Dianova, Hamburg, Germany
Rabbit-anti-H3K4triCH3	Abcam, Cambridge, UK
Rabbit-anti-H3K9triCH3	Millipore, Billerica, USA
Rabbit-anti-H3K27triCH3	Millipore, Billerica, USA
Goat-anti-Rabbit-Biotin	Dianova, Hamburg, Germany
Rabbit-anti-DNP	Sigma-Aldrich, Deisenhofen, Germany
Goat-anti-Rabbit-Alexa488	Molecular Probes, Carlsbad, USA

3.12.5 Buffers and solutions

Cryoprotection

Buffer/solutions	Ingredients	Volume
1M Na ₂ HPO ₄	Na ₂ HPO ₄ x H ₂ O	134g in 1l H ₂ O
1M NaH ₂ PO ₄	NaH ₂ PO ₄ x 2H ₂ O	178g in 1l H ₂ O
0.1M Phosphate buffer	1M Na ₂ HPO ₄ 1M NaH ₂ PO ₄	<u>400ml:</u> 23.08ml 1M Na ₂ HPO ₄ , 16.92ml 1M NaH ₂ PO ₄ , 360ml H ₂ O
5% Sucrose	Sucrose 0.1M Phosphate buffer	5g Sucrose in 1l 0.1M phosphate buffer
20% Sucrose	Sucrose 0.1M Phosphate buffer	20g Sucrose in 1l 0.1M phosphate buffer
95% Ethanol	Ethanol	<u>1l:</u> 950ml ethanol, 50ml H ₂ O

Whole mount RNA in situ

Buffer/solutions	Ingredients	Volume
Blocking solution whole mount RNAish	1x MABT horse serum salmon sperm	20 ml MABT 5 ml horse serum (fin.conc. 20%) 100 µl salmon sperm (stock: 10 mg/ml)
Pre-hybridisation-mix for whole mount RNAish	deionised formamide 20x SSC (pH= 4.5) Tween 20 Triton-X-100 salmon sperm	10 ml deionised formamide 5 ml 20x SSC (pH= 4.5) 40µl Tween 20 (=0.2 % final conc.) 100µl Triton-X-100 (=0.5% final conc.) 80µl salmon sperm (stock: 10 mg/ml)

	yeast RNA DEPC H ₂ O	40 µl yeast RNA (stock: 25 mg/ml) add 20 ml DEPC H ₂ O (=4,46 ml)
5x MABT	MAB Tween	<u>100 ml:</u> 100 ml MAB 400 ml dH ₂ O 1 ml Tween-20
25% Methanol	Methanol 1x PBS	<u>100 ml:</u> 25 ml MeOH + 75 ml PBS
50% Methanol	Methanol 1x PBS	<u>100 ml:</u> 50 ml MeOH + 50 ml PBS
75% Methanol	Methanol 1x PBS	<u>100 ml:</u> 75 ml MeOH + 25 ml PBS
NTMT-buffer	5M NaCl 2M Tris pH 9.5 MgCl ₂ Tween-20 H ₂ O	<u>50ml:</u> 1ml 5M NaCl 5ml 2M Tris pH 9.5 1.25ml MgCl ₂ 5ml 1% Tween-20 37.75ml H ₂ O
PBT	1x PBS 0.1% Triton-X-100	<u>100 ml:</u> 100 ml PBS + Triton
Sodium citrate	Sodium citrate	<u>1L:</u> 2.941g dissolve in 1000ml H ₂ O bidest, adjust to pH=6.0
Solution I	Formamide 5x SSC Tween-20 Triton-x-100	50% formamide 5x SSC 0.2% Tween-20 0.1% Triton-x-100
Solution II	2x SSC Tween-20 Triton-x-100	50% formamide 2x SSC 0.2% Tween-20 0.1% Triton-x-100
Solution III	5x SSC Tween Triton-x-100	5x SSC 0.2% Tween 0.1% Triton-x-100

RNA in situ to tissue sections

Buffer/solutions	Ingredients	Volume
Buffer 1	Tris NaCl	<u>500ml:</u> 6.07g Tris, 4.38g NaCl, adjust to pH 7.5
Buffer 2	Buffer 1	<u>10 ml:</u>

	Horse serum Salmon sperm	8 ml buffer 1, 2 ml horse serum, 40µl salmon sperm, heat for 30 min at 70°C
Buffer 3	Tris NaCl MgCl ₂	<u>500 ml:</u> 6.07g Tris, 2.92g NaCl, 2.38g MgCl ₂ adjust to pH 9.5
H ₂ O (DEPC)	H ₂ O DEPC	0.1% DEPC incubated over night under constant stirring
20x PBS (DEPC)	20x PBS DEPC	0.1% DEPC incubated over night under constant stirring
20x SSC (DEPC)	20x SSC DEPC	0.1% DEPC incubated over night under constant stirring
1x TE (wash)	Tris 10mM EDTA 1mM pH= 8.0	10 ml Tris 1 ml EDTA
Pre-hyb-mix for cryosections	Deionised formamide 5x SSC salmon sperm yeast RNA	5 ml deionised formamide, 5 ml 5x SSC, 40µl salmon sperm, 20µl yeast RNA

Nick Translation:

Buffer/solutions	Ingredients	Volume
dNTP-Mix for Nick Translation	dATP, dCTP, dGTP, dTTP (je 100mM Stock), H ₂ O bidest	2mM solution: 2µl 100mM Stock, 100µl H ₂ O bidest <u>400µl dNTP Mix:</u> each 100µl 2mM dATP,dGTP, dCTP, 20µl 2mM dTTP, 80µl H ₂ O bidest
NT-Puffer	NT-Puffer 1M Tris-HCl (pH = 7.5) 1M MgCl ₂ , BSA	<u>100ml :</u> 50ml 1M Tris-HCL, 50mg BSA, 45ml H ₂ O bidest
Mercaptoethanol (0,1M)	Mercaptoethanol H ₂ O bidest	0.1ml Mercaptoethanol + 14.4ml H ₂ O bidest

DOP-PCR:

Buffer/solutions	Ingredients	Volume
10x TAPS PCR Puffer (Nicht für die primäre Amplifikation)	250mM TAPS (pH9.3) 500mM KCl 20mM MgCl ₂	<u>40ml Ansatz:</u> 2,43g TAPS, 1,49g KCl, 800 µl 1M MgCl ₂ , 30ml H ₂ O, adjsut to pH 9,3 80µl 14.4M Mercaptoethanol, ad 40ml H ₂ O, adjust to

	14,4 M Mercaptoethanol H ₂ O	pH 8.5
W1 Detergenz	20x W1 H ₂ O bidest	<u>100ml:</u> 0.5g W1 + 100ml H ₂ O bidest
dNTP Mix für Markierungs-PCR	dATP, dCTP, dGTP, dTTP (each 100mM Stock), H ₂ O bidest	<u>500µl dNTP Mix:</u> je 10µl dATP, dCTP, dGTP + 8µl dTTP, ad 500µl H ₂ O bidest
dNTP Mix für Re-amplikations-PCR	dATP, dCTP, dGTP, dTTP (each 100mM Stock), H ₂ O bidest	<u>500µl dNTP Mix:</u> each 10µl dATP, dCTP, dGTP, dTTP ad 500µl H ₂ O bidest

Gelelectrophoresis:

Buffer/solutions	Ingredients	Volume
TAE-buffer (pH 8.0)	40mM Tris-acetate 1mM EDTA	<u>50x TAE:</u> 242.2g Tris + 18.6g EDTA+ 57,1ml conc. Acetic acid, ad 1L H ₂ O bidest, pH 8
1% Agarose in TAE-buffer	Agarose 1x TAE-buffer	<u>100ml:</u> 1g Agarose in 100ml 1xTAE-buffer dissolve in microwave oven
3M NaAc (pH= 5.2)	NaAc	
0.5M EDTA (pH = 8.0)	EDTA	<u>100ml:</u> 18.6g EDTA in 100ml H ₂ O (DEPC)
10xMOPS	MOPS NaAc EDTA	<u>1l:</u> 41.2g MOPS, 13.3ml 3M NaAc, 10ml 0.5M EDTA
RNA gel loading buffer	Glycerol EDTA Bromophenol blue	<u>10ml:</u> 5ml glycerol, 20µl 0.5M EDTA, 0.025g bromophenol blue, 5ml H ₂ O (DEPC)

DNA-FISH

Buffer/solutions	Ingredients	Volume
SSC pH 7	3 M NaCl, 0.3 M NaCitrate, H ₂ O bidest	<u>20x SSC:</u> 350.6g NaCl +176.4g NaCitrat ad 2l H ₂ O bidest, adjust pH 7.0, autoclave
PBS pH 7.4	140mM NaCl 2.7 mM KCL 6.5 mM Na ₂ HPO ₄ 17.6 mM KH ₂ PO ₄	<u>20xPBS:</u> 320g NaCl+ 8g Kcl +57.6g Na ₂ HPO ₄ + 9.6g KH ₂ PO ₄ ad 2l H ₂ O adjust pH 7,4, autoclave

	1.5 mM KH ₂ PO ₄ H ₂ O bidest	
4xSSC/ 0.2% Tween	4x SSC Tween 20	<u>1L:</u> 1000ml 4x SSC+ 2ml Tween 20
1xPBS/ 0.05% Tween	1x PBS Tween 20	<u>500ml:</u> 500 ml 1xPBS + 250µl Tween 20
3% BSA /4x SSC 0.2% Tween	4x SSC Tween 20 BSA (for SSC)	<u>100ml:</u> 3g BSA + 100ml 4x SSC 0.2% Tween; steril filtration of solution
1% BSA /4x SSC 0.2% Tween	4x SSC Tween 20 BSA (for SSC)	<u>100ml:</u> 1g BSA + 100ml 4x SSC 0.2% Tween; steril filtration of solution
2% BSA /4x SSC/0.1% Triton/ 0.05% Tween /0.1% saponin for tissue sections	4x SSC BSA Saponin TritonX100	<u>100 ml:</u> 2g BSA + 100 ml 4x SSC 100µl Triton, 1g saponin, 50 µl Tween-20
Paraformaldehyde-solution 4%	Paraformaldehyde PBS	<u>100ml:</u> Fibroblasts: 4g in 100ml 1xPBS, heat powder until dissolved, cool to rt
TritonX-100-solution(0.5%)	1x PBS Triton-X-100	<u>100ml:</u> 99.5ml 1xPBS + 0.5ml TritonX100

Hybridisation buffer	Formamide 50% Dextranulfate 20x SSC 1M NAPO ₄ Puffer 10%SDS 50x Denhardts H ₂ O bidest	<u>10ml Ansatz:</u> 5ml Formamide, 2ml 50% Dextranulfate, 1ml 20x SSC, 400µl 1M sodiumphosphate-buffer, 100µl 10% SDS, 200µl 50x Denhardts , 1,3ml H ₂ O
50% Dextranulfate	Dextranulfate H ₂ O bidest	<u>100ml:</u> 50g Dextranulfate ad 100ml H ₂ O, dissolve at 60°C
1M Natriumphosphate-buffer	1M Na ₂ HPO ₄ 1M NaH ₂ PO ₄	577µl 1M Na ₂ HPO ₄ , 423µl 1M NaH ₂ PO ₄
10% SDS solution	SDS H ₂ O	<u>100ml:</u> 10g SDS ad 100ml H ₂ O
Denaturation solution: 70% Formamide in SSC	Formamide 2x SSC	<u>100ml:</u> 70ml Formamide + 30ml 2x SSC
Stringency- washing	Formamide	<u>200ml:</u>

solution 50% formamide in SSC	2x SSC	100 ml Formamide + 100ml 2x SSC
DAPI (0.2µg/ml)	DAPI-Stock solution (500µg/ml)	<u>50ml</u> : 50ml 4xSSC/T + 0.2ml DAPI-Stock solution
NaCl-solution (5M)	NaCl H ₂ O	<u>100ml</u> : 29.2g NaCl ad 100ml H ₂ O bidest
MgCl ₂ (1M)	MgCl ₂ x 6H ₂ O H ₂ O	<u>100ml</u> : 20.33g MgCl ₂ x 6H ₂ O dissolve in 80ml H ₂ O , ad 100ml H ₂ O
Tris HCL (1M)	Tris-HCL H ₂ O	<u>100ml</u> : 12.11g Tris-HCL ad 100ml H ₂ O bidest, pH 9.5
Hypotonic solution: 0.075M KCL	KCL H ₂ O bidest	<u>100ml</u> : 0.56g KCL in H ₂ O bidest

Fixative	Methanol Glacial acid	Methanol, glacial acid 3:1 (v/v)
HCl-solution (0.1N, 0.01 N)	1N Hcl H ₂ O dest	1N HCL dilute with H ₂ O bidest 1:10 or 1:100
Pepsin-solution	10% Pepsin in H ₂ O 0,01M HCL	<u>100ml</u> : <u>Metapaphases</u> (0.005% Pepsin): 100ml 0.01M HCL + 50µl Pepsin (10%) <u>3D</u> : (0,0025% Pepsin): 100ml 0.01M HCL + 25µl Pepsin (10%)
Sodium acetate (3M), pH 7	NaAc (water free) H ₂ O bidest	<u>100ml</u> : 24.6g NaAc dissolve, 70ml H ₂ O bidest, adjust to pH 7 adjust, ad 100ml H ₂ O

3.12.6 Commercial Kits, Solutions and Consumables

Kit/Solution	Manufacturer
Affinity Script™ QPCR cDNA Synthesis kit	Stratagene, Amsterdam, Netherlands
Bio RNA labeling Kit	Roche, Mannheim, Germany
Brilliant II QPCR Maser Mix	Stratagene, Amsterdam, Netherlands
DIG RNA labeling Kit	Roche, Mannheim, Germany
Illustra genomiPhi V2 DNA amplification kit	GE Healthcare, Munich, Germany
Qiaquick gel extraction kit	QiaGen, Hilden, Germany
QuickPick™ RNA SML mRNA kit	BioNobile, Turku, Finland
peqGold RNAPure™	PeqLab, Erlangen, Germany
Pheno-Chloroform-Isoamylalcohol (25:24:1)	Roth, Karlsruhe, Germany

RNAeasy Mini Kit	QiaGen, Hilden, Germany
RNA later	Applied Biosystems, Darmstedt, Germany
SuperScript™ II/III RT kit	Invitrogen, Scotland, UK
Tissue freezing medium	JUNG, Nussloch, Germany
Vectashield Antifade Medium	Vector, Burlingame, USA

Consumables	Manufacturer
1mm PEN-Membrane Slides	Zeiss, Jena, Germany
Cover Slips	Menzel, Braunschweig, Germany
Choplin Jars	Duran, Mainz, Germany
Eppendorf tubes (0.2ml, 1.5ml, 2.0ml)	Eppendorf, Hamburg, Germany
Falcons 14ml	greiner-bio-one, Frickenhausen, G.
Falcons 15ml	greiner-bio-one, Frickenhausen, G.
Filterpaper 125nm	Schleicher & Schuell, Dassel, G.
Fixogum	Marabu, Tamm, Germany
Glass Pasteur pipets	NeoLab, Heidelberg, Germany
Object Slides	R. Langenbrinck, Teningen, Germany
Optical Adhesive Cover	Applied Biosystems, USA
Optical 96-well Reaction Plate	Applied Biosystems, USA
PALM AdhesiveCaps (0.2ml)	Zeiss, Jena, Germany
PickPen® 1-M magnetic tool	BioNobile, Turku, Finland
PickPen® Tips (bulk 96)	BioNobile, Finland
Pipets (10µl, 20µl, 200µl, 1000µl)	Eppendorf, Hamburg, Germany
PipetBoy	Vitaris, Baar, Germany
Pipet tips (10µl, 20µl, 200µl, 1000µl)	MolecularBioproducts, SanDiego, USA
Poly-A-Way® Disposable Embedding molds (T-12)	Polyscience inc., Warrington, USA
Razor Blades	Wilkinson Sword, Solingen, Germany
Scissors, Forceps, Spatula	FST, Heidelberg, Germany
Serological pipets	Sarstedt, Nümbrecht, Germany
SuperFrost® Plus Slides	Menzel, Braunschweig, Germany

3.12.7 Technical devices

Device	Manufacturer
ABI 7500 Fast qPCR system	Applied Biosystems, Foster City, USA
Axiovert 25 microscope	Zeiss, Jena, Germany
Axiovert 40c microscope	Zeiss, Jena, Germany
Canon PowershotG5	Canon, Krefeld, Germany
Centrifuge Biofuge pico	Heraeus Instruments, Hanau, Germany
Centrifuge Jouan C 3i	Jouan, Frenwald, Germany
Certomat® R/H Incubator	Vitaris, Baar, Germany
CM3000 Cryostat	Zeiss, Jena, Germany
Consort-E835 power supply	Consort, Brussels, Belgium
Easy-Cast Gelelectrophoresis system	Owl, Portsmouth, USA
Gel-Imaging machine	MWG-Biotech, Ebersberg, Germany

Lauda E100 waterbath	Lauda, Königshofen, Germany
LCS SP1	Leica, Wetzlar, Germany
LCS SP2 AOBS	Leica, Wetzlar, Germany
LCS SP5 AOBS	Leica, Wetzlar, Germany
Microwave Samsung Selection	Samsung, Schwalbach, Germany
Hera cell incubator	Heraeus Instruments, Hanau, Germany
Hera safe laminar flow workbench	Heraeus Instruments, Hanau, Germany
PALM Microbeam	Zeiss, Jena, Germany
Polytron homogenizer Ultra Turrax	Janke & Kunkel, Staufen, Germany
RNA/DNA calculator Gene Quant II	Pharmacia Biotech, Wien, Austria
Stemi 2000-C	Zeiss, Jena, Germany
Techne TC-312 thermal cycler	Techne, Burlington, USA
Techne Dry Blot DB-20	Techne, Burlington, USA
Test-Tube-Rotator	Snijders, Tilburg, Netherlands
Thermo Block TDB-120	BioSan, Riga, Latvia
Ultra Sonificator SW 200 F	Heat-Systems-Ultrasonic, USA

3.12.8 Software

Software	Source
3D-RRD	Johann v. Hase, Heidelberg, Germany
7500 Fast System Software	Stratagene, Amsterdam, Netherlands
Adobe Photoshop 7.0	Adobe, San Jose, USA
Amira 3.0	Visage imaging, Carlsbad, USA
DistAng	Tobias Thormeyer, Munich, Germany
EDMT	Tobias Thormeyer, Munich, Germany
Huygens Essential 3.5	Scientific Volume Imaging, Hilversum, NL
Image J	http://rsb.info.nih.gov/ij/ , open source
Primer express 3.0	Stratagene, Amsterdam, Netherlands

4. Results

The results section is divided in two parts. The first part focuses on nuclear topological analyses of genomic regions with the deepest conserved sequence identity in vertebrates, represented by *Dach1* and *Bcl11a*. The second part is dedicated to investigations of evolutionary genomic sequence innovations, which separate the mammals from other vertebrates, represented by the casein gene cluster. Thus, we studied certain aspects of nuclear architecture related to genomic conservation and innovation in the evolutionary context by comparing the distantly related vertebrates mouse and chicken. A common strategy of both parts was to analyze the influence of tissue specification and active gene expression on the higher-order nuclear chromatin conformation.

In this comparative 3D FISH study a unique DNA probe color code was used throughout all experiments for all images and graphs, with exception of paragraph 4.1.1. Referring the locus orientation in mouse the target genes *Dach1*, *Bcl11a* and the *Csn* cluster are depicted in green, sequences 5' to the target gene in red and sequences 3' to the target gene in blue (see 4.1.2.1, 4.1.3.1, 4.2.1, respectively). Chromosome territories (CTs) are shown in yellow. The color code for chicken orthologous segments is maintained irrespectively to inverted locus orientations in this species.

The data was evaluated in three ways referencing different nuclear structures. Firstly, the nuclear relative radial distribution of target genes, flanking regions and harboring chromosome paints was evaluated using 3D-RRD software (4.1.1.2, 4.1.2.3, 4.1.3.3, 4.2.3). Secondly, the distance to the surface of the CT comprising the target genes and flanking regions was determined by the EDMT programme (4.1.2.4, 4.1.3.4, 4.2.4). Thirdly, distances and angles between signal gravity centers of the target genes and both flanking regions were measured with DistAng software (4.1.2.5, 4.1.3.5, 4.2.5) (see 3.9 for evaluation procedures). These measurements resulted in the triangular higher order chromatin conformation of the locus. Statistical tests for all evaluations were based on the rank up sum test (see 3.10). For conciseness of the results chapter supplemental material is annex to this work for which the detailed content can be obtained from chapter 6. In brief all radial and distance to surface distribution curves can be obtained from figures S1 and figures S2. Further statistical data on the distribution curves and angles and distances measurements can be found in table S3. Finally table S4 shows nuclear volumes, surfaces and roundness factors of all evaluated cell types.

4.1 Nuclear topology of ultraconserved noncoding sequence (UCS) clusters

Apart from the well conserved gene coding sequences a second fraction of ultraconserved noncoding sequences (UCS) was recently described. UCS have a strong tendency to cluster in proximity to trans-dev genes that. Importantly, only UCS clusters in gene deserts were targeted, in the study presented here to relate findings with accuracy to the UCS description itself.

Firstly, five hotspots UCS clusters were targeted. Preferential histone modifications of UCS and the radial arrangement were determined in embryonic fibroblasts. Further the nuclear localization of these UCS hotspots was identified in tissue nuclei of mesodermal and ectodermal cells in mouse and chicken embryos before organogenesis and with advanced organogenesis.

Secondly, the RNA expression pattern of the trans-dev genes *Dach1* and *Bcl11a* was investigated and relatively quantified in embryos of mouse and chicken. Then the nuclear conformation of *Dach1* and *Bcl11a* and of the flanking UCS clusters was defined, in relation to certain tissues and the gene expression status by combining RNAish and DNA FISH. These two genes were chosen because *Dach1* is flanked on both sides by clusters of UCS whereas *Bcl11a* is situated in-between a gene-rich region with no UCS and a gene desert with clustered UCS.

4.1.1 Hot spots of conserved noncoding sequences

4.1.1.1 Experimental design

Five of the most prominent UCS clusters, close to the trans-dev genes *Dach1*, *Foxp2*, *Meis1*, *Zfp536* and *Zfhx1b* were selected and targeted by BAC clones from mouse and chicken (figure 4.1). Notably, the BAC clones were selected from non-genic regions and for UCS clusters localized on separate chromosomes in mouse and chicken to allow for independent positioning in the nucleus.

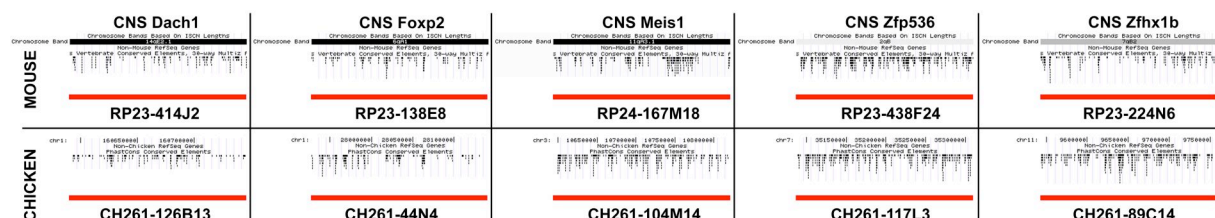


Figure 4.1: Comparative map of 5 orthologous UCS cluster hotspots (= CNS) in mouse and chicken. Evolutionarily sequence conservation is shown as PhasCons Vertebrate Conserved Elements, Multiz Alignment (30-way or 10-way alignment see Siepel et al. 2005). Mouse and chicken BAC clones (for detailed mapping see 3.12.3) depict UCS clusters in proximity to the trans-dev genes *Dach1*, *Foxp2*, *Meis1*, *Zfp536* and *Zfhx1b*. (modified from www.ensembl.org)

The five BAC clones were then pooled, fluorescently labeled and hybridized to tissue cryosections of mouse E7.0 (figure 4.2 A,B,G), mouse E13.0, chicken E21h (figure 4.2 H), chicken E5.5 and to embryonic fibroblasts of both species. Early embryos were staged prior to organogenesis (primitive streak stage) whereas in later stage embryos the organogenesis and the body plan development were far advanced. Radial 3D-evaluations with respect to the nucleus highlighted potential changes between evaluated mesodermal and ectodermal tissue from both developmental stages and between mouse and chicken. Further, the data was analyzed with respect to preferential co-localization of UCS e.g. for obvious cluster formation. Since it was not possible to distinguish ectodermal cells from mesodermal nuclei in tissue sections from chicken E21h, cells from both germ lines were pooled. (see 4.1.1.2) Finally, hybridizations to embryonic fibroblasts of mouse and chicken in combination with immunofluorescence detection of histone modifications marking constitutive heterochromatin (H3K9me3), facultative heterochromatin (H3K27me3) or euchromatin (H3K4me3) gave an idea to which extent UCS regions are modified by histone landmarks and allowed estimations to which chromatin class UCS cluster belong (figure 4.2 C-F).

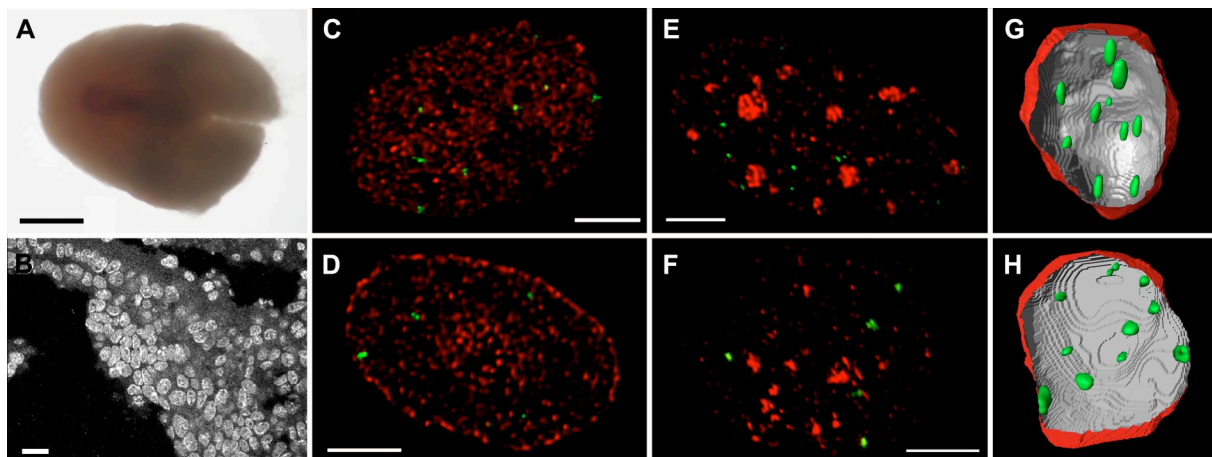


Figure 4.1: (A) Mouse E7.0 (scale bar 150µm). (B) DAPI counterstained tissue cryosection from mouse E7.0 neuronal ectoderm (scale bar 10µm). (C-E) Z-Projection of three consecutive deconvoluted confocal slices (3x 150nm) (scale bar 5µm). (C-E) Mouse embryonic fibroblast nuclei: UCS cluster (green), (C) anti H3K4triCH₃ immuno staining (red), (D) anti H3K27me₃ immuno staining (red), (E) anti H3K9me₃ immuno staining (red). (F) Chicken embryonic fibroblast nucleus: UCS hotspots (green and) anti H3K9me₃ immuno staining (red). (G-H) Amira 3.1.1 3D reconstruction of a midbrain nucleus from (G) mouse E13.0 and (H) chicken E5.5: DAPI counterstain (red) and 5x UCS cluster (green.)

4.1.1.2 Nuclear radial arrangement of of UCS clusters

The radial arrangement of UCS cluster was determined with 3D-RRD in nuclei from the head (neopallial cortex), the hind limb (mesenchymal cells in the interdigit zone), the ectoderm and/or the mesoderm before organogenesis in mouse and chicken. The nuclear distribution in all evaluated tissues indicated a tendency for UCS to be located in the periphery but no strictly defined radial position or UCS colocalization

was found. Although UCS clusters in mouse were located constantly in the nuclear periphery, in the mouse E13.0 hind limb (ARR 70.8% \pm 0.53) the UCS cluster showed a significant tendency towards the nuclear center compared to mouse E13.0 head (ARR 74.95% \pm 0.48), mouse E7.0 ectoderm (ARR 76.64% \pm 0.34) and mouse E7.0 mesoderm (ARR 78.60% \pm 0.59). Orthologous UCS clusters to mouse were also investigated in chicken embryos. Here, the orthologous five UCS clusters in chicken E5.5 head (ARR 86.49%, $\text{sdm} \pm 0.41$) were positioned significantly more in the nuclear exterior than in chicken E.5.5 hind limb (ARR 80.90%, $\text{sdm} \pm 0.50$) and chicken E21h (ARR 77.9% \pm 0.63%) (figure 4.3, table S3 for statistics).

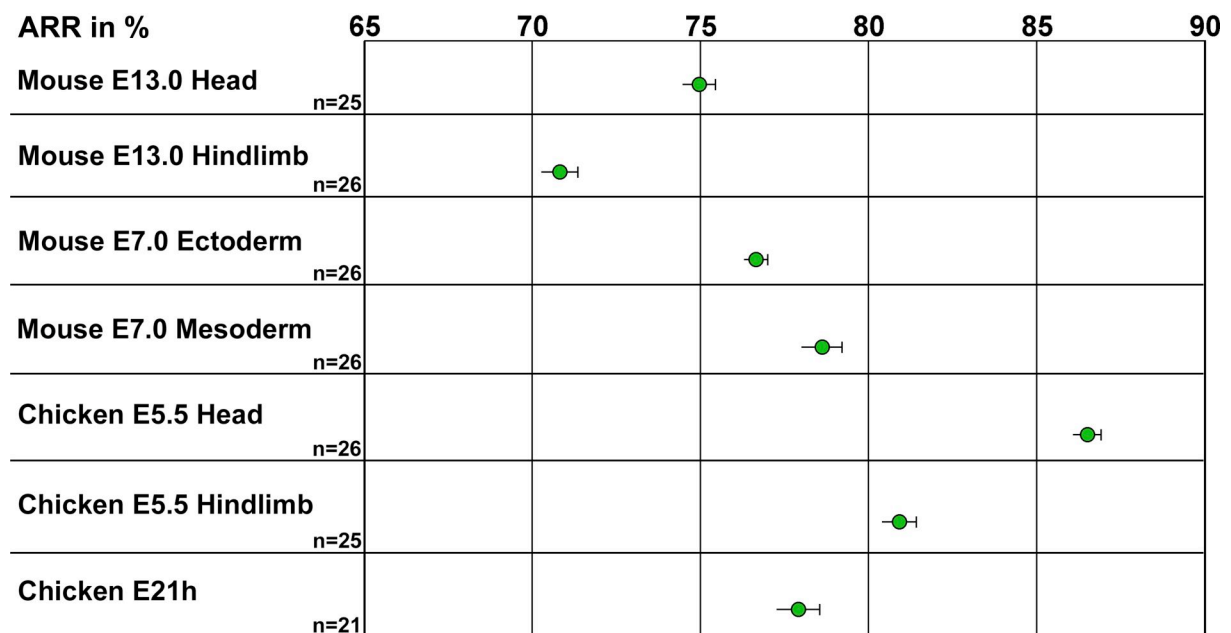


Figure 4.3: Absolute relative radii (ARR) from 3D-RRD evaluations of five ortholog UCS cluster in embryos of mouse and chicken (green). (n = number of evaluated nuclei, error bars indicate the sdm, ARR in % = Absolute relative radial distance to the nuclear center in percent).

Further, to evaluate the radial distribution, of each UCS hotspot separately the fiveselected BACs were detected with five different fluorophors in embryonic fibroblasts of mouse and chicken. The mean ARR of all UCS clusters and also the individual ARR values were surprisingly evolutionarily conserved between mouse and chicken (figure 4.4, table S3 for statistics, mean ARR MMU: 69.0%, $\text{sdm} \pm 1.4$, mean ARR GGA 69.1%, $\text{sdm} \pm 1.5$). The radial position of ortholog UCS cluster pairs was changed only by 1.0% to 4.4% comparing mouse and chicken.

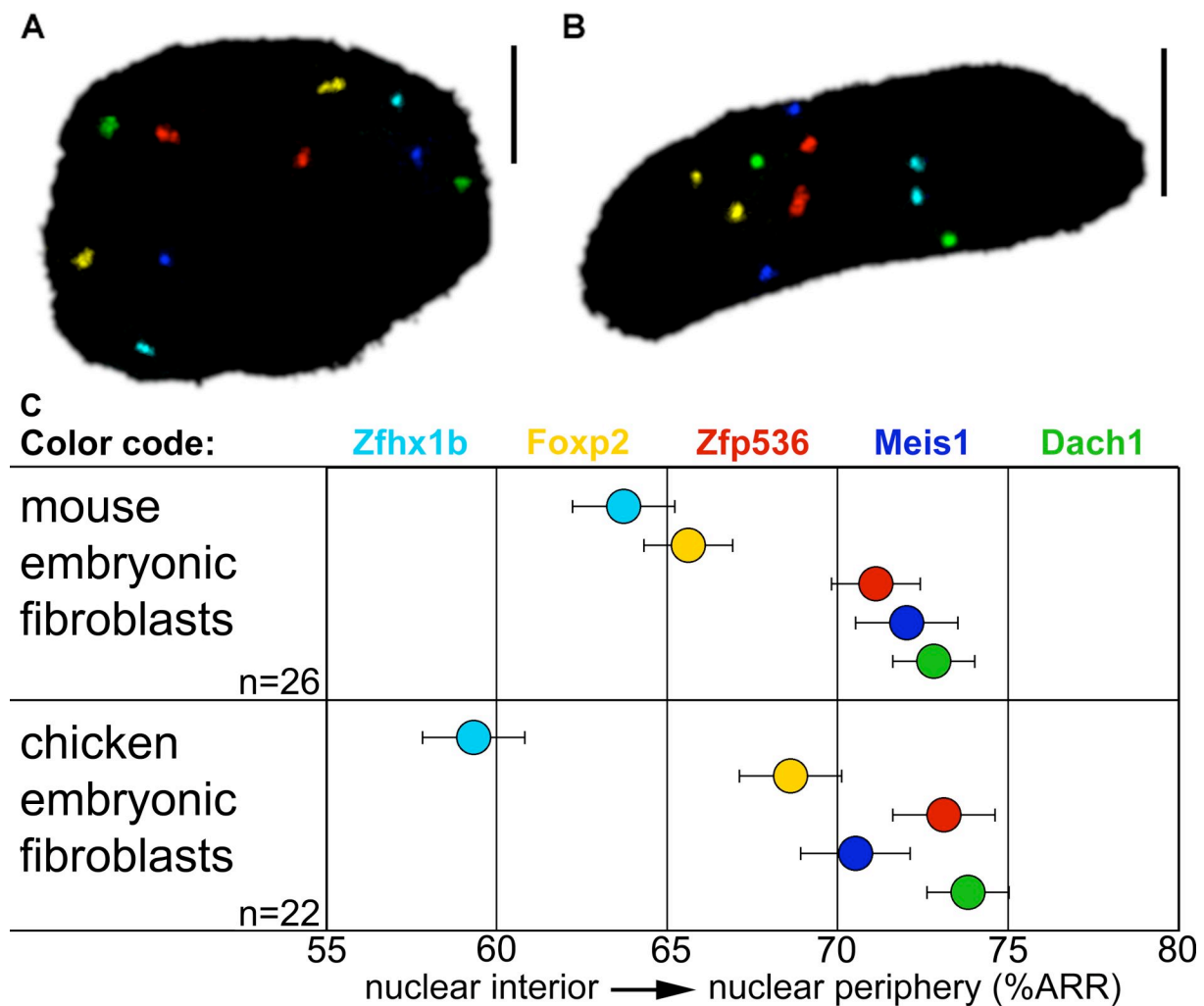


Figure 4.4: Z-projections of confocal image stacks from (A) a mouse and (B) a chicken embryonic fibroblasts, showing five ortholog UCS hotspots. (C) ARR (absolute relative radius referred to the nuclear center) blot of five ortholog UCS hotspots in nuclei of mouse and chicken embryonic fibroblasts (n = number of evaluated nuclei, error bars indicate the sdm). The color code indicates the trans-dev gene in proximity to the UCS cluster.

4.1.1.3 Histone modifications in UCS cluster regions

Embryonic fibroblasts from mouse and chicken were hybridized with the UCS hotspot BAC clone set also used on tissue sections (see 4.1.1.1). In addition, FISH was combined with immunohistochemistry to detect colocalization frequencies with the histone modifications H3K4me3, H3K9me3 and H3K27me3. Image deconvolution was performed, deconvolution parameters and user-defined thresholds, selecting voxels included in the evaluation were set in accordance with (Zinner et al. 2006). UCS clusters from mouse and chicken showed only little overlap with the marker for constitutive heterochromatin (H3K9me3, MMU: 5.4% sdm± 0.5, GGA: 17.0% sdm± 0.8) and colocalized to a higher extend both with facultative heterochromatin (H3K27me3, MMU: 30.4% sdm± 0.7, GGA: 30.3% sdm± 0.7) and euchromatin (H3K4me3, MMU: 28.0% sdm± 0.8, GGA: 37.9% sdm± 0.9) (figure 4.5).

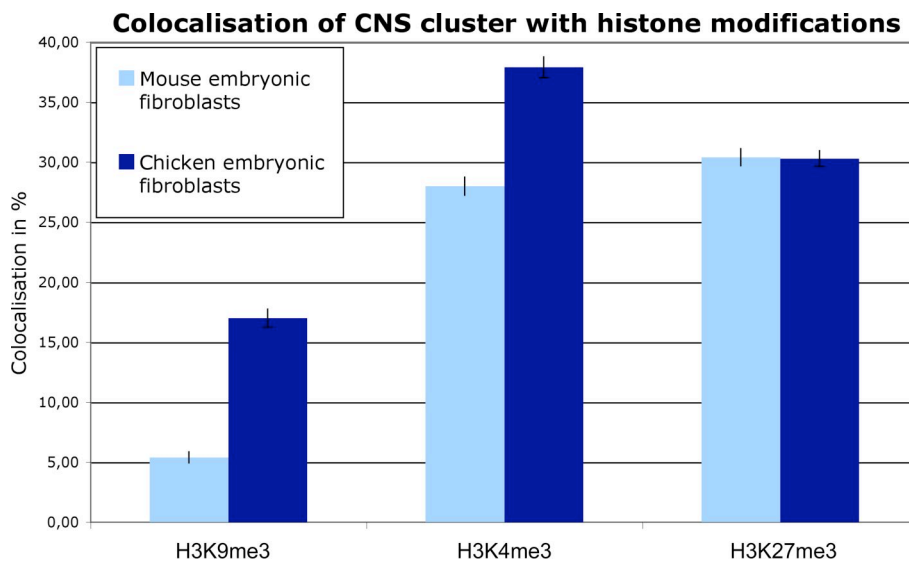


Figure 4.5: One-way Manders (Manders et al. 1992) colocalization analysis of histone modifications with five orthologous UCS clusters in embryonic fibroblasts of mouse and chicken (error bars show the sdm).

4.1.1.4 Results summary of UCS hot spots

The five UCS hotspots were preferentially localized in the nuclear periphery in all evaluated tissues. Nevertheless they showed a broad distribution leading to significantly different radial distributions among certain tissues. These findings could not be linked with evolutionary change, or species developmental stage or the germ line layer, but showed that UCS have no common preferential radial localization in the nucleus or cluster in a specific compartment of the nucleus. In contrast the radial arrangement of each of the five selected UCS hotspots in embryonic fibroblasts was evolutionarily highly conserved.

For embryonic fibroblasts it could be demonstrated that the selected UCS hotspots were not part of constitutive heterochromatin but belong to facultative heterochromatin or euchromatin.

Taken together the data indicate that UCS clusters are not heterochromatic and are coordinately organized in the nucleus. Instead the results suggest that each UCS cluster is an independent functional unit operating within its local genomic environment.

4.1.2 Dach1 and flanking conserved noncoding sequence clusters

4.1.2.1 Experimental design

The genomic region of the trans-dev gene Dach1 is otherwise free of coding sequences. In this genes desert both 5' and 3' to the gene UCS clusters were identified (see 2.4.3). To study the Dach1 region in mouse and chicken BAC clones were chosen from public databases to target the Dach1 gene (green) and the UCS

cluster 5' and 3' of the gene, further referred as UCS cluster A (red) and UCS cluster B (blue), respectively (figure 4.6).

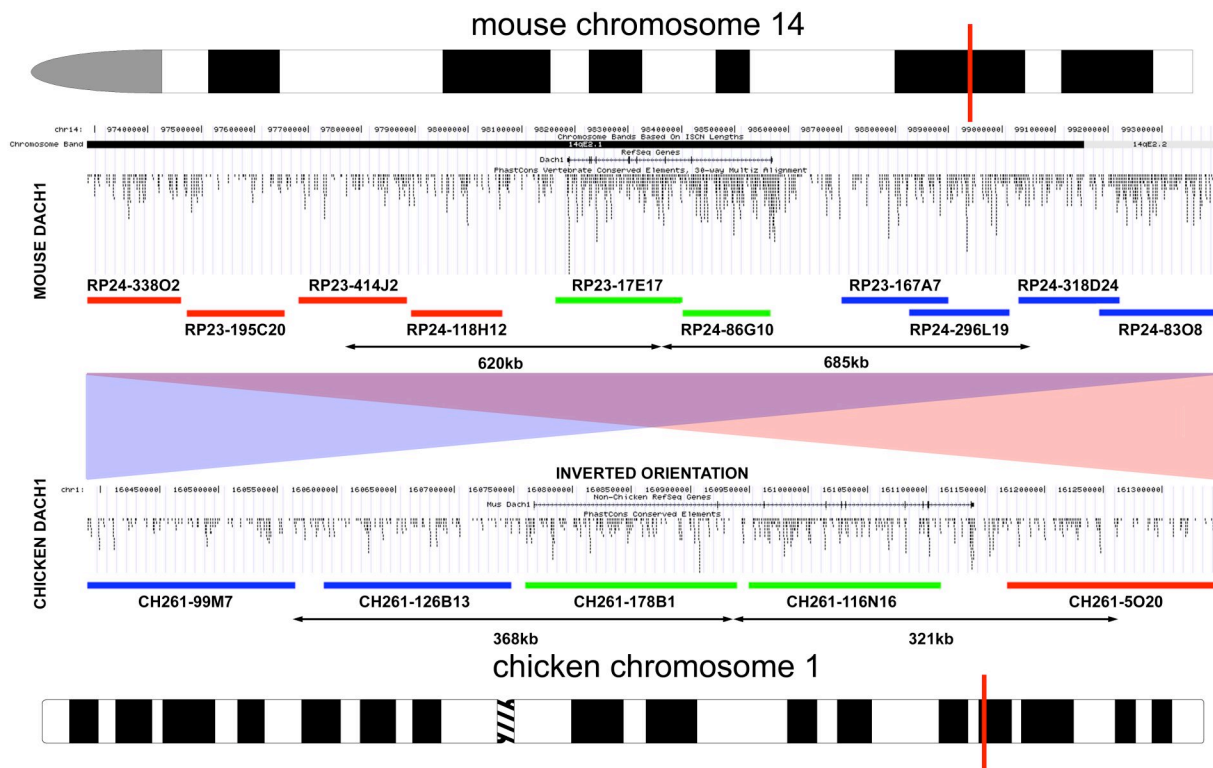


Figure 4.6: Comparative experimental design map for the *Dach1* locus of mouse and chicken. Evolutionary sequence conservation is shown as PhasCons Vertebrate Conserved Elements, Multiz Alignment (30-way or 10-way alignment). Mouse BAC clones depict *Dach1* (green) and flanking clusters of UCS in the gene desert A (red) and B (blue). The orientation of the locus is evolutionarily inverted in chicken compared to mouse. (adapted from <http://genome.ucsc.edu/>, mouse assembly July 2007, chicken assembly May 2006).

Chromogenic RNAish to whole mount embryos and tissue sections (E13.0 in mouse, E5.5 in chicken, figure 4.7 A) showed that *Dach1* expression is restricted to certain tissues. These tissue expression differences were validated and quantified by RNA FISH and qPCR analysis from laser microdissected native tissue material. Then, by combining RNAish with DNA FISH on tissue-sections we addressed if the expression state of the *Dach1* gene, in afore selected tissues and species influences the nuclear architecture of the *Dach1* region (figure 4.7 B-F). Differentially labeled fluorescent probe sets for *Dach1*, UCS A and UCS B and the chromosome paint probe allowed us to analyze the genomic architecture of the *Dach1* region in respect to the nucleus and the harboring CT (figure 4.7 F). Further, the local higher order chromatin conformation of the *Dach1* gene, UCS A, UCS B to each other was determined by measuring distances and angles between the BAC FISH signals (figure 4.7 G).

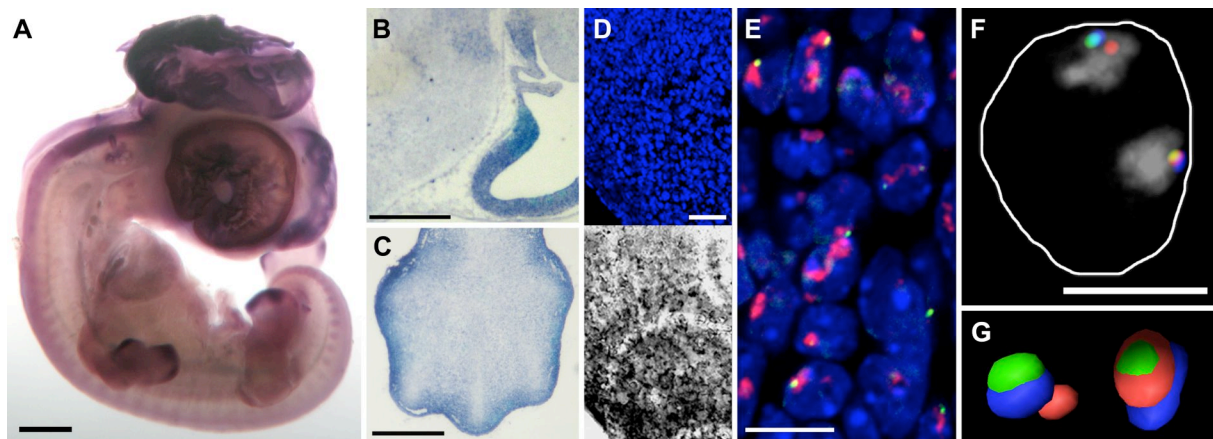


Figure 4.7: (A-C) RNAish on chicken E5.5 with a Dach1 RNA antisense probe. (A) Whole mount mouse E5.5 (scale bar 1mm) (B-C) 20µm tissue cryosection of mouse E13.0: (B) brain sagittal, third ventricle, (C) hind limb horizontal (scale bar 0.5mm). (D) Confocal image of mouse E5.5 midbrain: DAPI counterstain (blue) and brightfield image of NBT/BCIP precipitate (grey). (E) Unprocessed confocal image slice of mouse E13.0 midbrain nuclei (z step = 150nm): DAPI counterstain (blue), mouse chromosome 14 (red), mouse Dach1 gene (green). (F) Mouse E13.0 midbrain nucleus: Z-projection of a processed confocal image stack (103 slices), counterstain outlined (white), mouse chromosome 14 (grey), Dach1 (green), 5'UCS cluster (red), 3'UCS cluster (blue) (scale bar 5µm). (G) 3D reconstruction (AMIRA 3.1.1) of the local chromatin conformation between Dach1 (green), UCS cluster A (red), UCS B (blue).

4.1.2.2 Dach1 mRNA expression pattern and quantification

Whole mount RNAish with a Dach1 T7 RNA antisense probe on mouse E13.0 and chicken E5.5 results were identical with previous works and are described in detail therein (Caubit et al. 1999; Davis et al. 1999; Kida et al. 2004). Both the tissue expression pattern and the relative expression levels were conserved between mouse and chicken (figure 4.8).

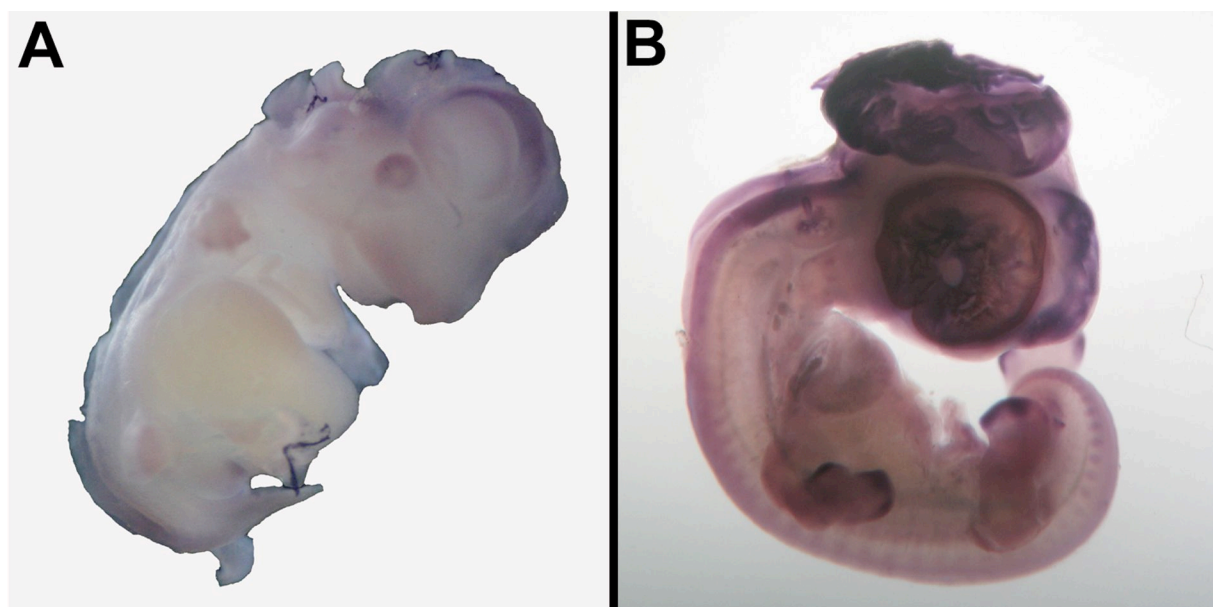


Figure 4.8: Whole mount RNAish with a Dach1 DIG RNA anti-sense probe: (A) Mouse E13.0, (B) Chicken E5.5. Amongst others Dach1 was strongly expressed in the brain ventricles and in the tips of the limb buds.

Based on the results of the whole mount RNAish we repeated RNAish on sagittal tissue sections of the head and on horizontal tissue sections of the hind limb bud of mouse E13.0 and chicken E5.5. Dach1 was strongly expressed in neurons surrounding the brain ventricles and in the tips of the developing digits in the limbs whereas in the striatum, the cephalic mesenchyme or the hind limb plate no expression was detected (figure 4.6 A-D). The chromogenic RNAish treated cryosections were further proceeded to 3D-FISH hybridizations (figure 4.6, 4.1.2.3-5). To validate and to quantify the expression differences obtained by RNAish we performed 2-step quantitative PCR from mouse E13.0 head tissue. About 300-400 laser-microdissection cells, were separately collected from brain ventricles, showing high expression activity by RNAish and from cephalic mesenchyme, where no gene expression could be identified by RNAish. Next, mRNAs were isolated, reversely transcribed to cDNA and the cDNA was then used as input for the qPCR reactions. Finally, after the qPCR run the relative expression level difference between brain ventricle cells and cephalic mesenchyme cells was calculated, set against a passive reference and normalized by two the house keeping genes Gapdh and Actb. The mean relative expression difference between expressional active and silent tissue in triplicate experiments was 29.6 (sdm \pm 8.1), and thus obtained results confirmed RNAish.

4.1.2.3 Nuclear radial arrangement of the Dach1 locus

3D-FISH was performed on RNAish treated cryosections of the head and the hind limb bud from mouse E13.0 and chicken E5.5. This combination of RNAish and FISH allowed to evaluate the nuclear architecture of the Dach1 region in the context of its expression status (figure 4.6).

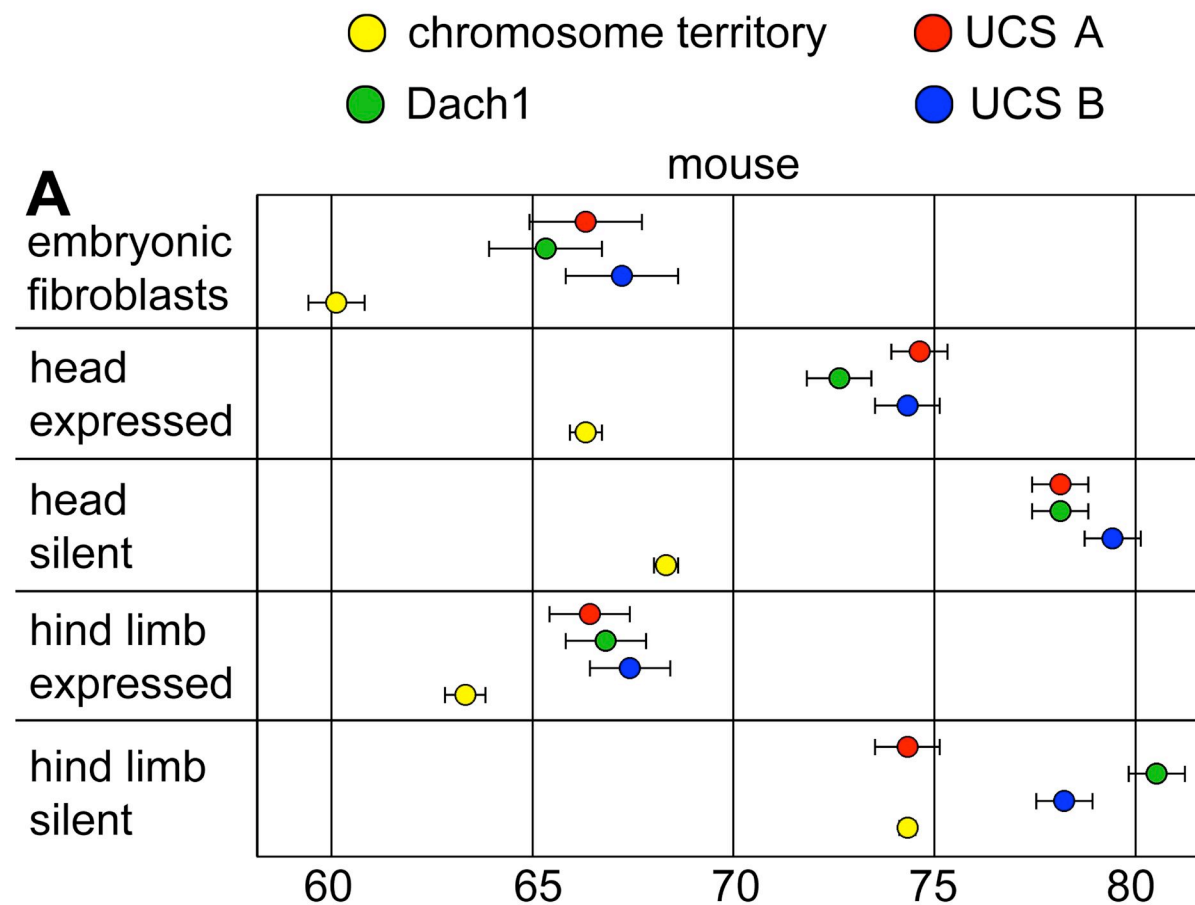
The Dach1 region displayed a remarkably stable peripheral position in all four evaluated tissues and in embryonic fibroblasts of mouse and chicken. The maximal difference in the mean radial position of the UCS A, the Dach1 gene and the UCS B in a single evaluation was 1.0-6.2%. Thus the entire Dach1 region resided closely at the same radial position in the nucleus (figure 4.9). We observed no major relocalization of the Dach1 region upon transcriptional activation of Dach1 with respect to flanking UCS clusters, in different cell types nor between mouse and chicken.

At a first glance the Dach1 region in mouse E13.0 showed a tendency to be more internal in the Dach1 expressing tissue (Dach1 gene - neopallial cortex: 72.6%, \pm sdm 0.8 and hind limb mesenchyme: 66.8%, sdm \pm 0.8) compared to the tissue where Dach1 was silent (striatum: 78.1%, sdm \pm 0.7 and hind limb plate: 80.5%, sdm \pm 0.7) (table S3 for statistics). Since these position differences were also observed for the position of the chromosome 14 paint (ARR Dach1 gene – neopallial cortex: 66.3%

sdm \pm 1.4, hind limb mesenchyme: 63.3% sdm \pm 0.5, stitatum: 68.3% sdm \pm 0.4 and Hind limb plate: 74.3% sdm \pm 0.2), the effects were not necessarily connected with the Dach1 region itself but with cell type specific differences of the entire chromosome 14. When correcting for the CT position differences in mouse the Dach1 gene position varied between evaluations by 6.3% instead of 13.7%.

As the chicken chromosome 1 paint position showed a maximal deviation of only 1.9% between experiments the position of the Dach1 region in this species was even more stable, ranging between 72.7%, sdm \pm 1.2 and 77.4%, sdm \pm 0.8 for the Dach1 gene (figure 4.9). Normalized by the chromosome 1 paint position differences, the Dach1 gene position in chicken E5.5 varied only by 2.7% (figure 4.9). Notably, mouse and chicken homologous tissues did not statistically differ in their Dach1 positioning with the exception of head silent (table S3 for statistics).

The radial distribution of the Dach1 gene in embryonic fibroblasts was most internal in mouse (65.3%, sdm \pm 1.4), but most external in chicken (79.6%, sdm \pm 1.3) compared with the results in tissue sections. However, the localization was in close accordance with the peripheral localization of Dach1 in tissues (mouse tissue ARR: 60.8% - 80.5% chicken tissue ARR: 72.7-77.4%) (figure 4.9).



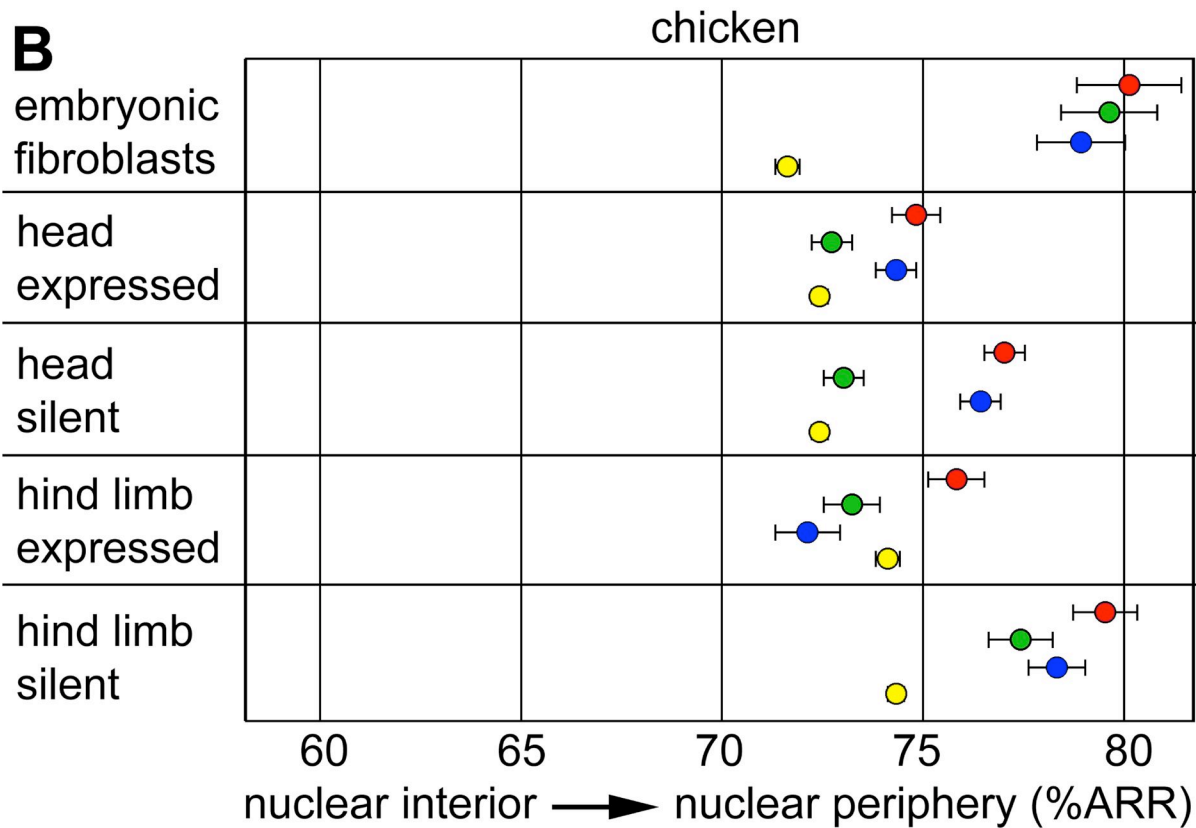


Figure 4.9: ARR dot blot of the Dach1 region. (A) Mouse chromosome 14 (yellow) or (B) chicken chromosome 1 (yellow), the Dach1 gene (green) and flanking UCS cluster A and B two both sides (red, blue) in tissue sections of mouse E13.0, chicken E5.5 and embryonic fibroblasts, respectively. (error bars indicate the sdm, figure S1 for distribution curves)

To exclude the possibility of having distinct populations of nonexpressing and expressing cells in a tissue with a positive RNAish pattern we performed RNA FISH with a Dach1 RNA antisense probe to a tissue section of mouse E13.0. RNA FISH sites in the neopallial cortex were also found nearly exclusively in the nuclear periphery and matched with the peripheral Dach1 gene localization obtained by FISH. Further, sites of expression were found in the vast majority of nuclei from tissue shown before to be positive by chromogenic RNAish and qPCR. Confirmatively, a blank control without a RNA probe in the hybridization mix produced equal background as in silent tissue (figure 4.10). By conclusion, the Dach1 localization of Dach1 in expressing tissue was not influenced by extensive expression level variations in individual cells in a given tissue (figure 4.10).

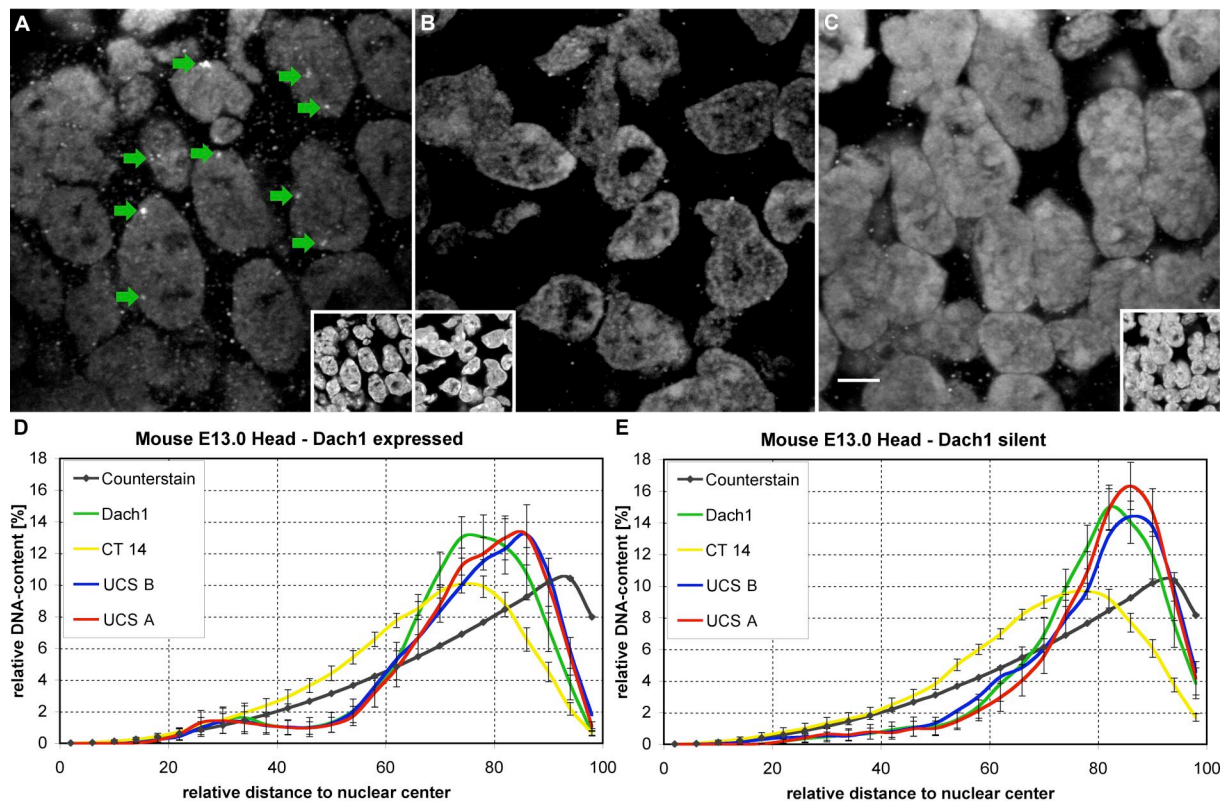


Figure 4.10: RNA FISH with a Dach1 RNA antisense probe on mouse E13.0 tissue sections. (A) Neopallial cortex: Sites of expression are exemplarily indicated with green arrows (2 μ m z-projection). (B) Head mesenchyme: No sites of expression were detected. (C) RNA FISH blank control without an RNA anti-sense probe in the hybridization mix on mouse E13.0 tissue section. Neopallial cortex: No specific signal was detected and the background equals to the (B) head mesenchyme. (D) The peripheral position of expression sites matches the relative radial distribution of the Dach1 gene evaluated from 3D-FISH. (E) The Dach1 region showed a stable peripheral position also in transcriptionally silent nuclei.

4.1.2.4 Distance to the chromosome territory surface of the Dach1 locus

The distance to the CT surface of the Dach1 gene, the UCS A and the UCS B cluster was measured with EDMT software.

The mouse Dach1 region resided stably close to the territory surface of mouse chromosome 14 without statistical differences (Dach1 gene: 126nm – 177nm, table S3 for statistics, figure 4.11). In contrast, the Dach1 region resided inside the chicken chromosome 1 territory (Dach1 gene: 225nm – 317nm) exhibiting more positional flexibility compared with mouse. No preferential polarity of mean distances in a chromosome territory among the UCS A, the Dach1 gene and the UCS B was revealed in the different evaluations. The maximal deviation when comparing the position of UCS A, Dach1 and UCS B in one evaluation was, 91nm in mouse and 83nm in chicken (table S3). Taken together the position inside the CT was remarkably stable in cultured fibroblasts and in tissue cells of one species but significantly different between mouse and chicken. We observed no effect of the Dach1 expression status or the nuclear morphology on position of the Dach1 region position with respect to CTs.

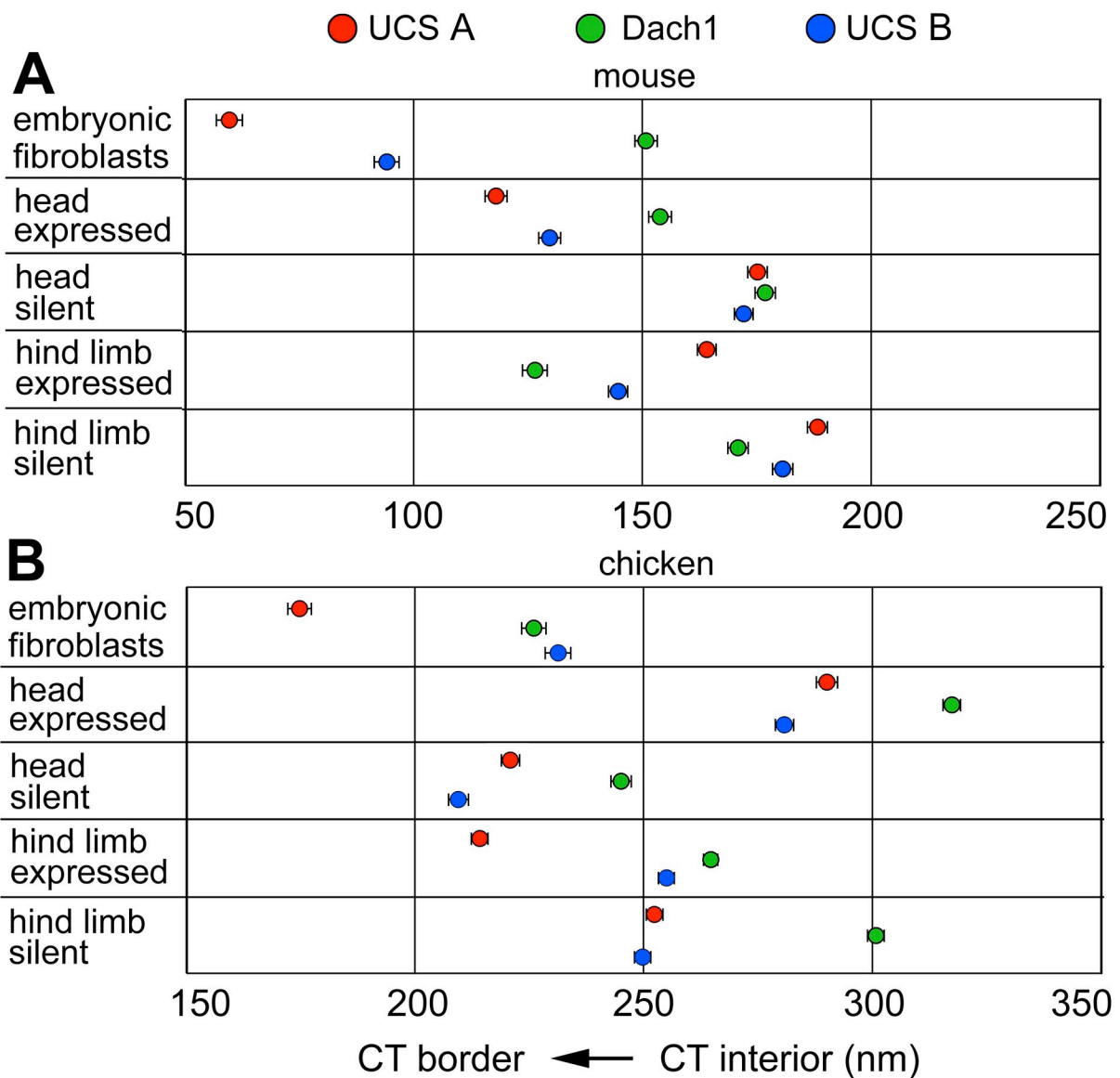


Figure 4.11: Dot blot of mean distances to (A) mouse chromosome 14 or (B) chicken chromosome 1 surface harboring the Dach1 gene (green) and the UCS clusters A and B (red, blue) in tissue sections of mouse E13.0, chicken E5.5, and in embryonic fibroblasts of both species. (error bars indicate the sdm, figure S2 for distribution curves)

4.1.2.5 Mean higher order chromatin conformation of the Dach1 region

We measured 3D interphase distances and angles drawn to the geometrical centers of UCS A, Dach1 and UCS B BAC FISH signals to determine the triangular higher order chromatin conformation of the region. Interphase distances were normalized against genomic distances resulting in a measure for the chromatin compaction in kbp/nm (figure 4.14).

The mean genomic 3D angles using Dach1 as apex and UCS A and UCS B as sides was nearly equilateral in tissue of mouse E13.0 (52.4° - 75.7°), whereas the mean genomic angle around chicken Dach1 in E5.5 was close to a rectangle (77.5° - 108.9°) (figure 4.12, table S3 for statistics). The genomic angle around Dach1 in embryonic fibroblast nuclei of both species differed considerably from those in

tissues (MMU: 66.2°, GGA: 71.0°, table S3 for statistics). A high cell-to-cell variation of genomic angles was commonly observed for each individual experiment. The angles around mouse Dach1 were in 66.52% below 60°, in 25.22% between 60° and 120° and only in 8.26% over 120°. In chicken 33.0% of angles around Dach1 were 0°-60°, 37.4% were 60°-120° and 29.6% were 120°-180° (figure 4.13). Thus we observed a species difference of the chromatin folding of the Dach1 region.

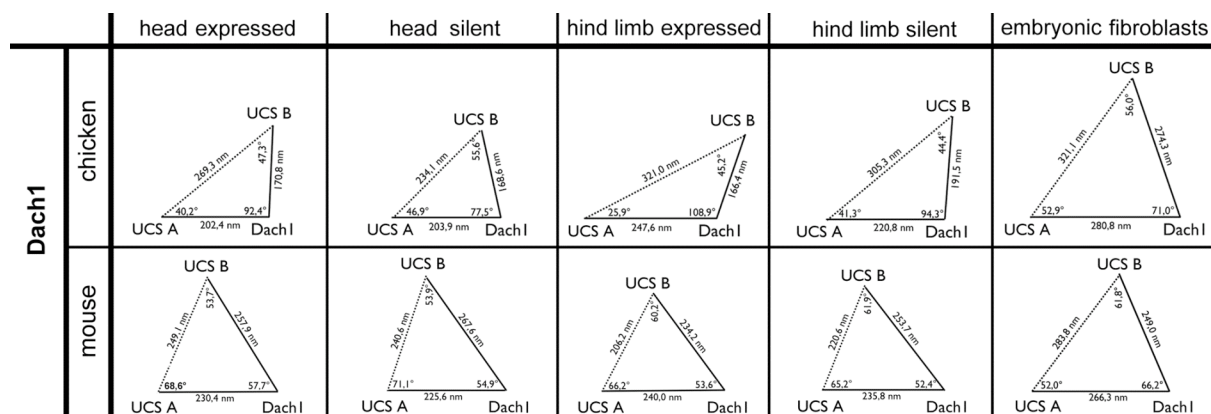


Figure 4.12: Triangular display of the mean higher order chromatin conformation obtained by distances and angles measurements in mouse tissue E13.0 between UCS A, Dach1 and UCS B.

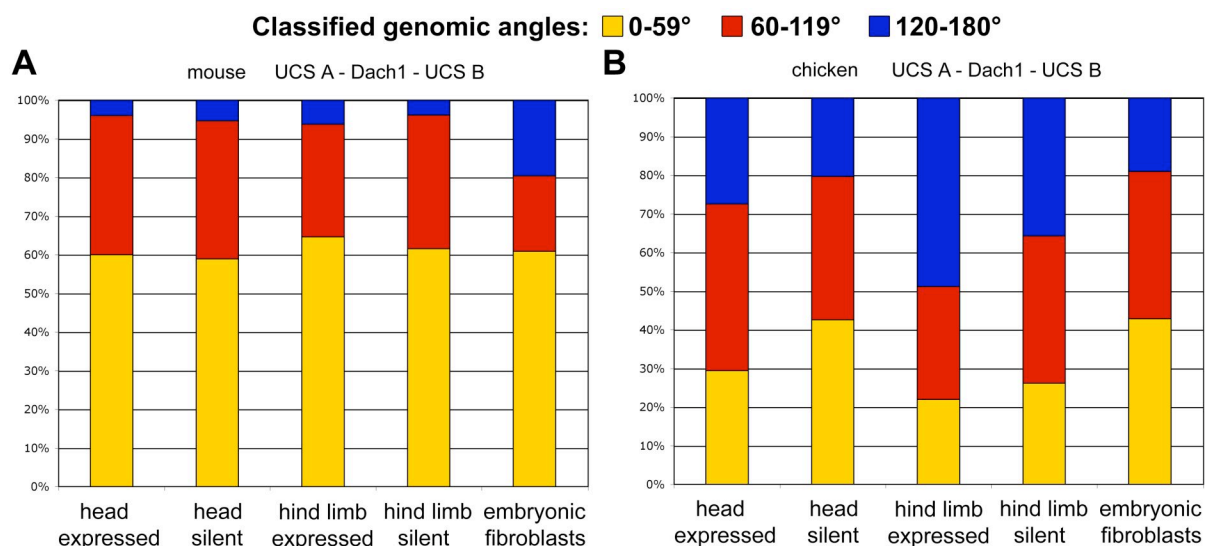


Figure 4.13: Genomic UCS A-Dach1-UCS B angles, with Dach1 as apex classified between 0-59°(yellow), 60-119° (red) and 120-180° (blue) in interphase nuclei of (A) mouse and (B) chicken.

The chromatin compaction in the mouse Dach1 region obtained from UCS A to Dach1 (2.33-2.75 kbp/nm) and from UCS B to Dach1 (2.56-2.92 kbp/nm) was very stable without statistically valid differences among evaluations. Similarly constant was the chromatin compaction at the UCS A side (1.34-2.21 kbp/nm) and at the UCS B side (1.30-1.59 kbp/nm) in chicken nuclei (figure 4.14, table S3 for statistics). Chromatin was less compacted in embryonic fibroblasts compared to all tissue in both species and chromatin was less compact in chicken compared to mouse (table

S3 for statistics). Neither the genomic angles nor the chromatin compaction in the Dach1 region could be correlated with the expressional activity of Dach1.

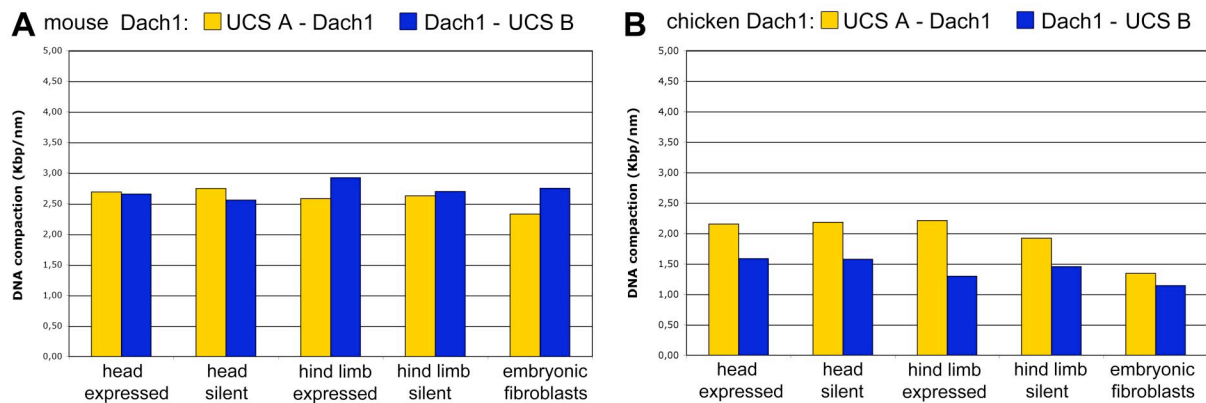


Figure 4.14: Chromatin compaction in kbp/nm calculated from distance measurements between UCS A to Dach1 (yellow) and UCS B to Dach1 (blue) in (A) mouse and (B) chicken interphase nuclei.

In a control experiment one BAC clone for the 5' site of the Dach1 gene and the two BAC clones marking the distal ends end of the UCS clusters A and B were hybridized on mouse embryonic fibroblasts (figure 4.15).

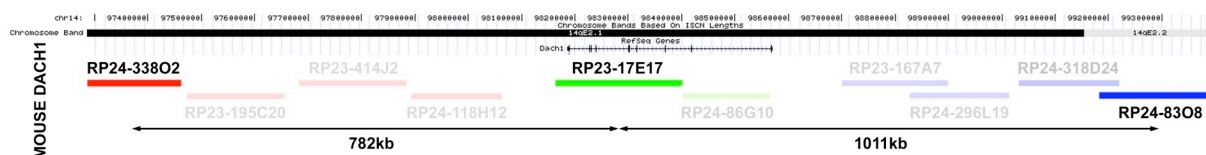


Figure 4.15: FISH probe set to control the resolution of distance and angle measurements in mouse embryonic fibroblasts. Only the BAC clones marking the 5' site of the Dach1 gene (green) or distal ends of the UCS cluster were used (blue and red). Large insert clones excluded from the original clone set for this experiment are shown in light colors.

The chromatin compaction was remarkably similar between the the entire clone set (UCS A: 2.07 kbp/nm, UCS B: 2.42 kbp/nm) and the control experiment (UCS A: 2.33 kbp/nm, UCS B: 2.56 kbp/nm). However, as expected from the increased genomic distances between BAC probes in this control experiment we observed significantly higher interphase distances compared with the entire BAC clone set for UCS A (MMU: 385.8nm-266.3nm=119.5nm) or UCS B (MMU: 417.3nm-249.0nm=168.3nm, GGA: 367.9nm-280.8nm=87.1nm). Therefore it can be concluded that the undertaken measurements of mean distances, were above the resolution limit in our experimental setup.

4.1.2.6 Results summary of Dach1

Taken together, the Dach1 gene displayed an evolutionarily conserved nuclear peripheral position, irrespective of the expression status of Dach1 or the species. qPCR analysis, together with RNA FISH independently confirmed the Dach1 expression differences in the tissues analyzed. Slight position changes between

tissues were comprehensible by chromosome paint position variations and therefore not specific to the Dach1 region per se. Overall the mouse chromosome 14 position was more changed between different tissues than chicken chromosome 1.

Concerning the localization inside the harboring CT an evolutionary diversification was statistically evident: The Dach1 region was stably positioned close to the surface of mouse chromosome 14. In contrast the chicken Dach1 gene was found in the interior of chromosome 1.

Angles and chromatin compaction were species-specific and non of these parameters showed a correlation with gene expression.

4.1.3 Bcl11a and its flanking genomic regions

4.1.3.1 Experimental design

Bcl11a (green) marks the border between a gene rich region (red) devoid of UCS and a gene desert with clustered UCS (blue). BAC clones for mouse Bcl11a, the gene-rich control region, UCS cluster and the respective chicken orthologs with inverted chromosomal orientation were selected from public databases (figure 4.16).

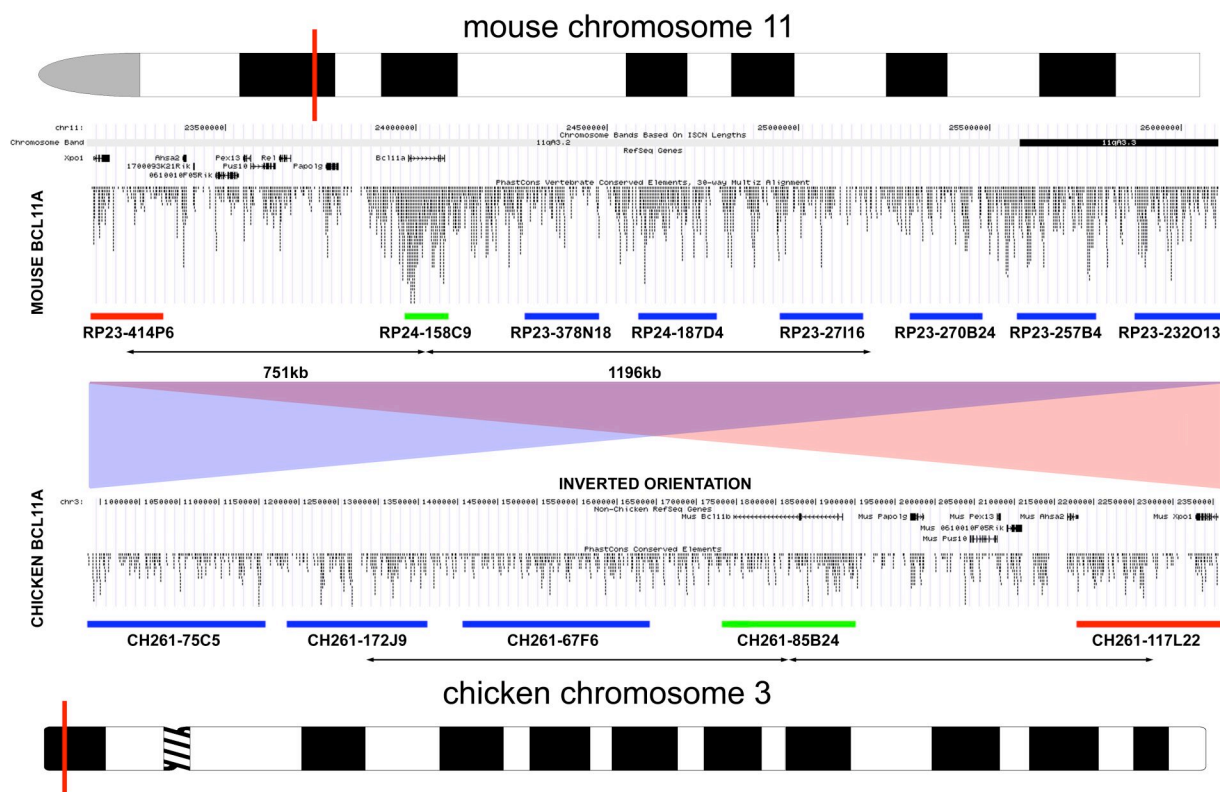


Figure 4.16: Comparative map for the Bcl11a region of mouse and chicken. Evolutionary sequence conservation is shown as PhasCons Vertebrate Conserved Elements, Multiz Alignment (30-way or 10-way alignment). Mouse BAC clones depict Bcl11a (green), the flanking gene rich Xpo1 control region (red) and the 3' flanking cluster of conserved noncoding sequences in a gene desert (blue). The orientation of the locus is evolutionarily inverted in chicken compared to mouse (chicken BAC clones: Bcl11a green, 5' conserved noncoding elements blue, 3' Xpo1 control red). (adapted from <http://genome.ucsc.edu/>, mouse assembly july 2007, chicken assembly may 2006).

The experimental strategy was the same as for the Dach1 experiments. First RNAish with a Bcl11a antisense probe was performed on whole mount embryos (figure 4.17 A) and tissue sections (figure 4.17 B,C) from mouse E13.0 and chicken E5.5. Next, Bcl11a nascent mRNA expression was visualized by RNA FISH. Then the expression was relatively quantified between expressional active and silent tissues by qPCR.

Further, RNAish treated tissue sections and embryonic fibroblasts as ex vivo control were hybridized in situ with fluorescently labeled BAC probes together with the chromosome paint harboring the Bcl11a region (figure 4.17 D-G). Confocal image stacks of tissue nuclei with or without detectable Bcl11a expression and of embryonic fibroblasts were recorded and three dimensionally evaluated referring the localization in the nucleus and in the harboring CT. Measurements of angles and distances among signal gravity centers of Bcl11a, the gene-rich control and the UCS cluster were performed to determine the higher order chromatin conformation of the Bcl11a region.

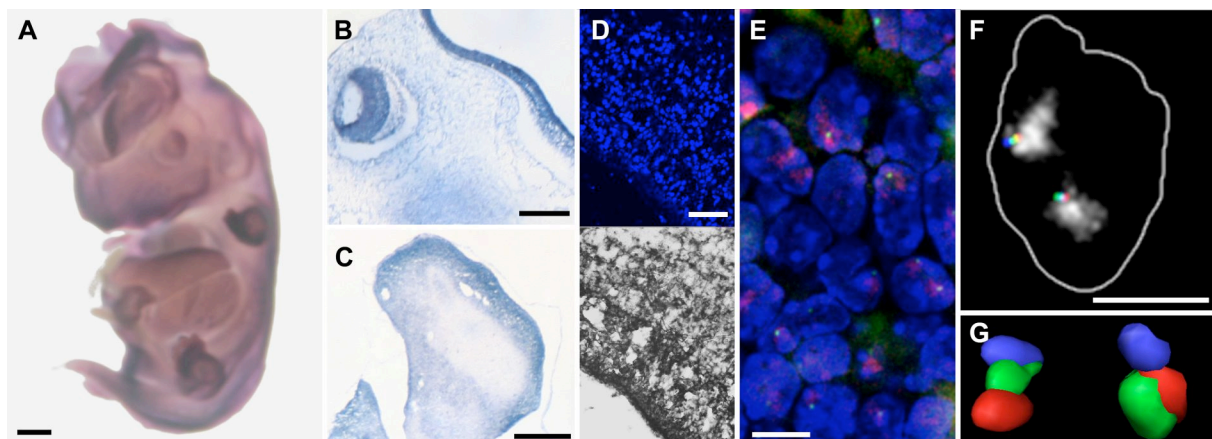


Figure 4.17: (A-C) RNAish on mouse E13.0 with a Bcl11a RNA antisense probe. (A) Whole mount mouse E13.0 (scale bar 1mm) (B-C) 20µm tissue cryosection of chicken E5.5: (B) brain sagittal, between eye and lateral ventricle, (C) hind limb horizontal (scale bar 0.5mm). (D) Confocal image of the chicken E5.5 neopallial cortex: DAPI counterstain (blue) and brightfield image of NBT/BCIP RNAish precipitate (grey). (E) Unprocessed confocal image slice of mouse E13.0 neopallial cortex nuclei (z step = 150nm): DAPI counterstain (blue), mouse chromosome 11 (red), mouse Bcl11a gene (green). (F) Processed mouse E13.0 neopallial cortex nucleus: Z-projection of a confocal image stack (97 slices), counterstain outlined (white), mouse chromosome 11 (grey), Bcl11a (green), gene-rich control (red), UCS cluster (blue) (scale bar 5µm). (J) 3D reconstruction (AMIRA 3.1.1) of the local chromatin conformation between Bcl11a (green), Xpo1 (red) and the UCS cluster (blue).

4.1.3.2 Bcl11a mRNA expression pattern

Chromogenic whole mount RNA in situ hybridization with a DIG-T7-Bcl11a antisense probe on mouse E13.0 (figure 4.18) produced the same expression pattern as published by Leid et al. 2004 and is described in detail therein. The Bcl11a expression pattern was determined the same way in whole mount chicken E5.5 and was found to be evolutionarily conserved between mouse E13.0 and chicken E5.5,

with respect to tissue specificity and relative expression intensities. Besides other tissues, strong expression in brain and the limbs was detected (figure 4.18).

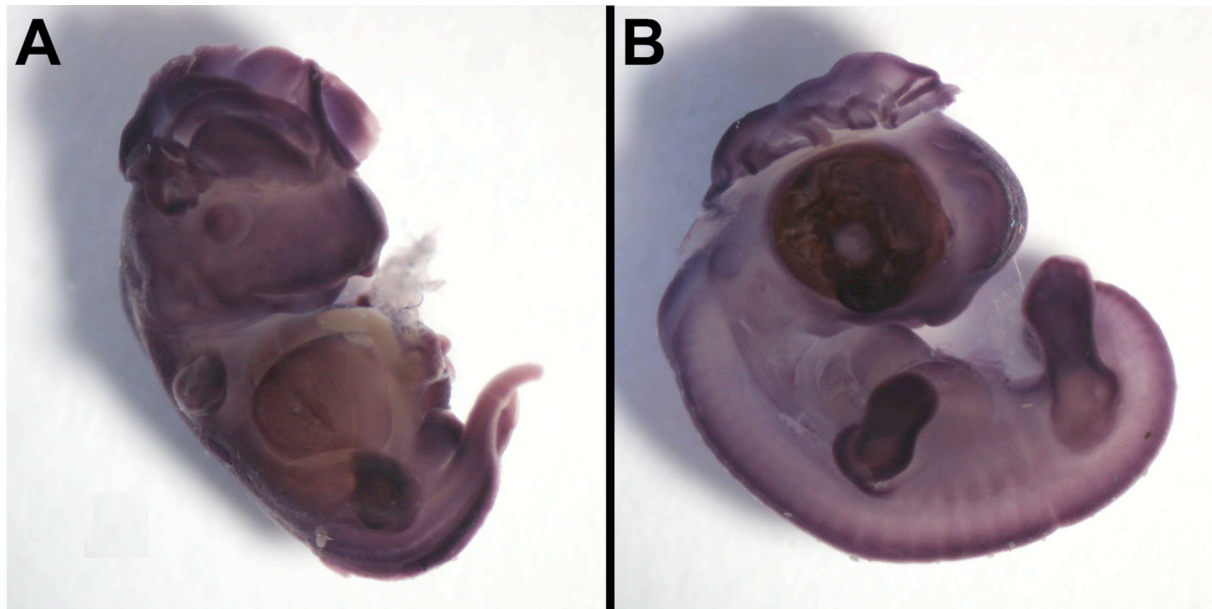


Figure 4.18: Whole mount RNAish with a Bcl11a DIG RNA anti-sense probe detected with NBT/BCIP: (A) Mouse E13.0, (B) Chicken E5.5. Among other organs Bcl11a was strongly expressed in the brain and in the limb buds.

We repeated RNA in situ hybridization on sagittal brain and horizontal hind limb bud tissue sections (figure 4.17 A-D). Bcl11a was broadly expressed in the brain and in particular strong in the brain ventricles and in the striatum, while parts of the midbrain and the cephalic mesenchyme no expression was detected. In the hind limb bud Bcl11a expression was demonstrated in the mesenchyme underlying the entire hind limb bud but not in the hind limb plate. Therefore both selected body regions, were used in FISH experiments, and thus allowed the parallel analysis of transcriptionally active and inactive tissue.

RNA FISH in tissue sections of mouse E13.0 visualized sites of nascent Bcl11a mRNA expression in head nuclei. The expression pattern was comparable to that observed by chromogenic RNAish (see 4.1.3.3).

The observed expression differences were validated and relatively quantified from laser microdissected tissue of mouse E13.0 with qPCR in the same way as for Dach1 (see 4.1.2.2). Bcl11a mRNA from expressional active and silent brain regions was isolated by laser microdissection, from each 200-300 cells, reversely transcribed to cDNA and relatively quantified with TaqMan based qPCR. Triplicate experiments from three independent tissue sections resulted in a relative expression difference of $34.4 \text{ sdm} \pm 12.3$, and thus confirmed the RNAish observations.

4.1.3.3 Nuclear radial arrangement of the Bcl11a region

The radial localization of BAC clones for Bcl11a, the gene rich control region, the UCS cluster and the respective chromosome paint probe was determined with respect to the nucleus using the 3D-RRD software. We obtained statistically considerable position differences for the Bcl11a region that could not be correlated with CT position variegations (table S3) nor could be linked to the expression status of Bcl11a, however the radial nuclear position was strongly conserved between homologous tissues from mouse and chicken.

In mouse E13.0 the Bcl11a gene was localized more internally in expressing forebrain ventricles (ARR 66.4% $\text{sdm} \pm 1.0$) than in the silent midbrain (ARR 72.1% $\text{sdm} \pm 1.0$). In contrast the Bcl11a gene was positioned closer to the nuclear periphery in the expressing mouse hind limb mesenchyme (67.4% $\text{sdm} \pm 1.0$) than in the silent limb bud plate (63.1% $\text{sdm} \pm 1.1$). Accordingly, the Bcl11a gene was statistically significantly more peripheral in the midbrain versus the hind limb bud plate (table S3 for statistics). Likewise, in tissues of chicken E5.5 the Bcl11a region was more internal in the telencephalon (ARR 67.1% $\text{sdm} \pm 1.0$) and in the limb bud plate (61.6% $\text{sdm} \pm 1.0$) compared to the midbrain (71.7% $\text{sdm} \pm 0.9$) and the hind limb mesenchyme (73.1% $\text{sdm} \pm 1.0$), irrespectively of the Bcl11a expression status. Notably, no significant differences of Bcl11a radial distributions between orthologous tissue of mouse and chicken were identified (figure 4.19).

The evolutionary nuclear position conservation of the Bcl11a gene between mouse and chicken was also found for embryonic fibroblasts. The ARR of the Bcl11a gene was nearly identical for mouse (ARR 61.4% $\text{sdm} \pm 1.5$) and chicken (ARR 61.2% $\text{sdm} \pm 1.3$) and slightly more internal compared to tissue. The flanking gene-rich control and the UCS cluster resided in close proximity (max Δ ARR 1.7% in mouse and 0.8% in chicken).

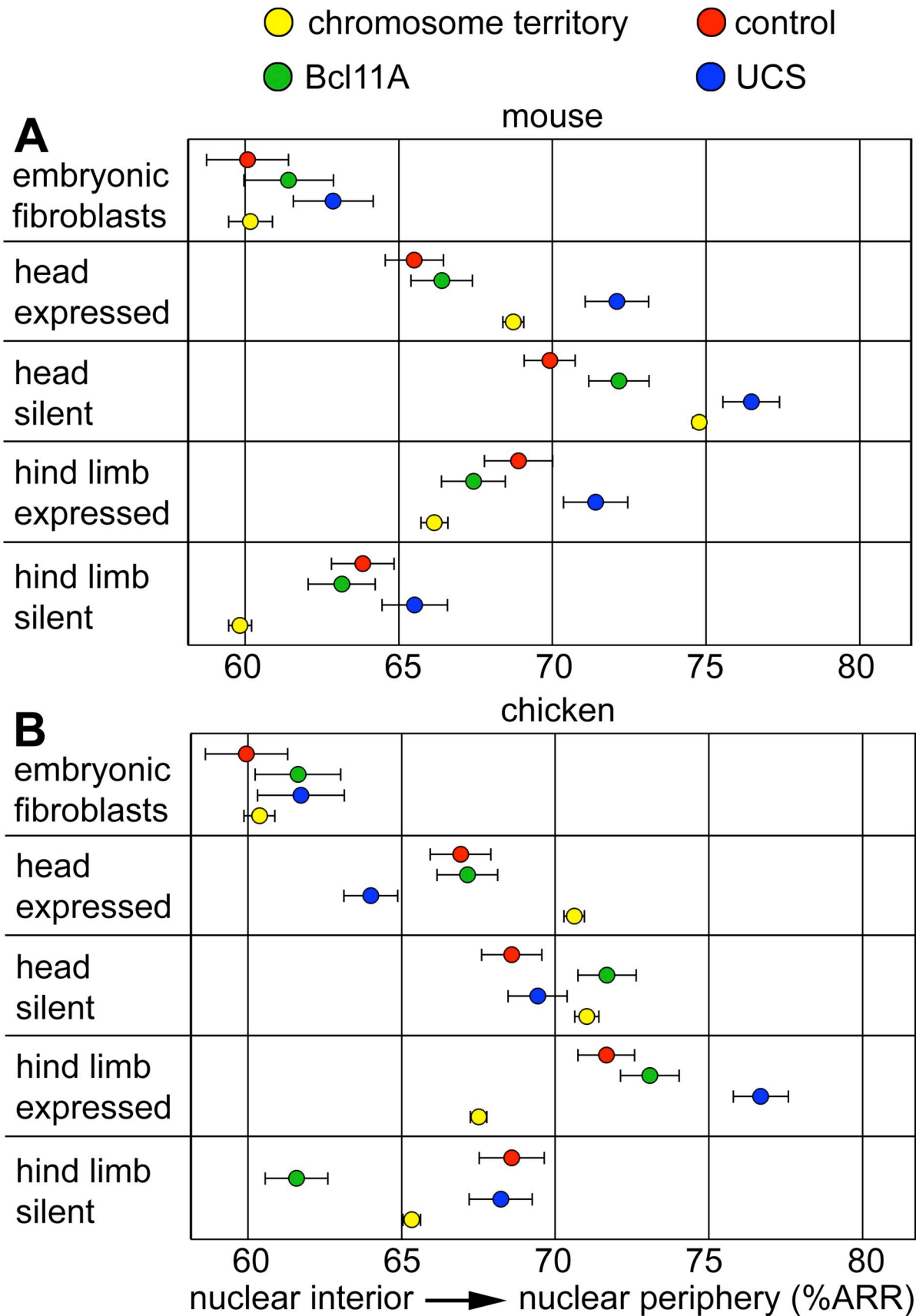


Figure 4.19: ARR dot blot of the Bcl11a region. (A) mouse chromosome 11 (yellow) or (B) chicken chromosome 3 (yellow), the Bcl11a gene (green), the gene-rich control UCS cluster A and B two both sides (red, blue) in tissue sections of mouse E13.0 or chicken E5.5, respectively. (error bars indicate the sdm, figure S1 for distribution curves)

To verify if the radial localization of Bcl11a in expressing cells in the nucleus refers to sites to nascent Bcl11a mRNA expression in tissue we performed RNA FISH in tissue sections of mouse E13.0 head (figure 4.20). RNA expression was only detected in tissue areas afore shown to express Bcl11a by chromogenic RNAish. In the brain ventricles sites of expression were flexibly localized in the nuclear center as well as in the nuclear periphery, in accordance to the broad radial distribution of the Bcl11a gene determined by DNA FISH (figure 4.20). By conclusion the radial distance was not directly influenced by the expression status of Bcl11a in single tissue cells, and Bcl11a expression can be driven from different nuclear positions.

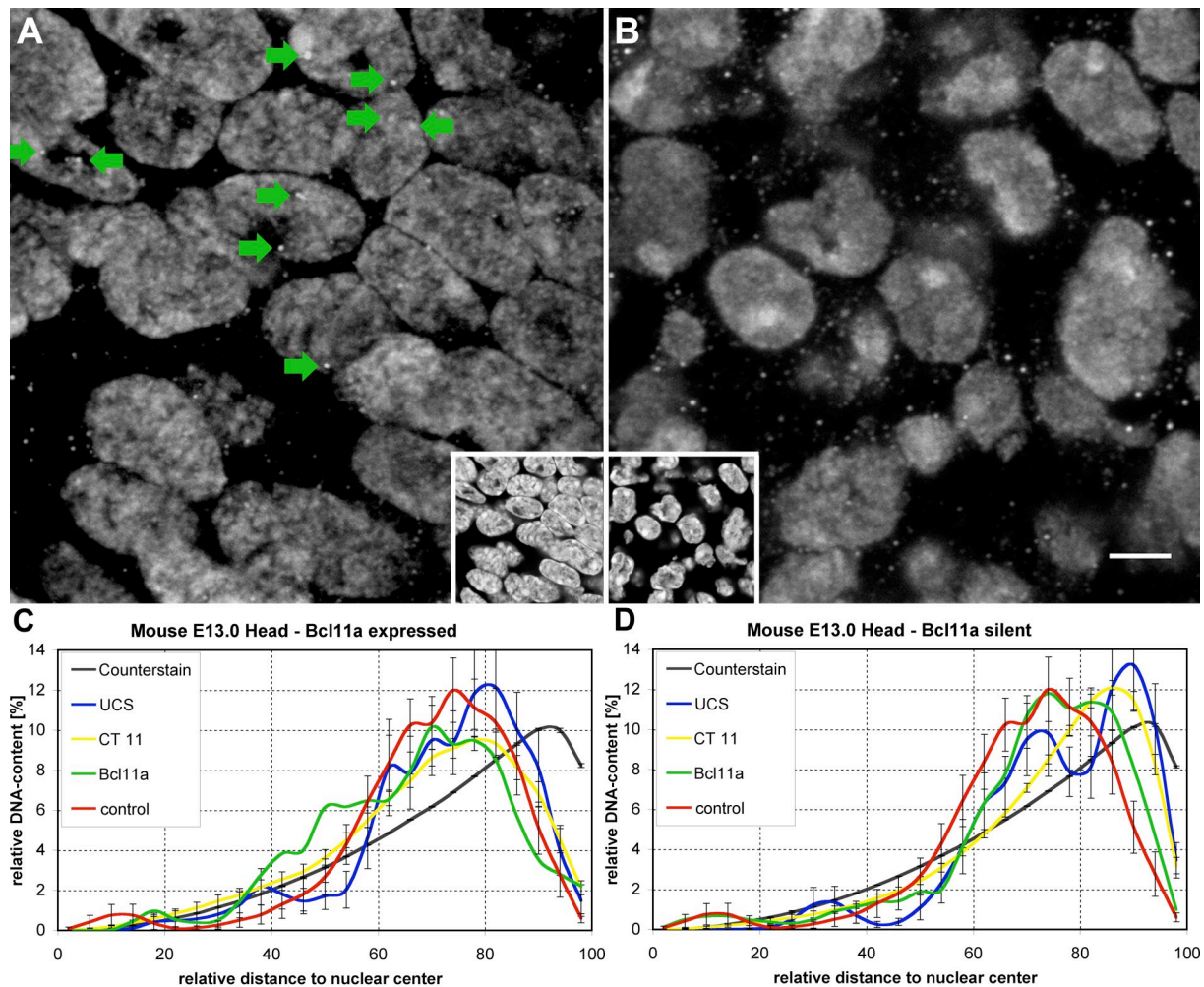


Figure 4.20: RNA FISH with a Bcl11a RNA antisense probe on mouse E13.0 tissue sections. (A) Neopallial cortex: Sites of expression are exemplarily indicated with green arrows (2 μ m z-projection). (C) The flexible position of expression sites matches the relative radial distribution of the Bcl11a gene evaluated from 3D-FISH (B) Head mesenchyme: No sites of expression were detected. (D) The Bcl11a region showed a more stable and more peripheral radial position also in expressional silent nuclei. A blank control without a RNA probe in the hybridization mix produced equal background as in silent tissue (figure 4.10)

4.1.3.4 Distance to the chromosome territory surface of the Bcl11a region

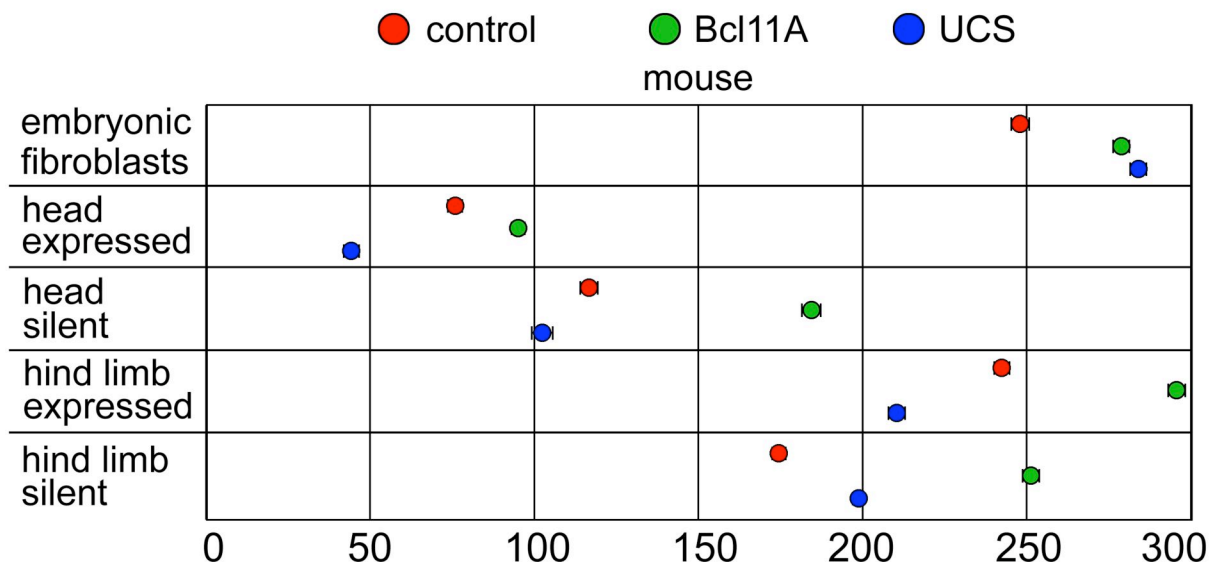
The physical distance of the Bcl11a gene, the gene rich control and the UCS cluster referencing the interphase CT surface was calculated utilizing the software EDMT. In

all five evaluated cell types per species the resulting mean e for the Bcl11a gene to the surface was rather flexible. In mouse the mean distance of the Bcl11a gene from the CT 11 surface in the E13.0 hind limb bud mesenchyme (288nm) and hind limb plate was significantly higher (244nm) than in the telencephalon ventricle (67nm) and the midbrain (167nm) (table S3 for statistics, figure 4.21). The flanking regions always resided at closely the same distance to the territory border (max Δ 92nm).

In chicken the Bcl11a gene was most positioned internally of chicken chromosome 3 in all evaluations compared to the UCS cluster and the gene rich control region. The maximum intra experimental distance difference among the region varied considerably between 60nm in the expressing hind limb mesenchyme and 273nm in the silent hind limb plate. In the hind limb plate (230nm) the Bcl11a gene was significantly orientated towards the territory interior compared with the hind limb mesenchyme (119nm) and both evaluated tissue in the head. Further, in the head a significant trend towards the territory surface was determined in the expressing brain ventricles (79nm) compared with the silent parts of the midbrain (159nm) (table S3 for statistics).

The distance to the territory surface in embryonic fibroblast was is in the range found in tissue sections. The mouse Bcl11a gene was 258nm and the chicken Bcl11a gene was located 215nm to the inside of the harboring CT.

Notably, in all evaluated tissue on average around 14% of the gene rich control signal volumes were found outside of the core territory determined by computing mouse CT11 paint with a maximal distance of around 0.5 μ m but 27% outside the chicken core CT 3 with a maximal distance of 0.8 μ m to the territory border.



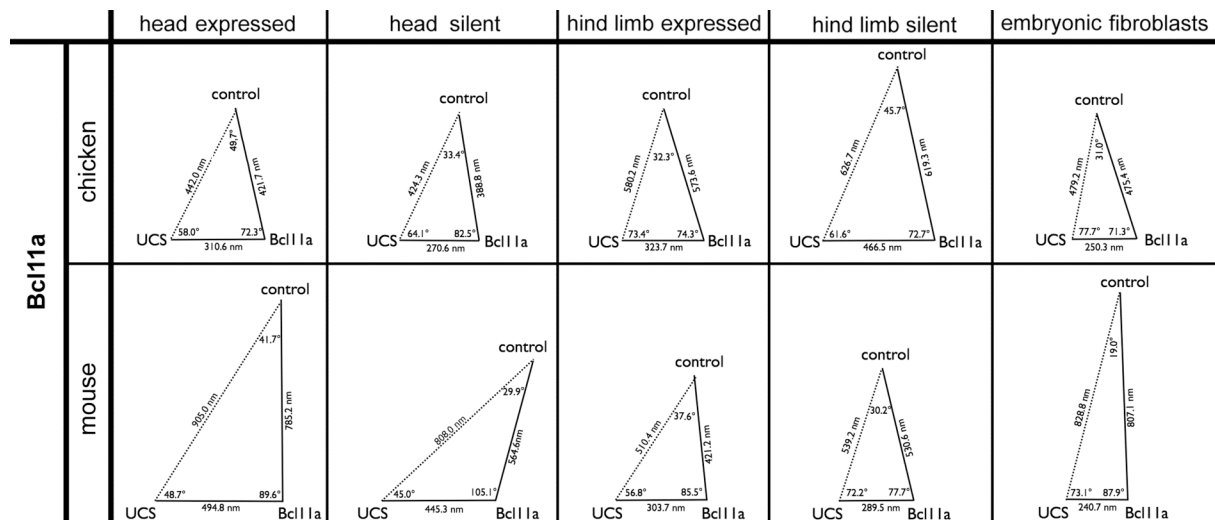


Figure 4.22: Triangular display of the higher order chromatin conformation obtained by mean distances and angles measurements in mouse tissue E13.0 between the gene-rich control, Bcl11a and UCS.

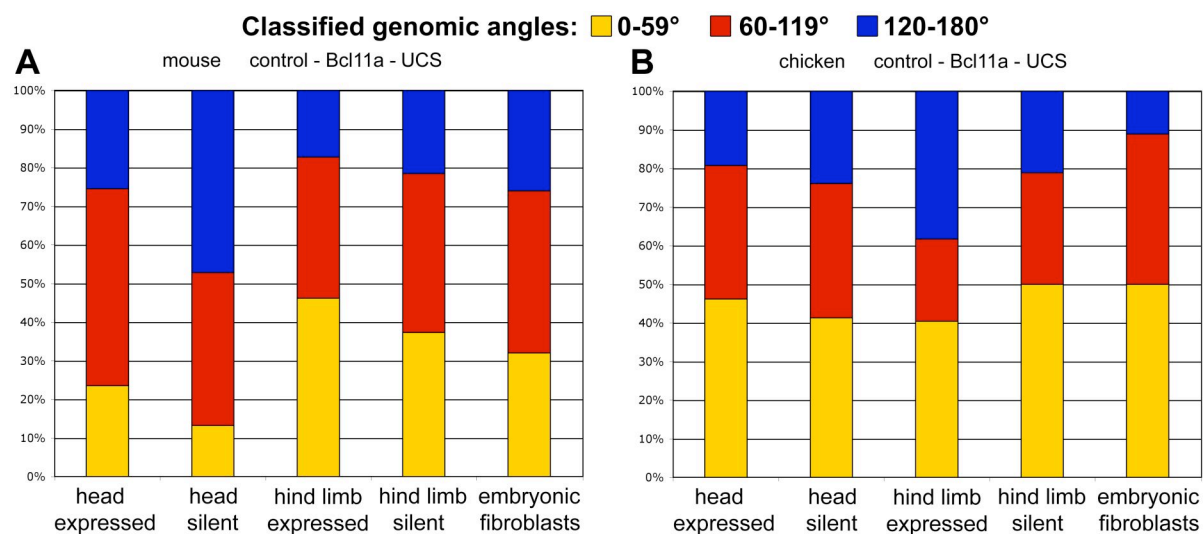


Figure 4.23: Genomic angles gene-rich control-Bcl11a-UCS angles, with Bcl11a as apex classified between 0-59°(yellow), 60-119° (red) and 120-180° (blue) in interphase nuclei of (A) mouse and (B) chicken.

Interestingly, the chromatin compaction between the Bcl11a gene and the gene rich control region (MMU: 0.93-1.78 kbp/nm, GGA: 0.73-1.16 kbp/nm) versus the chromatin compaction between the Bcl11a gene and the UCS cluster (MMU: 2.43-4.97 kbp/nm, GGA: 1.13-2.11 kbp/nm) was significantly different for each evaluation of mouse and chicken (see table S3 for statistics). The gene-rich chromatin reproducibly displayed a more open chromatin conformation compared with the gene desert containing the UCS cluster. Next, significant differences of chromatin compactions amongst different tissue were found, highlighting the flexibility concerning the chromatin compaction of the locus between different cell types, which in no case was functionally linked with Bcl11a expression differences (figure 4.24, table S3 for statistics).

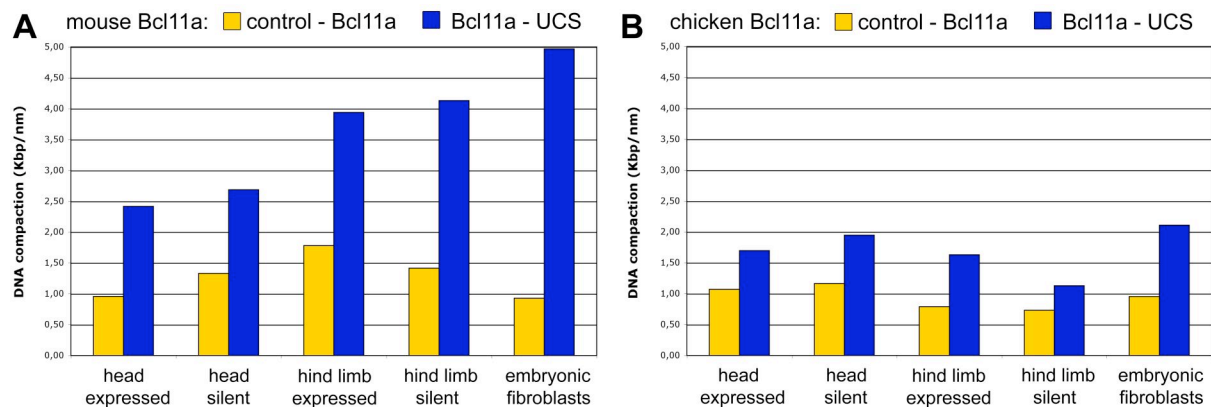


Figure 4.24: Chromatin compaction in kbp/nm calculated from distance measurements between gene-rich control to Dach1 (yellow) and UCS to Dach1 (blue) in (A) mouse and (B) chicken interphase nuclei.

Again, control experiments were carried out on mouse embryonic fibroblasts to verify the accuracy of distance measurements with single BAC clones for the gene rich control, Bcl11a and the center of the UCS cluster (figure 4.26).

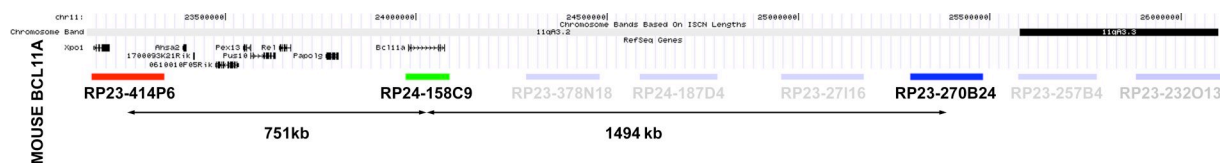


Figure 4.25: Probe set to control distances and angles measurements in mouse and chicken embryo fibroblasts. The BAC clones for Bcl11a (green), the gene rich Xpo1 control and the central part of the UCS (red) cluster were used (blue).

The genomic angle around the Bcl11a gene in fibroblasts of mouse (87.9°) displayed no significant difference to the control experiments (84.2°). The mean distance between the Bcl11a gene and the gene-rich control was measured twice, in the experiment with the entire (figure 4.16) and in the control (figure 4.25) BAC clone set, and matched closely between the two independent experiments ($\Delta 36.0\text{nm}$, chromatin compaction 0.97 kbp/nm and 0.93 kbp/nm). Also the chromatin compaction comparing the entire BAC clone set and the central BAC clone for UCS cluster was highly similar (4.97 kbp/nm and 5.63 kbp/nm , respectively). This again underpinned the accuracy and reproducibility of the distance measurements obtained in this study.

4.1.3.6 Results summary of Bcl11a

The radial position of Bcl11a in the nucleus was rather flexible at the single-cell level, as well as between tissues from one species. Sites of nascent RNA expression showed an equally broad radial distribution in tissue nuclei. Despite this, the Bcl11a expression status was found not to influence the radial nuclear distribution in a direct way. Surprisingly, the radial position between homologous tissues and embryonic

fibroblasts of mouse and chicken was evolutionarily conserved and statistically indistinguishable.

The *Bcl11a* locus in mouse could be shown to reside close to the CT 11 surface. In contrast, the chicken ortholog showed more positional freedom in the different tissues, resulting in frequent localization of the gene-rich control outside the core CT 3.

The genomic angle around *Bcl11a*, was nearly gaussian distributed in all evaluations. The chromatin compaction showed significant differences between cell types, however the chromatin of the gene-rich control side was always less condensed compared with the chromatin to the UCS side.

4.2 Nuclear topology of mammalian genomic innovative genomic region

Innovative genomic changes frequently mark key evolutionary steps, which may also be relected by nuclear topological changes. As an example we focused on the analysis of the genomic region involved in the complex rearrangement events leading to the formation of the mammalian casein (*Csn*) gene cluster, coding for the major milk protein. In addition to the effects of the gene duplication events in mouse compared to chicken, the casein genes offer the possibility to trace the effects of profound gene expression activation in mouse during lactation.

4.2.1 Experimental design

Three BAC clones were identified from public databases, each for mouse and chicken. Mouse clones covered the exclusively mammalian *Csn* cluster and the conserved genes flanking vertebrate orthologous sequences represented by *Igj* (5') and *Sult1b1* (3'). Two of the chicken clones also mapped to the vertebrate orthologous segments starting with *Igj* (3') and *Sult1b1* (5') genes. The third clone in between mimicked the mapping of the *Csn* cluster (termed pseudo *Csn*). In addition to the casein linked gene duplication the order of more distal reference genes is highly changed between mouse and chicken due to intrachromosomal rearrangements since the separation from the last common ancestor. Therefore the chicken pseudo *Csn* clone is homolog directly 5' to the mouse *Alb1* gene locus, outside the mouse *Csn* cluster, 3' to *Igj* (see 2.5, figure 4.26).

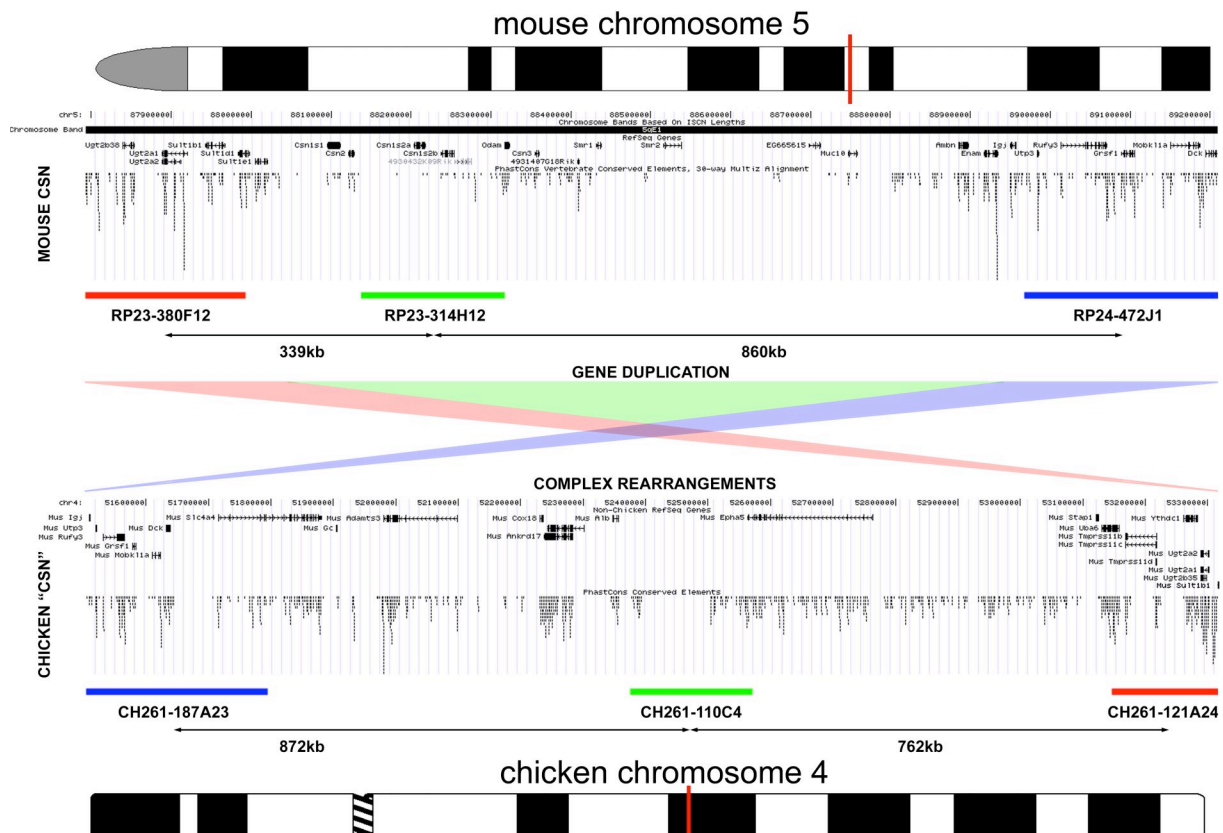


Figure 4.26: Comparative experimental design map for the *Csn* locus of mouse and chicken. The *Csn* gene cluster originated from a gene duplication event in the mammalian lineage and is not present in avians. Evolutionary sequence conservation is shown as PhasCons Vertebrate Conserved Elements, Multiz Alignment (30-way or 10-way alignment see Siepel et al. 2005). Mouse BAC clones depict the *Csn* gene cluster (green), and the flanking vertebrate ortholog sequences beginning with *Sult1b1* (5', red) and *Igj* (3', blue). Complex evolutionary rearrangements inverted the orientation of the vertebrate orthologs in the chicken genome (*Sult1b1* 3' red, *Igj* 5' blue). A BAC clone directly 3' to the *Alb1* gene mimics the presence of the *Csn* cluster in chicken (pseudo *Csn*, green). The *Alb1* locus is (adapted from <http://genome.ucsc.edu/>, mouse assembly July 2007, chicken assembly May 2006) located 3' to the *Igj* in the mouse genome.

The three selected mouse BAC clones were differentially fluorescently labeled and were used together with a mouse chromosome 5 painting probe for in situ hybridizations tissue sections of mouse mammary gland of three postnatal developmental stages (figure 4.27 F-H) and mouse hair follicle (figure 4.27 D), as well as to mouse embryonic fibroblasts as an ex vivo control. Mammary glands were obtained from a juvenile mouse, a lactating mouse and a retired breeder mouse after several cycles of pregnancy. Chromogenic RNAish was further employed to visualize expression differences of *Csn* genes among the postnatal developmental stages of mammary gland (figure 4.27 A-C). The three differentially labeled chicken BAC clone probes were combined with a chicken chromosome 4 painting probe and hybridized in situ to tissue sections from chicken feather follicles (figure 4.27 E) and to cultured chicken embryonic fibroblasts. Notably, all investigated organs of mouse and chicken are evolutionary developments of the skin and use epithelial cells as source of cyclical growth (see 2.7).

The position of the FISH probes in reference to the nucleus and the harboring CT was evaluated selectively from epithelial cells. The local, triangular higher order chromatin conformation was quantified by distance and angle measurements among the three BAC probes (figure 4.27 I,J).

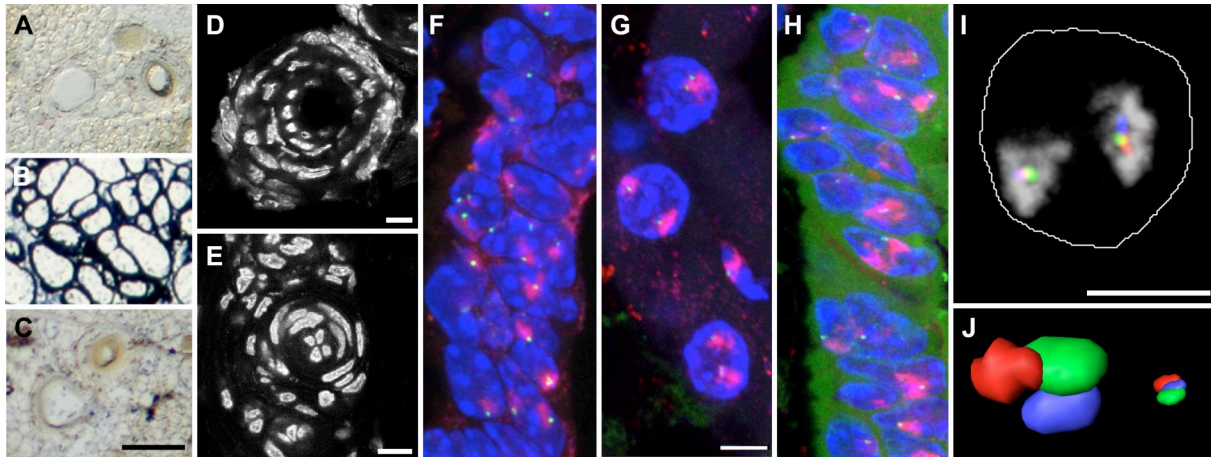


Figure 4.27: (A-C) RNAish on 20 μ m mouse mammary gland cryosections with a Csn3 RNA antisense probe (staining 12h, each): (A) juvenile (16-18wk) before pregnancy (B) lactating with strong Csn3 expression (C) retired breeder after complete involution (scale bar 250 μ m). (D-E) DAPI (grey) stained cross sections through a mouse hair follicle (D) and a chicken downy feather follicle (E) (scale bar 20 μ m). (F-H) Unprocessed confocal image slice (z step = 150nm): DAPI counterstain (blue), mouse chromosome 5 (red), mouse Csn gene cluster (green). (F) Epithelial cells of lactal duct in a juvenile mouse, (G) secreting epithelial cells of an alveoli in lactating mouse and (H) epithelial cells of lactal duct in a retired breeder mouse after complete involution (scale bar 5 μ m). (I) Lactating epithelial cell: Z-projection of a processed confocal image stack (106 slices), counterstain outlined (white), mouse chromosome 5 (grey), Csn gene cluster (green), Sult1b1 region (red), Igj region (blue) (scale bar 5 μ m). (J) 3D reconstruction (AMIRA 3.1.1) of the local chromatin conformation between Csn gene cluster (green), Sult1b1 region (red), Igj region (blue).

4.2.2 Casein genes mRNA expression pattern

Tissue sections of three postnatal developmental stages of mouse mammary gland were hybridized with RNA antisense probes for Csn3 (4.27 A-C) and Csn1s2a (data not shown) and detected chromogenically. RNA expression of both Csn genes was detected at high levels exclusively during lactation in the epithelial cells around the alveoli and lactal ducts. No expression of Csn3 or Csn1s2a was detected in the remaining adipose tissue during lactation, in the juvenile or in the involuted mammary gland. Hence RNA expression from the Csn gene cluster was confirmed to be limited to epithelial cells during lactation.

4.2.3 Nuclear radial arrangement of Casein region

We hybridized multi color FISH probes covering the Csn gene cluster, the flanking regions harboring Sult1b1 and Igj and a mouse chromosome 5 paint to tissue cryosections of juvenile, lactating, retired breeder mammary gland, hair follicles and embryonic fibroblasts of mouse. In chicken, embryonic fibroblasts and feather follicles were hybridized with probes detecting chicken CT 4, Sult1b1, Igj and pseudo

Csn in between Igj and Sult1b1. The nuclear radial arrangement was evaluated from this material using 3D-RRD software.

We determined the mean volume and mean surface to volume ratio of all nuclei in each experiment, because already by visual inspection we observed pronounced morphological differences between lactating and non-lactating mammary epithelial cell nuclei. During lactation epithelial cells in mouse increased their nuclear volume by approximately 1/3 compared with non-lactating mammary epithelial nuclei. Together with a decreasing surface to volume ratio a significant swelling and rounding of the secretory epithelial cells was evident (figure 4.27 F-H and figure 4.28, table S 4).

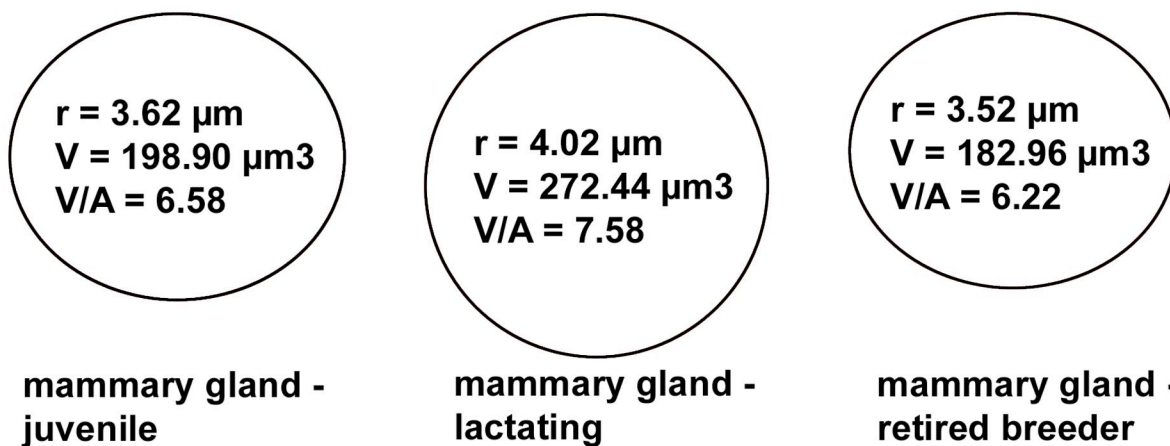


Fig 4.28: Changes of the morphology of mouse mammary epithelial cell nuclei in the course of lactation. In the lactating state the nuclear volume increased about 1/3 and the nuclei became more spherical (r = radius, V = volume, V/A = Volume to surface ration = roundness factor) (figure 4.27 F-H). (table S4 for details)

In line with the nuclear morphology changes during lactation a clear radial relocation of the Csn gene cluster including the flanking Sult1b1 and Igj regions to the nuclear center was observed (figure 4.29).

In Csn non-expressing, non-secretory mammary epithelial nuclei of juvenile and involuted mice the casein locus was positioned in the nuclear periphery (ARR 78,0% $\text{sdm} \pm 0.7$ and 71,7% $\text{sdm} \pm 0.6$, respectively, figure 4.30). The position difference in the juvenile compared to the involuted mammary gland was corrected with the position difference of the chromosome 5 paint resulting in a Δ ARR of only 1.7% in the Csn position after correction. Thus the position difference between juvenile and retired breeder mammary epithelial nuclei was caused by a position variation of the entire CT and not only the Csn region. In contrast, in Csn expressing secretory epithelial cells of lactating mammary gland the casein locus was highly significantly shifted to the nuclear center (ARR: 56,4%, $\text{sdm} \pm 0.9$) including the flanking reference regions. Besides, the relative orientation of the casein flanking loci was conserved in all mouse epithelial nuclei of hair and mammary gland. Sult1b1 was always

orientated towards the nuclear periphery in reference to Igj (Δ ARR juv 7.1% lact 4.6% invol 8.6%). This orientation was most prevalent and statistically valid in the juvenile and involuted mammary gland. The harboring chromosome paint was astonishingly stably positioned in all tissues (juv 69.2% lact 66.3% invol 64.5%), and therefore the relocalization can specifically attributed to the Csn region. In addition, the Csn locus was significantly more internal localized than the entire chromosome 5 in casein expressing nuclei but significantly more peripheral in all non-expressing tissue (table S3 for statistics). Further, the casein genes (ARR 74.6% $\text{sdm} \pm 0.8$) and the flanking regions were located in the hair follicle almost in the same radial position as in inactive mammary gland epithelial cells. Again Sult1b1 (ARR 74.4% $\text{smd} \pm 0.8$) tended to locate peripheral to Igj (ARR 70.1% $\text{sdm} \pm 0.9$). In contrast, cultured embryonic fibroblasts no preferential locus orientation was found. Here the chromosome 5 paint (ARR 63.7% $\text{sdm} \pm 0.5$) and more pronounced the Csn genes (ARR 67.6% $\text{sdm} \pm 1.3$) were slightly shifted more to the nuclear interior compared to the non-expressing tissue.

When comparing non-expressing mouse and chicken tissues the genomic innovation of caseins in this region did not change the nuclear position of the orthologous genes in the two species. Sult1b1 and Igj stably retained their position in the nuclear periphery in the follicular structures (ARR mouse: Sult1b1 74.4% and Igj 70.1%, ARR chicken: Sult1b1 70.5% Igj 71.5%) and in embryonic fibroblasts. Moreover, chicken Sult1b1 and Igj resided at about the same radial distance without an obvious orientation preference (figure 4.29, table S3).

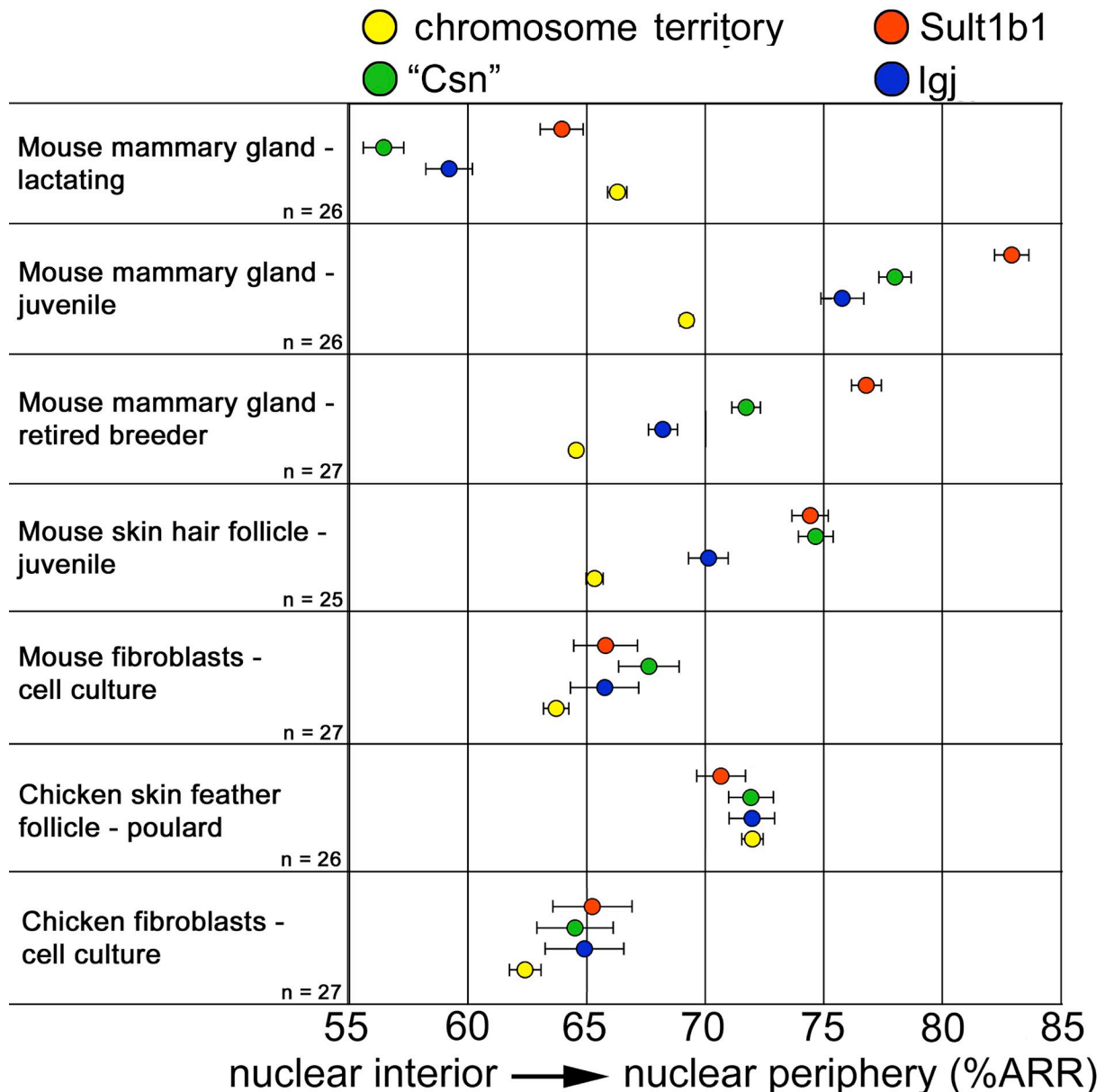


Figure 4.29: ARR dot blot of the Csn region encompassing mouse chromosome 5 (yellow) or chicken chromosome 4 (yellow), the Csn genes (mouse) or the pseudo Csn (chicken) (green), Sult1b1 (red) and Igj (blue) in tissue sections of mouse mammary gland, mouse hair, chicken feather and embryonic fibroblasts of both species. (error bars indicate the sdm, figure S1 for distribution curves)

4.2.4 Distance to the chromosome territory surface of the Casein region

By measuring the absolute distance of the Csn genes to the CT surface in mouse with EDT software we did not find looping away from the CT upon transcriptional activation in any cell nucleus (figure 4.30). In all mouse mammalian epithelial cells of the three postnatal developmental stages the Csn genes and the flanking loci encompassing Sult1b1 and Igj here located in the interior proximity to the CT 5 surface (Csn mean distance 80-146nm) and without displaying any significant differences (table S3 for statistics).

The Csn genes in epithelial cells of mouse hair were found closer to the territory surface (35nm) whilst they were more to the territory inside in mouse embryonic fibroblasts (258nm) compared with mammary gland epithelial cells (table S3). The orthologous segments, Sult1b1 and Igj in chicken chromosome 4 of epithelial cells in feathers and of embryonic fibroblasts showed on average less positional flexibility and were located slightly more to the inside of the CT (150-200nm). However, distances were still in the range observed for mouse orthologs (figure 4.30).

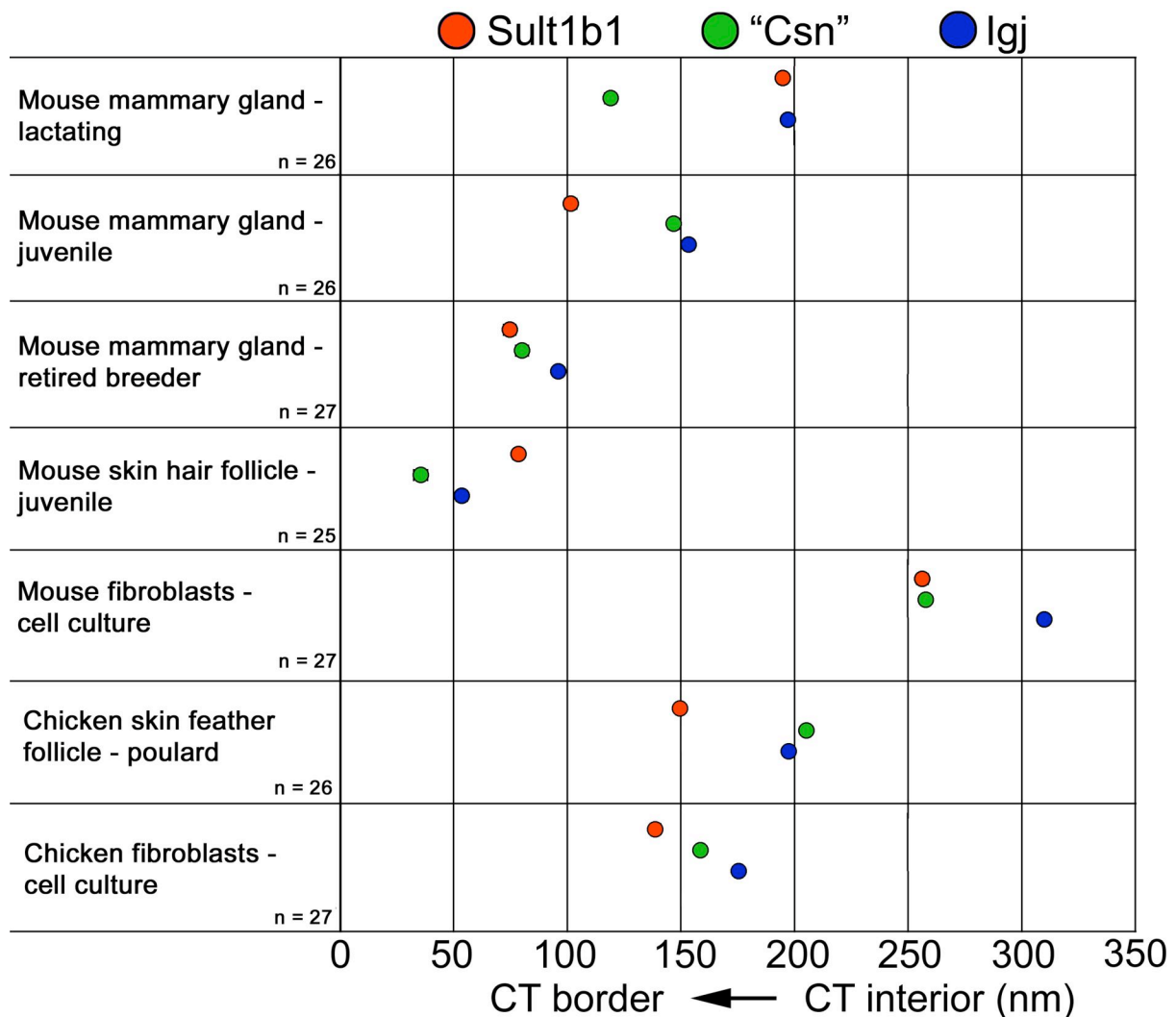


Figure 4.30: Dot blot of mean distances to mouse chromosome 5 or chicken chromosome 4 surface harboring the Csn genes (mouse) or the pseudo Csn (chicken) (green), Sult1b1 (red) and Igj (blue) in tissue sections of mouse mammary gland and hair, chicken feather and embryonic fibroblasts of both species. (error bars indicate the sdm, figure S2 for distribution curves)

4.2.5 Mean higher order chromatin conformation of the Csn region

Together with the flanking regions Igj and Sult1b1 the central Csn gene cluster presented a genomic triangle in the interphase (figure 4.31). By measuring 3D interphase distances and angles we determined the average triangular higher order chromatin conformation of the Csn locus (DistAng software). To normalize between different genomic distances the chromatin compaction in kbp/nm was calculated.

In mouse the mean genomic angle around the casein cluster in mammary gland was significantly more pointed during casein expression (71.5°) than before first gene activity in the juvenile stage (97.5°) and after closed expression with complete involution (96.9°) (figure 4.32, 4.33). Moreover, the genomic angle around casein in mouse fibroblasts (85.8°) and hair follicle (81.3°) was comparatively intermediate and showed no significant difference to any mammary gland developmental stage (figure 4.31, 4.32). In chicken the genomic angle distribution around the pseudo Csn was not statistically distinguishable between the two evaluations in feather hair follicle and embryonic fibroblasts (table S3 for statistics).

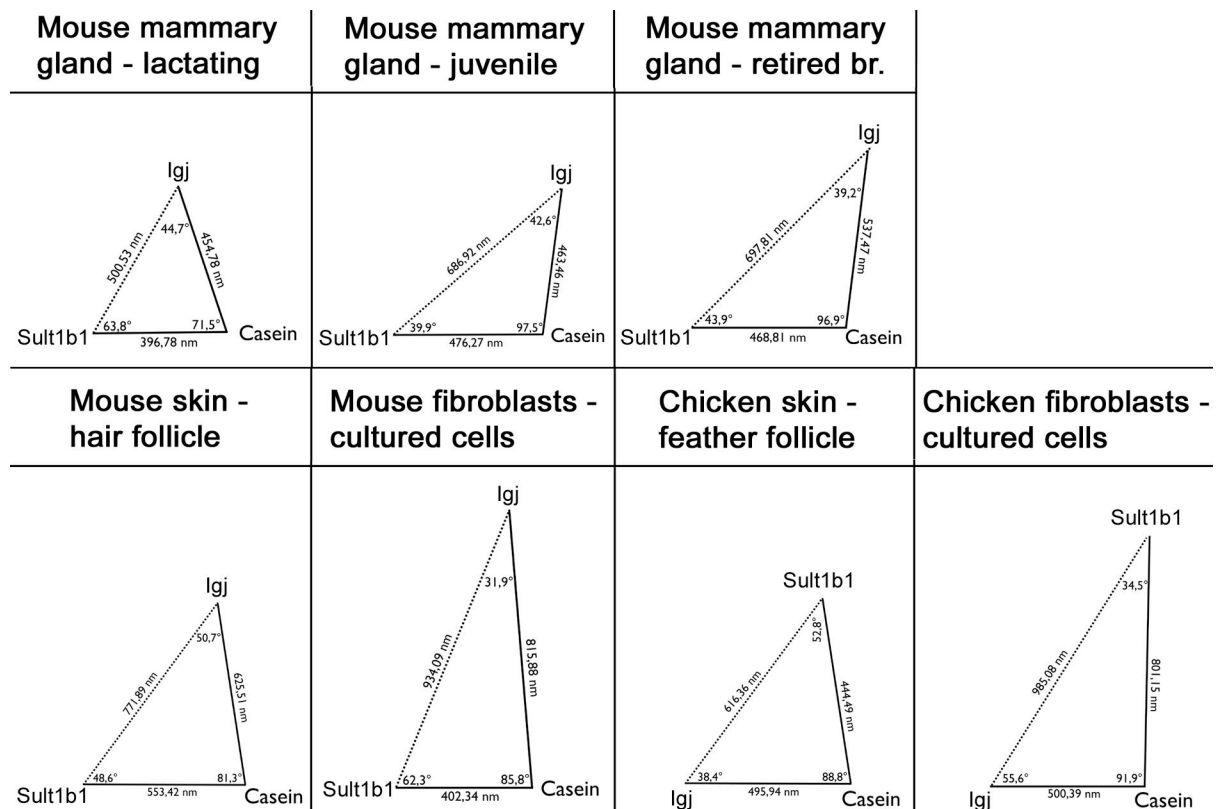


Figure 4.31: Triangular display of the higher order chromatin conformation obtained by distance and angle measurements in mammary gland of a juvenile, a lactating and a retired breeder mouse, mouse hair follicle, chicken feather follicle and embryonic fibroblasts of mouse and chicken between Sult1b1, the Csn genes (mouse) or the pseudo Csn (chicken) and Igj.

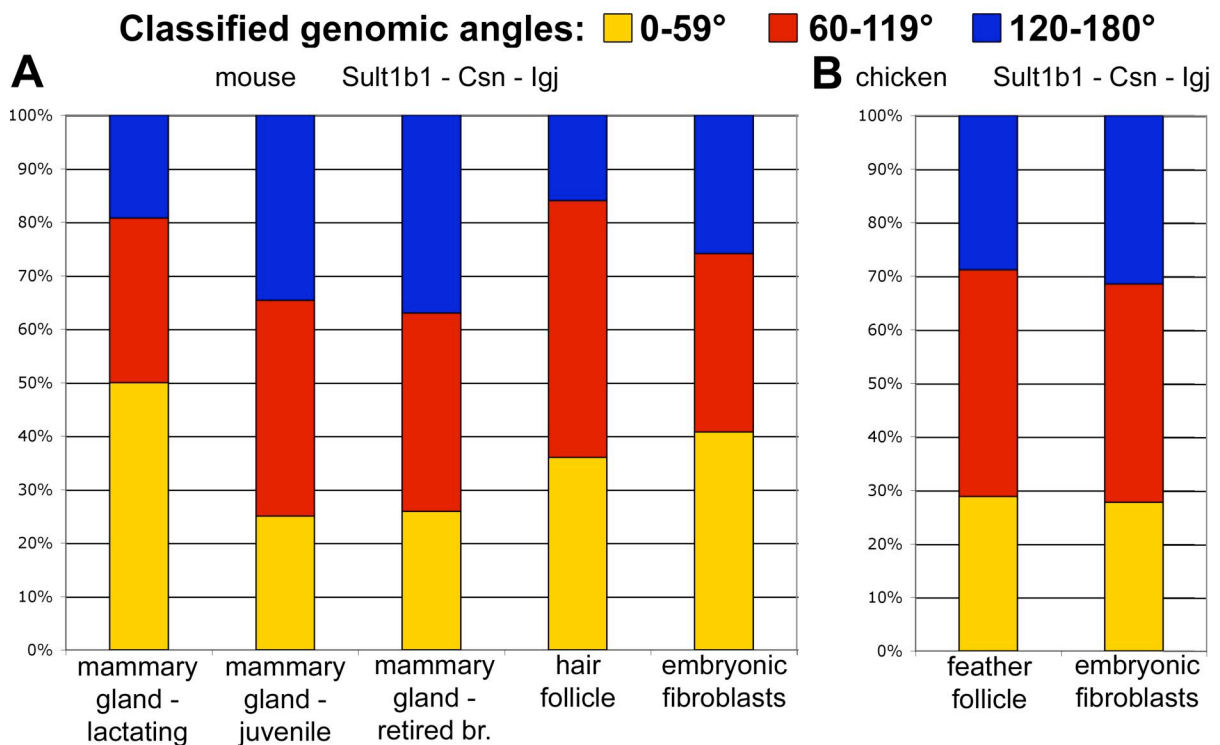


Figure 4.32: Classified genomic angles Sult1b1-Csn-Igj angles, with Csn as apex classified between 0-59° (yellow), 60-119° (red) and 120-180° (blue) in interphase nuclei of (A) mouse and (B) chicken.

In contrast the observed angles of genomic angles, the DNA compaction in the Sult1b1-Csn (0.72-0.85 kbp/nm) or Igj-Csn (1.60-1.89 kbp/nm) showed no significant differences in any of the three developmental stages, irrespective of lactating or non-lactating status of the mouse mammary gland. However, underlining the observation on chromatin back folding, the DNA compaction between Sult1b1 and Igj loci was significantly increased during lactation (2.40 kbp/nm) compared to the two non-expressing states, juvenile (1.72 kbp/nm) and involution (1.72 kbp/nm). Further the chromatin compaction at the Sult1b1-Csn side (0.64 kbp/nm) and the Igj-Csn side (1.38 kbp/nm) in the hair follicle was more open and exhibited significant differences to the lactating and juvenile state (figure 4.33, table S3 for statistics). Embryonic fibroblast of mouse and chicken displayed a significantly more open chromatin conformation in comparison to hair and feather follicle, respectively, and possibly linked to the increased nuclear volume of fibroblast nuclei (table S4). As the sequences between the orthologous segments encompassing Sult1b1 and Igj was different between mouse and chicken a direct evolutionary side to side comparison was not possible. Nevertheless, the chromatin Sult1b1-Igj in chicken embryonic fibroblasts and chicken feather follicle was significantly less compact compared with the chromatin in mouse embryonic fibroblasts and mouse hair follicle (table S3 for statistics).

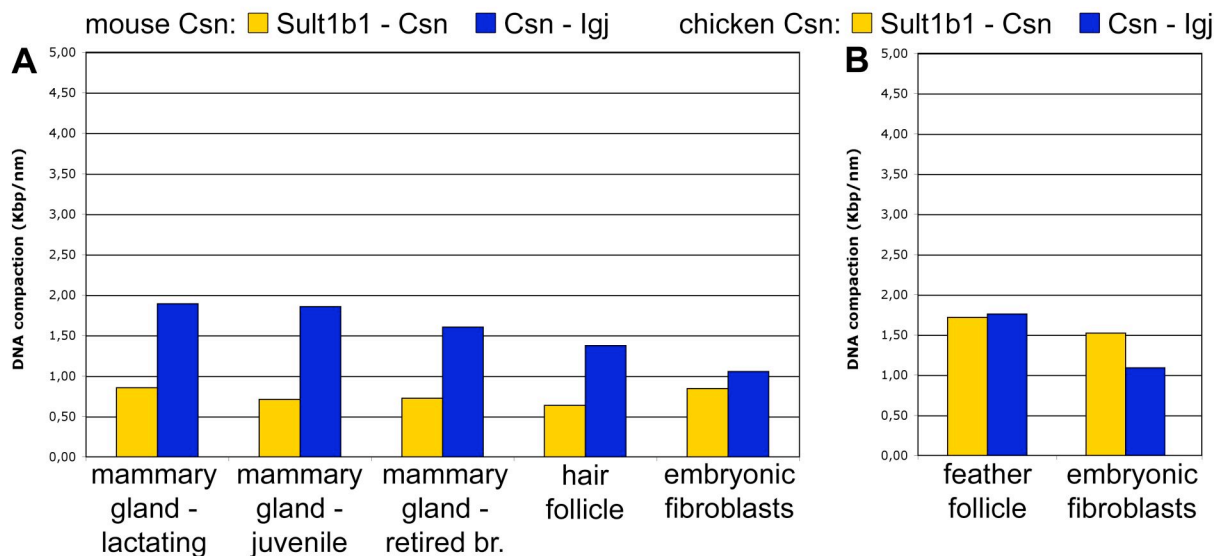


Figure 4.33: Chromatin compaction in kbp/nm calculated from distance measurements between Sult1b1-Csn (yellow) and Csn-Igj (blue) in (A) mouse and (B) chicken interphase nuclei.

4.2.6 Results summary of Csn genes

The evolutionary genomic innovation of the casein gene cluster formation did not affect the peripheral nuclear positioning of the orthologous regions encompassing Igj and Sult1b1 when comparing mouse and chicken.

In contrast the chromatin structure is fully reversibly remodelled during postnatal mouse mammary gland development in adaptation to lactation involving the expression of caseins. This gross chromatin remodelling was characterised at three levels investigated. Firstly, the nuclear volume and surface to volume ratio was considerable increased in lactating epithelial cells. Secondly, the casein locus including flanking genomic regions was visibly drawn to the nuclear center during gene expression. Thirdly, an increase of small angles, together with a decrease of the chromatin compaction between 5'Sult1b1 and 3'Igj, flanking the Csn genes was statistically evident, highlighted an extensive long-range back folding of the flanking regions in relation to the Csn cluster.

Most notably at all three levels this complex chromatin reorganisation during lactation was almost fully reversible and resulted in a highly similar chromatin structure before and after pregnancy.

5. Discussion

To date, the vast majority of published data on vertebrate nuclear architecture was obtained on cultured cells of only some cell types. Presently a general lack of information on in vivo fixed tissue material still exists, that would offer the advantage to investigate different cell types in their native tissue environment (Mateos-Langerak et al. 2007). The only exception is the Hox genes, which were investigated in mouse embryonal tissue sections by the Bickmore group (Chambeyron et al. 2005; Morey et al. 2007). In particular the publication by Morey et al. 2007 gave insight to the great potential of in vivo analysis by showing that upon gene expression even the same genes can respond differentially between tissue cell types.

We took advantage of this approach and, moreover our experiments were carried out in an evolutionarily comparative context during defined developmental stages, in homologous tissues of mouse and chicken. Evolutionary conservation of nuclear arrangements despite extensive sequence and karyotype diversification is a strong indication for functional importance (Woolfe et al. 2005). In addition to the evolutionary approach the data was referred to the expressional status of the target genes by combining chromogenic RNAish with DNA FISH. Furthermore, sites of nascent RNA expression were validated by RNA FISH and the expression levels were then relatively quantified by qPCR from little amount of laser-microdissected tissue material. Finally the nuclear localization of Dach1, Bcl11a and Csn was quantitatively evaluated referencing the nuclear center, the CT border and the signals centroids of flanking loci to measure interphase distances and angles within the respective region. Hence we obtained comprehensive high-resolution data to characterize the higher order chromatin conformation of the depicted loci at three different levels.

In summary, the present work took yet unexplored path by including ontogenical and phylogenical aspects of nuclear genome architecture in the attempt to contribute to close the still existing gap of knowledge.

We investigated the nuclear topology of Dach1, the Bcl11a and the Csn genes including the flanking genomic loci by multi color 3D FISH with selected BAC clones including the harboring chromosome paint in tissue sections of mouse and chicken. Whereas Dach1 is flanked by gene deserts to both sides, Bcl11a is flanked to one side by a gene desert and to the other side by a gene-dense region. These gene deserts are characterized by clusters of evolutionary ultraconserved non-coding sequences (UCS) with putative enhancer or boundary element function. Moreover, the trans-dev transcriptional factors Dach1 and Bcl11a themselves are evolutionarily remarkably conserved. In addition five of the most prominent UCS clusters were analyzed for specific pattern formation concerning histone modifications, radial

nuclear positioning and colocalization. Hence, these experiments focused on chromatin with the highest degree of evolutionary sequence identity among vertebrates. In contrast, the *Csn* genes represent an evolutionary innovation of the mammalian lineage flanked by two gene-dense regions, with well-preserved orthology in non-mammalian vertebrates. Thus the impact of novel sequence insertion in a genomic region flanked by orthologous segments could be analyzed.

The discussion critically highlights technical aspect of the procedure beginning with cell material fixation to the point of quantitative evaluations. Next the obtained results on UCS and the three target regions are related to each other and in the light of gene density, gene expression, tissue specification, geometrical constraints and evolutionary conservation vs. innovation.

5.1 Technical aspects of this work

5.1.1 RNA expression analysis

All data obtained on the nuclear topology of chromatin loci in tissue was directly conferred to the transcriptional activity of the targeted genes by the sequential combination of chromogenic RNAish and DNA FISH. Thus visualization of RNA expressing regions of the tissue section with the confocal microscope allowed us to link the nuclear architecture with the gene expression status in a given tissue. This was in particular important in tissue with non-uniform structure at cellular resolution (e.g. brain and limb buds). Chromogenic RNAish with enzymatic detection of Dig riboprobes is a very sensitive method (Kubota et al. 2006) and the obtained tissue expression patterns give information about the relative expression levels even by visual inspection. However, to quantify expression by RNAish using Dig riboprobes is still very difficult, because it is not possible to account for all aspects of variability like differences among riboprobe efficiency, density of labeled cells, dynamic signal range in tissue, signal saturation, threshold for low or no expression or signal to noise ratio. Despite the fact that valuable attempts have been made the results remain assailable (Jonker et al. 1997; Lee et al. 2008).

Although chromogenic RNAish only visualized expression on the tissue level but individual, sites, of RNA expression on the single cell level stayed covered and therefore the method was not quantifiable. Therefore, in addition to chromogenic RNAish, RNA FISH and qPCR from laser-microdissected tissue were used to detect and quantify gene expression in tissue. All three techniques provided verifying and complementary information.

RNA FISH visualized nascent RNA, confirmatively only in tissue showing the chromogenic RNAish expression pattern of *Dach1* or *Bcl11a*. Further, the genomic locus position of *Dach1* and *Bcl11a* DNA obtained by 3D FISH in mouse E13.0 brain

matched with the respective expression sites of nascent RNA. Similarly, on the single-cell level expression sites were observed throughout the nucleus proving evidence that mRNA expression shows probabilistic nuclear positioning and is not restricted in space. Moreover within expressing tissue we could not identify sites of nascent RNA in all nuclei either because these cells did not express, the expression level was below the detection sensitivity or because of reagent penetration failed. However in most nuclei of expressing tissue we observed biallelic expression driven from both homologs and monoallelic expression was not observed. 91% of about 4000 human genes, among them also DACH1 were shown to be expressed biallelically, with monoallelic gene expression restricted to imprinted regions, the inactive X chromosome and some autosomal genes (Gimelbrant et al. 2007). Notably pulses of gene activity (on average 5-6min) in vivo may tune the expression level over time (Chubb et al. 2006), which can explain expression differences and maybe also RNA FISH signal intensity differences between cells. Notwithstanding, to quantify expression levels by individual brightness or size of nascent RNA signals were affected by the essentially same technical difficulties as chromogenic RNAish quantification (C. Lanctôt, unpublished data). In addition, due to probe penetration problems, a top to bottom RNA FISH signal intensity gradient in the 14µm cryosections was observed. Further to combine RNA FISH and DNA FISH in the same cells was avoided because RNA hybridization requires non-denaturing conditions.

Consequently, the method of choice to quantify gene expression from tissue material is quantitative PCR. Here it is necessary to isolate mRNA from tissue, and by that the spatial information of the expression pattern is destroyed. To circumvent this we laser-microdissected 200-400 cells from an area previously identified to be transcriptionally active or inactive by RNA in situ techniques, followed by mRNA extraction. Notably Dach1 and Bcl11a, the targeted genes were only moderately expressed transcription factors. In comparison we were able to reliably quantify expression from only five cells for the highly expressed house-keeping gene Gapdh (data not shown). Finally the expression differences between expressing and non-expressing tissue were relatively quantified. A 2-step qPCR assay using TaqMan probes was performed, which increases the sensitivity compared to 1-step qPCR directly from mRNA. Moreover the site-directed TaqMan probe (see 3.5.5.2) further increased the detection specificity compared to quantification by SYBR green DNA double strand incorporation. In addition, the reactions were set against a passive reference dye, the data were normalized against the geometrical mean of two house-keeping genes (Vandesompele et al. 2002) and each experiment was performed in a triplicate. In summary, the qPCR results for Dach1 and Bcl11a could confirm the expression differences of RNA in situ techniques, resulting in approximately 30-fold

relative expression differences for both genes between tissue defined as expressing or non-expressing by RNAish.

5.1.2 3D image acquisition, processing and analysis

Laser confocal microscopy was used to acquire 3D image stacks separately all fluorescent channels. Therefore, FISH probes were labeled with organic dyes (A 488, A 514, Cy5, Tamara, Texas Red), which are light sensitive although embedded with vectashield. In comparison to organic dyes quantum dots, which are photo stable semiconductor nanocrystals (Excitation: UV light, Emission: defined by size, 2-8nm) offer in combination with organic dyes the simultaneous visualization of up to six DNA probes (Müller et al. submitted). By now quantum dots do not penetrate tissue well, however, technical improvements might solve this drawback and will lead to more sensitive and more variable 3D-FISH probes. The accuracy of the obtained results on confocal serial light optical sections was ensured by correction for chromatic shift (focus difference by optical lenses for light of different wave length between fluorescent channels) (Walter et al. 2006), applying a z-step of only 150nm between confocal serial sections, and by averaging 20-30 nuclei.

The relative radius measurements for nuclei did normalize for size but applied equidistant shells following the nuclear shape and increasing in volume from the inside to the outside. Noteworthy, the more the nuclear morphology differs from the perfect sphere the more the radial arrangement can be subjected to inaccurate evaluation. This was in particular relevant for evaluations in the flattened ellipsoid nuclei of cultured fibroblasts. The irregular shaped CTs could not be radially evaluated because not all voxels could be directly linked to the geometric center by a vector, which is a precondition for this evaluation type. Instead the topology within CTs was evaluated by distance to surface measurements, independent from shape differences but not normalizing for size differences. Hence, each applied evaluation method corrects for the most prominent weaknesses, but hazards some unavoidable drawbacks (reviewed in Ronneberger et al. 2008).

Interphase distance and angle measurements did not require a reference structure and genomic distances for normalization are known from the database (UCSC). The measurements are based on the geometrical centers of signals which were largely unaffected by data processing and were in particular suitable for error-free high-resolution analysis (Ronneberger et al. 2008). Confirmatively, control experiments on embryonic fibroblast of mouse and chicken proofed the reproducibility of high-resolution mean interphase distance measurements between gravity centers of FISH signals between independent data sets using the same probes and cell material (see 4.2.2.5). On the other hand side they revealed discriminable distances by using different clone sets from the same region (see 4.1.2.5), although the performed distance measurements break the resolution of confocal microscopy in xyz-direction

($xy = 210\text{nm}$, $z = 550\text{nm}$, (Ronneberger et al. 2008). Furthermore also other groups performed similar high-resolution interphase measurements (Lanzuolo et al. 2007; Morey et al. 2007; Jhunjhunwala et al. 2008). Hence, the performed distance and angle measurements reliably captured the mean higher order 3D chromatin conformation. Measurements on centroids were shown not to benefit from deconvolution (Albiez et al. in preparation), whereas out of focus signals misleadingly increase colocalization measurements (Landmann 2002; Sedarat et al. 2004). Therefore deconvolution was applied to all light optical serial sections before colocalization measurements of genomic loci with certain histone codes (see 4.1.1.3) but not for 3D interphase distance and angle measurements.

Statistical significance based on the Mann-Whitney U-test, a parameter free test based on the comparison of rank sums which were assigned to the sample values. Therefore the test allowed the statistical evaluation of the independent but similar distributed datasets herein and has been recommended by Ronneberger et al. 2008 and <http://www.vislab.ch/Lehre/EST/est.html> for 3D-RRD, EDMT and DistAng results. Furthermore the handling and processing of light-optical serial sections with Adobe Photoshop, Image J and Amira is subjected to the assessment of the user. Also the implementation of a user-set threshold and a minimal object size in the quantitative evaluation programs can affect the outcome. These implementations most severely perturb the rendering of the CT surface with its fine structures and considerable intensity differences and therefore evaluations of probe distribution with respect to the CT surface. In contrast BAC signals and the nucleus showed a homogenous brightness and thus were not very sensitive to image processing artefacts.

5.2 Nuclear chromosome territory and gene positioning

5.2.1 Chromosome territory positioning

In general gene density in spherical nuclei (Croft et al. 1999) and chromosome size in flattened ellipsoid nuclei (Bolzer et al. 2005; Sun et al. 2000) was previously shown to be major determinants of the radial nuclear position of CTs. Even though the exact reasons for preferential radial positioning are not known some theories try to explain the function. The bodyguard hypothesis argues that gene-poor material orientated to the periphery protects interior genes from DNA damage by external factors, like UV-light, chemical agents or radicals (Gazave et al. 2005; Hsu 1975). Other hypotheses favor that densely packed chromatin in the periphery enhances the structural integrity of the nucleus in response to tension or mechanical exposure (Caille et al. 2002; Gladilin et al. 2007; Maniotis et al. 1997; Vinogradov 2005). Notably, these theories lack convincing experimental evidence and are questionable with the finding of an inverted nuclear architecture with gene-dense and decondensed material to the

periphery in mouse rod cells (Solovei et al. in preparation). More likely the radial position groups the chromatin in domains of similar properties that may help to organize the nuclear processes (Mateos-Langerak et al. 2007). Also the non-random distribution of non-chromatin sites in the nucleus, like histone modifications (Zinner et al. 2006), replication foci (O'Keefe et al. 1992) RNA pol II sites (Osborne et al. 2004), transcription and splicing factors (SC 35 speckles) (Shopland et al. 2003) militate for a non-random nuclear architecture separated in evolutionary conserved functional domains with a radial nuclear organization. However, apart from preferential radial positioning reports revealed developmental, cell type or species CT position differences (Foster et al. 2005; Kuroda et al. 2004; Parada et al. 2004; Wiblin et al. 2005; Stadler et al. 2004; Bridger et al. 2000; Mehta et al. 2007; Neusser et al. 2007). Moreover the karyotype organization between mouse and chicken was reshuffled extensively leaving only small homologous blocks of conserved synteny. Therefore the position of entire mouse and chicken CTs cannot be directly compared. In mouse cell nuclei a tendency of gene rich and small chromosomes to the nuclear interior was found (Mayer et al. 2005). Because mouse chromosomes display only little differences in size (maximum threefold) and gene density (maximum twofold) the nuclear arrangement differences were not clearly defined and CTs displayed frequently cell type specific differences in CT positioning. E.g. the small CT 14 with an average gene content was found significantly more internal in embryonic stem cell nuclei compared to lymphocyte nuclei (Mayer et al. 2005). Confirmatively, we revealed significant differences in the chromosome territory position of investigated mouse chromosomes 5, 11 and 14. Out of the three CTs, chromosome 5 was most stably positioned and only significantly more peripheral in the juvenile mammary epithelial cells compared to epithelial cells in hair and mammary glands of retired breeder. Chromosome 14 in embryonic fibroblasts was significantly more to the nuclear interior compared to tissue nuclei in the stiratum, hind limb mesenchyme and hind limb plate. Among evaluated tissues chromosome 14 territories were significantly more inside in the neopallial cortex and hind limb mesenchyme compared to the hind limb plate. Chromosome 11 was most diversely positioned. Only the comparison between Bcl11a expressing brain tissue and the silent hind limb plate was not statistically different (table S3). The cause of differential chromosome positioning is unclear (Mayer et al. 2005; Parada et al. 2004) and maybe driven by the cell type specific transcriptome, proteome, epigenetic modifications or nuclear morphology constrains (see 5.2.3). These adaptations may result in significantly different positions of CTs between cell types. Therefore the high gene content of chromosome 11, the second gene-richest chromosome of mouse could facilitate the formation of cell type specific position patterns compared to chromosomes 5 and 14, both of average gene density.

In contrast to mouse CTs the paints for chicken chromosome 1,3 and 4 were quite stably positioned in the nucleus. Neither CT 1 nor CT 4 of chicken showed statistically valid position variegation among analyzed cell types. Only chicken chromosome 3 in embryonic fibroblasts was more internally compared to all tissues analyzed (table S3). In addition, CT3 was significantly positioned to the nuclear interior in the hind limb bud tissue compared to the brain tissue. The noticeably extended flexibility of CT3 compared to CT 1 and 4 could not be explained by chromosome size or gene density. It can be speculated that genes, prone to tissue-specific differences like histone modifications or expression are enriched on chromosome 3. Overall the stable peripheral position of the investigated chicken macrochromosomes results from the pronounced chromosome-size and gene density differences in the chicken genome (see 2.3.2, Habermann et al. 2001). Hence, both criteria for maintaining a stable peripheral CT position of chicken macrochromosomes, large size and low gene density (Bolzer et al. 2005) apply and are less pronounced in mouse.

5.2.2 Nuclear radial gene positioning

5.2.2.1 Correlation with gene density

Gene density over regions in the mbp-range was frequently shown to be the best predictive parameter for radial gene positioning in the nucleus (Kupper et al. 2007; Murmann et al. 2005; Grasser et al. 2008). At face value the radial positions of Dach1 and Bcl11a fitted this assumption (table 5.1).

Genes/mbp	Dach1	Bcl11a	Csn
+/- 1mbp	2.94	7.63	19.42
+/- 2mbp	3.42	7.08	16.64
+/- 5mbp	3.47	6.34	11.30
Genome	6.43	6.43	6.43

Table 5.1: Mouse genome gene density windows around the genes Dach1, Bcl11a and Csn genes (based on Ensembl Gene IDs, NCBI m37). Compared to the average genome gene density Dach1 resides in a gene-poor region, Bcl11a in a gene-medium region and Csn in a gene-dense region.

The gene-poor Dach1 region resided more peripheral in the nucleus compared to the gene-average Bcl11a region in mouse (Dach1: 65.3%-80.5%, Bcl11a: 61.4%-72.1%) and chicken (Dach1: 72.7%-79.6%, Bcl11a: 61.6%-73.1%). Despite Bcl11a displays a median gene density the genes are not equally distributed in the region. Whereas the chromatin to the one side of Bcl11a is gene-rich the reference sequence lacks any gene annotation for 1.44Mbp in mouse to the other side (see 2.4.4). This gradient correlated well with a polar trend in all evaluated mouse cells. The gene-rich region was slightly more internal compared to the gene desert (MMU: Δ ARR 1.7%-6.5%).

Shopland et al. 2006 and Goetze et al. 2007 also observed a polar orientation of directly adjacent gene-dense versus gene-poor regions and, moreover polarity of subchromosomal segments in CTs was frequently identified (Visser et al. 1998; Grasser et al. 2008; Kupper et al. 2007; Neusser et al. 2007; Nogami et al. 2000). In contrast, no polar orientation was evident in the chicken *Bcl11a* region maybe because of the specific locus position in the chromosome subtelomere (see 5.2.3). Also no regional polarity was evident in any experiment in the mouse or chicken the *Dach1* region, flanked by gene deserts to both sides.

Astonishingly, the very gene-rich region comprising Casein genes (table 5.1), with the exception to lactating mammalian epithelial cells, was located towards the nuclear periphery (MMU: 67.6%-78.0%, GGA: 65.1%-70.5%) comparable to the gene-poor *Dach1* region. Even-though the *Csn* region has a homogenous gene density distribution we determined a radial gradient of the flanking genes with *Sult1b1* significantly more to the periphery than *Igj* but only in mouse tissue sections (MMU: Δ ARR 4.3%-8.6%).

In conclusion, gene density can explain the nuclear radial arrangement of *Dach1* and *Bcl11a* but not of *Csn* that needs to be further explained (see 5.2.2.2).

5.2.2.2 Correlation with gene expression

The role of gene expression to establish the nuclear 3D genome architecture is less clear than for gene density. Both evidence for an adaptive (for review Fraser and Bickmore 2007; Lanctot et al. 2007) or a conservative nuclear architecture (Gilbert et al. 2005; Kupper et al. 2007) upon gene activation was published (see 2.1.2).

Dach1, a gene isolated within a gene desert showed a clearly conservative nuclear architecture. All observed radial position variations in the nucleus between evaluations of *Dach1* were not linked with the gene activity of *Dach1*, but with position differences of the harboring CT. In particular, in mouse when normalized against the territory position of mouse chromosome 14 the *Dach1* region was found stable to 6.3% among evaluated cell types instead of 13.7% without normalization. In chicken the nuclear position of chicken chromosome 1 and consequently that of *Dach1* was even more stable (*Dach1*: 2.7% variability between tissues), because chromosome architecture in chicken is more clearly defined, exhibiting pronounced size and gene density differences (Habermann et al. 2001) compared to mouse (see 5.2.2). Although Levisky et al. 2007 excluded gene expression in the nuclear periphery we detected gene expression of *Dach1* in high frequency directly at the nuclear border by RNA and DNA FISH. Concordantly, Shopland et al. 2006 found the genomic region directly upstream of *Dach1* on mouse chromosome 14 at the periphery. Moreover Hewitt et al. 2004 located the *Ifng* gene also stably positioned in the periphery, irrespectively to transcriptional activation and Kumaran and Spector

2008 observed a stably expressed transgenic locus, anchored to the nuclear periphery. It was further shown that some chromatin interacts directly with the nuclear lamina (Gruenbaum et al. 2005; Guelen et al. 2008). Maybe such binding sites in the Dach1 region link this locus with the periphery.

Bcl11a, together with the flanking gene-rich region and the gene desert was statistically different positioned among evaluated cell types in mouse and chicken. Nevertheless, like in the case of Dach1 these variations were not linked to the expression status of Bcl11a. The CT position could neither fully explain the difference between tissue. After normalization with mouse CT 11 positions the differences diminished by only about 2% and 9.3% variegation were still left. When compared with Dach1, the enhanced position flexibility might be dependent on transcription activity in the flanking gene rich region. Directly adjacent to Bcl11a protein coding genes like the ubiquitously expressed Xpo1, Paplog, Pex 13, or Ahsa2 and the Rel oncogene are located (table 5.2). The expression pattern of the flanking genes likely superimpose on the Bcl11a expression differences and may influence the nuclear position of the greater Bcl11a region in a combinatorial way.

A			C		
Region:	Chr14	97.28-99.40mbp	Region:	Chr5	87.79-89.21mbp
	brain	organogenesis		Mammary gland	skin
# ESTs	474115	128575	# ESTs	306321	118673
Dach1	22	7	Ugt2b38	0	0
			Ugt2a2	0	0
			Sult1b1	0	0
			Sult1d1	7	0
			Sult1e1	3	0
			Csn1s1	1925	0
			Csn2	4478	0
			Csn1s2a	1053	0
			Csn1s2b	1360	0
			4930432K09Rik	0	0
			EG654494	0	0
			Odam	3	0
			Csn3	1381	0
			4931407G18Rik	0	0
			2310003L06	0	0
			BO051076	0	0
			Smr1	0	13
			Smr2	n.a.	n.a.
			Muc10	0	0
			Amtn	0	0
			Ambn	0	0
			Enam	0	0
			Igj	0	31
			Rufy3	8	4
			Utp3	21	0
			Grsf1	30	13

B		
Region:	Chr11	23.14-.26.10mbp
	brain	organogenesis
# ESTs	474115	128575
Xpo1	28	51
usp34	28	13
Ahsa2	38	9
1700093K21Rik	0	0
0610010F05Rik	33	8
Pex13	15	9
Ccdc139	n.a.	n.a.
Rel	0	0
Paplog	18	1
Bcl11a	29	1

Tabel 5.2: EST expression profile from mouse mammary gland and skin or adult mouse brain and embryos during organogenesis (Uni Gene). (Red) Target genes Dach1 (A), Bcl11a (B) and the Casein gene cluster (C). (Blue) Genes in the casein region with orthologs in non-mammalian vertebrates. Casein genes are only and extremely highly expressed during lactation. Other genes in the Csn region display low or no expression activity.

In contrast to Dach1 and Bcl11a the Csn genes clearly demonstrated an adaptive nuclear architecture correlated with gene activation. In lactating mice the Csn locus, including the flanking regions relocated to the nuclear center. The mean ARR

difference in lactating mammary epithelial cells constituted at least 15.3% compared to the silent states before and after lactation. Strikingly, the peripheral position of the Csn region was fully reversibly restored after lactation in retired breeder mice (ARR: 71.7%) compared to juvenile mice (ARR: 78.0%). Relocalization to the nuclear interior upon onset of expression was also found for few other selected genomic loci (Hewitt et al. 2004; Kosak and Groudine 2004a; Williams et al. 2006; Zink et al. 2004, see 2.1.2). Surprisingly, a stable peripheral relocalization upon Csn gene expression, induced by lactogenic hormones was found in cultured mammary epithelial cells (Ballester et al. 2008), which underlines the importance of studies in native tissue. In non-expressing cells the peripheral orientation of the Csn region and the polar orientation conflicts the high gene-content (see 5.2.2.1). When taking a closer look at the regional expression profile in the evaluated tissue types most of the genes are silent and the remaining ones are expressed at low levels (table 5.2). The polar orientation of Sult1b1 more external to Igj might also be linked to the higher expressional activity around Igj (table 5.2). Further, atypically for a gene-rich locus, the mouse casein gene locus displays an exceptionally low GC content of only 34.5%. This places the Csn gene cluster in the L1 isochore class with the lowest GC content in mammalian genomes (Costantini et al. 2006).

In summary we provide evidence indicating that gene activity can shape the nuclear radial position. However, it may be a precondition to provide a strong expressional input to dominate the impact of the genomic landscape. The activation of an isolated gene like Dach1 was not sufficient to change the radial arrangement. Whereas the conclusions concerning Bcl11a repositioning can be just indirectly drawn to assumed tissue-specific gene expression changes in the entire region the striking relocalization of the Csn genes is clearly a result of the strong gene expression during lactation.

5.2.2.3 Evolutionary genomic conservation and innovation

All experiments presented here were performed in the evolutionary context comparing the two distantly related vertebrate species mouse and chicken. We investigated orthologous genomic loci at comparable developmental stages and in homologous tissues (see 2.4-7). Conservation of biological patterns despite extensive chromosome reshuffling is strong evidence for a functional role (Woolfe et al. 2005). In general we found a striking conservation of the radial nuclear architecture by DNA FISH and the gene expression patterns by RNAish between mouse and chicken, confirming this principle in the case of nuclear architecture.

The RNA expression pattern of Dach1 and Bcl11a, obtained by chromogenic RNAish on mouse and chicken embryos of the same developmental stage were highly similar concerning the temporal control, tissue specificity and the relative expression levels. Previously, also Liao and Zhang 2006 showed that spatio-temporal expression patterns at least between human and mouse are highly conserved because gene

expression networks are frequently subjected to purifying selection (Tsaparas et al. 2006). Moreover coexpressed genes tend to cluster in the genome (Purmann et al. 2007; Semon and Duret 2006).

Hybridization of five different UCS clusters, located in gene deserts to mouse and chicken embryonic fibroblasts and embryos before and at advanced organogenesis showed that UCS from different chromosomes did not share a specific radial position nor formed clusters. Instead the selected UCS regions showed a broad nuclear distribution with a slight preference for the nuclear periphery. However the radial position of each individual orthologous UCS cluster was evolutionarily conserved in fibroblast showing a maximal radial difference of 1.0%-4.4% between mouse and chicken.

Furthermore, the radial nuclear position of *Dach1* and *Bcl11a* was conserved between homologous tissue of mouse and chicken embryos, displaying maximum differences of only 0.1% to 6.4%. For example, compared with the maximal position difference between tissue cell types in one species of 13.7% the radial arrangement of *Dach1* and *Bcl11a* was strikingly more conserved in homologous mouse and chicken tissue than in different tissues of one species. In addition even the nuclear arrangement of *Sult1b1* and *Igj* between epithelial cells from hair and feather was conserved except for 3.2% and despite the genomic insertion of the *Csn* genes. This demonstrates that the genomic innovation did not modify the properties of the genomic region and that the nuclear arrangement is maintained regardless to new sequence insertions. In a similar way the formation of evolutionary neocentromeres in primates appears to be favored in genomic regions, which do not require nuclear repositioning of the locus (M. Lomiento, S. Müller, unpublished data). Moreover for primate cells it was repetitively shown that orthologous DNA segments largely maintain their radial position irrespectively of evolutionary chromosomal rearrangements (Cremer et al. 2003; Tanabe et al. 2002; Neusser et al. 2007; Grasser et al. 2008). Further, the basic structural organization of replication foci was even evolutionarily conserved down to *Hydra* (Alexandrova et al. 2003) and *Ciliates* (Postberg et al. 2005).

In particular the UCS regions that build syntenic units with trans-dev genes, like *Dach1* and *Bcl11a* most conserved in size and gene order between teleosts and mammals (Becker and Lenhard 2007). The interlocked order of UCS and trans-dev genes cannot be interrupted without a serious loss of fitness (Kikuta et al. 2007). Hence evolutionary rearrangements affecting UCS regions are likely negatively selected (figure 5.1).

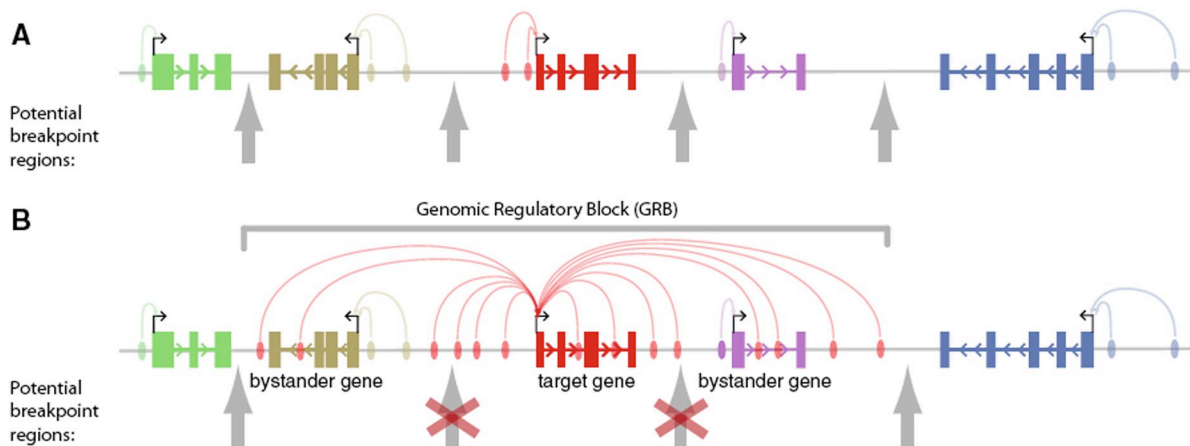


Figure 5.1: (A) In genomic regions without long-range cis regulatory elements chromosomal breakpoints are free to occur in intergenic regions. (B) In contrast in cis regulatory modules (= Genomic Regulatory Block) chromosomal rearrangements disrupt cis regulation. Hence chromosomal rearrangements are negatively selected. (taken from Becker and Lenhard 2007)

In contrast to the radial arrangement we could not identify any evolutionary conservation of the distance to the CT surface or the DNA compaction of genomic loci between mouse and chicken (see 5.3 and 5.4). In conclusion the nuclear radial position was well conserved despite 310mya years of evolution although mouse and chicken, irrespective of repetitive element, karyotype organization, genome size and nuclear size differences (table S4). Hence our results provide novel evidence, demonstrating that the radial nuclear arrangement is under evolutionarily selective pressure and consequently most likely functionally important.

5.2.3 Geometrical constraints

In addition to gene density and gene activity, the nuclear architecture is potentially influenced by geometrical constraints at various levels. Geometrical constraints are physical forces like steric hinderance, conformational changes at various scales, topological constraints, elastic properties, electrostatic changes (Lesne and Victor 2006) or macromolecular crowding effects (Hancock 2007), constricting the positional freedom of entire CTs, large chromosomal regions or individual genomic loci. Besides to physical constraints also biological factors like factor binding to chromatin motifs, factor recruitment or enzymatic reactions influence the chromatin positioning (see 5.4). Thus, biophysical constraints were postulated to define the general topology, which is then fine-tuned by biological processes (Lesne and Victor 2006). At the top-level, CT positioning might be non-functionally constrained by the nuclear shape. The nuclear shape can differ considerably from an ideal sphere lymphocyte by becoming elliptic, flattened or undulated and this can potentially result in deformation of genomic loci (figure 5.2). Next karyotype organization could directly influence the nuclear architecture. In contrast to the humans the karyotype of an old world monkey displayed chromosomes of a very homogenous size. Here, the

chromosome size correlation with the radial position in human flattened ellipsoid fibroblast nuclei (Bolzer et al. 2005) was not observed in this species and a gene-density-correlated radial position comparable to spherical nuclei was restored (Neusser et al. 2007).

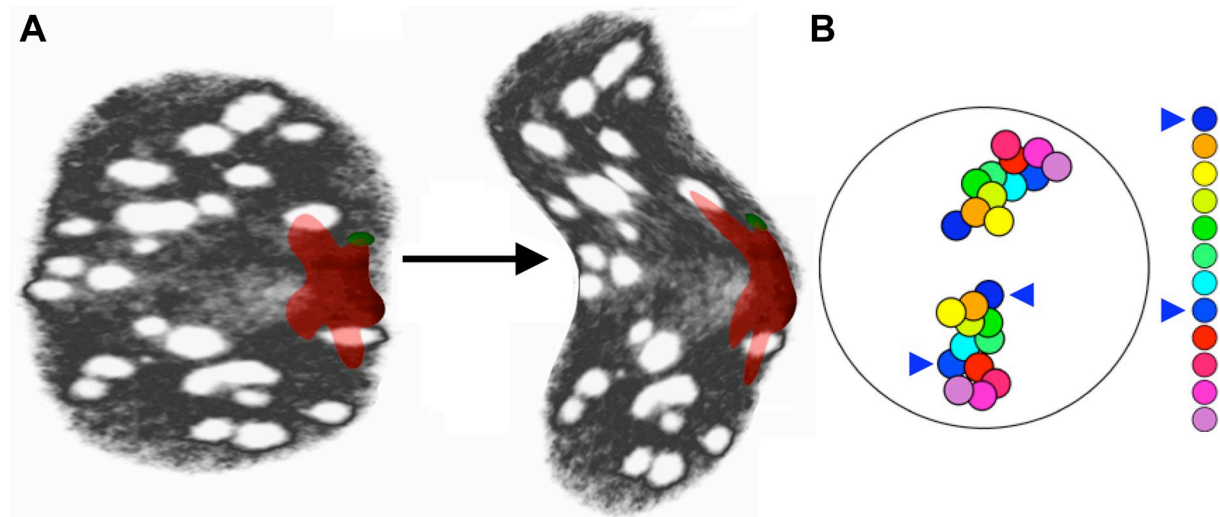


Figure 5.2: (A) The nuclear morphology can vary from the perfect sphere to flattened ellipsoids with undulations. Thus the nuclear morphology can impose constraints on the nuclear morphology of entire CTs (red) or genomic loci (green). (B) Chromatin persists in distinct domains throughout the interphase. The position of these domains is influenced by the relative order on the metaphase chromosome and maybe different between subtelomeric, centromeric and interstitial regions

To describe the nuclear morphology in a quantitative manner we measured the nuclear volume and the nuclear roundness factor (table S4). In general the nuclear volume of chicken tissue cells was about 55% smaller compared to mouse, partly correlated with the 2/3 smaller genome-size. Next the genome size divided by the nuclear volume resulted in $14.49 \text{ mbp}/\mu\text{m}^3$ in nuclei of mouse E13.0 and $9.93 \text{ mbp}/\mu\text{m}^3$ in nuclei of chicken E5.5, additionally showing that a linear correlation between genome size and nuclear volume was not present. Importantly, the dimensions of the chromatin-free space in the nucleus were beyond of the scope of these measurements. Specifically cultured embryonic fibroblasts differed extensively by their flattened ellipsoid nuclear morphology and by an at least 4 times bigger nuclear volume from native tissue nuclei. These findings underlined the problem to relate the results on cultured cells and in particular on fibroblasts, to the *in vivo* situation. Furthermore nuclear volume and roundness factor (Volume/Surface) between tissues showed only slight differences among tissue of one species (table S4). The exception were mouse lactating mammary epithelial cells, with increasing nuclear volume about 20% and significantly more spherical compared to non-lactating epithelial cells and hair epithelial cells in mouse. Thus during lactation the nuclear relocalization of the Csn region went along with a remodeling of the entire nuclear structure.

Another geometric constraint for their positioning might be the mapping position of individual genomic loci along the metaphase chromosome. Probably the mapping of the chicken *Bcl11a* locus very close to the telomere on chromosome 3pter resulted in notably positional flexibility compared to the interstitial mouse gene-rich locus. Astonishingly, 27% of the gene-rich region flanking *Bcl11a* in chicken was found outside of the core chromosome territory but only 14% of the ortholog segment in mouse. Also Mahy et al. 2002a detected a gene-rich segment on human chromosome 11pter and the orthologous segment on mouse 7qter in high frequency outside the core CT although only the high gene content but not the metaphase position was considered to be causal by the authors. Further the more internal position of the *Dach1* region in chicken CT1 compared to mouse CT14 might be caused by higher-order CT folding differences of the chromosome territory. Accordingly, evolutionary inversions of the human chromosome 7 in the orangutan, resulted in a pronounced polarity of gene-dense regions along the chromosome in this species and were shown to stretch the CT conformation compared to the more compacted human CT7. Notably the investigated genomic inversions, changing two neighborhoods influenced the genomic architecture to a larger extent compared to translocations, changing only one neighborhood (Grasser et al. 2008, figure 5.2).

Theoretically the chromatin in the interphase can be maximally expanded to the 2nm fiber (0.34 nm length per bp, Wakelin et al. 1984) and thus set the upper interphase DNA distance limit. In reality, the bulk chromatin is packed into higher-order chromatin structures of the 30nm fiber and higher (Staynov and Proykova 2008, see 2.1.3). These higher order structures from 100-300nm in diameter resulted from further giant loop formation or rosette like structures (Belmont and Bruce 1994; Sachs et al. 1995; Munkel et al. 1999; Yokota et al. 1995). Direct and indirect chromatin interaction and interactions with other nuclear components (e.g. matrix attachment regions, the lamina, nucleoli) may limit the position freedom (Chubb et al. 2002, see 2.1.3, 5.3). Confirmatively the position of the target genes *Dach1*, *Bcl11a* and the *Csn* genes and the flanking loci with respect to the nucleus or the CT was always closely identical with only little variation. The constrained orientation of neighboring genomic loci was in particular evident for the casein region. During lactation not only the *Csn* genes but also the flanking regions were drawn to the nuclear centre compared with the non-lactating state up to at least 9%. Presumably the *Csn* flanking regions were forced to follow the relocalization of the *Csn* cluster (relocated by at least 15.3%, ARR) but still aimed to retain their initial position. Furthermore these presumably non-functionally relocalization forces contributed to the frequent backfolding of the *Csn* region (see 5.2.3). Likewise, the *Mash1* locus together with the surrounding chromatin up to 2mpb relocated to the nuclear interior upon transcriptional activation (Williams et al. 2006). Further, the detected looping away from the CT surface upon transcriptional activation of the *Hox d* cluster

involved the flanking regions but with a sharp cut off 200kb 5' to the cluster (Chambeyron et al. 2005; Morey et al. 2007).

5.3 Gene positioning with respect to the chromosome territory

Gene dense segments were preferentially found to locate to the border of even outside of chromosome territories (Kupper et al. 2007; Mahy et al. 2002a; Visser et al. 1998). However the same and other studies revealed that this probabilistic orientation does not exclude gene-dense material and also gene expression from the CT interior (Visser et al. 1998; Kupper et al. 2007; Verschure et al. 1999; Sadoni et al. 2004). Previously, upon gene expression some genomic loci were shown to loop away from the harboring CT (Volpi et al. 2000; (Williams et al. 2002; Chambeyron and Bickmore 2004; Morey et al. 2007; Ragoczy et al. 2003). Initially CTs were believed to be rather impermeable structures (Kurz et al. 1996) and looping was postulated to allow contact of active chromatin to the transcriptional machinery in-between the CTs (Williams 2003). More recently it is either assumed that CTs are penetrated and separated by fine chromatin channels (Albiez et al. 2006) or that CTs overlap extensively (Branco and Pombo 2006). Moreover, studies revealed that in some instances active chromatin from different genomic loci loops to shared sites of expression (Osborne et al. 2004; Xu et al. 2006; Brown et al. 2006). To evaluate potential looping of Dach1, Bcl11a and Csn together with their flanking regions the distance to the chromosome territory surface was evaluated.

In brief, we could not identify any looping away from the CT surface in response to transcriptional activation of Dach1, Bcl11a or Csn genes. All investigated loci resided either closely outside to the CT border (max. distance ca. 0.8 μm away) or inside the CT. However, we could also not identify any evolutionary conservation of the distance to the CT surface between mouse and chicken. For example the Dach1 gene located species-specific close to the CT surface of mouse CT14 (126–177nm) and to the inside of chicken CT1 (225–317nm), and not correlated with gene expression. Even the strong gene expression of Csn genes during lactation did not result in chromatin loops, the Csn genes stayed stably associated with the CT in postnatal mammary epithelial cells at all developmental times (80-146nm) (see 4.2.1.4). Despite we identified some statistical significant differences in CT positioning among evaluated cell types in Dach1, Bcl11a and Csn, however without an obviously comprehensible functional pattern (figure S3). We cannot exclude data sampling or cell type variations, but species-specific CT folding patterns, resulting from evolutionary structural rearrangements also account for other differences observed. Interestingly our results on the gene-rich region adjacent to Bcl11a

indicated that a subtelomeric gene position in the CT may impose geometrical freedom and therefore could favor a position outside of the harboring CT (see 5.2.3).

5.4 Higher order chromatin structure

5.4.1 Global higher order chromatin conformation

Colocalization experiments of five independent UCS cluster with certain histone methylation patterns in embryonic fibroblasts showed that depicted UCS regions were not modified by H3K9me3 but rather by H3K27me3 and H3K4me3 in mouse and chicken (see 2.2). Thus, UCS regions did not belong to constitutive heterochromatic chromatin and therefore not to the most compacted and transcriptionally silent genome fraction. Instead UCS were part of facultative heterochromatin (H3K27me3) or euchromatin (H3K4me3). Facultative heterochromatin is a transcriptional repressive state for silencing tissue-specific genes that is in contrast to constitutive heterochromatin reversible (Schones and Zhao 2008) whereas euchromatin is referred to be the transcriptionally active part of the genome and is modified by histone acetylation leading to decondensed chromatin. Both H3K27me3 and H3K4me3 can also overlap leading to a bivalent chromatin state (Bernstein et al. 2006a). In contrast to heterochromatin euchromatin is probably maintained by active cellular processes (Gaszner and Felsenfeld 2006). Hence, although the selected UCS regions were located in gene deserts of several 100kbp their histone modifications were identical with coding regions.

In addition to evolutionary sequence conservation (Sandelin et al. 2004; Woolfe et al. 2005) and sequence prediction algorithms (McEwen et al. 2006; Pennacchio et al. 2007) the identified histone code, keeping UCS in an active or poised for activation chromatin state, underlines the functional role of UCS.

5.4.2 Local higher order chromatin conformation

An open chromatin conformation was found to correlate well with high gene density in a genome wide study by (Gilbert et al. 2004). In general chromatin decondensation is widely believed to control the access of transcription factor binding to chromatin and by that gene expression (reviewed in Nemeth and Langst 2004; Wegel and Shaw 2005). However, recent data using multimer nucleosome arrays showed a minor influence of the chromatin fiber organization on the accessibility but a strong effect of chromatin folding (Poirier et al. 2008). An alternative model suggested that chromatin compaction is mainly governed by self-assembly of chromatin dependent on the forces and concentrations of all macromolecules in the nucleus (Hancock 2007). UCS in the gene desert to both sites of Dach1 and to one side of Bcl11a were previously experimentally indicated or computationally predicted to induce long-range

enhancer activity (Sandelin et al. 2004; Woolfe et al. 2004). Whereas in the case of Dach1 selected UCS were already shown to drive tissue-specific gene expression from a transgene the UCS in Bcl11a region are still functionally uncharacterized (see 2.4.3 and 2.4.4). Next UCS were also annotated as boundary elements. Protein binding and thus site-specific chromatin folding between boundary elements help to establish discrete chromatin compaction domains in the nucleus and by that to control gene activity. Importantly, evolutionary conserved elements even in the same region can display various functions. For example in the hemoglobin beta region enhancer elements, boundary elements and intergenic promoters were identified (Chakalova et al. 2005). To establish chromatin interactions the chromatin has to form site-directed loops and potentially local decondensed chromatin states to span the genomic distance, e.g. between the promotor and the enhancer mediated by proteins to support gene expression. In fact still little is known about higher order chromatin folding (see 2.1.3) and only recently several groups focussed on this topic using FISH and interphase distance measurements (Goetze et al. 2007; Jhunjhunwala et al. 2008; Shopland et al. 2006).

We captured the higher order chromatin conformation in the Dach1, Bcl11a and Csn region by measuring interphase distances and angles between signal gravity centers of FISH probes for genomic loci using the centrally placed target gene as apex. The revealed chromatin folding and mean chromatin compactions in kbp/nm provided information about the local higher order 3D chromatin conformation in a combinatorial way that turned out to be influenced by species-specific factors, gene density and gene expression.

In general significantly less condensed chromatin was found in the investigated chicken genomic regions compared to the orthologous mouse regions (table S3). Noteworthy, chromatin was always less compact in cultured embryonic fibroblasts, that had an increased nuclear volume compared to tissue nuclei, (tables S3 and S4). Further, the mean genomic angle UCS A-Dach1-UCS B was always below 60°C (52.4°-57.7°C) in mouse but around 90°C (77.5°-108.9°) in chicken tissue presenting a species-specific folding. In contrast the mean detected angle control-Bcl11a-UCS in mouse (77.7°-105.1°) and in chicken (72.3°-82.5°) was mostly somewhat below 90°C. Therefore the higher order chromatin conformation of Dach1 and Bcl11a was highly similar between evaluated tissues of one species, but differed between loci and between species.

Apart from species-specific modifications the mean chromatin compaction in the Dach1, the Bcl11a and the Csn region revealed a significantly more open conformation of dene-rich chromatin compared to gene-desert chromatin. The gene-rich side flanking Bcl11a (MMU: 0.93-1.78 kbp/nm, GGA: 0.73-1.16 kbp/nm) and the gene-rich casein region (MMU: 0.64-1.89 kbp/nm) displayed a significantly smaller mean chromatin compaction compared to the gene-deserts flanking Bcl11a to one

side (MMU 2.42-4.97 kbp/nm, GGA: 1.13-2.11 kbp/nm) and both sides of Dach1 (MMU: 1.61-2.92 kbp/nm, GGA: 1.30-2.21 kbp/nm) in all experiments. Moreover the chromatin compaction of the Dach1 region was very constant, showing almost no statistical differences (table S3). In contrast the chromatin compaction to both sides of the Bcl11a gene differed statistically evident among evaluated experiments, presumably driven from tissue-specific chromatin patterns and expression of the flanking genes (table S3). In addition, the low chromatin compaction in the Csn region contrasts to other L1 isochores (<35% GC-content) that normally display a rather closed chromatin structure (Bernardi 2007).

Neither in the Dach1 nor in the Bcl11a region the genomic angles or chromatin compactions were comprehensively changed with the expression state of the respective gene. Instead the rarely detected significant differences among evaluated tissues could be due to other cell type specific differences, and stable chromatin interactions maintained in all tissue types may predominantly define the local chromatin state. Still we cannot exclude to have missed local, small-scale chromatin decondensations with the used FISH approach, e.g. constricted to promotor regions or chromatin loops that originate from an attachment point (MLS model, Münkler and Langowski 1998) and additional short-termed or less-frequent interactions. However, also Shopland et al. 2006 who determined the chromatin conformation of a 4.3mbp region could not link slight conformational changes in different cell types with the expression of the regional genes, even after total gene expression blocking with DRB. Further Goetze et al. 2007 showed that the chromatin compaction of RIDGEs and Anti-RIDGEs was not dependent on gene expression variation in six cell types. In contrast, a significant decondensation of the Hoxb cluster after its transcriptional onset (Morey et al. 2007) was also detected by FISH using BAC probes covering the target gene and flanking regions.

Once more the 3D conformation of the Csn locus showed an adaptation to expression. The genomic angle Sult1b1-Csn-Igj during lactation was significantly smaller (71.5°) compared to before (97.5°) and after (96.7°) lactation and remarkably, was nearly identical among the non-lactating states. Further the interphase distances between Sul1b1 and Igj were significantly smaller during lactation but not from Sult1b1 to Csn or Csn to Igj (tabel S3). The genomic angle in hair and feather was slightly below 90° (81.3° , 88.8°) and therefore in between and statistically indistinguishable from the angles found in mammary gland. Hence the higher order chromatin folding of the Csn region during lactation could permit specific long-range cis interactions, which may enhance the high transcriptional activity of Csn genes. Alternatively, the frequent chromatin backfolding might have been caused by geometrical force imposed by the nuclear relocalization of the Csn locus (see 5.2.3). Very recently an increased backfolding favoring cis-interactions was also detected in

the Igh locus when developing from pro-pre B cells to pre B cells (Jhunjhunwala et al. 2008).

In summary, in accordance with the genome wide array based study of Gilbert et al. 2004 and the local FISH approach of Goetze et al. 2007 gene density and not gene expression turned out to be the most reliable prediction parameter for the chromatin compaction.

5.5 Conclusions

In this study we compared the Dach1 region, an isolated gene within a gene desert, the Bcl11a region, marking the border of a gene dense region and a gene desert, and the Csn genes, embedded in a gene-rich region. Thus all three regions extensively differ with respect to their respective genomic environment. In addition we investigated the effects of gene expression, tissue and species specificity that are summarized in table 5.3.

Dach1	Nucleus	Chromosome territory	Chromatin conformation
Gene density	+	o	+
Gene expression	o	o	o
Tissue specificity	o	o	o
Evolutionary Conservation	+	o	o
Bcl11a	Nucleus	Chromosome territory	Chromatin conformation
Gene density	+	+	+
Gene expression	o	o	o
Tissue specificity	+	+	+
Evolutionary Conservation	+	o	o
Csn	Nucleus	Chromosome territory	Chromatin conformation
Gene density	-	o	+
Gene expression	+	o	+
Tissue specificity	o	o	o
Evolutionary Conservation	+*	o	o*

Table 5.3: Different properties influencing the positioning of Dach1, Bcl11a and Csn loci in the interphase nucleus. Dach 1 shows an evolutionary conserved peripheral nuclear radial position in accordance to the low gene content, species-specific distance to chromosome territory surface and chromatin conformation. Bcl11a displayed a flexible radial nuclear position, likely correlated to other expressed genes in the region. Despite Bcl11a was evolutionarily conserved among homologous tissue of mouse and chicken. Further subtelomeric position localization on the metaphase chromosome might enhance positional flexibility and allow for tissue-specific variation. The local chromatin compaction differed for the two sides in accordance with the antidromic gene-content. The peripheral position of Csn in non-lactating cells conflicted with the high gene-content and conserved between species. Gene expression of Csn led to relocalization to the nuclear center and enhanced chromatin backfolding. The open chromatin conformation was consistent with the high gene content. (+ positive correlation, - negative correlation, o no correlation, * only in tested non-lactating cells).

The position of the Dach1 locus was most stably maintained close to the nuclear periphery in all evaluated cell types in accordance with the low regional gene content. In contrast, the Bcl11a gene showed considerable position variegation, most likely linked to tissue specific gene expression from the adjacent genes to on side of the Bcl11a gene. Conversely, the moderate expression of trans-dev genes Dach1 or Bcl11a did not directly affect the radial gene positioning. Astonishingly, the nuclear

peripheral orientation of the Csn region in the silent state conflicted with the high gene content and instead followed the low expressional activity and the low GC content in the region. Importantly, the obvious relocalization of Csn genes to the nuclear center in lactating mammary glands (figure 5.3) is also clearly correlated with Csn expression.

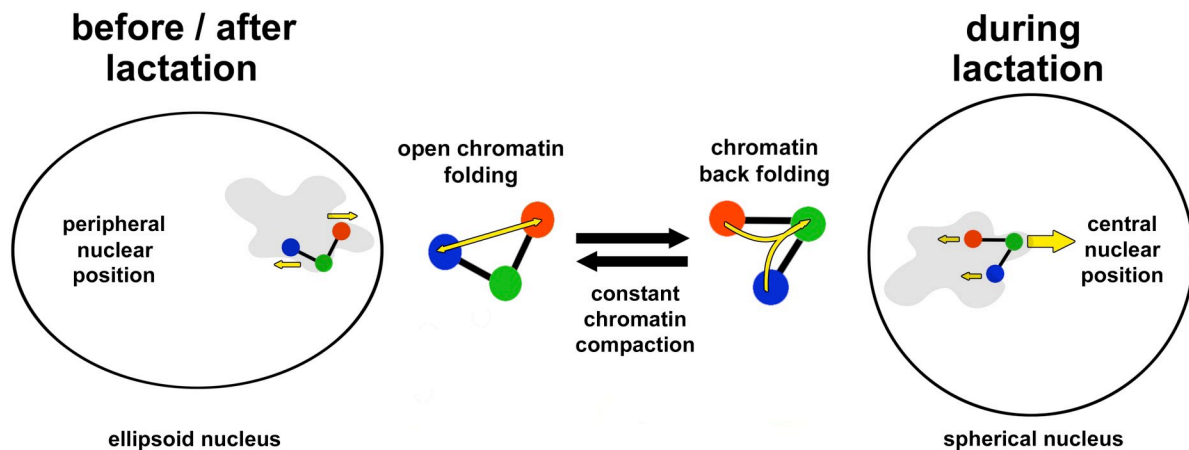


Figure 5.3: Nuclear genome architecture of the casein in mouse mammary epithelial cells locus before / after lactation (juvenile and retired breeder mouse) and during lactation (nursing mouse). (red) Sult1b1, (green) Csn genes, (blue) Igj, (yellow arrows) genomic forces affecting the Csn gene positioning.

Most importantly, the nuclear radial arrangement of Dach1, Bcl11a and silent Csn was deeper conserved between homologous mouse and chicken tissue than between different tissue types in one species, irrespectively of genomic rearrangements.

In no case the position of the investigated genomic loci with respect to the harboring CT was determined as functionally important, nor evolutionarily conserved. In particular no looping away from the CT surface, even for the highly transcriptional active Csn genes was evident. However, the Bcl11a locus indicated that CT position flexibility may be increased for subtelomeric genomic loci compared to mapping to interstitial regions.

Next, the local higher order chromatin architecture for all three loci indicated that gene density correlates well with an open chromatin conformation and is relatively inert to gene expression changes. Exceptionally, the Csn locus showed highly frequent chromatin backfolding during lactation compared to non-lactating states, either caused by geometrical forces deforming the chromatin fiber or by putative, intrachromosomal enhancer interactions (figure 5.3). Moreover, chromatin folding and compaction were not evolutionarily conserved.

In brief the strong evolutionary nuclear radial arrangement conservation of the investigated gene loci is strongly suggesting that a tissue-specific radial gene positioning is positively selected and a functionally indispensable feature of nuclear genome architecture. Moreover nuclear genome architecture was found to be

established by the dynamic interplay of different genomic properties, in particular gene density, gene expression and geometrical constraints. The weight of each factor clearly differs also between the Dach1, Bcl11a and Csn region (table 5.3) and potentially between species and tissue cell types. Only a careful inspection of the local genomic environment, considering most importantly gene density and the expression not only of single, but of all regional genes provide comprehensive information about expected results. Hence a simple rule of thumb, defining the nuclear architecture of genomic loci gene by gene does not exist.

6. Supplementary material

Supplement 1 (S1): 3-Dimensional radial distance distribution curves

Supplementary Figure 1.1: Dach1 – Mouse

Supplementary Figure 1.2: Dach1 – Chicken

Supplementary Figure 1.3: Bcl11a – Mouse

Supplementary Figure 1.4: Bcl11a - Chicken

Supplementary Figure 1.5: Csn – Mouse

Supplementary Figure 1.6: Csn – Chicken

Supplement (S2): Absolute distance measurement distribution to the CT surface

Supplementary Figure 2.1: Dach1 – Mouse

Supplementary Figure 2.2: Dach1 – Chicken

Supplementary Figure 2.3: Bcl11a – Mouse

Supplementary Figure 2.4: Bcl11a - Chicken

Supplementary Figure 2.5: Csn – Mouse

Supplementary Figure 2.6: Csn - Chicken

Supplement 3 (S3): ARR-values (Absolute relative radius), Absolute distance to the CT surface, Statistical evaluations

Supplementary Table 3.1: Dach1 and Bcl11a - ARR-values and absolute distance to the CT surface

Supplementary Table 3.2: Dach1 and Bcl11a - Statistical analysis of relative radial nuclear distribution

Supplementary Table 3.3: Dach1 and Bcl11a - Statistical analysis absolute distance to chromosome territory surface

Supplementary Table 3.4: Dach1 and Bcl11a - Statistical analysis of local 3D-conformation differences obtained from distance and angle measurements

Supplementary Table 3.5: Csn - ARR-values and absolute distance to the CT surface

Supplementary Table 3.6: Csn - Statistical analysis of relative radial nuclear distribution

Supplementary Table 3.7: Csn - Statistical analysis absolute distance to chromosome territory surface

Supplementary Table 3.8: Csn - Statistical analysis of local 3D-conformation differences obtained from distance and angle measurements

Supplement 4 (S4): Nuclear volumes, Roundness factor and Chromatin density

7. Literature

- Ahituv N, Zhu Y, Visel A, Holt A, Afzal V, Pennacchio LA, Rubin EM (2007) Deletion of ultraconserved elements yields viable mice. *PLoS Biol* 5: e234
- Albiez H, Cremer M, Tiberi C, Vecchio L, Schermelleh L, Dittrich S, Kupper K, Joffe B, Thormeyer T, von Hase J, Yang S, Rohr K, Leonhardt H, Solovei I, Cremer C, Fakan S, Cremer T (2006) Chromatin domains and the interchromatin compartment form structurally defined and functionally interacting nuclear networks. *Chromosome Res* 14: 707-33
- Albiez H, Zinner R, Tiberi C, Vecchio L, Weierich C, Schermelleh L, Strickfaden H, Solovei I, Fakan S, Cremer T (in preparation) Deconvolution of 3D confocal data sets improves image quality.
- Alexandrova O, Solovei I, Cremer T, David CN (2003) Replication labeling patterns and chromosome territories typical of mammalian nuclei are conserved in the early metazoan Hydra. *Chromosoma* 112: 190-200
- Arnone MI, Davidson EH (1997) The hardwiring of development: organization and function of genomic regulatory systems. *Development* 124: 1851-64
- Avram D, Fields A, Senawong T, Topark-Ngarm A, Leid M (2002) COUP-TF (chicken ovalbumin upstream promoter transcription factor)-interacting protein 1 (CTIP1) is a sequence-specific DNA binding protein. *Biochem J* 368: 555-63
- Ayres JA, Shum L, Akarsu AN, Dashner R, Takahashi K, Ikura T, Slavkin HC, Nuckolls GH (2001) DACH: genomic characterization, evaluation as a candidate for postaxial polydactyly type A2, and developmental expression pattern of the mouse homologue. *Genomics* 77: 18-26
- Backman M, Machon O, Van Den Bout CJ, Krauss S (2003) Targeted disruption of mouse Dach1 results in postnatal lethality. *Dev Dyn* 226: 139-44
- Ballester M, Kress C, Hue-Beauvais C, Kiêu K, Lehmann G, Adenot P, Devinoy E (2008) The nuclear localization of WAP and CSN genes is modified by lactogenic hormones in HC11 cells. 10.1002/jcb.21823
- Barski A, Cuddapah S, Cui K, Roh TY, Schones DE, Wang Z, Wei G, Chepelev I, Zhao K (2007) High-resolution profiling of histone methylations in the human genome. *Cell* 129: 823-37
- Becker TS, Lenhard B (2007) The random versus fragile breakage models of chromosome evolution: a matter of resolution. *Mol Genet Genomics* 278: 487-91
- Bejerano G, Siepel AC, Kent WJ, Haussler D (2005) Computational screening of conserved genomic DNA in search of functional noncoding elements. *Nat Methods* 2: 535-45
- Belmont AS, Bruce K (1994) Visualization of G1 chromosomes: a folded, twisted, supercoiled chromonema model of interphase chromatid structure. *J Cell Biol* 127: 287-302
- Bernardi G (2007) The neoselectionist theory of genome evolution. *Proc Natl Acad Sci U S A* 104: 8385-90
- Bernstein BE, Kamal M, Lindblad-Toh K, Bekiranov S, Bailey DK, Huebert DJ, McMahon S, Karlsson EK, Kulbokas EJ, 3rd, Gingeras TR, Schreiber SL, Lander ES (2005) Genomic maps and comparative analysis of histone modifications in human and mouse. *Cell* 120: 169-81
- Bernstein BE, Mikkelsen TS, Xie X, Kamal M, Huebert DJ, Cuff J, Fry B, Meissner A, Wernig M, Plath K, Jaenisch R, Wagschal A, Feil R, Schreiber SL, Lander ES

- (2006a) A bivalent chromatin structure marks key developmental genes in embryonic stem cells. *Cell* 125: 315-26
- Bernstein E, Duncan EM, Masui O, Gil J, Heard E, Allis CD (2006b) Mouse polycomb proteins bind differentially to methylated histone H3 and RNA and are enriched in facultative heterochromatin. *Mol Cell Biol* 26: 2560-9
- Bickmore WA, Teague P (2002) Influences of chromosome size, gene density and nuclear position on the frequency of constitutional translocations in the human population. *Chromosome Res* 10: 707-15
- Bolzer A, Kreth G, Solovei I, Koehler D, Saracoglu K, Fauth C, Muller S, Eils R, Cremer C, Speicher MR, Cremer T (2005) Three-dimensional maps of all chromosomes in human male fibroblast nuclei and prometaphase rosettes. *PLoS Biol* 3: e157
- Boveri T (1909) Die Blastomerenkerne von *Ascaris megalocephala* und die Theorie der Chromosomenindividualität. *Arch Zellforsch* 3: 181-268
- Boyer LA, Plath K, Zeitlinger J, Brambrink T, Medeiros LA, Lee TI, Levine SS, Wernig M, Tajonar A, Ray MK, Bell GW, Otte AP, Vidal M, Gifford DK, Young RA, Jaenisch R (2006) Polycomb complexes repress developmental regulators in murine embryonic stem cells. *Nature* 441: 349-53
- Braissant O, Whali W (1998) A Simplified In Situ Hybridization Protocol Using Non-radioactively Labeled Probes to Detect Abundant and Rare mRNAs on Tissue Sections. *BIOCHEMICA N O .* 1: 10-16
- Branco MR, Pombo A (2006) Intermingling of chromosome territories in interphase suggests role in translocations and transcription-dependent associations. *PLoS Biol* 4: e138
- Bridger JM, Boyle S, Kill IR, Bickmore WA (2000) Re-modelling of nuclear architecture in quiescent and senescent human fibroblasts. *Curr Biol* 10: 149-52
- Brisken C, Rajaram RD (2006) Alveolar and lactogenic differentiation. *J Mammary Gland Biol Neoplasia* 11: 239-48
- Brown JM, Leach J, Reittie JE, Atzberger A, Lee-Prudhoe J, Wood WG, Higgs DR, Iborra FJ, Buckle VJ (2006) Coregulated human globin genes are frequently in spatial proximity when active. *J Cell Biol* 172: 177-87
- Burt DW, Bruley C, Dunn IC, Jones CT, Ramage A, Law AS, Morrice DR, Paton IR, Smith J, Windsor D, Sazanov A, Fries R, Waddington D (1999) The dynamics of chromosome evolution in birds and mammals. *Nature* 402: 411-3
- Caille N, Thoumine O, Tardy Y, Meister JJ (2002) Contribution of the nucleus to the mechanical properties of endothelial cells. *J Biomech* 35: 177-87
- Caron H, van Schaik B, van der Mee M, Baas F, Riggins G, van Sluis P, Hermus MC, van Asperen R, Boon K, Voute PA, Heisterkamp S, van Kampen A, Versteeg R (2001) The human transcriptome map: clustering of highly expressed genes in chromosomal domains. *Science* 291: 1289-92
- Caubit X, Thangarajah R, Theil T, Wirth J, Nothwang HG, Ruther U, Krauss S (1999) Mouse Dac, a novel nuclear factor with homology to *Drosophila dachshund* shows a dynamic expression in the neural crest, the eye, the neocortex, and the limb bud. *Dev Dyn* 214: 66-80
- Chakalova L, Carter D, Debrand E, Goyenechea B, Horton A, Miles J, Osborne C, Fraser P (2005) Developmental regulation of the beta-globin gene locus. *Prog Mol Subcell Biol* 38: 183-206
- Chambeyron S, Bickmore WA (2004) Chromatin decondensation and nuclear reorganization of the HoxB locus upon induction of transcription. *Genes Dev* 18: 1119-30

- Chambeyron S, Da Silva NR, Lawson KA, Bickmore WA (2005) Nuclear re-organisation of the Hoxb complex during mouse embryonic development. *Development* 132: 2215-23
- Chuang CH, Carpenter AE, Fuchsova B, Johnson T, de Lanerolle P, Belmont AS (2006) Long-range directional movement of an interphase chromosome site. *Curr Biol* 16: 825-31
- Chubb JR, Bickmore WA (2003) Considering nuclear compartmentalization in the light of nuclear dynamics. *Cell* 112: 403-6
- Chubb JR, Boyle S, Perry P, Bickmore WA (2002) Chromatin motion is constrained by association with nuclear compartments in human cells. *Curr Biol* 12: 439-45
- Chubb JR, Trcek T, Shenoy SM, Singer RH (2006) Transcriptional pulsing of a developmental gene. *Curr Biol* 16: 1018-25
- Consortium CGS (2004) Sequence and comparative analysis of the chicken genome provide unique perspectives on vertebrate evolution. *Nature* 432: 695-716
- Costantini M, Clay O, Auletta F, Bernardi G (2006) An isochore map of human chromosomes. *Genome Res* 16: 536-41
- Cremer C, Cremer T, Gray JW (1982) Induction of chromosome damage by ultraviolet light and caffeine: correlation of cytogenetic evaluation and flow karyotype. *Cytometry* 2: 287-90
- Cremer M, Kupper K, Wagler B, Wizelman L, von Hase J, Weiland Y, Kreja L, Diebold J, Speicher MR, Cremer T (2003) Inheritance of gene density-related higher order chromatin arrangements in normal and tumor cell nuclei. *J Cell Biol* 162: 809-20
- Cremer M, von Hase J, Volm T, Brero A, Kreth G, Walter J, Fischer C, Solovei I, Cremer C, Cremer T (2001) Non-random radial higher-order chromatin arrangements in nuclei of diploid human cells. *Chromosome Res* 9: 541-67
- Cremer T, Cremer M, Dietzel S, Muller S, Solovei I, Fakan S (2006) Chromosome territories--a functional nuclear landscape. *Curr Opin Cell Biol* 18: 307-16
- Cremer T, Kreth G, Koester H, Fink RH, Heintzmann R, Cremer M, Solovei I, Zink D, Cremer C (2000) Chromosome territories, interchromatin domain compartment, and nuclear matrix: an integrated view of the functional nuclear architecture. *Crit Rev Eukaryot Gene Expr* 10: 179-212
- Croft JA, Bridger JM, Boyle S, Perry P, Teague P, Bickmore WA (1999) Differences in the localization and morphology of chromosomes in the human nucleus. *J Cell Biol* 145: 1119-31
- Davis RJ, Harding M, Moayed Y, Mardon G (2008) Mouse Dach1 and Dach2 are redundantly required for Mullerian duct development. *Genesis* 46: 205-13
- Davis RJ, Pesah YI, Harding M, Paylor R, Mardon G (2006) Mouse Dach2 mutants do not exhibit gross defects in eye development or brain function. *Genesis* 44: 84-92
- Davis RJ, Shen W, Heanue TA, Mardon G (1999) Mouse Dach, a homologue of *Drosophila dachshund*, is expressed in the developing retina, brain and limbs. *Dev Genes Evol* 209: 526-36
- Davis RJ, Shen W, Sandler YI, Heanue TA, Mardon G (2001) Characterization of mouse Dach2, a homologue of *Drosophila dachshund*. *Mech Dev* 102: 169-79
- de la Calle-Mustienes E, Feijoo CG, Manzanares M, Tena JJ, Rodriguez-Seguel E, Letizia A, Allende ML, Gomez-Skarmeta JL (2005) A functional survey of the enhancer activity of conserved non-coding sequences from vertebrate Iroquois cluster gene deserts. *Genome Res* 15: 1061-72
- de Laat W, Grosveld F (2007) Inter-chromosomal gene regulation in the mammalian cell nucleus. *Curr Opin Genet Dev* 17: 456-64

- Dean FB, Nelson JR, Giesler TL, Lasken RS (2001) Rapid amplification of plasmid and phage DNA using Phi 29 DNA polymerase and multiply-primed rolling circle amplification. *Genome Res* 11: 1095-9
- Dehal P, Boore JL (2005) Two rounds of whole genome duplication in the ancestral vertebrate. *PLoS Biol* 3: e314
- Dekker J (2008) Gene regulation in the third dimension. *Science* 319: 1793-4
- DeLange RJ, Fambrough DM, Smith EL, Bonner J (1969) Calf and pea histone IV. 3. Complete amino acid sequence of pea seedling histone IV; comparison with the homologous calf thymus histone. *J Biol Chem* 244: 5669-79
- Deng W, Tsao SW, Lucas JN, Leung CS, Cheung AL (2003) A new method for improving metaphase chromosome spreading. *Cytometry A* 51: 46-51
- Dermitzakis ET, Reymond A, Lyle R, Scamuffa N, Ucla C, Deutsch S, Stevenson BJ, Flegel V, Bucher P, Jongeneel CV, Antonarakis SE (2002) Numerous potentially functional but non-genic conserved sequences on human chromosome 21. *Nature* 420: 578-82
- Dietzel S, Jauch A, Kienle D, Qu G, Holtgreve-Grez H, Eils R, Munkel C, Bittner M, Meltzer PS, Trent JM, Cremer T (1998) Separate and variably shaped chromosome arm domains are disclosed by chromosome arm painting in human cell nuclei. *Chromosome Res* 6: 25-33
- Dundr M, Ospina JK, Sung MH, John S, Upender M, Ried T, Hager GL, Matera AG (2007) Actin-dependent intranuclear repositioning of an active gene locus in vivo. *J Cell Biol* 179: 1095-103
- Eichler EE, Johnson ME, Alkan C, Tuzun E, Sahinalp C, Misceo D, Archidiacono N, Rocchi M (2001) Divergent origins and concerted expansion of two segmental duplications on chromosome 16. *J Hered* 92: 462-8
- Engstrom PG, Fredman D, Lenhard B (2008) Ancora: a web resource for exploring highly conserved noncoding elements and their association with developmental regulatory genes. *Genome Biol* 9: R34
- Foster HA, Abeydeera LR, Griffin DK, Bridger JM (2005) Non-random chromosome positioning in mammalian sperm nuclei, with migration of the sex chromosomes during late spermatogenesis. *J Cell Sci* 118: 1811-20
- Francastel C, Schubeler D, Martin DI, Groudine M (2000) Nuclear compartmentalization and gene activity. *Nat Rev Mol Cell Biol* 1: 137-43
- Fraser P, Bickmore W (2007) Nuclear organization of the genome and the potential for gene regulation. *Nature* 447: 413-7
- Gaszner M, Felsenfeld G (2006) Insulators: exploiting transcriptional and epigenetic mechanisms. *Nat Rev Genet* 7: 703-13
- Gazave E, Gautier P, Gilchrist S, Bickmore WA (2005) Does radial nuclear organisation influence DNA damage? *Chromosome Res* 13: 377-88
- Gilbert N, Boyle S, Fiegler H, Woodfine K, Carter NP, Bickmore WA (2004) Chromatin architecture of the human genome: gene-rich domains are enriched in open chromatin fibers. *Cell* 118: 555-66
- Gilbert N, Gilchrist S, Bickmore WA (2005) Chromatin organization in the mammalian nucleus. *Int Rev Cytol* 242: 283-336
- Gimelbrant A, Hutchinson JN, Thompson BR, Chess A (2007) Widespread monoallelic expression on human autosomes. *Science* 318: 1136-40
- Gladilin E, Micoulet A, Hosseini B, Rohr K, Spatz J, Eils R (2007) 3D finite element analysis of uniaxial cell stretching: from image to insight. *Phys Biol* 4: 104-13
- Goetze S, Mateos-Langerak J, van Driel R (2007) Three-dimensional genome organization in interphase and its relation to genome function. *Semin Cell Dev Biol* 18: 707-14

- Gondor A, Rougier C, Ohlsson R (2008) High-resolution circular chromosome conformation capture assay. *Nat Protoc* 3: 303-13
- Graphodatsky AS, Yang F, Dobigny G, Romanenko SA, Biltueva LS, Perelman PL, Beklemisheva VR, Alkalaeva EZ, Serdukova NA, Ferguson-Smith MA, Murphy WJ, Robinson TJ (2008) Tracking genome organization in rodents by Zoo-FISH. *Chromosome Res* 16: 261-74
- Grasser F, Neusser M, Fiegler H, Thormeyer T, Cremer M, Carter NP, Cremer T, Muller S (2008) Replication-timing-correlated spatial chromatin arrangements in cancer and in primate interphase nuclei. *J Cell Sci* 121: 1876-86
- Griffin DK, Robertson LB, Tempest HG, Skinner BM (2007) The evolution of the avian genome as revealed by comparative molecular cytogenetics. *Cytogenet Genome Res* 117: 64-77
- Gritli-Linde A, Hallberg K, Harfe BD, Reyahi A, Kannius-Janson M, Nilsson J, Cobourne MT, Sharpe PT, McMahon AP, Linde A (2007) Abnormal hair development and apparent follicular transformation to mammary gland in the absence of hedgehog signaling. *Dev Cell* 12: 99-112
- Gruenbaum Y, Margalit A, Goldman RD, Shumaker DK, Wilson KL (2005) The nuclear lamina comes of age. *Nat Rev Mol Cell Biol* 6: 21-31
- Gu X, Wang Y, Gu J (2002) Age distribution of human gene families shows significant roles of both large- and small-scale duplications in vertebrate evolution. *Nat Genet* 31: 205-9
- Guelen L, Pagie L, Brasset E, Meuleman W, Faza MB, Talhout W, Eussen BH, de Klein A, Wessels L, de Laat W, van Steensel B (2008) Domain organization of human chromosomes revealed by mapping of nuclear lamina interactions. *Nature*
- Habermann FA, Cremer M, Walter J, Kreth G, von Hase J, Bauer K, Wienberg J, Cremer C, Cremer T, Solovei I (2001) Arrangements of macro- and microchromosomes in chicken cells. *Chromosome Res* 9: 569-84
- Hamburger V, Hamilton HL (1951) A series of normal stages in the development of the chick embryo. 1951. *Dev Dyn* 195: 231-72
- Hancock R (2007) Packing of the polynucleosome chain in interphase chromosomes: evidence for a contribution of crowding and entropic forces. *Semin Cell Dev Biol* 18: 668-75
- Hedges SB (2002) The origin and evolution of model organisms. *Nat Rev Genet* 3: 838-49
- Henikoff S, McKittrick E, Ahmad K (2004) Epigenetics, histone H3 variants, and the inheritance of chromatin states. *Cold Spring Harb Symp Quant Biol* 69: 235-43
- Hennighausen L (1997) Molecular mechanisms of hormone controlled gene expression in the breast. *Mol Biol Rep* 24: 169-74
- Hennighausen L, Robinson GW (2005) Information networks in the mammary gland. *Nat Rev Mol Cell Biol* 6: 715-25
- Hewitt SL, High FA, Reiner SL, Fisher AG, Merckenschlager M (2004) Nuclear repositioning marks the selective exclusion of lineage-inappropriate transcription factor loci during T helper cell differentiation. *Eur J Immunol* 34: 3604-13
- Hsu TC (1975) A possible function of constitutive heterochromatin: the bodyguard hypothesis. *Genetics* 79: 137-150
- Innis MA, Gelfand H (1990) PCR Protocols - Optimization of PCRs. Academic Press, New York
- Jenuwein T (2006) The epigenetic magic of histone lysine methylation. *Febs J* 273: 3121-35

- Jhunjunwala S, van Zelm MC, Peak MM, Cutchin S, Riblet R, van Dongen JJ, Grosveld FG, Knoch TA, Murre C (2008) The 3D structure of the immunoglobulin heavy-chain locus: implications for long-range genomic interactions. *Cell* 133: 265-79
- Jonker A, de Boer PA, van den Hoff MJ, Lamers WH, Moorman AF (1997) Towards quantitative in situ hybridization. *J Histochem Cytochem* 45: 413-23
- Kaufmann MH (1992) *The Atlas of Mouse Development*. Elsevier Academic Press, London, UK
- Kawasaki K, Buchanan AV, Weiss KM (2007) Gene duplication and the evolution of vertebrate skeletal mineralization. *Cells Tissues Organs* 186: 7-24
- Kawasaki K, Weiss KM (2006) Evolutionary genetics of vertebrate tissue mineralization: the origin and evolution of the secretory calcium-binding phosphoprotein family. *J Exp Zool B Mol Dev Evol* 306: 295-316
- Kida Y, Maeda Y, Shiraishi T, Suzuki T, Ogura T (2004) Chick Dach1 interacts with the Smad complex and Sin3a to control AER formation and limb development along the proximodistal axis. *Development* 131: 4179-87
- Kikuta H, Laplante M, Navratilova P, Komisarczuk AZ, Engstrom PG, Fredman D, Akalin A, Caccamo M, Sealy I, Howe K, Ghislain J, Pezeron G, Mourrain P, Ellingsen S, Oates AC, Thisse C, Thisse B, Foucher I, Adolf B, Geling A, Lenhard B, Becker TS (2007) Genomic regulatory blocks encompass multiple neighboring genes and maintain conserved synteny in vertebrates. *Genome Res* 17: 545-55
- Kim SH, McQueen PG, Lichtman MK, Shevach EM, Parada LA, Misteli T (2004) Spatial genome organization during T-cell differentiation. *Cytogenet Genome Res* 105: 292-301
- Kim TH, Barrera LO, Zheng M, Qu C, Singer MA, Richmond TA, Wu Y, Green RD, Ren B (2005) A high-resolution map of active promoters in the human genome. *Nature* 436: 876-80
- Kimura-Yoshida C, Kitajima K, Oda-Ishii I, Tian E, Suzuki M, Yamamoto M, Suzuki T, Kobayashi M, Aizawa S, Matsuo I (2004) Characterization of the pufferfish *Otx2* cis-regulators reveals evolutionarily conserved genetic mechanisms for vertebrate head specification. *Development* 131: 57-71
- Kleinjan DA, van Heyningen V (2005) Long-range control of gene expression: emerging mechanisms and disruption in disease. *Am J Hum Genet* 76: 8-32
- Knoch TA (2002) Approaching the Three-Dimensional Organization of the Human Genome: Structural-, Scaling-, and Dynamic-Properties in the Simulation of Interphase Chromosomes and Cell Nuclei, Long-Range Correlations in Complete Genomes, In Vivo Quantification of the Chromatin Distribution, Construct Conversion in Simultaneous Co- Transfections TAK Press, Mannheim, Germany
- Kohn M, Hogel J, Vogel W, Minich P, Kehrer-Sawatzki H, Graves JA, Hameister H (2006) Reconstruction of a 450-My-old ancestral vertebrate protokaryotype. *Trends Genet* 22: 203-10
- Kosak ST, Groudine M (2004a) Form follows function: The genomic organization of cellular differentiation. *Genes Dev* 18: 1371-84
- Kosak ST, Groudine M (2004b) Gene order and dynamic domains. *Science* 306: 644-7
- Kosak ST, Skok JA, Medina KL, Riblet R, Le Beau MM, Fisher AG, Singh H (2002) Subnuclear compartmentalization of immunoglobulin loci during lymphocyte development. *Science* 296: 158-62

- Kubota K, Ohashi A, Imachi H, Harada H (2006) Improved in situ hybridization efficiency with locked-nucleic-acid-incorporated DNA probes. *Appl Environ Microbiol* 72: 5311-7
- Kumaran RI, Spector DL (2008) A genetic locus targeted to the nuclear periphery in living cells maintains its transcriptional competence. *J Cell Biol* 180: 51-65
- Kupper K, Kolbl A, Biener D, Dittrich S, von Hase J, Thormeyer T, Fiegler H, Carter NP, Speicher MR, Cremer T, Cremer M (2007) Radial chromatin positioning is shaped by local gene density, not by gene expression. *Chromosoma* 116: 285-306
- Kuroda M, Tanabe H, Yoshida K, Oikawa K, Saito A, Kiyuna T, Mizusawa H, Mukai K (2004) Alteration of chromosome positioning during adipocyte differentiation. *J Cell Sci* 117: 5897-903
- Kurz A, Lampel S, Nickolenko JE, Bradl J, Benner A, Zirbel RM, Cremer T, Lichter P (1996) Active and inactive genes localize preferentially in the periphery of chromosome territories. *J Cell Biol* 135: 1195-205
- Lamond AI, Spector DL (2003) Nuclear speckles: a model for nuclear organelles. *Nat Rev Mol Cell Biol* 4: 605-12
- Lanctot C, Cheutin T, Cremer M, Cavalli G, Cremer T (2007) Dynamic genome architecture in the nuclear space: regulation of gene expression in three dimensions. *Nat Rev Genet* 8: 104-15
- Landmann L (2002) Deconvolution improves colocalization analysis of multiple fluorochromes in 3D confocal data sets more than filtering techniques. *J Microsc* 208: 134-47
- Lanzuolo C, Roure V, Dekker J, Bantignies F, Orlando V (2007) Polycomb response elements mediate the formation of chromosome higher-order structures in the bithorax complex. *Nat Cell Biol* 9: 1167-74
- Lee CK, Sunkin SM, Kuan C, Thompson CL, Pathak S, Ng L, Lau C, Fischer S, Mortrud M, Slaughterbeck C, Jones A, Lein E, Hawrylycz M (2008) Quantitative methods for genome-scale analysis of in situ hybridization and correlation with microarray data. *Genome Biol* 9: R23
- Leid M, Ishmael JE, Avram D, Shepherd D, Fraulob V, Dolle P (2004) CTIP1 and CTIP2 are differentially expressed during mouse embryogenesis. *Gene Expr Patterns* 4: 733-9
- Leitch AR (2000) Higher levels of organization in the interphase nucleus of cycling and differentiated cells. *Microbiol Mol Biol Rev* 64: 138-52
- Lemke J, Claussen J, Michel S, Chudoba I, Muhlig P, Westermann M, Sperling K, Rubtsov N, Grummt UW, Ullmann P, Kromeyer-Hauschild K, Liehr T, Claussen U (2002) The DNA-based structure of human chromosome 5 in interphase. *Am J Hum Genet* 71: 1051-9
- Lesne A, Victor JM (2006) Chromatin fiber functional organization: some plausible models. *Eur Phys J E Soft Matter* 19: 279-90
- Levsky JM, Shenoy SM, Chubb JR, Hall CB, Capodici P, Singer RH (2007) The spatial order of transcription in mammalian cells. *J Cell Biochem* 102: 609-17
- Liao BY, Zhang J (2006) Low rates of expression profile divergence in highly expressed genes and tissue-specific genes during mammalian evolution. *Mol Biol Evol* 23: 1119-28
- Liu CL, Kaplan T, Kim M, Buratowski S, Schreiber SL, Friedman N, Rando OJ (2005) Single-nucleosome mapping of histone modifications in *S. cerevisiae*. *PLoS Biol* 3: e328
- Liu H, Ippolito GC, Wall JK, Niu T, Probst L, Lee BS, Pulford K, Banham AH, Stockwin L, Shaffer AL, Staudt LM, Das C, Dyer MJ, Tucker PW (2006)

- Functional studies of BCL11A: characterization of the conserved BCL11A-XL splice variant and its interaction with BCL6 in nuclear paraspeckles of germinal center B cells. *Mol Cancer* 5: 18
- Livak KJ, Schmittgen TD (2001) Analysis of relative gene expression data using real-time quantitative PCR and the 2(-Delta Delta C(T)) Method. *Methods* 25: 402-8
- Lomvardas S, Barnea G, Pisapia DJ, Mendelsohn M, Kirkland J, Axel R (2006) Interchromosomal interactions and olfactory receptor choice. *Cell* 126: 403-13
- Mahy NL, Perry PE, Bickmore WA (2002a) Gene density and transcription influence the localization of chromatin outside of chromosome territories detectable by FISH. *J Cell Biol* 159: 753-63
- Mahy NL, Perry PE, Gilchrist S, Baldock RA, Bickmore WA (2002b) Spatial organization of active and inactive genes and noncoding DNA within chromosome territories. *J Cell Biol* 157: 579-89
- Manders EM, Stap J, Brakenhoff GJ, van Driel R, Aten JA (1992) Dynamics of three-dimensional replication patterns during the S-phase, analysed by double labelling of DNA and confocal microscopy. *J Cell Sci* 103 (Pt 3): 857-62
- Maniotis AJ, Chen CS, Ingber DE (1997) Demonstration of mechanical connections between integrins, cytoskeletal filaments, and nucleoplasm that stabilize nuclear structure. *Proc Natl Acad Sci U S A* 94: 849-54
- Mardon G, Solomon NM, Rubin GM (1994) dachshund encodes a nuclear protein required for normal eye and leg development in *Drosophila*. *Development* 120: 3473-86
- Martens JH, O'Sullivan RJ, Braunschweig U, Opravil S, Radolf M, Steinlein P, Jenuwein T (2005) The profile of repeat-associated histone lysine methylation states in the mouse epigenome. *Embo J* 24: 800-12
- Martini SR, Roman G, Meuser S, Mardon G, Davis RL (2000) The retinal determination gene, dachshund, is required for mushroom body cell differentiation. *Development* 127: 2663-72
- Mateos-Langerak J, Goetze S, Leonhardt H, Cremer T, van Driel R, Lanctot C (2007) Nuclear architecture: Is it important for genome function and can we prove it? *J Cell Biochem* 102: 1067-75
- Matsuya A, Sakate R, Kawahara Y, Koyanagi KO, Sato Y, Fujii Y, Yamasaki C, Habara T, Nakaoka H, Todokoro F, Yamaguchi K, Endo T, Oota S, Makalowski W, Ikeo K, Suzuki Y, Hanada K, Hashimoto K, Hirai M, Iwama H, Saitou N, Hiraki AT, Jin L, Kaneko Y, Kanno M, Murakami K, Noda AO, Saichi N, Sanbonmatsu R, Suzuki M, Takeda J, Tanaka M, Gojobori T, Imanishi T, Itoh T (2008) Evola: Ortholog database of all human genes in H-InvDB with manual curation of phylogenetic trees. *Nucleic Acids Res* 36: D787-92
- Mayer R, Brero A, von Hase J, Schroeder T, Cremer T, Dietzel S (2005) Common themes and cell type specific variations of higher order chromatin arrangements in the mouse. *BMC Cell Biol* 6: 44
- McEwen GK, Woolfe A, Goode D, Vavouri T, Callaway H, Elgar G (2006) Ancient duplicated conserved noncoding elements in vertebrates: a genomic and functional analysis. *Genome Res* 16: 451-65
- Meaburn KJ, Misteli T (2007) Cell biology: chromosome territories. *Nature* 445: 379-781
- Mehta IS, Figgitt M, Clements CS, Kill IR, Bridger JM (2007) Alterations to nuclear architecture and genome behavior in senescent cells. *Ann N Y Acad Sci* 1100: 250-63

- Miguel-Aliaga I, Allan DW, Thor S (2004) Independent roles of the dachshund and eyes absent genes in BMP signaling, axon pathfinding and neuronal specification. *Development* 131: 5837-48
- Mikkola ML (2007) Genetic basis of skin appendage development. *Semin Cell Dev Biol* 18: 225-36
- Misteli T (2005) Concepts in nuclear architecture. *Bioessays* 27: 477-87
- Morey C, Da Silva NR, Perry P, Bickmore WA (2007) Nuclear reorganisation and chromatin decondensation are conserved, but distinct, mechanisms linked to Hox gene activation. *Development* 134: 909-19
- Müller S, Cremer M, Neusser M, Grasser F, Cremer T (submitted) A technical note on quantum dots for multi-color fluorescence in situ hybridization. *Cytogenet Genome Res*
- Munkel C, Eils R, Dietzel S, Zink D, Mehring C, Wedemann G, Cremer T, Langowski J (1999) Compartmentalization of interphase chromosomes observed in simulation and experiment. *J Mol Biol* 285: 1053-65
- Münkel C, Langowski J (1998) Chromosome structure described by a polymer model. *Phys. Rev. E Stat. Plasmas Fluids Relat. Interdiscip. Topics* 57(5B) 5888-5896
- Murmann AE, Gao J, Encinosa M, Gautier M, Peter ME, Eils R, Lichter P, Rowley JD (2005) Local gene density predicts the spatial position of genetic loci in the interphase nucleus. *Exp Cell Res* 311: 14-26
- Mustafa A *Biology of Lactation*. Mc Gill University Montreal, Canada
- Nakamura T, Yamazaki Y, Saiki Y, Moriyama M, Largaespada DA, Jenkins NA, Copeland NG (2000) Evi9 encodes a novel zinc finger protein that physically interacts with BCL6, a known human B-cell proto-oncogene product. *Mol Cell Biol* 20: 3178-86
- Nakatani Y, Takeda H, Kohara Y, Morishita S (2007) Reconstruction of the vertebrate ancestral genome reveals dynamic genome reorganization in early vertebrates. *Genome Res* 17: 1254-65
- Nei M, Kumar S (2000) *Molecular evolution and phylogenetics*. Oxford University Press, New York
- Nemeth A, Langst G (2004) Chromatin higher order structure: opening up chromatin for transcription. *Brief Funct Genomic Proteomic* 2: 334-43
- Neusser M, Schubel V, Koch A, Cremer T, Müller S (2007) Evolutionarily conserved, cell type and species-specific higher order chromatin arrangements in interphase nuclei of primates. *Chromosoma* 116: 307-20
- Nobrega MA, Ovcharenko I, Afzal V, Rubin EM (2003) Scanning human gene deserts for long-range enhancers. *Science* 302: 413
- Nogami M, Nogami O, Kagotani K, Okumura M, Taguchi H, Ikemura T, Okumura K (2000) Intranuclear arrangement of human chromosome 12 correlates to large-scale replication domains. *Chromosoma* 108: 514-22
- Nunez E, Kwon YS, Hutt KR, Hu Q, Cardamone MD, Ohgi KA, Garcia-Bassets I, Rose DW, Glass CK, Rosenfeld MG, Fu XD (2008) Nuclear receptor-enhanced transcription requires motor- and LSD1-dependent gene networking in interchromatin granules. *Cell* 132: 996-1010
- O'Keefe RT, Henderson SC, Spector DL (1992) Dynamic organization of DNA replication in mammalian cell nuclei: spatially and temporally defined replication of chromosome-specific alpha-satellite DNA sequences. *J Cell Biol* 116: 1095-110
- Oftedal OT (2002a) The mammary gland and its origin during synapsid evolution. *J Mammary Gland Biol Neoplasia* 7: 225-52

- Oftedal OT (2002b) The origin of lactation as a water source for parchment-shelled eggs. *J Mammary Gland Biol Neoplasia* 7: 253-66
- Okada TA, Comings DE (1979) Higher order structure of chromosomes. *Chromosoma* 72: 1-14
- Osborne CS, Chakalova L, Brown KE, Carter D, Horton A, Debrand E, Goyenechea B, Mitchell JA, Lopes S, Reik W, Fraser P (2004) Active genes dynamically colocalize to shared sites of ongoing transcription. *Nat Genet* 36: 1065-71
- Osborne CS, Chakalova L, Mitchell JA, Horton A, Wood AL, Bolland DJ, Corcoran AE, Fraser P (2007) Myc dynamically and preferentially relocates to a transcription factory occupied by Igh. *PLoS Biol* 5: e192
- Parada LA, McQueen PG, Misteli T (2004) Tissue-specific spatial organization of genomes. *Genome Biol* 5: R44
- Pennacchio LA, Ahituv N, Moses AM, Prabhakar S, Nobrega MA, Shoukry M, Minovitsky S, Dubchak I, Holt A, Lewis KD, Plajzer-Frick I, Akiyama J, De Val S, Afzal V, Black BL, Couronne O, Eisen MB, Visel A, Rubin EM (2006) In vivo enhancer analysis of human conserved non-coding sequences. *Nature* 444: 499-502
- Pennacchio LA, Loots GG, Nobrega MA, Ovcharenko I (2007) Predicting tissue-specific enhancers in the human genome. *Genome Res* 17: 201-11
- Peters AH, Kubicek S, Mechtler K, O'Sullivan RJ, Derijck AA, Perez-Burgos L, Kohlmaier A, Opravil S, Tachibana M, Shinkai Y, Martens JH, Jenuwein T (2003) Partitioning and plasticity of repressive histone methylation states in mammalian chromatin. *Mol Cell* 12: 1577-89
- Pispa J, Thesleff I (2003) Mechanisms of ectodermal organogenesis. *Dev Biol* 262: 195-205
- Poirier MG, Bussiek M, Langowski J, Widom J (2008) Spontaneous access to DNA target sites in folded chromatin fibers. *J Mol Biol* 379: 772-86
- Pokholok DK, Harbison CT, Levine S, Cole M, Hannett NM, Lee TI, Bell GW, Walker K, Rolfe PA, Herbolsheimer E, Zeitlinger J, Lewitter F, Gifford DK, Young RA (2005) Genome-wide map of nucleosome acetylation and methylation in yeast. *Cell* 122: 517-27
- Postberg J, Alexandrova O, Cremer T, Lipps HJ (2005) Exploiting nuclear duality of ciliates to analyse topological requirements for DNA replication and transcription. *J Cell Sci* 118: 3973-83
- Purmann A, Toedling J, Schueler M, Carninci P, Lehrach H, Hayashizaki Y, Huber W, Sperling S (2007) Genomic organization of transcriptomes in mammals: Coregulation and cofunctionality. *Genomics* 89: 580-7
- Ragoczy T, Bender MA, Telling A, Byron R, Groudine M (2006) The locus control region is required for association of the murine beta-globin locus with engaged transcription factories during erythroid maturation. *Genes Dev* 20: 1447-57
- Ragoczy T, Telling A, Sawado T, Groudine M, Kosak ST (2003) A genetic analysis of chromosome territory looping: diverse roles for distal regulatory elements. *Chromosome Res* 11: 513-25
- Rijnkels M (2002) Multispecies comparison of the casein gene loci and evolution of casein gene family. *J Mammary Gland Biol Neoplasia* 7: 327-45
- Rijnkels M, Elnitski L, Miller W, Rosen JM (2003) Multispecies comparative analysis of a mammalian-specific genomic domain encoding secretory proteins. *Genomics* 82: 417-32
- Roh TY, Cuddapah S, Cui K, Zhao K (2006) The genomic landscape of histone modifications in human T cells. *Proc Natl Acad Sci U S A* 103: 15782-7

- Roix JJ, McQueen PG, Munson PJ, Parada LA, Misteli T (2003) Spatial proximity of translocation-prone gene loci in human lymphomas. *Nat Genet* 34: 287-91
- Ronneberger O, Baddeley D, Scheipl F, Verveer PJ, Burkhardt H, Cremer C, Fahrmeir L, Cremer T, Joffe B (2008) Spatial quantitative analysis of fluorescently labeled nuclear structures: Problems, methods, pitfalls. *Chromosome Res* 16: 523-62
- Sachs RK, van den Engh G, Trask B, Yokota H, Hearst JE (1995) A random-walk/giant-loop model for interphase chromosomes. *Proc Natl Acad Sci U S A* 92: 2710-4
- Sadoni N, Cardoso MC, Stelzer EH, Leonhardt H, Zink D (2004) Stable chromosomal units determine the spatial and temporal organization of DNA replication. *J Cell Sci* 117: 5353-65
- Sandelin A, Bailey P, Bruce S, Engstrom PG, Klos JM, Wasserman WW, Ericson J, Lenhard B (2004) Arrays of ultraconserved non-coding regions span the loci of key developmental genes in vertebrate genomes. *BMC Genomics* 5: 99
- Satterwhite E, Sonoki T, Willis TG, Harder L, Nowak R, Arriola EL, Liu H, Price HP, Gesk S, Steinemann D, Schlegelberger B, Oscier DG, Siebert R, Tucker PW, Dyer MJ (2001) The BCL11 gene family: involvement of BCL11A in lymphoid malignancies. *Blood* 98: 3413-20
- Schalch T, Duda S, Sargent DF, Richmond TJ (2005) X-ray structure of a tetranucleosome and its implications for the chromatin fibre. *Nature* 436: 138-41
- Schlake T (2007) Determination of hair structure and shape. *Semin Cell Dev Biol* 18: 267-73
- Schmid M, Nanda I, Hoehn H, Scharfl M, Haaf T, Buerstedde JM, Arakawa H, Caldwell RB, Weigend S, Burt DW, Smith J, Griffin DK, Masabanda JS, Groenen MA, Crooijmans RP, Vignal A, Fillon V, Morisson M, Pitel F, Vignoles M, Garrigues A, Gellin J, Rodionov AV, Galkina SA, Lukina NA, Ben-Ari G, Blum S, Hillel J, Twito T, Lavi U, David L, Feldman MW, Delany ME, Conley CA, Fowler VM, Hedges SB, Godbout R, Katyal S, Smith C, Hudson Q, Sinclair A, Mizuno S (2005) Second report on chicken genes and chromosomes 2005. *Cytogenet Genome Res* 109: 415-79
- Schones DE, Zhao K (2008) Genome-wide approaches to studying chromatin modifications. *Nat Rev Genet* 9: 179-91
- Schubeler D, MacAlpine DM, Scalzo D, Wirbelauer C, Kooperberg C, van Leeuwen F, Gottschling DE, O'Neill LP, Turner BM, Delrow J, Bell SP, Groudine M (2004) The histone modification pattern of active genes revealed through genome-wide chromatin analysis of a higher eukaryote. *Genes Dev* 18: 1263-71
- Sedarat F, Lin E, Moore ED, Tibbits GF (2004) Deconvolution of confocal images of dihydropyridine and ryanodine receptors in developing cardiomyocytes. *J Appl Physiol* 97: 1098-103
- Semon M, Duret L (2006) Evolutionary origin and maintenance of coexpressed gene clusters in mammals. *Mol Biol Evol* 23: 1715-23
- Senawong T, Peterson VJ, Leid M (2005) BCL11A-dependent recruitment of SIRT1 to a promoter template in mammalian cells results in histone deacetylation and transcriptional repression. *Arch Biochem Biophys* 434: 316-25
- Shen W, Mardon G (1997) Ectopic eye development in *Drosophila* induced by directed dachshund expression. *Development* 124: 45-52

- Shopland LS, Johnson CV, Byron M, McNeil J, Lawrence JB (2003) Clustering of multiple specific genes and gene-rich R-bands around SC-35 domains: evidence for local euchromatic neighborhoods. *J Cell Biol* 162: 981-90
- Shopland LS, Lynch CR, Peterson KA, Thornton K, Kepper N, Hase J, Stein S, Vincent S, Molloy KR, Kreth G, Cremer C, Bult CJ, O'Brien TP (2006) Folding and organization of a contiguous chromosome region according to the gene distribution pattern in primary genomic sequence. *J Cell Biol* 174: 27-38
- Siepel A, Bejerano G, Pedersen JS, Hinrichs AS, Hou M, Rosenbloom K, Clawson H, Spieth J, Hillier LW, Richards S, Weinstock GM, Wilson RK, Gibbs RA, Kent WJ, Miller W, Haussler D (2005) Evolutionarily conserved elements in vertebrate, insect, worm, and yeast genomes. *Genome Res* 15: 1034-50
- Solovei I, Cavallo A, Schermelleh L, Jaunin F, Scasselati C, Cmarko D, Cremer C, Fakan S, Cremer T (2002) Spatial preservation of nuclear chromatin architecture during three-dimensional fluorescence in situ hybridization (3D-FISH). *Exp Cell Res* 276: 10-23
- Solovei I, Grasser, F., Lanctôt, C. (2007) FISH on Histological Sections CSH Protocols doi:10.1101/pdb.prot4729
- Solovei I, Lanctôt C, Kösem S, Kreysing M, Guck J, Peichl L, Joffe B, Cremer T (in preparation) Nuclear architecture of rod photoreceptor cells adapts to vision in mammalian evolution.
- Spilianakis CG, Lalioti MD, Town T, Lee GR, Flavell RA (2005) Interchromosomal associations between alternatively expressed loci. *Nature* 435: 637-45
- Squazzo SL, O'Geen H, Komashko VM, Krig SR, Jin VX, Jang SW, Margueron R, Reinberg D, Green R, Farnham PJ (2006) Suz12 binds to silenced regions of the genome in a cell-type-specific manner. *Genome Res* 16: 890-900
- Stadler S, Schnapp V, Mayer R, Stein S, Cremer C, Bonifer C, Cremer T, Dietzel S (2004) The architecture of chicken chromosome territories changes during differentiation. *BMC Cell Biol* 5: 44
- Staynov DZ, Proykova YG (2008) Topological constraints on the possible structures of the 30 nm chromatin fibre. *Chromosoma* 117: 67-76
- Su AI, Cooke MP, Ching KA, Hakak Y, Walker JR, Wiltshire T, Orth AP, Vega RG, Sapinoso LM, Moqrich A, Patapoutian A, Hampton GM, Schultz PG, Hogenesch JB (2002) Large-scale analysis of the human and mouse transcriptomes. *Proc Natl Acad Sci U S A* 99: 4465-70
- Sun HB, Shen J, Yokota H (2000) Size-dependent positioning of human chromosomes in interphase nuclei. *Biophys J* 79: 184-90
- Tanabe H, Habermann FA, Solovei I, Cremer M, Cremer T (2002) Non-random radial arrangements of interphase chromosome territories: evolutionary considerations and functional implications. *Mutat Res* 504: 37-45
- Tremethick DJ (2007) Higher-order structures of chromatin: the elusive 30 nm fiber. *Cell* 128: 651-4
- Tsaparas P, Marino-Ramirez L, Bodenreider O, Koonin EV, Jordan IK (2006) Global similarity and local divergence in human and mouse gene co-expression networks. *BMC Evol Biol* 6: 70
- Van de Peer Y (2004) Computational approaches to unveiling ancient genome duplications. *Nat Rev Genet* 5: 752-63
- Vandesompele J, De Preter K, Pattyn F, Poppe B, Van Roy N, De Paepe A, Speleman F (2002) Accurate normalization of real-time quantitative RT-PCR data by geometric averaging of multiple internal control genes. *Genome Biol* 3: RESEARCH0034

- Verdone L, Caserta M, Di Mauro E (2005) Role of histone acetylation in the control of gene expression. *Biochem Cell Biol* 83: 344-53
- Verschure PJ, van Der Kraan I, Manders EM, van Driel R (1999) Spatial relationship between transcription sites and chromosome territories. *J Cell Biol* 147: 13-24
- Vinogradov AE (2005) Genome size and chromatin condensation in vertebrates. *Chromosoma* 113: 362-9
- Visser AE, Eils R, Jauch A, Little G, Bakker PJ, Cremer T, Aten JA (1998) Spatial distributions of early and late replicating chromatin in interphase chromosome territories. *Exp Cell Res* 243: 398-407
- Volpi EV, Chevret E, Jones T, Vatcheva R, Williamson J, Beck S, Campbell RD, Goldsworthy M, Powis SH, Ragoussis J, Trowsdale J, Sheer D (2000) Large-scale chromatin organization of the major histocompatibility complex and other regions of human chromosome 6 and its response to interferon in interphase nuclei. *J Cell Sci* 113 (Pt 9): 1565-76
- Wakelin LP, McFadyen WD, Walpole A, Roos IA (1984) Interaction of phenylthiolato-(2,2',2"-terpyridine)platinum(II) cation with DNA. *Biochem J* 222: 203-15
- Walter J, Joffe B, Bolzer A, Albiez H, Benedetti PA, Muller S, Speicher MR, Cremer T, Cremer M, Solovei I (2006) Towards many colors in FISH on 3D-preserved interphase nuclei. *Cytogenet Genome Res* 114: 367-78
- Walter J, Schermelleh L, Cremer M, Tashiro S, Cremer T (2003) Chromosome order in HeLa cells changes during mitosis and early G1, but is stably maintained during subsequent interphase stages. *J Cell Biol* 160: 685-97
- Wegel E, Shaw P (2005) Gene activation and deactivation related changes in the three-dimensional structure of chromatin. *Chromosoma* 114: 331-7
- Wiblin AE, Cui W, Clark AJ, Bickmore WA (2005) Distinctive nuclear organisation of centromeres and regions involved in pluripotency in human embryonic stem cells. *J Cell Sci* 118: 3861-8
- Wilkinson DG (1992) Whole mount in situ hybridization of vertebrate embryos. IRL Press, Oxford
- Williams RR (2003) Transcription and the territory: the ins and outs of gene positioning. *Trends Genet* 19: 298-302
- Williams RR, Azuara V, Perry P, Sauer S, Dvorkina M, Jorgensen H, Roix J, McQueen P, Misteli T, Merckenschlager M, Fisher AG (2006) Neural induction promotes large-scale chromatin reorganisation of the Mash1 locus. *J Cell Sci* 119: 132-40
- Williams RR, Broad S, Sheer D, Ragoussis J (2002) Subchromosomal positioning of the epidermal differentiation complex (EDC) in keratinocyte and lymphoblast interphase nuclei. *Exp Cell Res* 272: 163-75
- Woolfe A, Goodson M, Goode DK, Snell P, McEwen GK, Vavouri T, Smith SF, North P, Callaway H, Kelly K, Walter K, Abnizova I, Gilks W, Edwards YJ, Cooke JE, Elgar G (2005) Highly conserved non-coding sequences are associated with vertebrate development. *PLoS Biol* 3: e7
- Xu N, Tsai CL, Lee JT (2006) Transient homologous chromosome pairing marks the onset of X inactivation. *Science* 311: 1149-52
- Yokota H, van den Engh G, Hearst JE, Sachs RK, Trask BJ (1995) Evidence for the organization of chromatin in megabase pair-sized loops arranged along a random walk path in the human G0/G1 interphase nucleus. *J Cell Biol* 130: 1239-49
- Yue Z, Jiang TX, Widelitz RB, Chuong CM (2005) Mapping stem cell activities in the feather follicle. *Nature* 438: 1026-9

Zink D, Amaral MD, Englmann A, Lang S, Clarke LA, Rudolph C, Alt F, Luther K, Braz C, Sadoni N, Rosenecker J, Schindelbauer D (2004) Transcription-dependent spatial arrangements of CFTR and adjacent genes in human cell nuclei. *J Cell Biol* 166: 815-25

Zinner R, Albiez H, Walter J, Peters AH, Cremer T, Cremer M (2006) Histone lysine methylation patterns in human cell types are arranged in distinct three-dimensional nuclear zones. *Histochem Cell Biol* 125: 3-19

Publications

Journal Articles

- 2007 Solovei I., **Grasser F.**, Lanctôt C.. FISH on Histological Sections (CSH Protocols; 2007; doi:10.1101/pdb.prot4729)
- 2008 **Grasser F.**, Neusser M., Fiegler H., Thormeyer T., Cremer M, Carter NP., Cremer T. and Müller S.. Replication timing correlated spatial chromatin arrangements in cancer and primate interphase nuclei (J Cell Sci. 2008 Jun 1;121(Pt 11):1876-86. Epub 2008 May 13)
- 2008 Müller S., Cremer M., Neusser M., **Grasser F.**, and Cremer T.. A technical note on quantum dots for multi-color fluorescence in situ hybridization (Cytogenet Genome Res, in press)
- 2008 Bodega B., Brunelli S., **Grasser F.**, Belotti P., Tonlorenzi R., Mora M., Torrente Y., Meneveri A., Marozzi A., Müller S., Battaglioli E. and Ginelli E.. Impairment of Polycomb recruitment on D4Z4 contracted alleles does not affect FRG1 expression during FSHD myoblast differentiation (PNAS, under review)

Articles in preparation

Grasser F., Lanctôt C., Langer S., Witt V., Cremer T., Müller S., Nuclear topology of trans-dev genes and flanking ultra-conserved non-coding sequence clusters in mouse and chicken development

Grasser F., Lanctôt C., Cremer T., Müller S., Reversible nuclear repositioning of the casein gene cluster, a mammalian genomic innovation, during postnatal development

Congress Contributions

- 2005 Oral presentation: Replication timing dependent spatial chromatin arrangements in hominoids, 2nd Marie Curie Conference on arrayCGH and Molecular Cytogenetics, Bari, Italy
- 2006 Oral presentaion: Replication-timing-dependent spatial chromatin arrangements in different cell lines derived from cancer and hominoid primates, International Cytogenetics and Genome Society, Canterbury, England
- 2006 Oral presentation: Nuclear topology of ultra-conserved non-coding sequence clusters flanking the Dach1 locus in mouse and chicken development, 3rd Marie Curie Conference on arrayCGH and Molecular Cytogenetics, Leuven, Belgium

- 2007 Poster presentation: Nuclear topology of trans-dev genes and flanking ultra-conserved non-coding sequence clusters in mouse and chicken development, 16th International Chromosome Conference Amsterdam, Netherlands
- 2008 Poster presentation: Reversible nuclear repositioning of the casein gene cluster, a mammalian genomic innovation, during postnatal development, Interplay among genetics, epigenetics and non-coding RNA's , Madrid, Spain

Curriculum Vitae

Persönliche Daten

Name: Florian Grasser
Adresse: Arnulfstraße 275,
80639 München
Geburtsdatum: 23.11.1979
Geburtsort: München
Nationalität: Deutsch

Schule, Wehrdienst

25/06/1999 Allgemeine Hochschulreife, Carl-Spitzweg-Gymnasium,
Unterpfaffenhofen (Gesamtnote 2,0)
07/1999-04/2000 Grundwehrdienst, Ordonanz und Koch, Offizierkasino der
1.Gebirgsdivision, Gebirgspionierbataillon 8, Brannenburg

Studium

10/2000-06/2005 Diplomstudiengang Biologie, Ludwig-Maximilians-Universität,
München, Hauptfach: Anthropologie und Humangenetik,
Nebenfächer: Immunologie, Genetik, Zoologie (zellbiologische
Richtung, Vorlesungen in Englisch), organische Chemie
(zusätzliches Nebenfach)
11/10/2002 Diplom-Vorprüfung (Gesamtnote 1,6)
07/07/2005 Diplom-Hauptprüfung (Gesamtnote 1,0)
10/2004-06/2005 Diplom-Arbeit am Lehrstuhl für Humangenetik der Ludwig-
Maximilians-Universität, München (Note 1,0)
seit 08/2005 Doktorand am Lehrstuhl für Humangenetik der Ludwig-
Maximilians-Universität, München und Mitglied der International
Max Planck Research School of Cellular and Life Sciences

Zusatzqualifikationen

Seminare: Gewerblicher Rechtsschutz für Chemiker und Pharmazeuten I –
Patentrecht, Ludwig-Maximilians-Universität, München
Gewerblicher Rechtsschutz für Chemiker und Pharmazeuten II –
Marken-, Gebrauchs-, Geschmacksmusterrecht, Ludwig-Maximilians-
Universität, München
Effective Scientific Writing, Max-Planck- Institut für Biochemie,
Martinsried

Intercultural Communication, Max-Planck- Institut für Biochemie, Martinsried

Presenting with Confidence, Max-Planck- Institut für Biochemie, Martinsried

Politik und internationale Sicherheit, Seminar der Thomas Dehler Stiftung, Konstanz

Sprachen: Englisch (sicher in Wort und Schrift)

Französisch (Unterricht seit Januar 2006)

EDV: Windows, MacOSX und Linux Betriebssysteme

MSoftware, Excel, Powerpoint, Adobe Photoshop, SigmaStat

2D- und 3D- Bildbearbeitungs- und Auswertungsprogramme

Berufliche Tätigkeit

Seit 10/1997 Verkaufsberater (Bekleidung), Hirmer GmbH & Co., München,
vor und nach dem Studium: Geringfügige Beschäftigung (ca. 30h/Monat), während des Studiums: Werkstudent (ca. 85h/Monat)

Acknowledgement

PD Dr. Stefan Müller danke ich, für die inkl. der Diplomarbeit nun mehr fast 4 Jahre gemeinsamer Forschung, Vertrauen und seiner Zeit. Insbesondere dafür, dass er mir die richtige Mischung aus Freiraum und Betreuung gegeben hat.

Prof. Dr. Thomas Cremer danke ich dafür, dass er trotz schwieriger finanzieller Situationen immer wieder Geld aus dem Hut gezaubert hat, um meine Arbeit zu finanzieren und für seine Unterstützung.

Prof. Dr. Dirk Eick, PD Dr. Angelika Böttger, Prof. Dr. Gerhard Wanner und Prof. Dr. Manfred Schliwa danke ich für die Übernahme der Gutachten zu dieser Arbeit, sowie zusätzlich den beiden ersteren für die Teilnahme am Rigorosum, und somit allen für ein kostbares Gut - die Zeit.

Dr. Christian Lanctôt danke ich für unzählige kleine Tipps und Tricks als auch für sein stetes Interesse an meiner Arbeit. Sein Wissen und seine Ideen waren für viele Ergebnisse dieser Arbeit unerlässlich.

Dr. Sabine Langer danke ich für die geduldige Einweisung auf dem Gebiet der Lasermikrodissektion und dafür, dass sie eine tolle Büromitbewohnerin ist.

Dr. Michaela Neusser, verdanke ich noch immer die Geheimnisse einer gelungenen FISH und eine hervorragende Banknachbarschaft.

Dr. Marion Cremer danke ich dafür, dass sie den Laden am Laufen hält und für das nette Schwätzchen zwischendurch.

Dr. Irina Solovei für die gemeinsame Entwicklungen und Diskussionen zum Thema - FISH auf Gewebeschnitte.

Prof. Dr. Rüdiger Kölbl, PD Dr. Stefan Grund und Dr. Markus Moser danke ich für die unkomplizierte und schnelle Bereitstellung von diversen Zellmaterialien.

Tobias Thormeyer danke ich, dass er unseren Daten das DistAng Programm auf den Leib geschrieben hat.

Heidi Hahn-Henninger danke dafür, dass man in unserem Labor sogar vom Fußboden essen könnte.

Unseren Diplomanden Caroline Bernhard und Verena Witt danke ich für ihre Mitarbeit und im Besonderen Caroline, dass sie immer noch nicht aufgegeben hat meine Ernährung auf eine guten Weg zu bringen.

Des Weiteren danke ich allen PostDocs, Mitdoktoranden, Mitarbeitern – Prof. Dr. Stan Fakan, Dr. Jürgen Paar, Dr. Jaques Rouquette, Dr. Alessandro Brero, Dr. Charlotte Hauser, Dr. Steffen Dietzl, Dr. Iris Haas, Dr. Boris Joffe, Mariana Lomiento, Radka Symonova, Dani Köhler, Claudia Dahlem, Claudia Heppberger, Robert Mayer, Heiner Albiez, Roman Zinner, Alexandra Kölbl, Jens Nagel, Hilmar Strickfaden, Andreas Zunhammer, Doris Illner, Barbara Hübner, Roy Hessing und Caroline Bleese, Ming Zhao – unzähligen Diplomanden und Praktikanten für ihre Kollegialität, Hilfsbereitschaft zu allen Zeiten und die eifrige Teilnahme an den geselligen Feierabendbierrunden.

Meiner Familie, v.a. meiner Mama, meinem Papa und meiner Schwester danke ich sehr für ihre liebevolle Unterstützung und ihr Verständnis, die es mir erst ermöglicht haben den zeitlich hohen Aufwand für diese Dissertation und meinem samstäglichen Nebenjob zu treiben.

Ehrenwörtliche Versicherung

Hiermit bestätige ich, dass ich die vorliegende Dissertation selbstständig und nur mit den angegebenen Materialien und Quellen durchgeführt habe.

München, den .07.08

Florian Grasser

Erklärung über frühere Promotionsversuche

Hiermit bestätige ich, dass ich vor dieser Arbeit keine anderen Promotionsversuche unternommen habe. Dies ist meine erste Dissertation.

München, den .07.08

Florian Grasser